MONASH University

Computational Drug Formulation

Amali Galappaththi Guruge

B. Sc. (Hons), M. Phil

A thesis submitted for the degree of *Doctor of Philosophy* at

Monash University in 2021

Department of Medicinal Chemistry

Copyright notice

Dedication

To my mother, Irene Silva Guruge who sacrificed her everything so I could dream big…

and

To my father, Dr Kingsley G. Guruge, the epitome of my life…

පිදුම

මා වෙනුවෙන් ජීවිතයේ සියලු කැපකිරීම් කල ආදරණීය අම්මා, අයිරින් සිල්වා ගුරුගේටත් ජීවිතයේ මුල් කඩයිම් අසල නිස්කාරණයේ කඩාවැටුණු මා අස්වසාලමින් මගේ සෙවනැල්ල සහ ශක්තිය වූ ආදරණීය තාත්තා, ආචාර්ය කිංග්ස්ලි ගුරුගේටත් සෙනෙහෙ සිතින් පිළිගන්වමි.

Contents

Abstract

Understanding the fate of drug formulations after oral administration is essential to design improved lipid-based formulations (LBFs) for poorly water-soluble drugs emerge from drug discovery pipelines. However, due to the complexity in the gastrointestinal tract, experimental investigations are limited. In contrast, molecular dynamics (MD) is an attractive approach that can be used to explore complex environments at the atomic level. Information gained through this approach greatly helps to understand experimental observations of complex systems.

Polyethylene oxide (PEO) surfactants are widely used excipient in LBFs. Due to the unavailability of a proper force field (FF) to model PEO molecules, the exploring of the phase behavior of LBFs using MD approach lags behind. Thus, we started our work by identifying the most suitable FF to model different phase behaviors of a simple nonionic PEO surfactant $C_{12}E_6$. Out of the explored FFs, we found that 2016H66 FF better reproduced the experimental phase behavior of the surfactant. Further, starting from different liquid phases of $C_{12}E_6$, classical MD simulations, and replica-exchange MD simulations were performed to study how well MD reproduces the phase structures due to changes in concentration and temperature (i.e., phase transitions). This study showed that the 2016H66 FF successfully models the phase transitions and thus, this FF is independent from the starting structure and depends only on the conditions of the system. Moreover, this investigation provides insight into the colloidal behavior of experimentally less explored regions in the $C_{12}E_6$/water phase diagram. Also, both studies described above provide confidence in the use of the 2016H66 FF to model complex phase behavior of PEO surfactants.

To study the colloidal behavior of LBFs upon dispersion and dilution, we selected Type III formulations designed for the poorly water-soluble drug loratadine. We studied the phase behavior and the influence of excipient type and composition on the phase behavior of LBFs by running 50 long MD simulations (0.4 – 1.7 μs) for 5 LBFs.
Visual observations from MD were compared with the same in experiments. We found that MD successfully reproduced the experimental phase behavior, indicating that MD can be used as a predictive tool to determine the phase behavior of LBFs. This study also showed changes in general phase behavior in the presence of polymer, surfactant concentration and surfactant types. Overall, this study facilitates understanding the

experimental phase behavior at the atomic level and designing better formulations for poorly water-soluble drugs.

Since phospholipids and bile salts play a major role in drug absorption, they influence in the phase behavior of LBFs. Thus, having the intension of introducing phospholipids and bile components to LBFs, we conducted an investigation to test how well coarse-grained (CG) MD reproduces the experimental phase behavior of POPC/bile salt aqueous mixtures in the micellar and vesicular regions. In this investigation, we showed that the CG MARTINI models successfully reproduce the experimentally observed phase behavior of POPC/bile salt/water mixtures. Further, MD showed that the vesicle formation occurs through bicelle formation, which then curls up and forms a vesicle. This study provides confidence to use CG MARTINI models to explore the detailed phase behavior of LBFs in the gastrointestinal tract.

Thesis including published works declaration

I hereby declare that this thesis contains no material which has been accepted for the award of any other degree or diploma at any university or equivalent institution and that, to the best of my knowledge and belief, this thesis contains no material previously published or written by another person, except where due reference is made in the text of the thesis.

This thesis includes 1 original paper published in peer reviewed journals and 0 submitted publications. The core theme of the thesis is drug formulation. The ideas, development and writing up of all the papers in the thesis were the principal responsibility of myself, the student, working within the Faculty of Pharmacy and Pharmaceutical Sciences under the supervision of David K. Chalmers, Colin W. Pouton and Dallas B. Warren.

The inclusion of co-authors reflects the fact that the work came from active collaboration between researchers and acknowledges input into team-based research.

In the case of *Chapter 3* my contribution to the work involved the following:

Thesis Chapter	Publication Title	Status	Nature and % of student contribution	Co-author name(s) Nature and % of Co-author's contribution*	Co-author(s), Monash student Y/N
3	*Aqueous phase behavior of the PEO-containing non-ionic surfactant $C_{12}E_6$: A molecular dynamics simulation study*	*Published*	*75% Investigation, data analysis and writing first draft*	*1) Dallas B. Warren, Supervision, Writing - review & editing input into manuscript 6.25%* *2) Hassan Benameur, Conceptualization, Supervision, input into manuscript 6.25%* *3) Colin W. Pouton, Conceptualizati*	*No* *No* *No*

				on, Supervision, Writing - review & editing, input into manuscript 6.25% *4) David K. Chalmers, Conceptualization, Supervision, Resources, Writing - review & editing, input into manuscript 6.25%*	*No*

I have not renumbered sections of submitted or published papers in order to generate a consistent presentation within the thesis.

Student name: Amali G. Guruge

Student signature: **Date:** 03-06-2021

I hereby certify that the above declaration correctly reflects the nature and extent of the student's and co-authors' contributions to this work. In instances where I am not the responsible author I have consulted with the responsible author to agree on the respective contributions of the authors.

Main Supervisor name: Dr. David Chalmers

Main Supervisor signature: **Date:** 04-06-2021

Acknowledgements

First and foremost, I would like to extend my special thanks to my main supervisor, Dr. David Chalmers for giving me an opportunity to join his research group in 2017. Since the first email I sent him to express my interest in joining his research group to date, he guided, supported, and advised me to achieve goals of my PhD within the stipulated time period. My sincere thanks also go to my co-supervisors, Prof. Colin Pouton and Dr. Dallas Warren for their support and guidance throughout the project. I truly enjoyed many interesting talks with them on every meeting on Thursdays that guided me to keep my research on track and continuously improve my knowledge on drug formulation science.

I would also like to thank my PhD panel at Monash Institute of Pharmaceutical Sciences (MIPS), Dr. Natalie Trevaskis, Dr. David Manallack and Prof. Philip Thompson for their valuable comments during milestone panel meetings.

My thanks also go to Estelle Suys for being such a nice and close friend for me throughout my PhD journey and for many exciting discussions, which helped me get a better understanding of not just my research but of science in general. Also, I like to thank Sanjeevini Babu Reddiar, Amanda Handrisanto and Mitchell Silk for their friendly chats at MIPS.

I would also like to thank Monash University and Lonza Pharma Sciences for providing me with a 'Graduate Research Scholarship (MGS)' for my stipend and scholarship support for my tuition fee during my PhD.

I am grateful to my father, Dr. Kingsley Guruge, who always inspired and guided me to achieve my goals regardless of circumstances. He is my strength, guiding light and the role model who taught me to be unstoppable until I reach goals in life. Also, I am grateful to my mother, Irene Silva Guruge, who sacrificed everything for me. She used to do Paritta chant from Sri Lanka every time I was doing PhD milestones and blessed me unconditionally to reach success. Also, I would like to thank my sister, Dinushi Guruge, for encouraging me and helping me work on my PhD without any disturbance in my mind by taking care of our mother.

My sincere thanks also go to my husband, Shan Anjana Jayasinghe for being such a wonderful person who always stands behind and walks with me at every step I take. He used to wipe off my tears and tried bringing a smile to my face when I had hard times. Without him, I would not be able to be who I am today, thank you so much for choosing me as your life partner. Also, I am grateful to my son, Sanuka Hansitha Jayasinghe who is the cutest troublemaker in my life. Thank you so much for your kisses and hugs that helped me release my working stress.

I would also like to thank all my teachers at my school (Sujatha Balika Vidyalaya, Matara), the University of Colombo and the Institute of Chemistry Ceylon. I especially like to thank my mathematics tuition teacher, Mr. Sujith Jasingarachchi for laying the foundation in me toward science. Also, I especially thankful to Prof. Dhammike Dissanayake, Prof. Samantha Weerasinghe and Dr. Chandini Udawatte for their guidance, support and still advising me for a successful academic career.

Many thanks go to people who helped me and my husband since we landed in Australia. Thank you Kasun Shanaka and Jinani Nupehewa for hosting us for few weeks at your home until we find a house to rent ourselves. My aunt, Jayani Atapattu, thank you for everything you have done to feel that we are not alone in Australia. Your first visit to our apartment in Drummond Street to your surprised birthday cakes made us comfortable and feel like that we are surrounded by our own family. Thank you, my uncle, Saman de Silva and cousins for all pleasant gatherings at your home in Hampton Park. Also, thank you for all my friends in Australia for arranging fun times, picnics and trips around Victoria, New South Wales and Western Australia which, worked as a remedy for working stress and led to spend cheerful times as a family.

Finally, I also like to thank relatives and non-relatives who inspired me to walk the path my father followed. Special thanks go to my aunt, Indira de Silva for encouraging me to study since I was schooling primary. At last, but not least, many thanks go to relatives who tried pulling me down and discouraged me. Every effort they took to discourage me allowed me to gain more courage and inspired me to travel this journey this far strongly.

Publications

The following publications have been produced during the enrolment:

Guruge, A. G., Warren, D. B., Benameur, H., Pouton, C. W., & Chalmers, D. K. Aqueous Phase Behavior of the PEO-containing Non-ionic Surfactant $C_{12}E_6$: A Molecular Dynamics Simulation Study. J. Colloid and Interface Sci. 2021, 588, 257-268.

Chapter 1

Introduction

1.1 Oral Drug Delivery

Pharmaceutical drugs are introduced to the human body through different routes such as oral, injection, nasal, rectal, vaginal, sublingual, inhalation, ocular and other numerous ways.[1] Each route has advantages and disadvantages of using it. However, out of the above routes, oral administration is considered as one of the most convenient routes to deliver drugs into systemic circulation due to its simplicity, acceptability from the patient's perspective, safety, ease of ingestion and adaptability to use with various types of drugs.[2] Thus, this method has come a long way and is still developing with sophisticated technologies to deliver drugs with improved efficiency.[3] Different dosage forms such as pills, powders, suspensions and solutions are used to deliver drugs through this drug delivery method. Fundamentally, to use this drug delivery method, the drugs need to be solubilised in the aqueous environment for a sufficiently long period to be absorbed.[3] Yet, many drugs/drug leads that emerge from high-throughput screening with combinatorial chemistry in the current drug discovery pipelines are lipophilic and poorly water-soluble due to multifaceted reasons. However, the key causes include the pursuit of compound potency rather than good molecular properties[4-6], synthesis of nonpolar compounds is simpler than for polar compounds[7-8] and the pursuit of some targets, such as protein-protein interactions, requires physically large compounds to obtain adequate inhibitory activity.[9] Thus, physicochemical properties of these drugs and drug leads are beyond the Lipinski's[10] 'rule of 5' (no more than 5 hydrogen bond donors, no more than 10 hydrogen bond acceptors, molecular mass less than 500 Daltons, and an octanol-water partition coefficient less than 5). Consequently, emerging high molecular weight lipophilic compounds through drug discovery pipelines remains the major reason for hindering the simplest and pain-free drug delivery method, oral administration.

1.2 Biopharmaceutical Classification System (BCS)

The drugs that arise from drug discovery can be classified into four classes depending on their membrane permeability and solubility.[11] The typical representation for this classification is shown in Figure 1.[12]

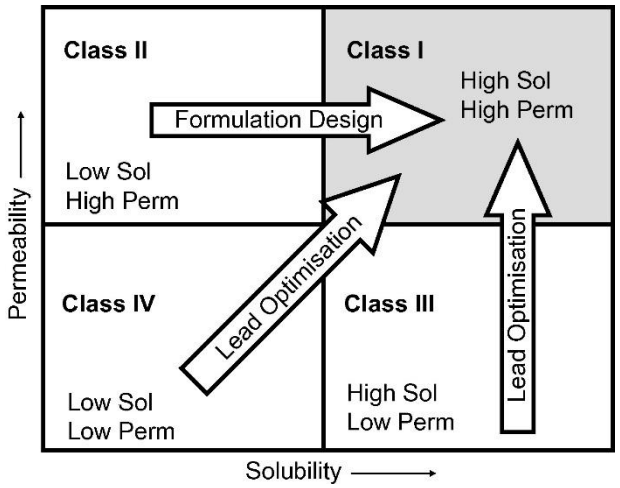

Figure 1 – Biopharmaceutical classification system. *Reprinted from European Journal of Pharmaceutical Sciences, 29 (3), Pouton, C. W., Formulation of Poorly Water-Soluble Drugs for Oral Administration: Physicochemical and Physiological Issues and the Lipid Formulation Classification System, 278-287, Copyright (2006), with permission from Elsevier.*

According to the classification, poorly water-soluble drugs are categorized into either class II or class IV. Poor water solubility is common to both classes, but the permeability of these two classes is different; class II drugs are highly permeable while class IV drugs are poorly permeable. To enhance the solubility of class IV drugs, a range of methods can be used, but their performance is hindered by low membrane permeability. Thus, the best way to improve the bioavailability of this class is to return to the lead optimisation step in the drug development process and modify the structure to obtain desirable properties.[13] Even though, class II drugs have good permeability, their bioavailability is compromised by the poor water solubility of the drug. Hence, the general approach to enhance the solubility of Type II drugs is through formulation strategies such as crystalline solid formulations, amorphous formulations, or lipid-based formulations (LBFs).[12, 14] Within these three formulation methods, our interest particularly lies in LBFs for delivering poorly water-soluble drugs through oral administration.

1.3 Lipid-Based Formulations (LBFs)

Many studies in the literature provide evidence that the absorption or bioavailability of poorly water-soluble drugs (class II in BCS) increases with the co-administration of a lipid-rich meal.[15-16] For example, work conducted with several poorly water-soluble drugs; griseofulvin[17], halofantrine[18] and danazol[19-20] showed improved bioavailability in the presence of co-administrated lipid-rich foods. Thus, developing LBFs for poorly water-soluble drugs gained increased attention. LBFs are one of the extensively studied formulation techniques that are currently used in many U.S Food and Drug Administration (FDA) approved drugs on the market.[21] In LBFs, poorly water-soluble drug blends with different pharmacologically inactive components (excipients) such as oils composed of pure triglycerides or mixed mono- and diglycerides, hydrophilic surfactants, hydrophobic surfactants and cosolvents together in different proportions. Most of the oil excipients used in LBFs are primarily derived from plant sources. These natural oils are mixtures of triglycerides that vary in the chain length of the fatty acid (long-chain and medium-chain triglycerides) and the degree of unsaturation.[22-23] Additionally, mixtures of mono/diglycerides obtained by partial hydrolysis of vegetable oils are also used in LBFs.[22] Typical examples of natural, long-chain triglyceride oil excipients utilized in LBFs are corn oil, olive oil, sesame oil and peanut oil. Some examples of medium-chain fatty acid triglyceride excipients are: Miglyol® 812, Captex® 355 and Labrafac®. Vegetable oil derived partial glycerides include excipients such as Capmul® MCM and Imwitor® 742.

Surfactants are classified as cationic, anionic, zwitterionic, or non-ionic according to the polar head group of the surfactant.[24] Out of these types, non-ionic surfactants are used in LBFs due to their low toxicity compared to cationic, anionic, and zwitterionic surfactants[25] and their ability to maintain the solubilising power against hydrophobic drugs in the gastrointestinal (GI) tract.[26-27] The partitioning tendency of the non-ionic surfactant in oil or water[28] is determined through the hydrophilic-lipophilic balance (HLB) where high HLB value surfactants have a higher affinity towards water. In LBFs, both high and low HLB surfactants are used in Type II-IV formulations in combination with oil excipients or cosolvents. Common examples of hydrophobic surfactants are polyoxyethylene (20) sorbitan trioleate (Tween® 85) and polyoxyethylene (20) glyceryl trioleate (Tagot® TO). Kolliphor® RH40, Kolliphor® RH60, and Tween® 80 are

examples of water-soluble surfactants used in LBFs. Many of the PEO surfactants such as polysorbates (Tween®) and polyoxyl castor oils (Kolliphor®), used in LBFs are heterogeneous mixtures and their composition can vary between manufacturer and batch.[29] Thus, the unclear chemical nature and heterogeneous nature of these PEO surfactants causes problems in establishing molecular models for them. Therefore, in our main investigation on LBFs with MD simulations, we used a single component representation to model this type of excipients as described in Chapter 5. However, for the initial studies conducted in Chapter 3 and Chapter 4, we used a PEO alkyl ether surfactant, which is a synthetic, pure compound in nature.

Cosolvents are particularly used in formulations to enhance the dispersion of the formulation. Commonly used cosolvents are polyethylene glycol (PEG-400), glycerol, ethanol and propylene glycol. However, care must be taken using hydrophilic cosolvents in LBFs since formulations with cosolvents sometimes tend to precipitate the hydrophobic drugs upon dispersion.

Details of typical excipients in LBFs that belong to oil, surfactant and cosolvent types are discussed in the literature.[30] Due to the critical roles of these excipients in drug formulations, many steps have been taken globally to regulate the manufacturing process and maintain the quality of these excipients since adulteration of these excipients could result in adverse effects in patients.[31-32] By mixing the above described excipients, a wide range of LBFs can be produced. Thus, to identify the performance of LBFs with different lipid systems and for simplification, a classification known as Lipid Formulation Classification System (LFCS) has been introduced initially by Pouton in 2000.[16] Lately, he updated the existing classification by introducing Type IV, which is a LBF type free from oil excipients.[12] This LFCS is based on the relative oil, surfactant and cosolvent composition included in a formulation and it has four main types (I to IV) of LBFs as shown in Table 1. [12] The drugs formulated with LBFs are typically in a liquid form inside a soft gelatin capsule. Detailed descriptions of Type I, II, III and IV formulations, and the effects of these formulations on drug solubility, absorption and dispersion, can be found in the literature.[30, 33]

Type I formulations are the simplest form of LBFs, which contain only oils. These formulations require digestion of the triglycerides in the oils into free fatty acids and 2-mono-glycerides by digestive enzymes to increase the dispersion and amphiphilicity

of the formulation but Type II-IV formulations contain sufficient surfactants to facilitate the spontaneous dispersion. Type II formulations are self-emulsifying drug delivery systems that contain oils and water-insoluble surfactants (hydrophilic-lipophilic balance; HLB<12). Type III formulations are self-microemulsifying drug delivery systems that contain oils, water-soluble surfactants (HLB>12) and cosolvents. The subclass Type IIIA includes greater proportions of oils but subclass Type IIIB includes a minor proportion of oils with a greater proportion of hydrophilic surfactants and cosolvents. Type IV formulations contain water-soluble surfactants, water-insoluble surfactants and hydrophilic cosolvents. By mixing water-soluble surfactant with cosolvent, Type IV offers high solvent capacity for the formulation on dilution compared to cosolvent alone.[12] Thus, Type IV formulations are extremely hydrophilic formulations. The general properties of LBFs are changed depending on the excipient content in a formulation and this is well described in the literature.[16, 34]

Table 1- Lipid formulation classification system[12]

Excipient in formulation	Content of formulation (% w/w)				
	Type I	Type II	Type IIIA	Type IIIB	Type IV
Oils: triglycerides or mixed mono- and diglycerides	100	40–80	40–80	<20	-
Water-insoluble surfactants (HLB<12)	-	20–60	-	-	0–20
Water-soluble surfactants (HLB>12)	-	-	20–40	20–50	30–80
Hydrophilic cosolvents (e.g., PEG, Transcutol)	-	-	0–40	20–50	0–50

Through all these formulations, the dissolution and solubility of the active pharmaceutical ingredient/drug are increased since the drug remains in solution (in the GI fluid) during its residence in the GI tract, which enhances the absorption. The properties of excipients and the criteria for selecting the excipients in lipid formulations have also been discussed by Pouton et al. in 2008.[35] Additionally, several useful reviews regarding the LBFs have been published focusing on broader aspects of LBFs.[34, 36-38]

Even when a poorly water-soluble drug is formulated in an LBF, its fate still depends on the dispersion, dilution, and exposure of the formulation to digestive enzymes in the GI tract, which alter the physical properties of the formulation.[12] Ultimately, the physical property changes in the LBFs affect the solubility of the drug. For example, the possibility of drug precipitation in Type IV formulation is high due to the hydrophilic nature of Type IV formulations upon dispersion/dilution in the GI tract. Thus, before using a LBF in a capsule, pre-investigations are required to predict the fate of drug formulations upon dispersion, dilution and digestion. In general, the performance/fate of these LBFs is evaluated through *in vivo* and *in vitro* studies.[39-43] Also, Pouton has established protocols to predict how the fate of the drug is affected by formulation design and to optimise the formulation design in a laboratory.[12] However, microstructural details such as the drug distribution within formulations and molecular interactions between excipients and drugs in formulations are difficult to study through experimental techniques. In contrast, the advancement of high-performance computing and *in silico* tools such as molecular dynamics (MD) have emerged as a new strategy to gain additional insight into complex systems at the atomic level and help understanding experimental observations. Thus, to study and understand the behavior of LBFs at the atomic level, we aimed to use MD simulations. The information we get from MD simulations will assist in the formulation development of poorly water soluble drugs.

1.4 Phase Diagrams

To characterize the fate of LBFs after oral administration, the experimental phase behavior and MD phase behavior were compared in the study in Chapter 5. Thus, the identification of various phases formed in different component systems is crucial.

A phase of a substance is a form of matter that is uniform throughout its physical state and its chemical composition.[44] As an example, the universal solvent; water can have three phases depending on the temperature and pressure conditions as liquid, solid and gas. A phase diagram is a graphical plot that shows the relationship between different phases that exist in a system under equilibrium conditions.[45] Therefore, phase diagrams provide information to understand conditions to form phases and transformation of phases due to changes commonly in temperature, pressure and composition.

The work described in this thesis includes phase diagrams for two-component or three-component (ternary phase diagrams) systems. The main two-component phase diagram we used in our work is the PEO surfactant $C_{12}E_6$/water phase diagram as shown in Figure 6.[46]

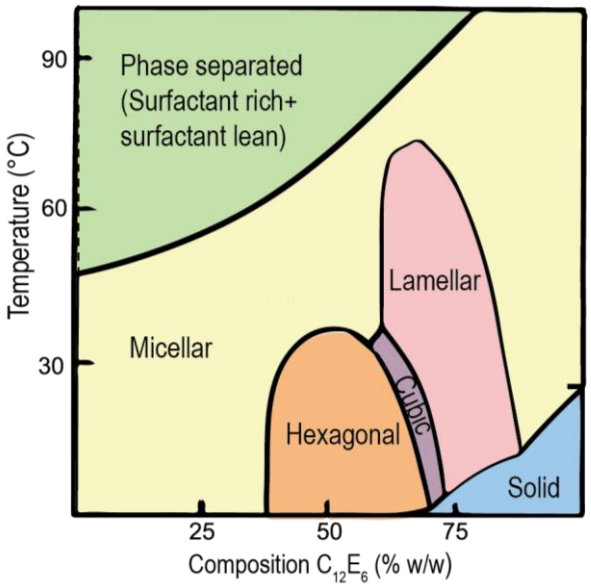

Figure 6 – Phase diagram of $C_{12}E_6$ in water[46]

According to the phase diagram, $C_{12}E_6$/water binary systems form micellar, hexagonal, lamellar, solid, cubic and phase separated phases. The temperature and pressure conditions required to form each phase can be identified through the plot. Similarly, the ternary phase diagram of 1-palmitoyl-2-oleoyl-sn-glycerol-3-phosphocholine, glycochenodeoxycholate and water (Figure 1 of Chapter 6) used in the current study shows the formation of micellar and vesicular phases under different compositions of three components.

1.5 Phase Structures

The molecular arrangement or phase structure is different from phase to phase. Since MD provides detailed atomic information, the exact molecular arrangement is essential to determine the phases formed in MD simulations of LBFs.

Phase Structures in Surfactant/Water Mixtures

Chapter 3 and Chapter 4 employed the binary system $C_{12}E_6$ and water. Since $C_{12}E_6$ is a surfactant that contains hydrophilic head and hydrophobic tail, the surfactant self-

assembled into different phase structures in the presence of water as shown in Figure 6. The simplest form of surfactant molecule arrangement is the micellar phase where hydrophilic head (pink segment in the surfactant, Figure 7) of the surfactant makes contact with the solvent (i.e., water) while hydrophobic tails (green segment in the surfactant, Figure 7) arrange in the middle of the micelle. As the concentration of the surfactant increases, other phases such as elongated micelles, which is also known as rod-like or wormy micelles, lamellar; a sheet like structure, hexagonal; infinite elongated micelles that are arranged in a honeycomb structure and other liquid crystalline phases such as lamellar and cubic are formed. Schematic representation of few surfactant phase structures is shown in Figure 7.[47]

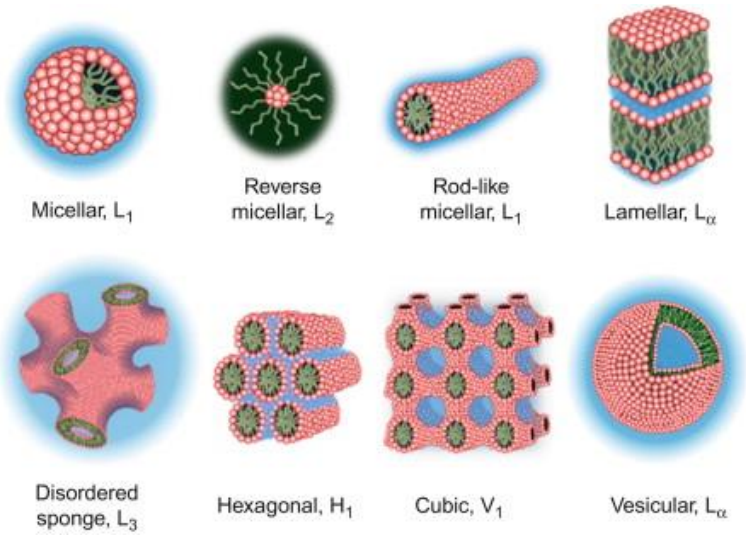

Figure 7 – Schematic representation of some surfactant phases.[47] *Reprinted from, Colloid Foundations of Nanoscience, Eastoe J. and Tabor R. F., Chapter 6 – Surfactants and Nanoscience, 135-157, Copyright (2014), with permission from Elsevier.*

The formation of different phases is controlled by factors such as the interactions between head and tail groups of the surfactants with the solvent and the geometric factors of the surfactant, which is defined with the packing parameter *P*. The packing parameter is defined as follows.[48]

$$P = \frac{V_c}{aL_c}$$

P – Packing parameter

V_c – Volume of tail group of the surfactant

a – Cross sectional area of the surfactant

L_c – Length of the tail group of the surfactant

Depending on the value for *P*, self- assembled structures are formed. When *P* is small; *P* < 1/3, spherical structures like micelles are favoured. When 1/3 < *P* <1/2, cylindrical structures such as hexagonal phase is formed. The lamellar phase is formed when *P* = 1. The phases like reversed hexagonal, reversed micelles and reversed cubic are formed when *P* > 1.

Phase Structures in Surfactant/Oil/Water Mixtures

Emulsion is a phase formed by mixing immiscible or partially miscible liquids. Since oil is a major component of a LBF and it is immiscible in water, once LBFs make contact with the aqueous environment of the gastric fluid, LBFs form emulsion phases. Emulsions can be oil-in-water (O/W), where oil droplets are dispersed in the water continuous phase or water-in-oil (W/O) where water droplets are dispersed in oil continuous phase.[47] The droplet size of these phase structures is very large and phases are thermodynamically unstable. Thus, emulsions tend to sperate or break.[49] However, microemulsion phase is thermodynamically stable and contains relatively small droplets and can be in W/O or O/W type. Furthermore, another phase called bicontinuous phase also exists in surfactant/oil/water systems where oil and water phases are continuous and separated by a surfactant layer. Schematic representation of O/W, W/O and bicontinuous microemulsion phases is shown in Figure 8.[50] Detailed information regarding phases formed in surfactant/oil/water mixtures are discussed in Chapter 5.

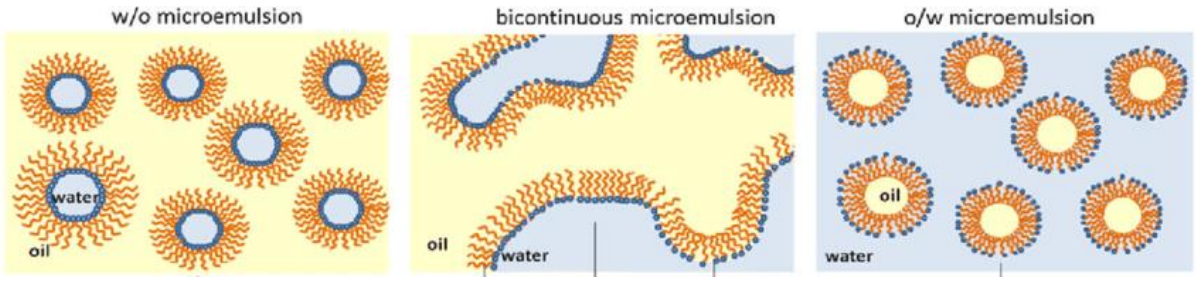

Figure 8 – Schematic representation of W/O, bicontinuous and O/W microemulsions. *Adapted by permission from Springer Nature, Food Engineering Reviews, High- and*

Low-Energy Emulsifications for Food Applications: A Focus on Process Parameters, R. C. Santana et al.[50] *Copyright (2013).*

1.6 Molecular Dynamics (MD)

The first MD simulation of a macromolecule was published 44 years ago.[51] Since then, this computational approach has evolved with the advancement of the computer. MD models the physical movements of atoms and molecules by solving the Newtonian equations of motions numerically.[52] MD is a powerful tool in molecular modelling and gives insight into the detailed picture of the structure and motion of individual particles as a function of time. Since MD relies on empirical approximations, reproducing quantum effects such as bond-forming or bond breaking is not feasible with classical MD simulations.[53]

1.6.1 Force Fields (FFs)

MD simulations are based on force fields. This includes an equation set to calculate potential energy and forces plus a collection of parameters that need to use within the defined equation set.[53] These force fields define the properties of atoms/molecules (e.g., bond lengths, bond angles, charges etc.), how atoms interact with neighbouring atoms in the system and calculate the forces on each atom every time step of MD simulations. Within the force field, functions that are used to calculate the potential energy are divided into two as ‘bonded interactions’ and ‘nonbonded interactions’. The first term includes potential energy due to the covalent bond stretching, angle bending, torsion potentials due to rotating around bonds and improper torsion potential due to rotating out of the plane. Bonds and angles are defined with harmonic constraints while dihedral defined with a cosine series (Figure 2, adapted from Reference 54). The second term, nonbonded interactions cover van der Waals (vdW) potential through Leonard-Jones equation and Coulomb potentials through Coulombic equation. These interactions are treated differently beyond cut-off distance and methods we used to calculate these long-range interactions are described in the methods section of each study in this thesis.

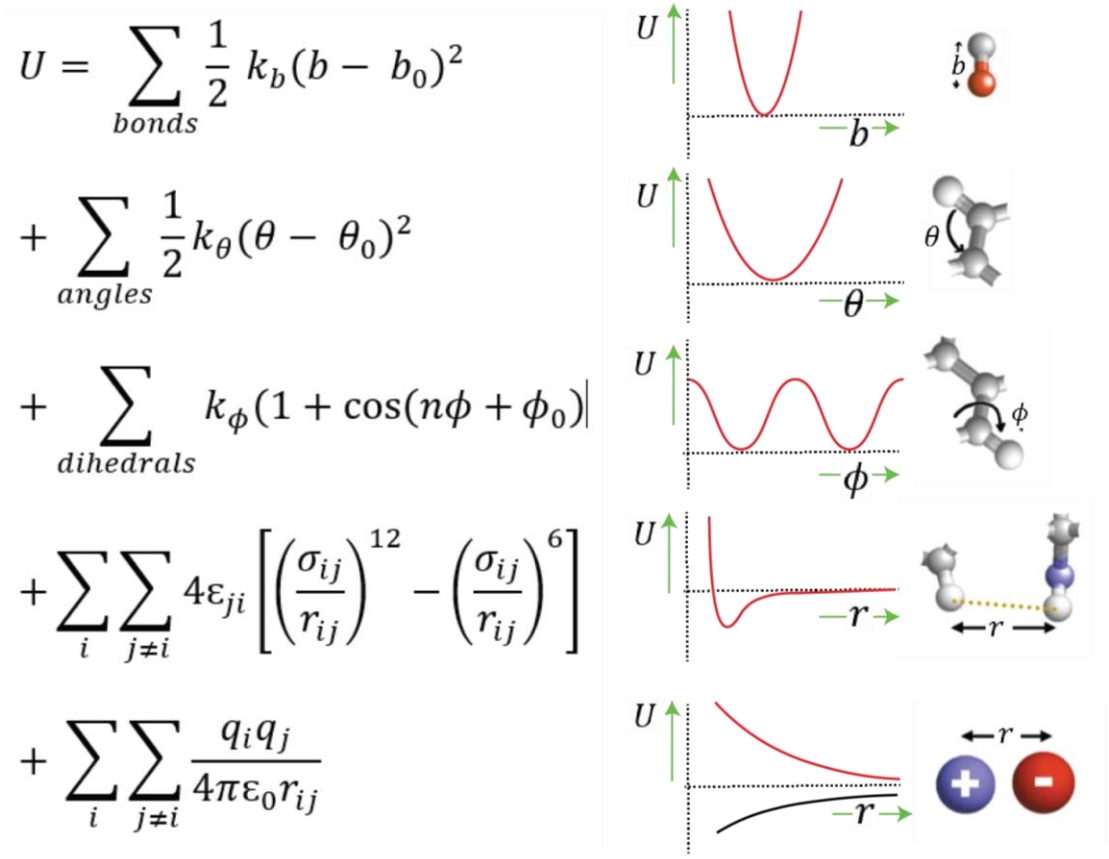

Figure 2 – General equations used in the GROMOS force field.[54] The potential energy (U) is equal to the sum of bond, angle, dihedral, vdW interaction and Coulombic interaction energetic terms. *Adapted by permission from Springer Nature, Nature Structural Biology, The birth of computational structural biology, Levitt, M. Copyright (2001).*

Many different force fields have been introduced in the literature, such as all-atom, united-atom, and coarse-grained (CG) using different principles. A simple representation for lipid, 1,2-dipalmitoyl-sn-glycero-3-phosphocholine (DPPC) from all three types of force fields is shown in Figure 3.[55]. As the name suggests, the all-atom force field (or molecular model) include all atoms in molecules explicitly. Thus, these force fields generate detailed information of a system at the atomic level, but due to the high spatial resolution in this type of force fields, simulations required more resources. Therefore, all-atom simulations are computationally expensive. Yet, simulations of large proteins and complexes have been performed using this force field in the literature.[56-57] Currently, CHARMM, AMBER and OPLS/AA are widely used all-atom FFs for proteins.

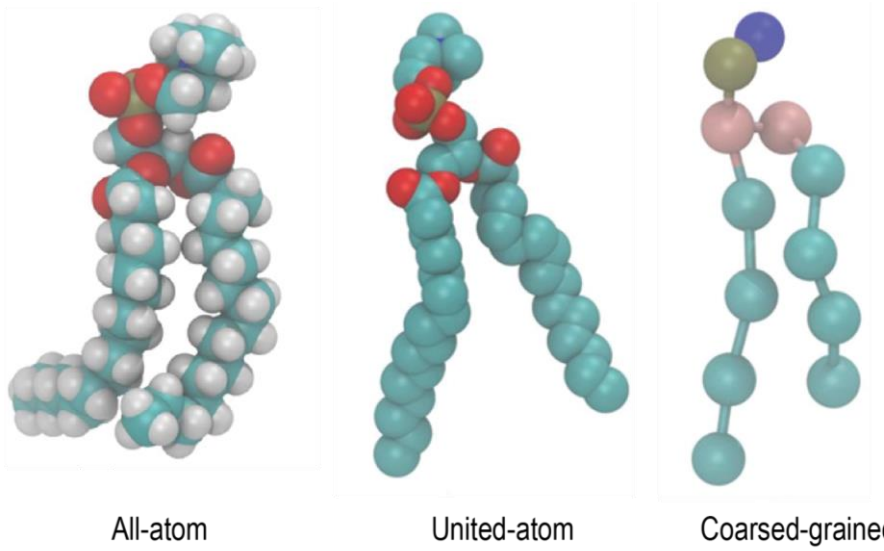

Figure 3 – van der Waals sphere representation of 1,2-dipalmitoyl-sn-glycero-3-phosphocholine (DPPC) with all-atom, united-atom, and coarse-grained force fields.[55] *© 2016, S. W. Leong, T. S. Lim, Y. S. Choong. Originally published in Bioinformatics for Membrane Lipid Simulations: Models, Computational Methods, and Web Server Tools. In Bioinformatics: Updated Features and Applications, pp.85-104 under CC BY license. Available from: DOI: 10.5772/62576*

United-atom force fields group nonpolar carbons with their bonded hydrogen atoms into a single particle (Figure 3). However, united-atom force fields still treat polar hydrogen separately. United atom force fields can be considered a coarse-grained force field, but it is at the lowest level. The GROMOS united-atom force field is a widely used force field which was introduced in 1984.[58-67] Since then, this force field has grown with various versions but none of the released versions provides proper parameterisation for oxy functional groups or vicinal ether (polyethylene oxide groups) groups.[68] Thus, conventional GROMOS 53A6 force fields fail to reproduce the experimental behavior of molecules with polyethylene oxides (PEO) which remained as the main hurdle for simulating PEO surfactants and many cosolvents in LBFs. However, this problem was solved in 2016 by introducing additional parameters (i.e., dihedral angles) to the conventional GROMOS force field with improved charges for oxy-functional groups, which were named as 2016H66 force field.[69-71] Alternatively, Warren et al. recently introduced another force field known as 56A6$_{DBW}$ by adjusting the Lennard-Jones interactions between CH_3 and CH_2 groups with water oxygen to model proper interaction of water with PEO chains.[72] Thus, the emerging of two united-

atom force fields in the field encouraged us to explore it for using it in LBFs. Especially, at the time my PhD began, these two force fields were less investigated and validated for different molecular systems, especially for PEO surfactant phase behavior. Thus, Chapter 3 discusses the extensive study of these two force fields against different colloidal regions of a simple PEO surfactant.

The choice of a force field is driven by the ability of the potential model to emulate experimental properties of the molecular system under investigation, the validity of the force field against the molecular system (e.g., the GROMOS force field is not recommended for simulations with nucleotides[73]) and the MD package used for the simulation. The most commonly use MD packages include CHARMM[74], GROMACS[75-76], NAMD[77] and AMBER[78] and our work employed GROMACS software.

1.6.2 The MD Algorithm

MD simulations are initiated with a potential energy calculation according to the force field. Subsequently, forces affecting each atom of the system are derived at each time step, which typically varies between 1 and 5 fs. Once the forces on atoms are obtained, Newton's equations of motion are used to determine the acceleration and velocities. Subsequently, new coordinates of the atoms are updated accordingly, and updated coordinates are used to calculate the forces on atoms again. Meanwhile, statistics/energy/coordinates are collected and written into trajectory files. This process is continued until a system reaches a stable configuration in the time scale of nanoseconds to microseconds. However, simulations with a millisecond time scale are also possible with specialized hardware in a high-performance computer.[79] The basic MD simulation algorithm is shown in Figure 4.[80] Molecular dynamics methods and the theory behind these MD simulations are well explained by Adcock et al. in 2006.[81] The detailed procedure of using MD simulations with one of the commonly used simulation tools, GROMACS, is described stepwise by Lindahl.[53]

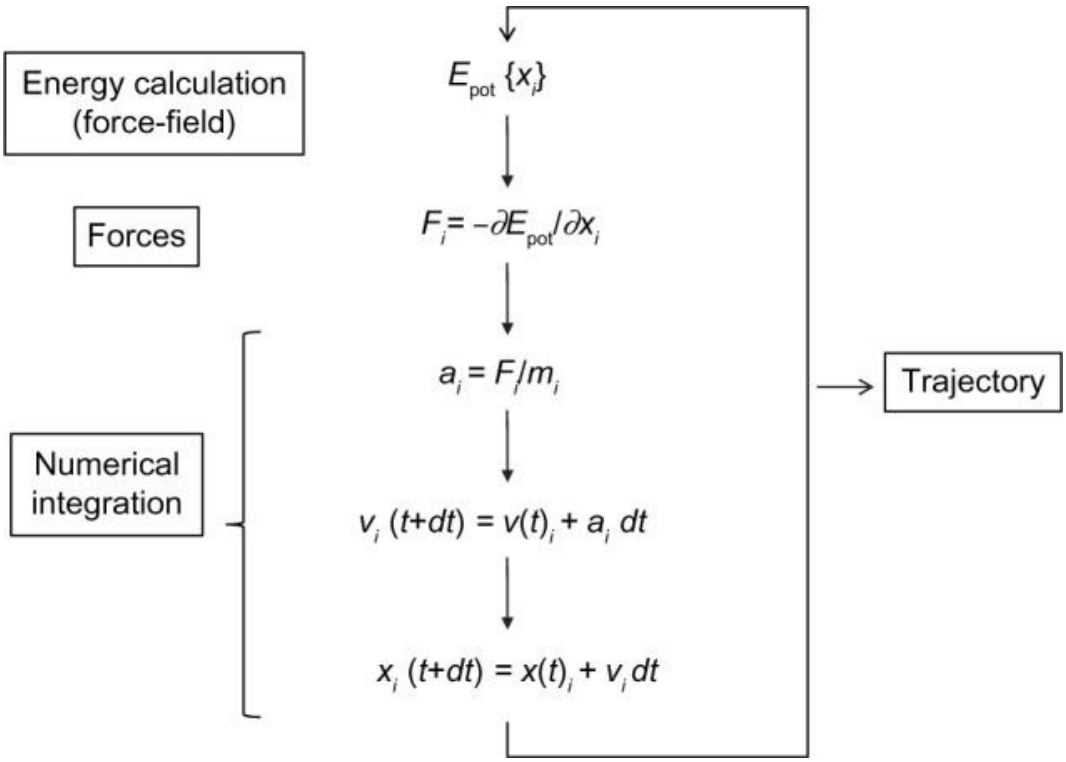

Figure 4 – Basic algorithm of MD simulations, E_{pot} – potential energy, t – simulation time, dt – iteration time. For each atom *i*, x – atom coordinate, F – forces, a – acceleration, m – atom mass, v -velocity.

1.6.3 MD Simulation Conditions

Time Step

To speed up MD simulations, the length of the time step is important. However, this time step is restricted by bond oscillations, which have high frequency. Thus, increasing the time step is challenging since errors are introduced in bond vibrations even at 1 fs.[82] Therefore, increasing the time step is done by introducing approximations for high-frequency bond oscillations such as setting fixed length bonds through bond constraint algorithms; SHAKE[83], SETTLE[84] and LINKS[85]. Furthermore, an increased time step is also possible with the heavy H atom method.[86] In this method, the hydrogen atom mass is modified to 4 a.m.u. and the additional mass of the hydrogen atom is balanced by reducing the mass of the attached heavy atom. This approach slows down the highest frequency bond angle vibrations and allows to

increase the time step to explore conformational space rapidly and save computational expense.

Ensemble

Molecular simulations require the generation of a statistically representative set of configurations called an ensemble.[52] The thermodynamic state of a statistical mechanical system can be described using different variables such as pressure, temperature, number of particles, etc. The micro-canonical (NVE) ensemble is used to describe possible states of a system with specified total energy. In this ensemble, the energy of the system (E), number of particles in the system or composition (N), and the volume of the system (V) are kept the same in all possible states of the system. In the canonical (NVT) ensemble, the number of particles (N), volume (V) and temperature (T) of the systems is conserved. Similarly, in the isothermal-isobaric (NPT) ensemble, composition (N), pressure (P), and temperature (T) are conserved. Within these ensembles, the MD algorithm generates a sequence of configurations and the average of any property over a generated sequence is an approximation to the measured value of that property for the thermodynamic state specified with N, V, E, and T.[52]

Thermostats and Barostats

MD in a canonical ensemble (NVT) uses an external bath (thermostat) to maintain the system temperature, which is known as temperature coupling. In these methods, temperature fluctuations are maintained within the ensemble and prevent energy drifts caused by accumulating numerical errors throughout MD simulations.[87] Various thermostat methods such as the Berendsen thermostat[88], velocity re-scaling thermostat[89] and the Nosé–Hoover thermostat[90] are commonly used with MD. Pressure coupling is applied similarly to the temperature coupling where a barostat is coupled with the system to modulate the pressure fluctuations. Through this approach, the average system pressure is maintained with by scaling the volume of the unit cell. Commonly used barostats include the Berendsen barostat[88] and the Parrinello-Rahman barostat[91].

Periodic Boundary Conditions

To ensure that the system does not have a border with a vacuum, a concept called ‘periodic boundary conditions' (PBC) is applied in MD. Under this condition, atoms leaving through a face of the unit cell (cubic, rhombic dodecahedron or truncated octahedron in shape) are considered as re-entering through the opposite face. PBC assembles infinite copies of the unit cell system in three-dimensional space. PBC methods make the system free from edge-effects and match with the real systems that do not have boundaries. Alternatively, PBC allows calculating long-range electrostatic interactions between individual charges in the unit cell and charges in all other copies through the particle-mesh Ewald (PME) technique,[92] rather than a simple cut-off scheme.[93] Yet, it is possible to introduce artifacts to the simulation through this PBC.[94]

Parallelisation of MD Simulations

A feature called parallelisation has been implemented in many MD packages to speed up simulations. In this method, the large simulation cell is partitioned into many smaller blocks including atoms in that specific block and each core of the computer performs calculations for blocks simultaneously.[95] However, to calculate interactions at the boundaries especially when a particle moves from one block to another, inter-processor communication is essential and this could decrease the performance of parallel computing.[96] Thus, different parallel methods have been introduced in the literature that differs from the distribution of subproblems in cores and communication algorithms between cores.[97-98]

1.6.4 Limitations of MD

Even though MD simulations have emerged as a powerful tool to study various systems at the atomic level, all-atom and united and all-atom force fields have limitations, particularly restrictions in simulation time and system size. However, CG force fields are a solution so far to the above limitations in all-atom and united-atom models, but CG force fields also introduce different limitations. Since this method groups several united atoms into a single bead, atomistic detail is lost in CG force fields and thus, CG models maintain more limited molecular description. Due to the simple representation in CG, the total number of particles in a system is significantly reduced[99] and thus very large systems can be modelled with this force field.

Alternatively, high-frequency degrees of freedom such as C-H vibrations are not counted in the force field and thus, CG force fields can enable larger time steps, which facilitates micro to millisecond range simulations. Because of all measures described above, CG force fields are two to three-fold faster compared to all-atom force fields. Currently, available CG models and applications have been discussed in detail by Ingólfsson and co-workers.[100] The most popular CG force field is MARTINI[101] and we used this force field for the preliminary investigation we carried out for modelling the phase behavior of phospholipid/bile salt/water mixture which is discussed in Chapter 6 in detail.

Another limitation of MD is trapping of simulations in local minima which obstruct the simulation from reaching the global minimum. For example, simulated systems in conventional MD can be trapped in local minimum conformational states and therefore, conventional MD simulations can rarely explore the whole conformational space within an accessible simulation time. In such instances, longer simulations and enhances sampling methods are essential to overcome the energy barriers associated with local minima and reach the global minimum state. Since performing longer simulations is computationally expensive, the best practical way is to use enhanced sampling methods.

1.6.5 Replica Exchange Molecular Dynamics

Many enhanced sampling methods are available in MD.[102] One method is 'Replica Exchange Molecular Dynamics (REMD)', a combination of conventional MD simulation and Monte Carlo algorithm that was initially introduced by Sugita and Okamoto.[103] In this method, several copies of the same system, known as replicas, are simulated simultaneously at different temperatures using conventional MD simulations. The Metropolis criterion is used to swap neighbouring systems periodically. Through this process, systems at low temperatures can swap with systems at high temperatures, which facilitates overcoming the high-energy barriers and explores conformational space more thoroughly. A single REMD simulation can produce detailed information about the system at wide range of temperatures, which is an added advantage of this method. An illustration of this process is shown in Figure 5.[104] The REMD technique is widely used in simulations of biological systems[105-114] and in a few studies on phase transitions[115-116].

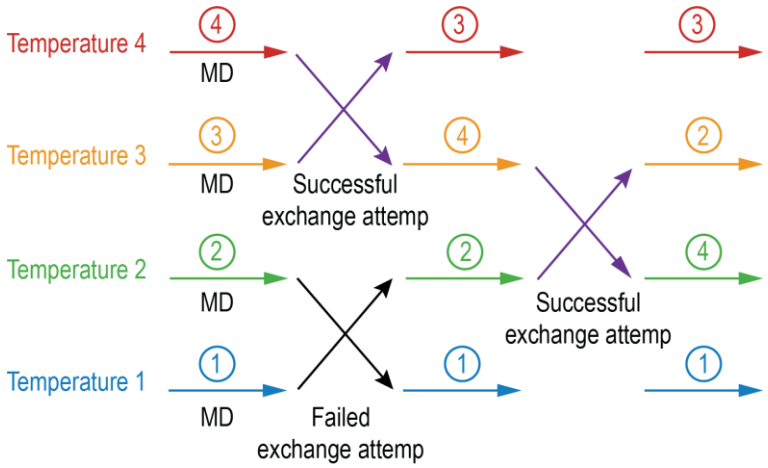

Figure 5 – The Replica exchange molecular dynamics method. *Adapted by permission from Springer Nature, Replica Exchange Molecular Dynamics: A Practical Application Protocol with Solutions to Common Problems and a Peptide Aggregation and Self-Assembly Example. In: Nilsson B., Doran T. (eds) Peptide Self-Assembly. Methods in Molecular Biology, Qi et al.*[104] *Copyright (2018).*

Even though this method explores the conformation space more efficiently compared to conventional MD[117], obtaining converged data from the REMD simulation method is still challenging. Thus, numerous investigations have been done in the literature to study and solve this issue.[118-119]

1.7 MD Simulations of LBFs

A limited number of MD simulation studies in the literature are directly related to LBFs.[120-124] Most of these studies have investigated Type I formulations that contain only oil excipients. Additionally, MD simulations with oil/surfactant excipients in LBFs have been done with interest in using these excipients in a formulation design.[125-131] Each of these studies is discussed in detail in the literature review manuscript in Chapter 2. Overall, there is a dearth of information on how well MD predicts the experimental phase behavior of LBFs containing PEO non-ionic surfactants. Additionally, to date, no one has investigated the fate of commercialized LBFs through MD simulations.

1.8 Aims and Scope of the Thesis

It has been known that MD simulations provide atomic information on the complex behavior of molecular systems, which aids in understanding experimental

observations. MD is an attractive approach where experimental investigations are limited or unable to perform. In our research, we are interested in determining the fate LBFs after oral administration. Since the GI tract is a heterogeneous, dynamic and complex environment, the fate of LBFs or the phase behavior of LBFs is difficult to study with experimental techniques such as spectroscopic methods and X-ray diffraction methods. In contrast, computational methods such as MD allow modelling of the complex mixtures to extract atomic information about phase behavior with time progression, which is not possible with experimental methods.

The literature provides evidence that MD can successfully predict the phase behavior of oil-rich formulations, particularly Type I formulations. However, there are no extensive MD studies of the phase behavior of LBFs composed of complex PEO surfactants. Therefore, there is a lack of information in the literature on how well MD models such mixed LBFs. Thus, this thesis explores the use of MD simulations to study PEO surfactant mixed LBFs. To fulfil our main aim, we worked under the following specific aims.

i. To explore whether existing force fields (i.e., 2016H66 and 53A6$_{DBW}$) can reproduce the experimental phase behavior of non-ionic PEO surfactants under different conditions (i.e., changes in temperatures/compositions) and there by selecting the most suitable force field to model molecules with PEO.
ii. To study whether the starting configuration of the MD simulation with selected force field from aim 1 affects reaching the equilibrated phases of non-ionic PEO surfactant.
iii. To study LBFs containing non-ionic PEO surfactants using MD to test the reproducibility of experimental phase behavior of LBFs upon dilution.
iv. To study the GI environment through MD with an interest in introducing bile components to LBFs to get a clear picture of the phase behavior of LBFs in the GI environment.

The work in this thesis will ultimately provide insight into the use of MD in designing efficient LBFs to develop the pharmaceutical field.

1.9 References

1. Aldridge, M., Miscellaneous Routes of Medication Administration. In *Medicines Management*, 2010; pp 239-261.

2. Sastry, S. V.; Nyshadham, J. R.; Fix, J. A., Recent Technological Advances in Oral Drug Delivery–A Review. *Pharmaceut. Sci. Tech. Today* **2000**, *3* (4), 138-145.

3. Kaur, G.; Arora, M.; Ravi Kumar, M. N. V., Oral Drug Delivery Technologies—A Decade of Developments. *J. Pharmacol. Exp. Ther.* **2019**, *370* (3), 529-543.

4. Hann, M. M., Molecular Obesity, Potency and Other Addictions in Drug Discovery. *MedChemComm* **2011**, *2* (5), 349-355.

5. Leeson, P. D.; Young, R. J., Molecular Property Design: Does Everyone Get It? *ACS Med. Chem. Lett.* **2015**, *6* (7), 722-5.

6. Meanwell, N. A., Improving Drug Design: An Update on Recent Applications of Efficiency Metrics, Strategies for Replacing Problematic Elements, and Compounds in Nontraditional Drug Space. *Chem. Res. Toxicol.* **2016**, *29* (4), 564-616.

7. Walters, W. P.; Green, J.; Weiss, J. R.; Murcko, M. A., What Do Medicinal Chemists Actually Make? A 50-Year Retrospective. *J. Med. Chem.* **2011**, *54* (19), 6405-16.

8. Nadin, A.; Hattotuwagama, C.; Churcher, I., Lead-Oriented Synthesis: A New Opportunity for Synthetic Chemistry. *Angew. Chem. Int. Ed. Engl.* **2012**, *51* (5), 1114-22.

9. Doak, B. C.; Over, B.; Giordanetto, F.; Kihlberg, J., Oral Druggable Space Beyond the Rule of 5: Insights from Drugs and Clinical Candidates. *Chem. Biol.* **2014**, *21* (9), 1115-42.

10. Lipinski, C. A.; Lombardo, F.; Dominy, B. W.; Feeney, P. J., Experimental and Computational Approaches to Estimate Solubility and Permeability in Drug Discovery and Development Settings. *Adv. Drug Deliv. Rev.* **1997**, *23* (1-3), 3-25.

11. Yu, L. X.; Amidon, G. L.; Polli, J. E.; Zhao, H.; Mehta, M. U.; Conner, D. P.; Shah, V. P.; Lesko, L. J.; Chen, M.-L.; Lee, V. H. L.; Hussain, A. S., Biopharmaceutics Classification System: The Scientific Basis for Biowaiver Extensions. *Pharm. Res.* **2002**, *19* (7), 921-925.

12. Pouton, C. W., Formulation of Poorly Water-Soluble Drugs for Oral Administration: Physicochemical and Physiological Issues and the Lipid Formulation Classification System. *Eur. J. Pharm. Sci.* **2006**, *29* (3), 278-287.

13. Kerns, E. H.; Di, L., Pharmaceutical Profiling in Drug Discovery. *Drug Discov. Today* **2003**, *8* (7), 316-323.

14. Fahr, A.; Liu, X., Drug Delivery Strategies for Poorly Water-Soluble Drugs. *Expert. Opin. Drug Deliv.* **2007**, *4* (4), 403-416.

15. Humberstone, A. J.; Charman, W. N., Lipid-Based Vehicles for the Oral Delivery of Poorly Water Soluble Drugs. *Adv. Drug Deliv. Rev.* **1997**, *25* (1), 103-128.

16. Pouton, C. W., Lipid Formulations for Oral Administration of Drugs: Non-Emulsifying, Self-Emulsifying and 'Self-Microemulsifying' Drug Delivery Systems. *Eur. J. Pharm. Sci.* **2000**, *11*, S93-S98.

17. Crounse, R. G., Human Pharmacology of Griseofulvin: The Effect of Fat Intake on Gastrointestinal Absorption. *J. Invest. Dermatol.* **1961**, *37*, 529-33.

18. Humberstone, A. J.; Porter, C. J. H.; Charman, W. N., A Physicochemical Basis for the Effect of Food on the Absolute Oral Bioavailability of Halofantrine. *J. Pharm. Sci.* **1996**, *85* (5), 525-529.

19. Charman, W. N.; Rogge, M. C.; Boddy, A. W.; Berger, B. M., Effect of Food and a Monoglyceride Emulsion Formulation on Danazol Bioavailability. *J. Clin. Pharmacol.* **1993**, *33* (4), 381-6.

20. Sunesen, V.; Vedelsdal, R.; Kristensen, H.; Christrup, L.; Müllertz, A., Effect of Liquid Volume and Food Intake on the Absolute Bioavailability of Danazol, a Poorly Soluble Drug. *Eur. J. Pharm. Sci.* **2005**, *24*, 297-303.

21. Savla, R.; Browne, J.; Plassat, V.; Wasan, K. M.; Wasan, E. K., Review and Analysis of FDA Approved Drugs Using Lipid-Based Formulations. *Drug Dev. Ind. Pharm.* **2017**, *43* (11), 1743-1758.

22. Kalepu, S.; Manthina, M.; Padavala, V., Oral Lipid-Based Drug Delivery Systems – An Overview. *Acta Pharm. Sin. B.* **2013**, *3* (6), 361-372.

23. Hauss, D. J., Oral Lipid-Based Formulations. *Adv. Drug Deliv. Rev.* **2007**, *59* (7), 667-76.

24. Myers, D., Surfactant Science and Technology. A John Wiley & Sons: New York, NY, 2006.

25. Rebello, S.; Asok, A. K.; Mundayoor, S.; Jisha, M., Surfactants: Chemistry, Toxicity and Remediation. In *Pollutant Diseases, Remediation and Recycling*, Springer, 2013; pp 277-320.

26. Koehl, N. J.; Holm, R.; Kuentz, M.; Jannin, V.; Griffin, B. T., Exploring the Impact of Surfactant Type and Digestion: Highly Digestible Surfactants Improve Oral Bioavailability of Nilotinib. *Mol. Pharm.* **2020**, *17* (9), 3202-3213.

27. Vinarov, Z.; Katev, V.; Burdzhiev, N.; Tcholakova, S.; Denkov, N., Effect of Surfactant–Bile Interactions on the Solubility of Hydrophobic Drugs in Biorelevant Dissolution Media. *Mol. Pharm.* **2018**, *15* (12), 5741-5753.

28. Hydrophilic–Lipophilic Balance (HLB): Classical Indexation and Novel Indexation of Surfactant. In *Encyclopedia of Biocolloid and Biointerface Science 2V Set*, 2016; pp 570-574.

29. Zhang, R.; Wang, Y.; Tan, L.; Zhang, H.; Yang, M., Analysis of Polysorbate 80 and Its Related Compounds by RP-HPLC with ELSD and MS Detection. *J. Chromatogr. Sci.* **2012,** *50* (7), 598-607.

30. Müllertz, A.; Ogbonna, A.; Ren, S.; Rades, T., New Perspectives on Lipid and Surfactant Based Drug Delivery Systems for Oral Delivery of Poorly Soluble Drugs. *J. Pharm. Pharmacol.* **2010**, *62* (11), 1622-1636.

31. Elder, D.; Kuentz, M.; Holm, R., Pharmaceutical excipients - Quality, Regulatory and Biopharmaceutical Considerations. *Eur. J. Pharm. Sci.* **2015**, *87*, 88-99.

32. Saluja, V.; Sekhon, B., The regulation of Pharmaceutical Excipients. *J. Excip. Food Chem.* **2013**, *4*, 95-106.

33. Mu, H.; Holm, R.; Müllertz, A., Lipid-Based Formulations for Oral Administration of Poorly Water-Soluble Drugs. *Int. J. Pharm.* **2013**, *453* (1), 215-224.

34. Feeney, O. M.; Crum, M. F.; McEvoy, C. L.; Trevaskis, N. L.; Williams, H. D.; Pouton, C. W.; Charman, W. N.; Bergström, C. A. S.; Porter, C. J. H., 50 Years of Oral Lipid-Based Formulations: Provenance, Progress and Future Perspectives. *Adv. Drug Deliv. Rev.* **2016**, *101*, 167-194.

35. Pouton, C. W.; Porter, C. J. H., Formulation of Lipid-Based Delivery Systems for Oral Administration: Materials, Methods and Strategies. *Adv. Drug Deliv. Rev.* **2008**, *60* (6), 625-637.

36. Kuentz, M., Lipid-based Formulations for Oral Delivery of Lipophilic Drugs. *Drug Discov. Today Technol.* **2012**, *9* (2), e97-e104.

37. Porter, C. J. H.; Pouton, C. W.; Cuine, J. F.; Charman, W. N., Enhancing Intestinal Drug Solubilisation Using Lipid-Based Delivery Systems. *Adv. Drug Deliv. Rev.* **2008**, *60* (6), 673-691.

38. Porter, C. J. H.; Trevaskis, N. L.; Charman, W. N., Lipids and Lipid-Based Formulations: Optimizing the Oral Delivery of Lipophilic Drugs. *Nat. Rev. Drug Discov.* **2007**, *6*, 231.

39. Williams, H. D.; Sassene, P.; Kleberg, K.; Bakala-N'Goma, J.-C.; Calderone, M.; Jannin, V.; Igonin, A.; Partheil, A.; Marchaud, D.; Jule, E., Toward the Establishment of Standardized In Vitro Tests for Lipid-Based Formulations, Part 1: Method Parameterization and Comparison of In Vitro Digestion Profiles Across a Range of Representative Formulations. *J. Pharm. Sci.* **2012**, *101* (9), 3360-3380.

40. Williams, H. D.; Anby, M. U.; Sassene, P.; Kleberg, K.; Bakala-N'Goma, J. C.; Calderone, M.; Jannin, V.; Igonin, A.; Partheil, A.; Marchaud, D.; Jule, E.; Vertommen,

J.; Maio, M.; Blundell, R.; Benameur, H.; Carrière, F.; Müllertz, A.; Pouton, C. W.; Porter, C. J., Toward the Establishment of Standardized In Vitro Tests for Lipid-Based Formulations. 2. The Effect of Bile Salt Concentration and Drug Loading on the Performance of Type I, II, IIIA, IIIB, and IV Formulations During In Vitro Digestion. *Mol. Pharm.* **2012**, *9* (11), 3286-300.

41. Williams, H. D.; Sassene, P.; Kleberg, K.; Calderone, M.; Igonin, A.; Jule, E.; Vertommen, J.; Blundell, R.; Benameur, H.; Müllertz, A.; Pouton, C. W.; Porter, C. J. H.; on behalf of the, L. C., Toward the Establishment of Standardized In Vitro Tests for Lipid-Based Formulations, Part 3: Understanding Supersaturation Versus Precipitation Potential During the In Vitro Digestion of Type I, II, IIIA, IIIB and IV Lipid-Based Formulations. *Pharm. Res.* **2013**, *30* (12), 3059-3076.

42. Williams, H. D.; Sassene, P.; Kleberg, K.; Calderone, M.; Igonin, A.; Jule, E.; Vertommen, J.; Blundell, R.; Benameur, H.; Müllertz, A.; Porter, C. J. H.; Pouton, C. W., Toward the Establishment of Standardized In Vitro Tests for Lipid-Based Formulations, Part 4: Proposing a New Lipid Formulation Performance Classification System. *J. Pharm. Sci.* **2014**, *103* (8), 2441-2455.

43. Porter, C. J. H.; Kaukonen, A. M.; Taillardat-Bertschinger, A.; Boyd, B. J.; O'Connor, J. M.; Edwards, G. A.; Charman, W. N., Use of In Vitro Lipid Digestion Data to Explain the In Vivo Performance of Triglyceride-Based Oral Lipid Formulations of Poorly Water-Soluble Drugs: Studies with Halofantrine. *J. Pharm. Sci.* **2004**, *93* (5), 1110-1121.

44. Atkins, P.; DePaula, J., Physical Transformations of Pure Substances. In Physical Chemistry, Oxford University Press, Oxford: 1994; pp 183-191.

45. Massalski, T. B.; Laughlin, D. E., Phase Diagrams. In Reference Module in Materials Science and Materials Engineering, Elsevier: 2017.

46. Mitchell, D. J.; Tiddy, G. J. T.; Waring, L.; Bostock, T.; McDonald, M. P., Phase Behaviour of Polyoxyethylene Surfactants with Water. Mesophase Structures and Partial Miscibility (Cloud Points). *J. Chem. Soc.*, Faraday Trans. 1 **1983**, 79 (4), 975-1000.

47. Eastoe, J.; Tabor, R. F., Chapter 6 - Surfactants and Nanoscience. In Colloidal Foundations of Nanoscience, Berti, D.; Palazzo, G., Eds. Elsevier: Amsterdam, 2014; pp 135-157.

48. Park, S.-J.; Seo, M.-K., Chapter 5 - Interface Applications in Nanomaterials. In Interface Science and Technology, Park, S.-J.; Seo, M.-K., Eds. Elsevier: 2011; Vol. 18, pp 333-429.

49. Capek, I., 3 - Preparation of polymer-based nanomaterials. In Nanocomposite Structures and Dispersions (Second Edition), Capek, I., Ed. Elsevier: Amsterdam, 2019; pp 175-265.

50. Santana, R.; Perrechil, F.; Cunha, R., High-and Low-energy Emulsifications for Food Applications: A Focus on Process Parameters. *Food Eng. Rev.* **2013**, *5* (2), 107-122.

51. McCammon, J. A.; Gelin, B. R.; Karplus, M., Dynamics of Folded Proteins. *Nature* **1977**, *267* (5612), 585-90.

52. Andersen, H. C., Molecular Dynamics Simulations at Constant Pressure and/or Temperature. *J. Chem. Phys.* **1980**, *72* (4), 2384-2393.

53. Lindahl, E. R., Molecular Dynamics Simulations. In *Molecular Modeling of Proteins*, Kukol, A., Ed. Humana Press: Totowa, NJ, 2008; pp 3-23.

54. Levitt, M., The Birth of Computational Structural Biology. *Nat. Struct. Biol.* **2001,** *8* (5), 392-393.

55. Leong, S.W.; Lim, T.S.; Choong, Y.S., Bioinformatics for Membrane Lipid Simulations: Models, Computational Methods, and Web Server Tools. In *Bioinformatics: Updated Features and Applications*, InTech: Croatia, 2016; pp.85-104.

56. Gumbart, J.; Trabuco, L. G.; Schreiner, E.; Villa, E.; Schulten, K., Regulation of the Protein-Conducting Channel by a Bound Ribosome. *Structure* **2009**, *17* (11), 1453-1464.

57. Yao, Y.; Harrison, C. B.; Freddolino, P. L.; Schulten, K.; Mayer, M. L., Molecular Mechanism of Ligand Recognition by NR3 Subtype Glutamate Receptors. *EMBO J.* **2008**, *27* (15), 2158-70.

58. Chandrasekhar, I.; Kastenholz, M.; Lins, R. D.; Oostenbrink, C.; Schuler, L. D.; Tieleman, D. P.; van Gunsteren, W. F., A Consistent Potential Energy Parameter Set for Lipids: Dipalmitoylphosphatidylcholine as a Benchmark of the GROMOS96 45A3 Force Field. *Eur. Biophys. J.* **2003**, *32* (1), 67-77.

59. Chandrasekhar, I.; Oostenbrink, C.; van Gunsteren, W. F., Simulating the Physiological Phase of Hydrated DPPC Bilayers: The Ester Moiety. *Soft Mater.* **2004**, *2* (1), 27-45.

60. Daura, X.; Mark, A. E.; Van Gunsteren, W. F., Parametrization of Aliphatic CHn United Atoms of GROMOS96 Force Field. *J. Comput. Chem.* **1998**, *19* (5), 535-547.

61. Hermans, J.; Berendsen, H. J. C.; Van Gunsteren, W. F.; Postma, J. P. M., A Consistent Empirical Potential for Water–Protein Interactions. *Biopolymers* **1984**, *23* (8), 1513-1518.

62. Lins, R. D.; Hünenberger, P. H., A New GROMOS Force Field for Hexopyranose-Based Carbohydrates. *J. Comput. Chem.* **2005**, *26* (13), 1400-1412.

63. Oostenbrink, C.; Villa, A.; Mark, A. E.; Van Gunsteren, W. F., A Biomolecular Force Field Based on the Free Enthalpy of Hydration and Solvation: The GROMOS

Force-Field Parameter Sets 53A5 and 53A6. *J. Comput. Chem.* **2004**, *25* (13), 1656-1676.

64. Schmid, N.; Eichenberger, A. P.; Choutko, A.; Riniker, S.; Winger, M.; Mark, A. E.; van Gunsteren, W. F., Definition and Testing of the GROMOS Force-Field Versions 54A7 and 54B7. *Eur. Biophys. J.* **2011**, *40* (7), 843.

65. Schuler, L. D.; Daura, X.; van Gunsteren, W. F., An Improved GROMOS96 Force Field for Aliphatic Hydrocarbons in the Condensed Phase. *J. Comput. Chem.* **2001**, *22* (11), 1205-1218.

66. Scott, W. R. P.; Hünenberger, P. H.; Tironi, I. G.; Mark, A. E.; Billeter, S. R.; Fennen, J.; Torda, A. E.; Huber, T.; Krüger, P.; van Gunsteren, W. F., The GROMOS Biomolecular Simulation Program Package. *J. Phys. Chem. A* **1999**, *103* (19), 3596-3607.

67. Soares, T. A.; Hünenberger, P. H.; Kastenholz, M. A.; Kräutler, V.; Lenz, T.; Lins, R. D.; Oostenbrink, C.; van Gunsteren, W. F., An Improved Nucleic Acid Parameter Set for the GROMOS Force Field. *J. Comput. Chem.* **2005**, *26* (7), 725-737.

68. Winger, M.; de Vries, A. H.; van Gunsteren, W. F., Force-Field Dependence of the Conformational Properties of α, ω-Dimethoxypolyethylene Glycol. *Mol. Phys.* **2009**, *107* (13), 1313-1321.

69. Horta, B. A. C.; Fuchs, P. F. J.; van Gunsteren, W. F.; Hünenberger, P. H., New Interaction Parameters for Oxygen Compounds in the GROMOS Force Field: Improved Pure-Liquid and Solvation Properties for Alcohols, Ethers, Aldehydes, Ketones, Carboxylic Acids, and Esters. *J. Chem. Theory. Comput.* **2011**, *7* (4), 1016-1031.

70. Fuchs, P. F. J.; Hansen, H. S.; Hünenberger, P. H.; Horta, B. A. C., A GROMOS Parameter Set for Vicinal Diether Functions: Properties of Polyethyleneoxide and Polyethyleneglycol. *J. Chem. Theory Comput.* **2012**, *8* (10), 3943-3963.

71. Horta, B. A. C.; Merz, P. T.; Fuchs, P. F. J.; Dolenc, J.; Riniker, S.; Hünenberger, P. H., A GROMOS-Compatible Force Field for Small Organic Molecules in the Condensed Phase: The 2016H66 Parameter Set. *J. Chem. Theory Comput.* **2016**, *12* (8), 3825-3850.

72. Warren, D. B.; McPhee, E.; Birru, W. A.; Benameur, H.; Chalmers, D. K.; Pouton, C. W., Improvement in the Predicted Partitioning of Alcohol and Polyethylene Oxide Groups between Water and Octanol (logP) in Molecular Dynamics Simulations. *J. Pharm. Sci.* **2019**, *108* (1), 214-222.

73. Ricci, C. G.; de Andrade, A. S.; Mottin, M.; Netz, P. A., Molecular Dynamics of DNA: Comparison of Force Fields and Terminal Nucleotide Definitions. *J. Phys. Chem. B* **2010**, *114* (30), 9882-93.

74. Brooks, B. R.; Brooks, C. L., 3rd; Mackerell, A. D., Jr.; Nilsson, L.; Petrella, R. J.; Roux, B.; Won, Y.; Archontis, G.; Bartels, C.; Boresch, S.; Caflisch, A.; Caves, L.; Cui, Q.; Dinner, A. R.; Feig, M.; Fischer, S.; Gao, J.; Hodoscek, M.; Im, W.; Kuczera, K.; Lazaridis, T.; Ma, J.; Ovchinnikov, V.; Paci, E.; Pastor, R. W.; Post, C. B.; Pu, J. Z.; Schaefer, M.; Tidor, B.; Venable, R. M.; Woodcock, H. L.; Wu, X.; Yang, W.; York, D. M.; Karplus, M., CHARMM: The Biomolecular Simulation Program. *J. Comput. Chem.* **2009**, *30* (10), 1545-1614.

75. Berendsen, H. J.; van der Spoel, D.; van Drunen, R., GROMACS: A Message-Passing Parallel Molecular Dynamics Implementation. *Comput. Phys. Commun.* **1995**, *91* (1-3), 43-56.

76. Pronk, S.; Páll, S.; Schulz, R.; Larsson, P.; Bjelkmar, P.; Apostolov, R.; Shirts, M. R.; Smith, J. C.; Kasson, P. M.; Van Der Spoel, D., GROMACS 4.5: A High-Throughput and Highly Parallel Open Source Molecular Simulation Toolkit. *Bioinformatics* **2013**, *29* (7), 845-854.

77. Phillips, J. C.; Braun, R.; Wang, W.; Gumbart, J.; Tajkhorshid, E.; Villa, E.; Chipot, C.; Skeel, R. D.; Kalé, L.; Schulten, K., Scalable Molecular Dynamics with NAMD. *J. Comput. Chem.* **2005,** *26* (16), 1781-802.

78. Case, D. A.; Cheatham, T. E., 3rd; Darden, T.; Gohlke, H.; Luo, R.; Merz, K. M., Jr.; Onufriev, A.; Simmerling, C.; Wang, B.; Woods, R. J., The Amber Biomolecular Simulation Programs. *J. Comput. Chem.* **2005**, *26* (16), 1668-1688.

79. Shaw, D.; Dror, R.; Salmon, J.; Grossman, J. P.; Mackenzie, K.; Bank, J.; Young, C.; Deneroff, M.; Batson, B.; Bowers, K.; Chow, E.; Eastwood, M.; Ierardi, D.; Klepeis, J.; Kuskin, J.; Larson, R.; Lindorff-Larsen, K.; Maragakis, P.; Moraes, M.; Towles, B., Millisecond-Scale Molecular Dynamics Simulations on Anton. In *Proceedings of the Conference on High Performance Computing Networking, Storage and Analysis,* 2009; pp 1-11.

80. Hospital, A.; Goñi, J. R.; Orozco, M.; Gelpí, J. L., Molecular Dynamics Simulations: Advances and Applications. *Adv. Appl. Bioinform. Chem.* **2015**, *8*, 37-47.

81. Adcock, S. A.; McCammon, J. A., Molecular Dynamics: Survey of Methods for Simulating the Activity of Proteins. *Chem. Rev.* **2006**, *106* (5), 1589-1615.

82. Lindahl, E., Molecular Dynamics Simulations. In *Molecular Modeling of Proteins*, Kukol, A., Ed. Springer New York: New York, NY, 2015; pp 3-26.

83. Ryckaert, J.-P.; Ciccotti, G.; Berendsen, H. J., Numerical Integration of the Cartesian Equations of Motion of a System with Constraints: Molecular Dynamics of n-Alkanes. *J. Comput. Phys.* **1977**, *23* (3), 327-341.

84. Miyamoto, S.; Kollman, P. A., Settle: An Analytical Version of the SHAKE and RATTLE Algorithm for Rigid Water Models. *J. Comput. Chem.* **1992**, *13* (8), 952-962.

85. Hess, B.; Bekker, H.; Berendsen, H. J. C.; Fraaije, J. G. E. M., LINCS: A Linear Constraint Solver for Molecular Simulations. *J. Comput. Chem.* **1997**, *18* (12), 1463-1472.

86. Feenstra, K. A.; Hess, B.; Berendsen, H. J. C., Improving Efficiency of Large Time-Scale Molecular Dynamics Simulations of Hydrogen-Rich Systems. *J. Comput. Chem.* **1999**, *20* (8), 786-798.

87. Hünenberger, P. H., Thermostat Algorithms for Molecular Dynamics Simulations. In *Advanced Computer Simulation: Approaches for Soft Matter Sciences I*, Dr. Holm, C.; Prof. Dr. Kremer, K., Eds. Springer Berlin Heidelberg: Berlin, Heidelberg, 2005; pp 105-149.

88. Berendsen, H. J. C.; Postma, J. P. M.; Gunsteren, W. F. v.; DiNola, A.; Haak, J. R., Molecular Dynamics with Coupling to an External Bath. *J. Chem. Phys.* **1984**, *81* (8), 3684-3690.

89. Bussi, G.; Donadio, D.; Parrinello, M., Canonical Sampling through Velocity Rescaling. *J. Chem. Phys.* **2007**, *126* (1), 014101.

90. Nosé, S.; Klein, M. L., Constant Pressure Molecular Dynamics for Molecular Systems. *Mol. Phys.* **1983**, *50* (5), 1055-1076.

91. Parrinello, M.; Rahman, A., Polymorphic Transitions in Single Crystals: A New Molecular Dynamics Method. *J. Appl. Phys.* **1981**, *52* (12), 7182-7190.

92. Darden, T.; York, D.; Pedersen, L., Particle mesh Ewald: An N·log(N) Method for Ewald Sums in Large Systems. *J. Chem. Phys.* **1993**, *98* (12), 10089-10092.

93. Kasahara, K.; Sakuraba, S.; Fukuda, I., Enhanced Sampling of Molecular Dynamics Simulations of a Polyalanine Octapeptide: Effects of the Periodic Boundary Conditions on Peptide Conformation. *J. Phys. Chem. B* **2018**, *122* (9), 2495-2503.

94. Weber, W.; Hünenberger, P. H.; McCammon, J. A., Molecular Dynamics Simulations of a Polyalanine Octapeptide under Ewald Boundary Conditions: Influence of Artificial Periodicity on Peptide Conformation. *J. Phys. Chem. B* **2000**, *104* (15), 3668-3675.

95. Nikolskii, V.; Stegailov, V., Domain-Decomposition Parallelization for Molecular Dynamics Algorithm with Short-Ranged Potentials on Epiphany Architecture. *Lobachevskii J. Math.* **2018**, *39* (9), 1228-1238.

96. Janežič, D.; Borštnik, U.; Praprotnik, M., Parallel Approaches in Molecular Dynamics Simulations. **2009**; pp 281-305.

97. Plimpton, S., Fast Parallel Algorithms for Short-Range Molecular Dynamics. *J. Comput. Phys.* **1995**, *117* (1), 1-19.

98. Jung, J.; Kobayashi, C.; Kasahara, K.; Tan, C.; Kuroda, A.; Minami, K.; Ishiduki, S.; Nishiki, T.; Inoue, H.; Ishikawa, Y.; Feig, M.; Sugita, Y., New Parallel Computing

Algorithm of Molecular Dynamics for Extremely Huge Scale Biological Systems. *J. Comput. Chem.* **2021**, *42* (4), 231-241.

99. Singh, N.; Li, W., Recent Advances in Coarse-Grained Models for Biomolecules and Their Applications. *Int. J. Mol. Sci.* **2019**, *20* (15), 3774.

100. Ingólfsson, H. I.; Lopez, C. A.; Uusitalo, J. J.; de Jong, D. H.; Gopal, S. M.; Periole, X.; Marrink, S. J., The Power of Coarse Graining in Biomolecular Simulations. *Wiley Interdiscip. Rev. Comput. Mol. Sci.* **2014**, *4* (3), 225-248.

101. Marrink, S. J.; Risselada, H. J.; Yefimov, S.; Tieleman, D. P.; de Vries, A. H., The MARTINI Force Field: Coarse Grained Model for Biomolecular Simulations. *J. Phys. Chem. B* **2007**, *111* (27), 7812-7824.

102. Lazim, R.; Suh, D.; Choi, S., Advances in Molecular Dynamics Simulations and Enhanced Sampling Methods for the Study of Protein Systems. *Int. J. Mol. Sci.* **2020**, *21* (17), 6339.

103. Sugita, Y.; Okamoto, Y., Replica-Exchange Molecular Dynamics Method for Protein Folding. *Chem. Phys. Lett.* **1999**, *314* (1), 141-151.

104. Qi, R.; Wei, G.; Ma, B.; Nussinov, R., Replica Exchange Molecular Dynamics: A Practical Application Protocol with Solutions to Common Problems and a Peptide Aggregation and Self-Assembly Example. *Methods Mol. Biol.* **2018**, *1777*, 101-119.

105. Zhou, P.; Deng, L.; Wang, Y.; Lu, J. R.; Xu, H., Interplay between Intrinsic Conformational Propensities and Intermolecular Interactions in the Self-Assembly of Short Surfactant-Like Peptides Composed of Leucine/Isoleucine. *Langmuir* **2016**, *32* (18), 4662-4672.

106. Ngo, S. T.; Hung, H. M.; Tran, K. N.; Nguyen, M. T., Replica Exchange Molecular Dynamics Study of the Amyloid Beta (11–40) Trimer Penetrating a Membrane. *RSC Adv.* **2017**, *7* (12), 7346-7357.

107. Rhee, Y. M.; Pande, V. S., Multiplexed-Replica Exchange Molecular Dynamics Method for Protein Folding Simulation. *Biophys. J.* **2003**, *84* (2), 775-786.

108. Nishino, M.; Sugita, Y.; Yoda, T.; Okamoto, Y., Structures of a Peptide Fragment of β2-Microglobulin Studied by Replica-Exchange Molecular Dynamics Simulations – Towards the Understanding of the Mechanism of Amyloid Formation. *FEBS Lett.* **2005**, *579* (24), 5425-5429.

109. Ho, B. K.; Dill, K. A., Folding Very Short Peptides Using Molecular Dynamics. *PLoS Comput. Biol.* **2006**, *2* (4), e27.

110. Zhang, J.; Qin, M.; Wang, W., Folding Mechanism of β-Hairpins Studied by Replica Exchange Molecular Simulations. *Proteins* **2006**, *62* (3), 672-685.

111. Watts, C. R.; Gregory, A. J.; Frisbie, C. P.; Lovas, S., Structural Properties of Amyloid β(1-40) Dimer Explored by Replica Exchange Molecular Dynamics Simulations. *Proteins* **2017**, *85* (6), 1024-1045.

112. Zerze, G. H.; Uz, B.; Mittal, J., Folding Thermodynamics of β-Hairpins Studied by Replica-Exchange Molecular Dynamics Simulations. *Proteins* **2015**, *83* (7), 1307-1315.

113. Blinov, N.; Khorvash, M.; Wishart, D. S.; Cashman, N. R.; Kovalenko, A., Initial Structural Models of the Aβ42 Dimer from Replica Exchange Molecular Dynamics Simulations. *ACS Omega* **2017**, *2* (11), 7621-7636.

114. Lim, G. S.; Klähn, M., On the Stability of Proteins Solvated in Imidazolium-Based Ionic Liquids Studied with Replica Exchange Molecular Dynamics. *J. Phys. Chem. B* **2018**, *122* (39), 9274-9288.

115. Nagai, T.; Ueoka, R.; Okamoto, Y., Phase Behavior of a Lipid Bilayer System Studied by a Replica-Exchange Molecular Dynamics Simulation. *J. Phys. Soc. Jpn.* **2012**, *81* (2), 024002.

116. Nagai, T.; Okamoto, Y., Replica-Exchange Molecular Dynamics Simulation of a Lipid Bilayer System with a Coarse-Grained Model. *Mol. Simul.* **2012**, *38* (5), 437-441.

117. Sanbonmatsu, K. Y.; García, A. E., Structure of Met-Enkephalin in Explicit Aqueous Solution Using Replica Exchange Molecular Dynamics. *Proteins* **2002**, *46* (2), 225-234.

118. Okur, A.; Roe, D. R.; Cui, G.; Hornak, V.; Simmerling, C., Improving Convergence of Replica-Exchange Simulations through Coupling to a High-Temperature Structure Reservoir. *J. Chem. Theory Comput.* **2007**, *3* (2), 557-568.

119. Zhang, W.; Wu, C.; Duan, Y., Convergence of Replica Exchange Molecular Dynamics. *J. Chem. Phys.* **2005**, *123* (15), 154105.

120. Warren, D. B.; Chalmers, D. K.; Pouton, C. W., Structure and Dynamics of Glyceride Lipid Formulations, with Propylene Glycol and Water. *Mol. Pharm.* **2009**, *6* (2), 604-614.

121. Warren, D. B.; King, D.; Benameur, H.; Pouton, C. W.; Chalmers, D. K., Glyceride Lipid Formulations: Molecular Dynamics Modeling of Phase Behavior During Dispersion and Molecular Interactions Between Drugs and Excipients. *Pharm. Res.* **2013**, *30* (12), 3238-3253.

122. Birru, W. A.; Warren, D. B.; Han, S.; Benameur, H.; Porter, C. J. H.; Pouton, C. W.; Chalmers, D. K., Computational Models of the Gastrointestinal Environment. 2. Phase Behavior and Drug Solubilization Capacity of a Type I Lipid-Based Drug Formulation after Digestion. *Mol. Pharm.* **2017**, *14* (3), 580-592.

123. Larsson, P.; Alskär, L. C.; Bergström, C. A. S., Molecular Structuring and Phase Transition of Lipid-Based Formulations upon Water Dispersion: A Coarse-Grained Molecular Dynamics Simulation Approach. *Mol. Pharm.* **2017**, *14* (12), 4145-4153.

124. Benson, S. P.; Pleiss, J., Molecular Dynamics Simulations of Self-Emulsifying Drug-Delivery Systems (SEDDS): Influence of Excipients on Droplet Nanostructure and Drug Localization. *Langmuir* **2014**, *30* (28), 8471-8480.

125. Moghaddasi, F.; Housaindokht, M. R.; Darroudi, M.; Bozorgmehr, M. R.; Sadeghi, A., Soybean Oil-Based Nanoemulsion Systems in Absence and Presence of Curcumin: Molecular Dynamics Simulation Approach. *J. Mol. Liq.* **2018**, *264*, 242-252.

126. Mobasheri, M.; Attar, H.; Rezayat Sorkhabadi, S. M.; Khamesipour, A.; Jaafari, M. R., Solubilization Behavior of Polyene Antibiotics in Nanomicellar System: Insights from Molecular Dynamics Simulation of the Amphotericin B and Nystatin Interactions with Polysorbate 80. *Molecules* **2015**, *21* (1), E6-E6.

127. Suys, E. J. A.; Warren, D. B.; Pham, A. C.; Nowell, C. J.; Clulow, A. J.; Benameur, H.; Porter, C. J. H.; Pouton, C. W.; Chalmers, D. K., A Nonionic Polyethylene Oxide (PEO) Surfactant Model: Experimental and Molecular Dynamics Studies of Kolliphor EL. *J. Pharm. Sci.* **2019**, *108* (1), 193-204.

128. Kozlowska, M.; Rodziewicz, P.; Utesch, T.; Mroginski, M. A.; Kaczmarek-Kedziera, A., Solvation of Diclofenac in Water from Atomistic Molecular Dynamics Simulations – Interplay between Solute–Solute and Solute–Solvent Interactions. *Phys. Chem. Chem. Phys.* **2018**, *20* (13), 8629-8639.

129. Ghattas, M. A.; Bryce, R. A.; Al Rawashdah, S.; Atatreh, N.; Zalloum, W. A., Comparative Molecular Dynamics Simulation of Aggregating and Non-Aggregating Inhibitor Solutions: Understanding the Molecular Basis of Promiscuity. *ChemMedChem* **2018**, *13* (6), 500-506.

130. Kasimova, A. O.; Pavan, G. M.; Danani, A.; Mondon, K.; Cristiani, A.; Scapozza, L.; Gurny, R.; Möller, M., Validation of a Novel Molecular Dynamics Simulation Approach for Lipophilic Drug Incorporation into Polymer Micelles. *J. Phys. Chem. B* **2012**, *116* (14), 4338-4345.

131. Omolo, C. A.; Kalhapure, R. S.; Agrawal, N.; Rambharose, S.; Mocktar, C.; Govender, T., Formulation and Molecular Dynamics Simulations of a Fusidic Acid Nanosuspension for Simultaneously Enhancing Solubility and Antibacterial Activity. *Mol. Pharm.* **2018**, *15* (8), 3512-3526.

Chapter 2

Molecular Dynamics Simulations for Lipid-Based Drug Formulations – A Review

LBFs are a widely used approach to enhance the solubility of poorly water-soluble drugs. Furthermore, MD is an attractive tool that provides atomic information of a complex system to understand experimental observations. Therefore, MD has been used in the formulation field to understand the complex phase behavior of LBFs at the atomic level. However, none of the published work in the literature provides an extensive overview of the MD technique used in the drug formulation field. Therefore, to provide insight into how MD has been used in the LBF field, we have written an extensive review of MD for LBFs that covers how MD simulations of LBFs, force fields involved in these studies and the strengths and weakness in simulating such systems, the problems or complications of performing MD simulation related to LBF field and future directions for improving using this method in formulation design. This chapter is a manuscript to be submitted for publication.

Molecular Dynamics Simulations for Lipid-Based Drug Formulations – A Review

Amali G. Guruge[1], Dallas B. Warren[2], Colin W. Pouton[2], David K. Chalmers[1]*

[1]Medicinal Chemistry, [2]Drug Delivery, Disposition and Dynamics, Monash Institute of Pharmaceutical Sciences, Monash University, 381 Royal Parade, Parkville, Victoria 3052, Australia

Keywords

Drug formulations, Molecular dynamics simulations, Lipid-based formulations, Gastrointestinal tract, Colloids, Solubility, Bile salts, Surfactants, Fatty acids.

Abstract

Delivery of poorly water-soluble drugs remains a challenging task in drug development. Lipid-based formulation (LBF) is a useful approach to delivering hydrophobic drugs into the systemic circulation by oral administration. While lipid formulations can be demonstrated to be effective *in vivo* using experimental methods, much of the physical detail regarding the behavior of LBFs is not well characterised, due to the complex nature of the formulations themselves and of the gastrointestinal (GI) environment where they must work to retain the drug in a solubilised state for sufficient time to be absorbed. Since the GI tract is a heterogeneous, dynamic and complex environment, the fate of the lipid-based formulation cannot easily be studied by experimental methods such as spectroscopic techniques. Recently, many researchers have started to use molecular dynamics (MD) simulations to complement *in vitro* studies of LBF systems. MD is a computational method based on classical mechanics, which simulates physical movements of atoms and provides atomic-scale information that cannot be retrieved from experimental investigations. MD can potentially provide insight for drug formulations in a cost and time-effective manner. This review summarizes the application of MD simulation to the study of LBFs and the interaction of LBFs with the GI environment and, further, it discusses the difficulties that arise for modelling the lipid-based drug formulation systems in the presence or absence of bile. Lastly, we discuss future directions for improving computational drug formulations.

Introduction

Oral administration is the preferred method for the delivery of many drugs into the systemic circulation, particularly due to its simplicity and acceptability from the patient's perspective. Yet, the outward simplicity of oral administration hides many complexities. Fundamentally, orally administered drugs must be dissolved in the principally aqueous environment of the gastrointestinal (GI) tract, and remain dissolved, for a sufficiently long to be absorbed. However, the pharmaceutical industry continues to develop significant numbers of more hydrophobic or water-insoluble drugs. The reasons for this are multifaceted, but key causes include: pursuit of compound potency rather than good molecular properties,[1-3] that the synthesis of nonpolar compounds is inherently simpler than for polar compounds[4-5] and that many drug targets require physically large compounds to obtain adequate inhibitory activity, such as protein-protein interactions.[6] Therefore, the physicochemical properties of many new drug molecules are outside Lipinski's[7] 'rule of 5'. As a consequence, lipophilic drugs arising from drug discovery pipelines hinder the most simple and convenient method of drug delivery.

Many drug compounds developed through today's drug discovery pipelines can be categorized into Class II of the biopharmaceutical classification system (BCS). This classification system is based on aqueous solubility and membrane permeability of drug compounds.[8] The classification is composed of the five types of formulation shown in Table 1. Class II compounds have good permeability with poor solubility, which is the main cause of poor bioavailability. One important method for solubilising class II compounds is the use of formulation strategies: crystalline solid formulations, amorphous formulations and lipid-based formulations (LBFs).[9-10] In this review, we are particularly interested in LBFs.

Table 1 – Lipid formulation classification system[10]

Excipient in formulation	Content of formulation (% w/w)				
	Type I	Type II	Type IIIA	Type IIIB	Type IV
Oils: triglycerides or mixed mono- and diglycerides	100	40–80	40–80	<20	-
Water-insoluble surfactants (HLB<12)	-	20–60	-	-	0–20
Water-soluble surfactants (HLB>12)	-	-	20–40	20–50	30–80
Hydrophilic cosolvents (e.g., PEG, Transcutol)	-	-	0–40	20–50	0–50

LBFs can contain a broad range of excipients such as oils, lipophilic surfactants, hydrophilic surfactants and water soluble cosolvents are blended with an active pharmaceutical ingredient. In Type I formulations, lipid components, including mono, di- and triglycerides in oils, are combined with the hydrophobic drug. Triglycerides and diglycerides in this type of formulation are rapidly digested into fatty acids and 2-mono-glycerides in the GI tract, making a colloidal dispersion of mixed micelles in combination with bile salts. The hydrophobic drug in the formulation is solubilised by the mixed micelles, resulting in a reservoir for the drug which enables efficient absorption.[9] In Type II formulations, addition of water-insoluble surfactants into the oils improves the solvent capacity and drives the self-emulsification, creating an average dispersion droplet size >200 nm. Type III formulations are self-microemulsifying drug delivery systems (SMEDDS) that consist of oils, hydrophilic surfactants and cosolvents which have an average dispersion droplet size <200 nm. This type of formulation is further categorised into Type IIIA or Type IIIB, depending on the proportion of oils in it. The last formulation type, Type IV, contains a high proportion of hydrophilic surfactants and cosolvents. This formulation type has an advantage of high solvent capacity on dilution due to the blending of surfactants with cosolvent.[10] Thus, LBFs are mixtures that can vary from simple vegetable oils (triglycerides) to complex mixtures containing oil, surfactant, co-surfactant and co-solvent. The properties of excipients used in LBFs, and the criteria for selection of these excipients in different

LBFs, have been investigated by Pouton and Porter.[11] Further, strategies used in self-emulsifying drug delivery systems, methods used to assess the efficiency of emulsification and other practical considerations required for the use of self-emulsifying drug delivery systems have been discussed by Pouton in 1997.[12] Moreover, a useful protocol has been established by Pouton to predict how the fate of a drug is affected by a formulation design and to optimise the formulation design depending on the drug by testing the bioavailability in a laboratory.[10] Also, several useful reviews have been published based on lipid-based formulations. [13-19]

On entering the GI tract, these LBFs experience a dynamically changing pH environment where LBFs make contact with bile, digestive enzymes, foods and the digested products of food. Ingested LBFs are initially dispersed in the stomach where the presence of the digestive enzyme gastric lipase initiates hydrolysis of dietary triglycerides and triglycerides to produce diglycerides and free fatty acids. Shear in the stomach further facilitates the emulsification of the formulation when combined with amphiphilic products (diglycerides and free fatty acids) of the initial digestion. Within the small intestine, pancreatic lipase and its cofactor, co-lipase complete the breakdown of triglycerides to diglycerides, monoglycerides and free fatty acids. The presence of exogenous lipids in the small intestine stimulates the secretion of bile salts, phospholipid and cholesterol from the gall bladder. Ultimately, the increased concentration in bile salt, monoglycerides and fatty acids then self-assembled into a series of colloidal structures mainly in micelles, mixed micelles, unilamellar and multilamellar vesicles that significantly increase the solubilization of lipid digestion products and drugs in the small intestine. This process is shown in Figure 1 which is adapted from Reference 18.

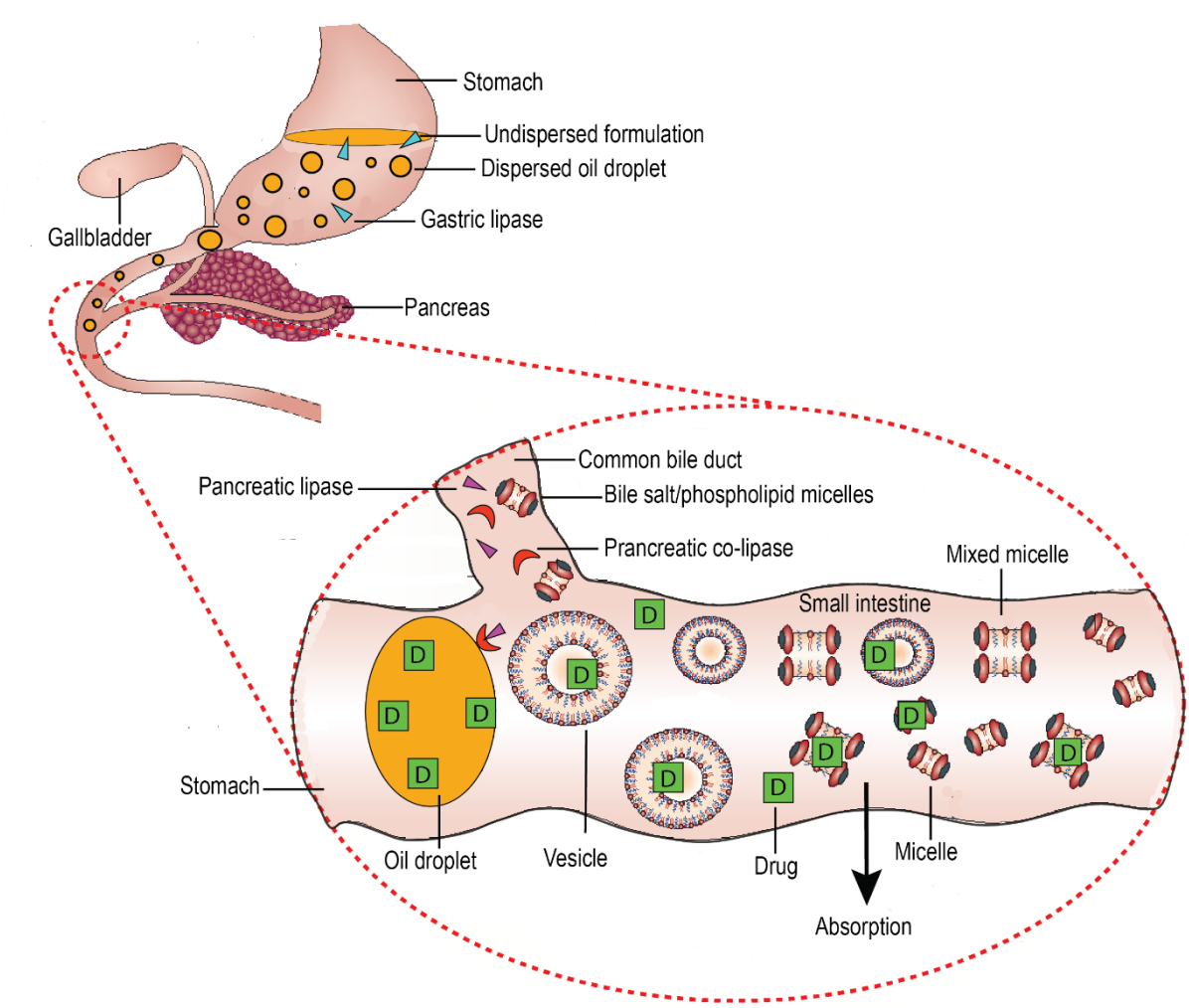

Figure 1 – Lipid digestion and drug absorption in the small intestine. *Adapted by permission from Nature/Springer/Palgrave, Nature Reviews Drug Discovery, Lipids and lipid-based formulations: optimizing the oral delivery of lipophilic drugs, Christopher J. H. Porter et al.*[18] *Copyright (2007).*

The gastric environment has a major impact on drug absorption and the behavior of drug/drug formulations.[11, 20] The phase behavior of drug formulations in the GI tract can be modified by dispersion and dilution of the drug formulation as well as the influence of digestive enzymes. Subsequently, these phase changes can alter the solubilization capacity of the formulation, which may lead to the precipitation of the drug. Thus, the proper understanding of drug trafficking between lipid and bile components and the fate of lipid formulations in the GI tract enables the optimization of lipid-formulated drug delivery methods for poorly water-soluble drugs.

However, designing a formulation is an intensive work that requires many experimental tests to optimize formulation properties. Some steps involved in this process are: the selection of excipients and testing solubility, assessing the encapsulation efficiency, testing the stability of formulations and testing drug absorption. Additionally, it is interesting to study fine molecular structural details such as types of colloids formed in the GI tract, the location of drug molecules within the colloidal structures and the state of the drug - whether it is dissolved or precipitated. These types of information help understand the complex phase behavior of lipid-based formulations and assist in designing efficient formulations. However, experimental investigations for obtaining these fine molecular details are difficult to conduct due to the number of various components present in the complex environment at the GI tract as well as the polymeric nature of many excipients uses in drug formulations.

Molecular dynamics (MD) simulations serve as a potential tool to understand this type of complex systems. In this method, physical movements of atoms are simulated by solving Newton's equations of motion numerically and thus, the dynamic evolution of the system can be captured with respect to time. The atomic movements are modelled using small time steps, typically an order of 1-5 fs, to execute stable dynamics through the numerical integration of the equation of motion.[21] However, to obtain a certain molecular event (i.e., spontaneous aggregation, crystal growth, protein folding, etc) or thermodynamic properties (e.g., heat capacity, density, free energy, etc), simulation times in this computational method vary from ~1 ps to μs range depend on the phenomenon we are interested in. More information regarding concepts in MD simulations can be found in the review article by Katiyar and Jha.[21] "Force fields" (FFs) are the heart of these simulations, which are responsible for calculating the potential energy of the system using molecular mechanics (e.g., harmonic oscillator and Coulombic potentials). Various FFs, such as united atom, all-atom and coarse-grained FFs are employed in the MD simulations discussed in this review. Also, the influence of these FFs on LBFs will be discussed in the last section of this review. Further information for MD simulations can be found in papers in the literature.[22-23]

Numerous computational approaches are accelerating today's drug delivery pipeline. The use of computational tools in different steps in formulation design has been discussed by Mehta et al. in 2019.[24] In the same year, Hossain et al. discussed how

classical MD simulations used for solubility calculations/predictions in pharmaceutical systems.[25] Further, Albano et al. have discussed MD simulations in applications of drug delivery carriers: liposomes, polymeric micelles, and polymersomes in 2018.[26] Similarly, various chapters in the "Introduction to Computational Pharmaceutics" book by Ouyang and Smith discussed applications of molecular modelling in drug delivery.[27-28]

MD simulations can provide precise atomic or microscopic information that can help our understanding of complex LBF systems and predict the colloidal behavior of drug formulations where experimental investigations are difficult or impossible to perform. In this review, we summarize MD studies of different lipid formulation types under four main topics:

I. an overview of the available MD studies for GI environment and lipid-based drug formulations.
II. FFs involved in investigations in the literature.
III. implementation of MD studies in drug formulations.
IV. future directions for computational drug formulation.

The Gastro-Intestinal Tract Lumen

The colloidal behavior of bile in the GI tract has a great influence on drug absorption.[11, 20] To gain insight into the phase behavior of bile components, numerous MD simulations have been reported in the literature and are summarized below.

The principal site of absorption for most oral drugs is the small intestine.[29] After passing through the stomach, a LBF will encounter bile and pancreatic enzymes. Bile is a complex mixture, synthesized and secreted from the liver, stored in the gall bladder and then delivered into the small intestine. It is mainly composed of bile salts (67% w/w), phospholipids (22% w/w), protein (4.5% w/w), cholesterol (4% w/w) and bilirubin (0.33% w/w).[30] The most abundant component, bile salts, are derived from cholesterol. These salts are conjugated with glycine or taurine and a rich variety of bile salts species present in the bile. Glycocholate, glycochenodeoxycholate, taurocholate, taurochenodeoxycholate and glycodeoxycholate are the major components of bile.[30] The structures of these principal bile acid species are shown in Figure 2.

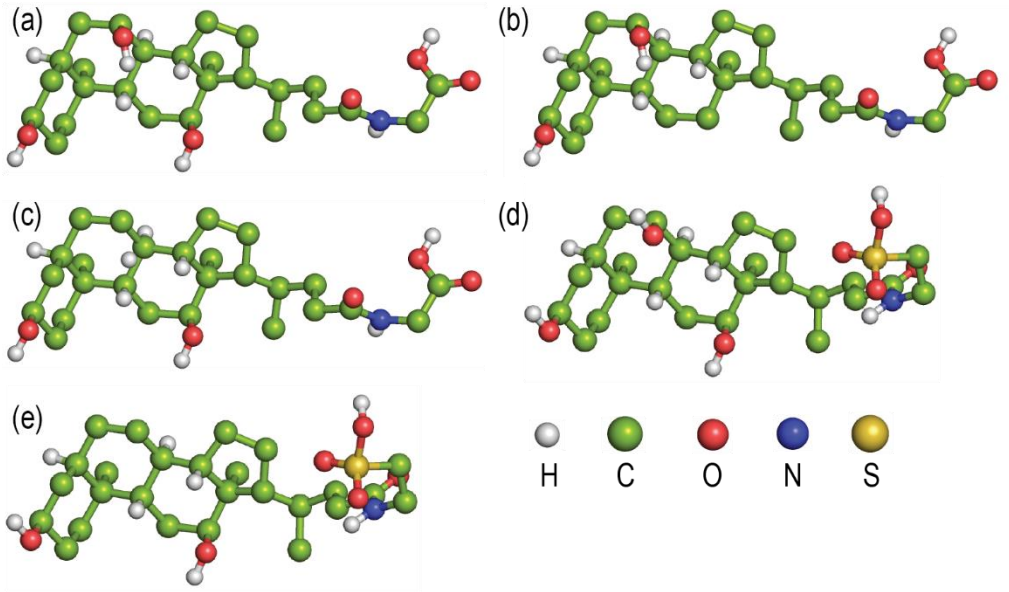

Figure 2 – 3D Chemical structures of abundant bile acid species in bile, (a) Glycocholic acid, (b) Glycodeoxycholic acid, (c) Glycochenodeoxycholic acid, (d) Taurocholic acid, (e) Taurochenodeoxycholic acid. Hydrogen atoms important for stereochemistry are shown.

Bile salts are amphiphilic molecules, responsible for the solubilisation of lipids, cholesterol, fatty acids and fat-soluble vitamins. Due to their amphiphilic nature, bile salts spontaneously aggregate into micelles in an aqueous environment. In the GI tract, these aggregates also combine with lipid products to form mixed micelles. In contrast to classical amphiphiles, which contain a separate hydrophilic head and a flexible hydrophobic tail, bile salts are rigid steroid backbone molecules with weakly separated hydrophilic and hydrophobic faces denoted as the α and β side of the molecule. The chemical structures of some bile acids (i.e., cholic acid, chenodeoxycholic acid, deoxycholic acid and lithocholic acid) with their α and β sides are shown in Figure 3.[31]

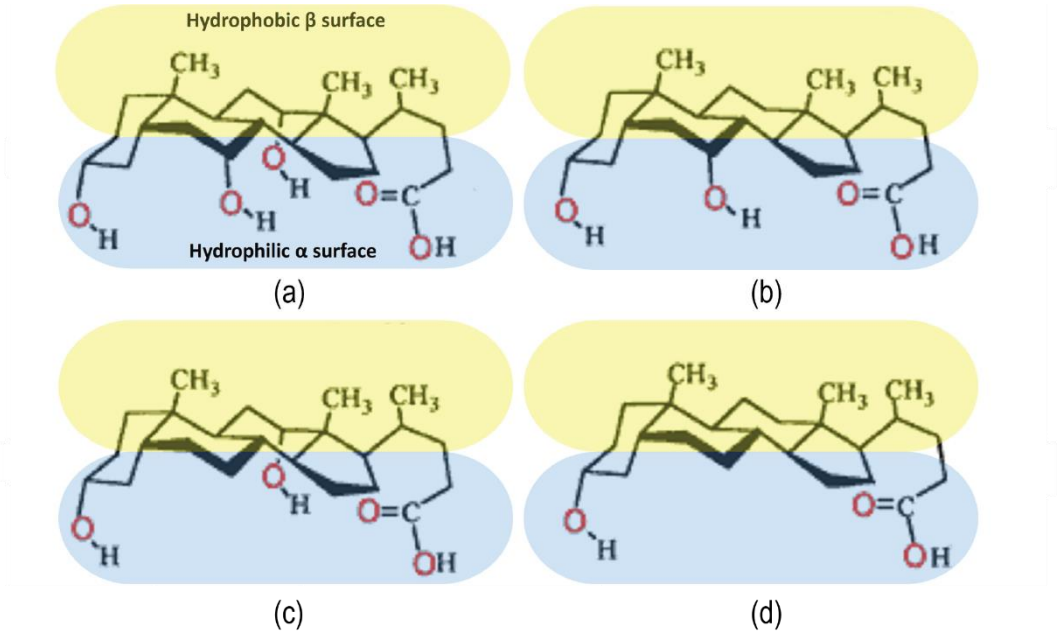

Figure 3 – α and β sides/surfaces of (a) cholic acid, (b) chenodeoxycholic acid, (c) deoxycholic acid and (d) lithocholic acid. *© 2018, Pavlović et al.[31] Originally published in Bile Acids and Their Derivatives as Potential Modifiers of Drug Release and Pharmacokinetic Profiles, Front. Pharmacol., 9 (1283) under CC BY license. Available from: DOI: 10.3389/fphar.2018.01283*

This facial polarity is due to the presence of hydroxy groups on one face and the methyl groups on the opposite side of the molecule. The bile salts differ in the number of hydroxyl groups attached to the steroid moiety where the three hydroxyl groups attached are more soluble. Due to the hydrophilic and hydrophobic facial arrangement, bile salts have unusual physicochemical properties in critical micellar concentration, shape and size of bile salts micelles and micellar structures compared to classical surfactants.[32] However, these salts have drawn attention due to their importance in drug formulation behavior and drug absorption.[20, 33-34] Thus, it has a long history of research. Recently, Hofmann and Hagey discussed the bile acid research in the last eight decades including information in extraordinary advances in the field of bile acids.[35] Many experimental studies have explored the properties of bile salt aggregates and some of these investigations are supported by simple models to deduce bile salt/phospholipid mixed micelles.[36-43] Though several models are available, the stacked disk model and radial shell model have been discussed widely in the literature. A schematic representation of these two models is shown in Figure 4.[44] The stack disc model was proposed by Shankalnd[45], which is based on a mixed

micelle disc model initially proposed by Small[46]. In the stacked disc model, mixed micelle disks are stack on one into another to form a rod-like micelle in which mixed micelle model, discoid phospholipid bilayer coated with bile acids. In contrast, Ulminus et al. proposed that phospholipids are oriented radially (radial shell model) with respect to the centre of the micelle.[38] Further, the bile salts in this model act as wedges that fill the spaces between phospholipid head groups and are arranged with their long axis parallel to the surface. This model is in accordance with a small angle neutron scattering study of conjugated bile salts and fatty lipids.[47]

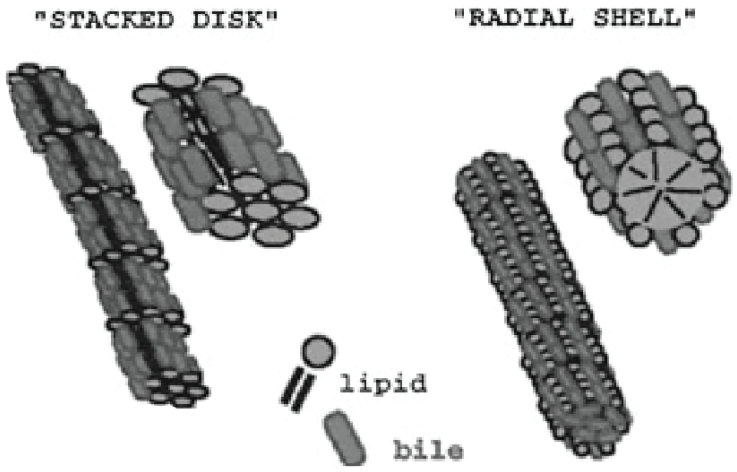

Figure 4 – Schematic representation of stacked disk model and radial shell model for bile salt/phospholipid mixed micelles.[44] *Reprinted from Current Opinion in Colloid & Interface Science, 28, Euston, S. R., Molecular Simulation of Biosurfactants with Relevance to Food Systems, 110-119, Copyright (2017), with permission from Elsevier.*

Bile Salts & Cholesterol

To understand structure of bile aggregates under different environmental conditions, MD simulation is a useful approach Several MD studies have investigated bile salts and bile using a united atom model.[48-55] In an early study, Marrink and Mark investigated the structure of a mixed micelle of palmitoyloleoylphosphatidylcholine (POPC) and cholate and also a ternary micelle formed with POPC, cholate and cholesterol.[48] Starting from the random distribution of molecules, they observed the spontaneous formation of mixed micelles in their simulations. In a mixed micellar structure, the phospholipid molecules are oriented radially with head groups at the surface while tails of the phospholipid pointing toward the micelle centre. Bile salts sit

at the surface by filling the spaces between phospholipid headgroups. These molecular arrangements resemble the radial shell model[38] proposed in the literature. Further, their simulations of the ternary micelle indicated that the hydroxy group of cholesterol is at the mixed micellar interface while steroid moiety is solvated by the phospholipid chains. A limitation of the Marrink and Mark study is that it is restricted to a single micelle where the number of constituent molecules was selected based on experimental measurements of an average mixed micelle. A more realistic model requires the simulation of larger systems that can form multiple micelles in the simulation cell.

An extensive study of the self-assembly behavior in the aqueous environment of six bile salt species; cholate, glycocholate, taurocholate, glycochenodeoxycholate, glycodeoxycholate and lycolithocholate was performed by Warren et al. in 2006.[49] They showed that these bile species spontaneously form highly dynamic aggregates, sizes ranging from 8 to 17 molecules. Further, they found that the size, structure and dynamics of the micelles are greatly influenced by the intermolecular hydrogen bonding within the micelle. The inter-micellar interactions allow the formation of primary and secondary micelles as proposed by the Carey and Small model[43] are observed in their simulated systems. Alternatively, they observed that the average shape of micelles as oblate, which is a feature of the model proposed by Kawamura and co-workers.[41] Even though Warren et al. observed some features of the literature models, they demonstrated dynamic and disordered behavior in bile salt aggregation. Thus, their model is a better model to represent bile salt behavior compared to the older rigid and structured molecular arrangement models in the literature.

Another study by Pártay and co-workers in 2007 studied the aggregation behavior of sodium cholate and sodium deoxycholate in three aqueous concentrations (30, 90 and 300 mM) .[50] This study thoroughly discussed the formation of primary and secondary micelles with respect to the concentrations and the bile salt species. The primary-secondary micelle behavior observed for the deoxycholate is fully in accordance with the model proposed by Small[40] in the literature. In the following year, the same authors, Pártay and co-workers, investigated the counterion binding in micelles formed with bile salt species, sodium cholate and sodium deoxycholate at three concentrations.[51] Their study provides insight to resolve discordant values obtained

from different experiments for the degree of counterion binding. Turner et al. have explored the aggregation behavior and physicochemical properties of glycocholate micelles at two physiological concentrations (the concentration in the gallbladder and the concentration in the small intestine under fed state) using MD simulations.[52] They found that the glycocholate aggregated into small micelles with an average aggregation number of 8.5. This self-assembly process was mainly driven by the hydrophobic interactions of the nonpolar faces of steroid backbones and hydrogen-bonding interactions among monomers. The dynamic process of micelle formation and the micellar structure information that emerged from the MD simulations support the previous models proposed by Mazer et al.[37] and Small et al. [40]

Holmboe et al. performed MD simulations to understand the structure and molecular interactions of colloids present in fasted state intestinal fluid considering taurocholate bile salt and phospholipid, phosphatidylcholine 1,2-dilinoleoyl-sn-glycero-3-phosphocholine.[53] They further investigated the partitioning of water, ethanol and drugs (carbamazepine, felodipine and danazol) in the lipid bilayers formed with taurocholate and phospholipid. The study demonstrated that intermolecular hydrogen bonding between taurocholate molecules is an important factor in bilayers, these intermolecular hydrogen bonds resulted in embedded transmembrane taurocholate clusters. In terms of drug-partitioning study, they found that the diffusion of hydrophilic to moderate lipophilic molecules through the bilayer is facilitated by the embedded taurocholate molecules since the capacity of drug molecules to form hydrogen bonds strongly related to taurocholate. Birru et al. used MD simulation to investigate the colloidal structure formation of the bile before digestion.[54] They computationally constructed the phase diagram for bile before digestion, however, they noticed a discrepancy in the predicted and experimental phase boundary. According to the composition of the bile, cholesterol is one of the major species present in the bile. The impact of this substance on the colloidal behavior of bile has been explored by Suys et al. more recently. They investigated the influence of cholesterol and pH on the colloidal structure formation in the GI tract upon lipid digestion using MD simulation and experimental techniques.[55] Their investigation indicated a reduction in aggregate size with increasing pH. Further, the study demonstrated that cholesterol does not significantly affect the size, number, shape or dynamics of aggregates. MD results in

this study help to understand the pH and cholesterol conditions that influence the self-assembly process in the GI tract.

A coarse-grained model was used by Verde and co-workers to investigate the bile salts in aqueous solutions using the dihydroxy bile salts at physiological temperature and counterion concentrations.[56] Their coarse-grained model retains sufficient information to provide atomic-scale understanding for bile salt aggregation. In another study, the hydration structure and dynamics of chenodeoxycholate bile species have been investigated by Nakashima et al. using MD simulations with all-atom FF.[57] They mainly focused on the distribution of water molecules in chenodeoxycholate, specifically around the oxygen atoms in COO^- and OH groups and the hydrophobic carbon atoms in the CH_3 groups. Strong hydrogen bonds of water with oxygen atoms in hydroxyl and carboxyl groups were identified, in addition to a strong hydration shell around the hydrophobic region of chenodeoxycholate.

These MD simulation models provide atomic information about bile salt colloidal behavior under various conditions, which helps to understand experimental observations. Further, these models could be used to continue investigations with lipid-based drug formulations.

Digestion Products of Bile

Phospholipids are one of the major components in bile and, due to the gastric and pancreatic lipases in the GI tract, these molecules are quickly hydrolysed/digested to lysophosphatidylcholine and free fatty acids.[58] A study by Birru et al. showed the changes in phase behavior in systems with bile salts/phospholipids and bile salts/digested phospholipids using *in vitro* models considering the concentration of the components in the gut lumen.[59] They particularly noticed a significant shift in the phase boundary in the bile salts/digested phospholipid system toward higher mass faction of phospholipids. Alternatively, oils containing free fatty acids are widely used in drug formulations. In water, fatty acids assemble to form micelles of various sizes and structures. Thus, there is a growing interest in MD investigations related to fatty acid phase behavior and we discussed MD simulations conducted with fatty acids to get proper awareness of how fatty acids influence aggregation formation with bile salts.

To investigate the titration behavior of oleic acid in different environments specifically oleic acid in small aggregates and oleic acid in dioleoylphosphatidylcholine (DOPC) bilayer, constant pH MD simulations with coarse-grained Martini model have been performed by Bennett and co-workers.[60] They found that titration behavior depends on the chemical environment where pH increases with the micellar size and was correlated with the deprotonated fraction of oleic acid. Similar to Bennett et al.'s study but with the all-atom model, Morrow and co-workers performed constant pH MD simulations with pH-based replica-exchange method to study the self-assembly and phase behavior of pH-sensitive lauric acid.[61] They observed the spontaneous formation of bilayer at low pH conditions while micelle formation at high pH conditions that agree with experimental investigations.

Another coarse-grained study investigated the interactions of oleic acid in dipalmitoylphosphatidylcholine (DPPC) bilayer.[62] The results of this study indicate that oleic acid disperses homogeneously in the bilayer at all oleic acid concentrations without much perturbation. All-atom MD simulation has been performed by Ngo in water with a pure oleic acid membrane consists of three layers to investigate the molecular mechanism of flip-flop events.[63] Ngo observed that COOH surrounding water molecules help reduce the barriers at the hydrophobic interfaces to trigger flip-flop events. Alternatively, the middle layer of the membrane serves as an intermediate for oleic acid and water molecules to migrate easily from one leaflet to another. United atom model MD simulations have been performed by Cerezo et al. to elucidate the structural and dynamic changes of 1,2-dimyristoyl-sn-glycero-3phosphocholine (DMPC) and 1,2-dipalmitoyl-sn-glycero-3-phosphocholine (DPPC) bilayers in the presence of oleic and 2-hydroxyoleic fatty acids at rising concentrations.[64] They found accumulation of both fatty acids in bilayer up to high concentrations induces small structural changes. Further, at rising fatty acid concentrations they noticed an increase mobility of lipid and fatty acid chains along with permeability enhancement of bilayers to hydrophobic penetrants.

The phase behavior of fatty acids in an aqueous medium has been investigated. These investigations are more important compared to the previously discussed investigations since fatty acid colloidal behavior impacts designing drug formulation and drug absorption in the GI tract. King et al. has been demonstrated that the complete ternary

phase diagram for sodium oleate, sodium laurate and water found experimentally can be reproduced with computational models[65]. Figure 5 shows the experimental phase diagram of sodium oleate/sodium laurate/water system at 348 K overlaid with the phase behavior observed with the MD simulations.[65] This study demonstrated that the spontaneous self-assembly of micellar, hexagonal and lamellar phases is feasible with MD simulations starting from the random arrangement of molecular components. Having investigated sodium oleate, sodium laurate surfactant systems, they intended to extend the modelling approach to explore systems relevant to drug formulations/absorption.

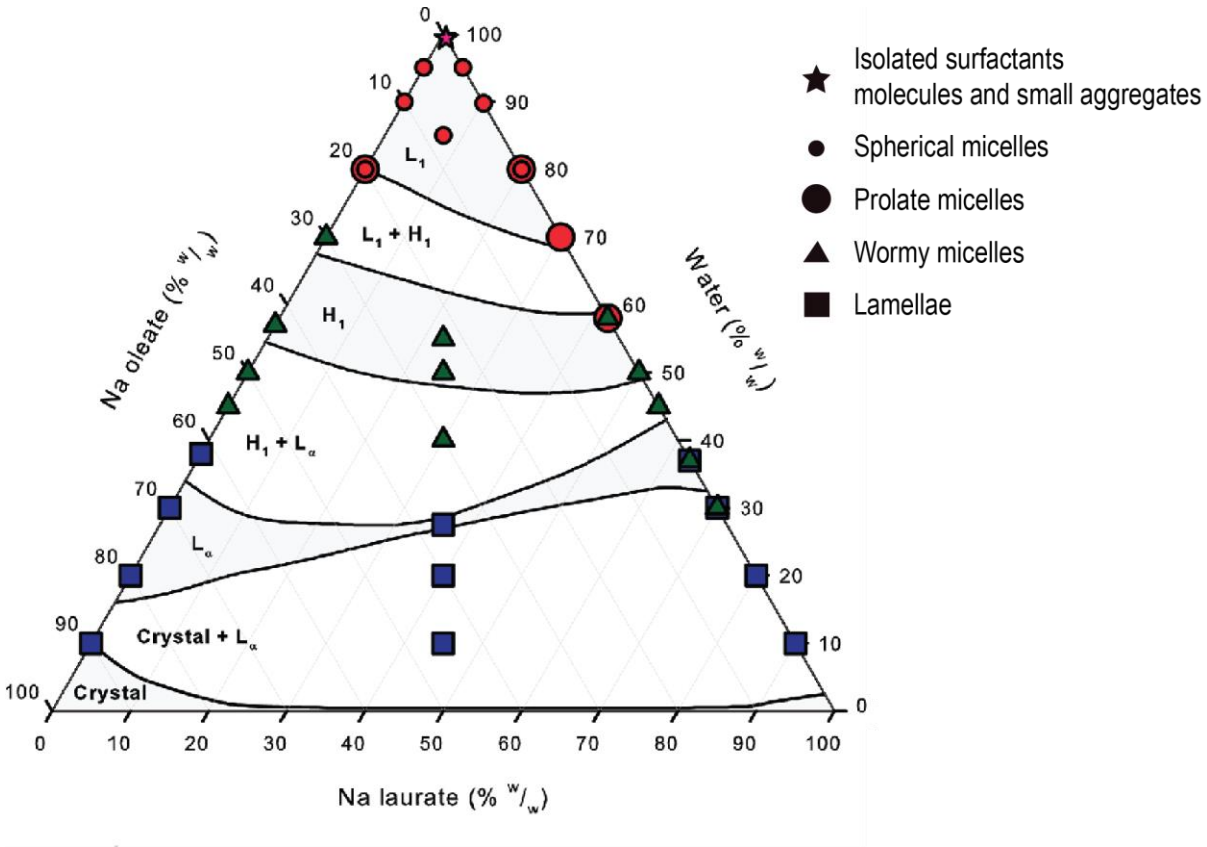

Figure 5 – Comparison of experimental and MD derived phase behavior of sodium oleate/sodium laurate/water system at 348 K.[65] Single phases are coloured in grey and white regions consist of a mixture of two adjoining phases. L_1 denotes the micellar phase, H_1 denotes the hexagonal phase and L_α denotes the lamellar phase. Points indicate the compositions of each simulation and the phase observed in the final frame of MD simulations. The colouring represents micelles (red), the hexagonal phase (green) and the lamellar phase (blue). *Adapted with permission from King, D. T.; Warren, D. B.; Pouton, C. W.; Chalmers, D. K., Using Molecular*

Dynamics to Study Liquid Phase Behavior: Simulations of the Ternary Sodium Laurate/Sodium Oleate/Water System. Langmuir ***2011,*** *27 (18), 11381-11393. Copyright (2011) American Chemical Society.*

Similar to the study by King et al., Janke and co-workers investigated the phase behavior of oleic acid using a coarse-grained model[66] where they observed the aggregation of oleic acids into micelles, vesicles, and oil phases depending on the protonation state of the oleic acid head group. The observed phases were compared with experimental observations. Further, their free energy calculations provided information about the thermodynamics of oleic acid aggregation. Recently, coarse-grained molecular dynamics simulations have been performed to investigate critical micellar concentration (CMC) and the aggregation behavior of four medium-chain fatty acids.[67] Their study calculated CMC values that were 1.8 to 3.5 fold lower than experiential measurements. The aggregate properties in terms of aggregate size, aggregate number and morphologies as a function of carbon chain length at different pH conditions are consistent with the experiential observations. Overall, this investigation indicates the coarse-grained Martini model is suitable for studying colloidal systems with medium chain fatty acids. The phase behavior of DPPC, palmitic acid and water 1:2:20 mixture was studied by Knecht and co-workers.[68] Starting from randomly distributed molecules, they observed the formation of gel phase and inverted hexagonal phase depending on temperature, which agrees with the experimental observation. During the transformation from the gel to the hexagonal phase they found the existence of a metastable lamellar intermediate on the nanosecond time scale.

Additionally, several MD simulation studies provide insight into the bile salt aggregation behavior with different fatty acids. Turner et al. investigated the influence of lipid digestion products in bile salt micelles.[52] Using glycocholate bile salt and oleic fatty acid in the bile salt-fatty acids mixed micelles, they observed how hydrocarbon chains of the oleate anions penetrated into to the centre of the micelle. They also found an increment of the averaged micellar diameter from 1.86 to 2.35 nm when glycocholate micelle associated with fatty acid. The phase diagram for the digested bile was constructed by Birru et al. using MD simulations.[54] Further, they explored the effect of fatty acid ionization on the phase behavior of digested bile. The phase boundary obtained through MD simulation agreed well with the experimental phase

boundary and they also found that increased ionization enhances micelle formation, indicating the fatty ion ionization plays a significant role in the phase behavior of bile.

Lipid-Based Drug Formulations

Dispersion/dilution and digestion of LBFs can modify the solvent properties and capacity of drug formulations, and may cause the precipitation of the drug. Once a drug precipitates, any re-dissolution is slow compared to the intestinal transit time. Consequently, the absorption of the drug and bioavailability is poor. Therefore, to establish a successful oral drug delivery product, it is essential to understand the colloidal behavior of drug formulations in terms of colloids themselves and the drug within the colloid in the processes of dispersion, dilution or digestion and this information can be obtained from MD simulations. Therefore, in this section, we mainly discussed MD simulations related to LBFs.

In terms of drug formulations, only a limited number of MD studies are available in the literature, and these are, for the simplest Type I formulations.[69-70] These studies focus on the colloidal structure formation of lipid formulations (with or without drug) and the changes in the structure on the dispersion in aqueous media. Warren et al. studied mixed glyceride formulations containing a trace amount of water (1% w/w) to model the microstructure of a drug formulation (without a drug in it) when in the soft-gelatine capsule.[69] They further explored mixed glyceride formulations during the dilution process up to a water concentration of 20% w/w in addition to exploring the influence of the water-soluble cosolvent, propylene glycol in those formulations. They found that all systems investigated in their study are in the reverse micellar structure. This work was extended in 2013. The phase behavior of a Type I formulation containing a 1:1 molar ratio of mono-lauroyl glyceride and di-lauroyl glyceride was investigated using more concentrations compared to their previous study (10 concentrations versus 6 concentrations) with improvements in simulation time and better simulation techniques.[70] The colloidal structure formations at different water contents (0%-75% w/w) were studied to identify the phases formed upon the dispersion of the formulation in an aqueous medium as their previous study. Importantly, the distribution of the five selected poorly water-soluble drugs during the dispersion of drug formulation was also investigated. The study revealed that the Type I formulation/water mixture forms a single reverse micelle-like phase with isolated water molecules at low water content,

a single reverse micelle phase at intermediate water content and a two-phase system (lamellar glycerides and bulk water) at high water content. Simulations of Type I formulations and drugs in different aqueous contents indicated that all drugs are localized within the system where the polar region of drugs in contact with water or polar lipid atoms, while the hydrophobic region of the drug contacts with lipids. Once a Type I formulation reaches the intestine, digestive enzymes convert the triglycerides in the formulation into free fatty acids and monoglycerides that are solubilized by bile and form a spectrum of colloidal phases within the GI environment. The previously modelled GI environment,[54] was used by Birru et al. to study the phase behavior of digested triglycerides in the GI tract.[71] Also, they explored the impact of triglycerides on the solubilization process of poorly water soluble drug; danzol. Their investigation includes MD simulation model and *in vitro* experimental model of the upper GI tract. The results of this study implied that formulation lipids improve the solubility of poorly water-soluble drug; danzol. Specifically, the solubility of danzol increases with the concentration of digested triglycerides, which agrees with published reports on the solubility of the related compound hydrocortisone.[72]

Recently, Larsson et al. explored LBFs composed of either medium chain or long chain lipids varying tri, di- and monoglyceride proportions in it using coarse-grained (CG) MD simulations.[73] The long-term goal of Larsson and co-worker was to establish a CG Martini model[74] for complex systems that increases the simulation speed for a better understanding of solubilization of drugs in LBFs. The study demonstrated the self-assembly of lipids into different colloidal structures at different water contents. This model has the added advantage of drastically reducing the computation time, which gives the opportunity to explore these systems with large simulation cells.

When self-emulsifying drug delivery systems disperse into microemulsions in the GI tract, nanoscale lipid droplets are formed and this type of lipid droplet has been modelled by Benson and Pleiss using MD simulations.[75] They studied the influence of excipients in terms of fatty acid chain length, surfactant concentration and variations in mono, di- and triglycerides composition. Besides, they also explored the localization of the drug cyclosporin A on the droplet. To our knowledge, this is the first MD simulation of a formulation that contains polyethylene oxide/polyethylene glycol (PEG-6) surfactants. Benson and Pleiss observed a clear change in droplet association

patterns with changes in the fatty acid chain length. In detail, they observed random, lamellar-like and vesicle-like association of hydrophilic triglyceride moieties with C6, C10, and C14 fatty acid chain lengths, respectively. Further, they found that the addition of monoglycerides leads to the stabilization of the drug molecule at the triglyceride core of the droplet.

It is important to understand the localisation of drug molecules within LBF or surfactant phases. Warren at al. recently investigated solubilized location of series of probe molecules in octaethylene glycol monododecyl ether ($C_{12}E_8$) micelles.[76] Even though this investigation is particularly unfocused on LBFs, the investigation provides confidence to conduct similar studies to understand the solubilization of drug molecules in LBFs with mixed micelles in the GI tract. The probe molecules in Warren et al.'s study include: alkane molecules (hexane, cyclohexane and hexanol), aromatic molecules (benzene and toluene) and drug molecules (2-hydroxybenzoic acid, 4-hydroxybenzoic acid, acyclovir and danzol). According to a figure in Martin's Physical Pharmacy and Pharmaceutical Sciences[77] (Figure 6), benzene and toluene are solubilized within the alkane core of a non-ionic surfactant micelle (the core of the $C_{12}E_8$ micelle) while 2-hydroxybenzoic acid is solubilized at the interface between the core and the ethylene oxide chains, protruding polar groups into the aqueous medium. Alternatively, 4-hydroxybenzoic acid is solubilized out of the micellar core, between the water-solvated polyethyleneoxide chains. However, with the MD investigation, Warren and co-workers found that benzene and toluene are in fact excluded from the core and 4-hydroxybenzoic acid favours maintaining contact with the core. Further, this study demonstrated that cyclic compounds move out from the micelle core and polar groups anchored to polyethyleneoxide mantle of the micelle.

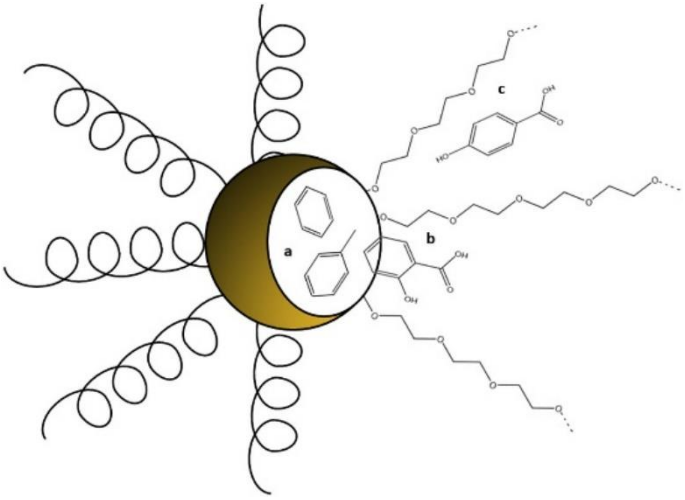

Figure 6 – Schematic diagram of solubilisation of probe molecules with in a spherical, non-ionic surfactant micelle from the textbook Martin's Physical Pharmacy and Pharmaceutical Sciences.[77] (a) – Non polar molecules solubilised within nonpolar region, (b) – more polar molecule partially embedded in both polar and nonpolar regions, (c) – polar molecule positioned well out in the polar regions, within the polyethyleneoxide chains. These distributions are challenged by the MD simulations of Warren et al.[76] *Reprinted from Journal of Pharmaceutical Sciences, 108 (1), Warren et al.[76], Location of Solvated Probe Molecules Within Nonionic Surfactant Micelles Using Molecular Dynamics, 205-213, Copyright (2019), with permission from Elsevier.*

The MD simulations of lipid-based drug formulations discussed so far are restricted to the oily systems which are mainly Type I formulations. This section will discuss the investigations with surfactants used LBFs. The soybean oil-based nanoemulsion system has recently been investigated by Moghaddasi and co-workers using MD simulations in the presence and absence of curcumin.[78] The emulsion systems in this study include palmitic acid, oleic acid, linolecic acid and α-linolenic acid to represent the soybean oil and polysorbate 80/Tween 80® surfactant with curcumin as a drug. This system corresponds to the Type III formulation in LFCS. To our knowledge, this investigation is the first MD study incorporated with complex polysorbate surfactants with lipid-based formulations. The study demonstrated that molecules self-assemble into spherical or prolate spheroid-shaped aggregates. However, the presence of curcumin accelerates the system reaching equilibrium and creates more symmetrical and compact colloidal systems. The particle size and the shape obtained from MD simulation agreed well with experimental data. In another study with a coarse-grained

MD simulation method investigated the solubilization behavior of polyene antibiotics amphotericin B and nystatin in polysorbate 80 micellar solution.[79] The main objective of this study was to gain insight into the use of polysorbate 80 in the formulation development of amphotericin B and nystatin. The study confirmed the experimentally evident solubilizing ability of polysorbate 80 for polyene antibiotics. The localization of these drug molecules in the polysorbate 80 micelles is also consistent with the experimental observation. The study also showed the heterogeneous distribution of polyene antibiotics among micelles. Overall, the study indicates that the lack of water molecules at interior sites of polysorbate 80 micelles and the large lateral occupied space of polyene antibiotic molecules impacts the penetration of polyene antibiotics, amphotericin B and nystatin.

Kolliphor EL® is another polyethoxylated, non-ionic surfactant used in LBFs, similar to Tween 80®. This excipient has complex heterogeneous compositions that vary from batch to batch and, thus, the phase behavior and microstructure of this surfactant in the aqueous medium is poorly understood. Suys and co-workers aimed to experimentally characterize the phase behavior of Kolliphor EL® and establish a computational model for the surfactant.[80] They simplified the Kolliphor EL® mixture into a single component and used the GROMOS 53A6, 2016H66, and 53A6$_{DBW}$ FFs to model this surfactant. They also conducted cryogenic transmission electron microscopy (cryo-TEM), light scattering measurements, and small-angle X-ray scattering (SAXS) to investigate the colloidal behavior of the surfactant in water. They found that their single-component model reproduced the aqueous phase behavior of commercial Kolliphor EL® mixture well.

Apart from simulating specific formulation types defined in the LFCS, a combined study of *ab initio* and classical molecular dynamics has been used to investigate the solvation of the BCS class II drug diclofenac in water.[81] They used ionized, non-ionized and a mixture of an ionized and non-ionized diclofenac to investigate the solute-solute interactions that influence the drug precipitation at gastric pH. This study revealed that the formation of micelle-like aggregates of diclofenac due to the intermolecular interactions and observed that the formation of these aggregates depends on the drug concentration, the protonation state of the drug and the temperature. Also, they observed that the presence of a small amount of protonated diclofenac with

deprotonated diclofenac significantly increases the self-association properties of the drug. Further, their analysis for aggregate formation showed higher solubility of the deprotonated diclofenac compared to protonated diclofenac.

In addition to investigations in branches of LBFs, MD simulation has been conducted more recently focusing on promiscuous inhibitor aggregation behavior to get useful information for drug discovery and formulation design.[82] The study included strong aggregator miconazole and known non-aggregator, fluconazole, to investigate aggregation behavior. The results showed that aggregation of miconazole into a micelle-like colloid occurred within 50 ns while no aggregation over a 500 ns simulation time with fluconazole.

The MD studies we have discussed so far imply that there is a lack of information in the phase behavior of Type II-IV formulations in the GI tract. There are no extensive MD investigations related to drug formulations with complex surfactants such as polysorbates and castor oil. However, it could be useful for formulators to have atomic information related to biological incidents happening for Type II-IV drug formulations in the GI tract to design effective oral drug delivery product.

In addition to the MD simulations stated in this review, there are several MD studies available for other formulation techniques. MD simulations performed to study the formulation of poorly water-soluble drugs with polymeric micelles.[83] In this method, amphiphilic copolymers are used which differ from classical surfactants used in lipid-based formulation types in LFCS. Another study combined with *in vitro*, *in silico* and *in vivo* methods has been conducted to formulate a nanosuspension that enhances the aqueous solubility and antibacterial activity of fusidic acid.[84] The formation of amorphous solid is another technique used to enhance the oral bioavailability of poorly water-soluble drugs. Xiang and Anderson carried out several MD simulations to understand various properties of the amorphous solids.[85-91]

Force Fields used in MD Studies of Drug Formulations

The force field is the heart of a MD simulation, since this includes functional forms and parameters used to calculate the potential energy of the system. However, FFs are substantially different from one another in terms of the functional form and parameters. The previously discussed MD simulations of LBFs have been conducted with a large

variety of FFs, mainly CHARMM, MARTINI or GROMOS, which can be categorized as all-atom, united atom and coarse-grained FFs. Thus, in this section, we summarized each of these FFs. A schematic representation of 1,2-dipalmitoyl-sn-glycero-3-phosphocholine (DPPC) with all-atom, united-atom and coarse-grained force fields is presented in Figure 7.[92]

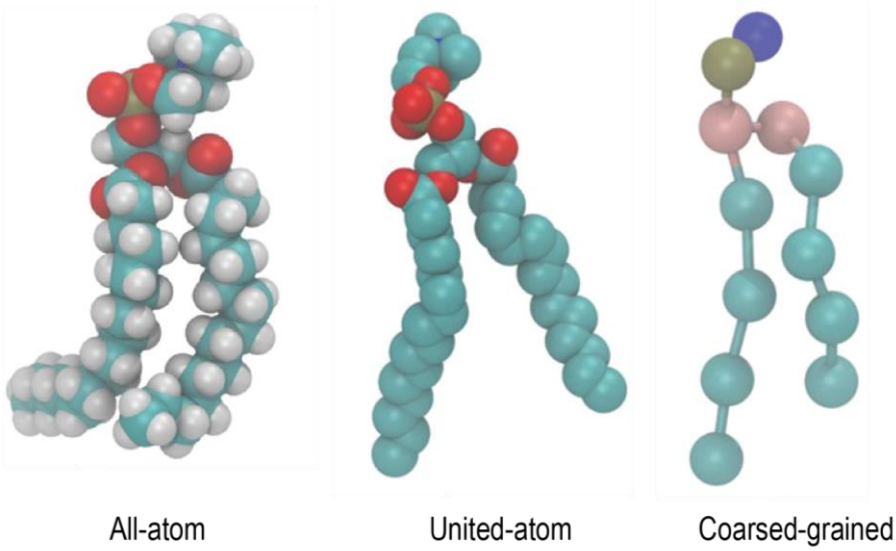

Figure 7 – van der Waals sphere representation of 1,2-dipalmitoyl-sn-glycero-3-phosphocholine (DPPC) with all-atom, united-atom, and coarse-grained force fields.[92]

According to the previous studies discussed in this review, few studies have been conducted using all-atom FFs.[57, 61, 63, 78, 81] As the name suggests, in this FF, all the atoms in each molecule are considered explicitly (Figure 7, all-atom model). As a result, all-atom FFs generate detailed atomistic information about the system, but they demand more computational resources without ensuring necessarily much better results.[93] Thus, enhanced sampling algorithms, such as metadynamics, are useful techniques to reduce the computational cost in all-atom FF models. Also, recent innovations in accelerating all-atom MD simulations on processing units and volunteer-computing projects have been reviewed by Buch and co-workers.[94]

The united atom FFs have been used in many investigations covering a broad range of the LBF field[48-55, 64-65, 68-71, 75-76, 80] and many studies have utilized GROMOS FFs for these simulations. The GROMOS FF, which was introduced in 1984, is one of the main united atom FFs used for MD simulations.[95-104] In this united atom FF, nonpolar carbons are grouped into single-particle with their bonded hydrogen atoms (Figure 7, united-atom model) and thus, it represents the lowest level of coarsening. Also, the literature supports evidence for the poor parametrisation of standard GROMOS 53A6 FF for molecules containing PEO, implying the parameterization issue was closely related to the oxy-functional groups and vicinal ether groups (PEO).[105-108] On the other hand, commercially available surfactants such as Tween 20®, Tween 40®, Tween 60®, Tween 80®, Tween 85®, Kolliphor EL®, Kolliphor RH 40® and Kolliphor RH 60®[109] and cosolvents including Transcutol® and polyethylene glycols in LBFs are PEO molecules. Thus, MD simulations of Type II, III and IV formulations lag behind. However, subsequent efforts have been made to improve GROMOS FF since proper force field parameters, which accurately model the experimental conformational behavior of PEO molecules (the stereo-electronic effect 'gauche effect'[110-111] present in PEO chains at lower temperatures) are pivotal for the accurate prediction of thermodynamic and structural properties of these molecules. To improve the parameters for compounds with oxy-functional groups such as alcohols, ethers, aldehydes, ketones, carboxylic acids and esters, Horta et al. introduced the $53A6_{OXY}$ parameter set by optimizing atomic charges, Lennard-Jones interaction parameters and the covalent parameters.[106] Later on, Fuchs et al. extended the $53A6_{OXY}$ parameter set to $53A6_{OXY+D}$, which appropriately accounts for the 'gauche effect' present in the PEO chains.[105] More recently, the parameter set developed for the oxy-functional groups and vicinal oxyethylene groups: $53A6_{OXY+D}$ was expanded by Horta et al. for amine, amide, thiol, sulfide, disulfide as well as aromatic compounds and nucleic-acid bases and named it as 2016H66.[107] In 2017, Senac et al. used this parameter set to simulate bilayers of PEO monoalkyl ethers, $C_{12}E_2$, $C_{12}E_3$, $C_{12}E_4$, $C_{12}E_5$ and $C_{14}E_4$ and they found that 2016H66 is an appropriate parameter set for simulating C_iE_j systems.[112] In 2019, Warren et al. introduced another parameter set known as $53A6_{DBW}$ by changing the Lennard-Jones interactions between CH_2 and CH_3 with water oxygen to model proper interaction of water with PEO chains.[113]

Even though there are two FFs (2016H66 and 53A6$_{DBW}$) available to model PEO, to date, there is only one study of the suitability of 2016H66 or 53A6$_{DBW}$ parameter sets for branched, oligomeric surfactants used in drug formulations. This study of Kolliphor EL® has been conducted by Suys et al. in 2019 by modelling its aqueous phase behavior.[80] They found that the 2016H66 parameter set reproduced the experimental aggregate size of Kolliphor EL® more accurately than 53A6$_{DBW}$. Alternatively, we investigated the suitability of 2016H66 and 53A6$_{DBW}$ FFs to model surfactants with PEO using a simple non-ionic surfactant $C_{12}E_6$ and we found that 2016H66 FF reproduced the experimental phase behavior more accurately than 53A6$_{DBW}$.[114] Those investigations have so far indicated that 2016H66 FF is appropriate for modelling PEO molecules. However, to achieve high-quality predictions, it is important to validate the FFs using different systems, considering various conditions of the PEO surfactant model in terms of concentration and temperature, before using it. In the context of FFs, a high degree of transferability of the FF is also required to use the FFs reliably. Since we are interested in colloidal structure formation of surfactants, the degree of transferability between different morphologies (i.e., phase transitions) is essential. Thus, we (Guruge et al. unpublished data) investigated the degree of transferability of 2016H66 by simulating phase transitions using the same $C_{12}E_6$/water phase diagram[115]. In our work, we observed adequate transferability of 2016H66 FF confirming that the FF is appropriate for investigating PEO molecule's phase behavior. Even though the parameter issue of PEO has been improved, there are, yet, no MD studies related to Type II-IV formulations. However, our investigations provide confidence to use 2016H66 FF to explore complex formulations more precisely in the future. Interestingly, the recent study by Benson and Pleiss used polyethylene oxide/polyethylene glycol (PEG-6) surfactant in nanoscale lipidic droplets in a microemulsion.[75] To parametrize polyethylene glycol in their study, they used 53A6_OE charges and Lennard-Jones parameters.[108] More recently, another study by Moghaddasi and co-workers[78] used Tween 80® surfactant, which is a PEO surfactant, for an investigation on soybean oil-based nanoemulsion system. They conducted the MD simulation with CHARMM all-atom force field, which is not problematic in modelling vicinal ethylene oxide groups.

Coarse-grained (CG) FFs are popular for modelling complex biomolecular systems. A few studies have been done in MD simulations related to the LBFs.[56, 60, 62, 66-67, 73, 79

These FFs are used when we do not need the full atomistic detail because in these FFs, a group of atoms is represented by beads (Figure 6, coarse-grained model) and thus atomistic detail is lost. However, the molecular description is maintained. Since several atoms (e.g., 3, 4 or 6 atoms) are represented by a single bead, the total number of particles in the system is significantly reduced and thus larger systems can be modelled (i.e., vesicles). For example, a system volume up to 100 × 100 × 100 nm containing millions of particles can be efficiently modelled with CG FFs. Alternatively, high-frequency degrees of freedom (i.e., C-H vibrations) are not considered in the dynamics and thus, MD simulations with CG FFs can use larger timesteps. Because of the fewer degrees of freedom and larger integration time step, CG models are two- to three-fold faster than to all-atom models and, therefore, the simulation time scale in the micro- to millisecond range. Ingólfsson and co-workers provided an overview of CG models used in biomolecular applications in the literature. Furthermore, through the discussed CG models in the study, the authors were able to show the diversity of CG models in molecular modelling.[116] However, there are many drawbacks in CG simulations where the main issues lie with inaccuracy, non-transferability and neglect of non-native interactions.[117]

Challenges in MD Studies of Drug Formulations

One of the hurdles in simulating LBFs in united atom FFs is the size of the simulation system that can be modelled with available computer capabilities. Currently, a system size ~15 nm and simulation time of ~100 ns MD simulations are achievable with modern computational resources.[21] Most studies of LBFs have been conducted with united atom FFs. The individual size of some colloids formed by LBF systems is larger than the currently computationally feasible simulation box size (i.e., vesicles and droplets in an emulsion). However, it is essential to use a larger simulation cell size in MD simulations compared to the experimental measurements of these colloids (i.e., the diameter of a vesicle or oily droplet) since the restricted space in the simulation cell affects the spontaneous self-assembly process and influences the relevant colloidal structure formation. As an example, a recent MD study carried out by Hage et al. for human haemoglobin showed that the effect of the simulation box size on thermodynamics quantities.[118] They showed that unliganded tetramer of haemoglobin (dimensions of 5.4 × 4.9 × 5.0 nm) is stable only in solution when the periodic solvent

box contains ten times more water than the standard size (a 7.5 nm cubic box) of solvent box. Alternatively, some of the polymeric excipient molecules used in LBFs are large molecules (e.g., Kollidon® 30 and Kollidon® 90 F). To represent a particular weight amount of the polymer in the model system, the number of polymeric molecules that can be included in the computationally feasible simulation cell is small. Therefore, modelling of the actual impact of some of the polymeric molecules in the colloidal structure formation in LBFs is not feasible using united atom FFs.

Another problem coupled with the simulation cell size is the simulation time scale. We experienced in our investigations that randomly distributed molecules require lengthy simulation time (~100 ns to µs range) to equilibrate, which is computationally expensive. If the chemical structure is in polymeric nature or complex, the self-assembly process is even more time-consuming. Similarly, the simulation process is slower when the size of the simulation box is increased. The literature also provides evidence that longer simulations are required to observe some molecular events such as protein folding.[119] All this information confirms that simulation time is an influential factor in MD technique. Coarse-grained simulations are one approach to accelerate this type of simulation. Fewer particles and the increased time step in CG models enable longer simulations to be performed. However, capturing atomistic details are still a concern in CG FFs.

Trapping of a MD simulation in local minima is also a potential issue in MD. In such situations, longer simulations are required which is again computationally expensive.[111] Alternatively, we can use more complex methods such as simulated annealing (SA) or replica exchange molecular dynamics (REMD) simulations[120] or metadynamics[121] to explore the conformational space. However, the disadvantage of these techniques is a larger number of computational resources are required to perform these simulations.

MD simulations require a topology that defines the charges of atoms, bond distances, bond angles, dihedral angles for each molecule in the simulation. The automated topology builders are available for conventional FFs such as GROMOS[122-123], CHARMM[124-126] and MARTINI (http://cgmartini.nl/index.php). However, to date, automated topology builders are not available for some recently released FFs (i.e.,

2016H66 or 53A6$_{DBW}$). Therefore, special care must be required when generating topologies for recently released FFs.

To model water molecules in MD simulations, there are two principal methods implicit and explicit are currently available. Implicit water models treat surrounding water as an isotropic continuous medium while in explicit models surrounding water molecules are present. Thus, explicit models are capable of modelling solute-solvent interactions and solvent specific effects at the molecular level. These explicit models are more accurate but computationally much more expensive and time-consuming.[127]

Future Directions

It is advantageous to couple *in vitro* studies of Types I to IV formulations with MD simulations to enhance the understanding of experimental observations. Proper understanding of the colloidal structure formation in the GI tract of Type II to IV formulations will facilitate development of formulations for regular use.

The availability of topologies for complex surfactant mixtures (e.g., Tween® surfactants) used in LBFs in the literature[128] is beneficial to simulate Type II-IV LBFs. However, it is significant to validate these available topologies before simulations. In our lab, we are currently working on validating available topologies to use in MD simulations with LBFs. Our ultimate goal is to develop atomic-scale models that will give detailed insights into the behavior of Type II-IV formulations in the GI tract, which will aid drug formulators to quickly design effective drug formulations for poorly water-soluble drugs.

Alternatively, coarse-grained models have been tested for different bile salts aggregation[56], fatty acid phase behavior[66-67] and phase behavior of Type I lipid formulations[73]. A coarse-grained model for non-ionic polyethylene oxide surfactant $C_{12}E_2$[127] has been successfully developed. Since coarse-grained models accelerate the simulation time, it would be good to use these models with larger simulation cells to study LBF behavior. Even though there is a possibility of losing detailed atomic information due to the coarse-grain model, this method has great potential of modelling large systems (i.e., vesicle formation), which is not currently feasible with atomistic models.

To date, MD studies of LBFs are using simple models with pure molecular components. The available computational models do not consider the effect of foods on lipid-based formulation and drug absorption. In future models, it could be possible to include carbohydrate and lipid components coming from foods to some extent. The benefit of this type of model is it would more closely represent the GI environment compared to models with bile salt and phospholipids alone.

It is clear from our review that when computational models can adequately capture the dynamic behavior of complex systems, then the phase behavior/fate of lipid-based drug formulations and the performance of these formulations can be predicted with MD simulations. Further, the atomic information we obtain from these MD simulations facilitates to understand its behavior at the GI tract and optimize the formulation toward a successful orally delivery product.

References

1. Hann, M. M., Molecular Obesity, Potency and Other Addictions in Drug Discovery. *MedChemComm* **2011,** *2* (5), 349-355.

2. Leeson, P. D.; Young, R. J., Molecular Property Design: Does Everyone Get It? *ACS Med. Chem. Lett.* **2015,** *6* (7), 722-5.

3. Meanwell, N. A., Improving Drug Design: An Update on Recent Applications of Efficiency Metrics, Strategies for Replacing Problematic Elements, and Compounds in Nontraditional Drug Space. *Chem. Res. Toxicol.* **2016,** *29* (4), 564-616.

4. Walters, W. P.; Green, J.; Weiss, J. R.; Murcko, M. A., What Do Medicinal Chemists Actually Make? A 50-Year Retrospective. *J. Med. Chem.* **2011,** *54* (19), 6405-16.

5. Nadin, A.; Hattotuwagama, C.; Churcher, I., Lead-Oriented Synthesis: A New Opportunity for Synthetic Chemistry. *Angew. Chem. Int. Ed. Engl.* **2012,** *51* (5), 1114-22.

6. Doak, B. C.; Over, B.; Giordanetto, F.; Kihlberg, J., Oral Druggable Space Beyond the Rule of 5: Insights from Drugs and Clinical Candidates. *Chem. Biol.* **2014,** *21* (9), 1115-42.

7. Lipinski, C. A.; Lombardo, F.; Dominy, B. W.; Feeney, P. J., Experimental and Computational Approaches to Estimate Solubility and Permeability in Drug Discovery and Development Settings. *Adv. Drug Deliv. Rev.* **1997**, *23* (1-3), 3–25.

8. Yu, L. X.; Amidon, G. L.; Polli, J. E.; Zhao, H.; Mehta, M. U.; Conner, D. P.; Shah, V. P.; Lesko, L. J.; Chen, M.-L.; Lee, V. H. L.; Hussain, A. S., Biopharmaceutics Classification System: The Scientific Basis for Biowaiver Extensions. *Pharm. Res.* **2002,** *19* (7), 921-925.

9. Pouton, C. W., Lipid Formulations for Oral Administration of Drugs: Non-Emulsifying, Self-Emulsifying and 'Self-Microemulsifying' Drug Delivery Systems. *Eur. J. Pharm. Sci.* **2000,** *11*, S93-S98.

10. Pouton, C. W., Formulation of Poorly Water-Soluble Drugs for Oral Administration: Physicochemical and Physiological Issues and the Lipid Formulation Classification System. *Eur. J. Pharm. Sci.* **2006,** *29* (3), 278-287.

11. Pouton, C. W.; Porter, C. J. H., Formulation of Lipid-Based Delivery Systems for Oral Administration: Materials, Methods and Strategies. *Adv. Drug Deliv. Rev.* **2008,** *60* (6), 625-637.

12. Pouton, C. W., Formulation of Self-Emulsifying Drug Delivery Systems. *Adv. Drug Deliv. Rev.* **1997,** *25* (1), 47-58.

13. Savla, R.; Browne, J.; Plassat, V.; Wasan, K. M.; Wasan, E. K., Review and Analysis of FDA Approved Drugs Using Lipid-Based Formulations. *Drug Dev. Ind. Pharm.* **2017,** *43* (11), 1743-1758.

14. Mu, H.; Holm, R.; Müllertz, A., Lipid-Based Formulations for Oral Administration of Poorly Water-Soluble Drugs. *Int. J. Pharm.* **2013,** *453* (1), 215-224.

15. Kuentz, M., Lipid-Based Formulations for Oral Delivery of Lipophilic Drugs. *Drug Discov. Today Technol.* **2012,** *9* (2), e97-e104.

16. Müllertz, A.; Ogbonna, A.; Ren, S.; Rades, T., New Perspectives on Lipid and Surfactant Based Drug Delivery Systems for Oral Delivery of Poorly Soluble Drugs. *J. Pharm. Pharmacol.* **2010,** *62* (11), 1622-1636.

17. Porter, C. J. H.; Pouton, C. W.; Cuine, J. F.; Charman, W. N., Enhancing Intestinal Drug Solubilisation Using Lipid-Based Delivery Systems. *Adv. Drug Deliv. Rev.* **2008,** *60* (6), 673-691.

18. Porter, C. J. H.; Trevaskis, N. L.; Charman, W. N., Lipids and Lipid-Based Formulations: Optimizing the Oral Delivery of Lipophilic Drugs. *Nat. Rev. Drug Discov.* **2007,** *6*, 231.

19. Feeney, O. M.; Crum, M. F.; McEvoy, C. L.; Trevaskis, N. L.; Williams, H. D.; Pouton, C. W.; Charman, W. N.; Bergström, C. A. S.; Porter, C. J. H., 50 Years of Oral Lipid-Based Formulations: Provenance, Progress and Future Perspectives. *Adv. Drug Deliv. Rev.* **2016,** *101*, 167-194.

20. Holm, R.; Müllertz, A.; Mu, H., Bile salts and Their Importance for Drug Absorption. *Int. J. Pharm.* **2013,** *453* (1), 44-55.

21. Katiyar, R. S.; Jha, P. K., Molecular Simulations in Drug Delivery: Opportunities and Challenges. *Wiley Interdiscip. Rev. Comput. Mol. Sci.* **2018,** *8* (4), e1358.

22. Adcock, S. A.; McCammon, J. A., Molecular Dynamics: Survey of Methods for Simulating the Activity of Proteins. *Chem. Rev.* **2006,** *106* (5), 1589-1615.

23. Hospital, A.; Goñi, J. R.; Orozco, M.; Gelpí, J. L., Molecular Dynamics Simulations: Advances and Applications. *Adv. Appl. Bioinform. Chem.* **2015,** *8*, 37-47.

24. Mehta, C. H.; Narayan, R.; Nayak, U. Y., Computational Modeling for Formulation Design. *Drug Discov. Today* **2019,** *24* (3), 781-788.

25. Hossain, S.; Kabedev, A.; Parrow, A.; Bergström, C. A. S.; Larsson, P., Molecular Simulation as a Computational Pharmaceutics Tool to Predict Drug Solubility, Solubilization Processes and Partitioning. *Eur. J. Pharm. Biopharm.* **2019,** *137*, 46-55.

26. Albano, J. M.; de Paula, E.; Pickholz, M., Molecular Dynamics Simulations to Study Drug Delivery Systems. In *Molecular Dynamics* 2018; IntechOpen, pp 74-90.

27. Ouyang, D. ; Smith, S.C., Introduction to Computational Pharmaceutics. In *Computational Pharmaceutics* 2015; pp 1-5.

28. Kang, M.; Lam, D.; Discher, D.E; Loverde, S.M., Molecular Modeling of Block Copolymer Self-Assembly and Micellar Drug Delivery. In *Computational Pharmaceutics* 2015; pp 53-80.

29. Orme, M., Drug Absorption in the Gut. *BJA: Br. J. Anaesth.* **1984,** *56* (1), 59-67.

30. O'Connor, C. J.; Wallace, R. G., Physico-Chemical Behavior of Bile Salts. *Adv. Colloid Interface Sci.* **1985,** *22* (1), 1-111.

31. Pavlović, N.; Goločorbin-Kon, S.; Đanić, M.; Stanimirov, B.; Al-Salami, H.; Stankov, K.; Mikov, M., Bile Acids and Their Derivatives as Potential Modifiers of Drug Release and Pharmacokinetic Profiles. *Front. Pharmacol.* **2018,** *9* (1283).

32. Madenci, D.; Egelhaaf, S. U., Self-Assembly in Aqueous Bile Salt Solutions. *Curr. Opin. Colloid Interface Sci.* **2010,** *15* (1), 109-115.

33. Stojančević, M.; Pavlović, N.; Goločorbin-Kon, S.; Mikov, M., Application of Bile Acids in Drug Formulation and Delivery. *Front. Life Sci.* **2013,** *7* (3-4), 112-122.

34. Van Den Abeele, J.; Rubbens, J.; Brouwers, J.; Augustijns, P., The Dynamic Gastric Environment and Its Impact on Drug and Formulation Behaviour. *Eur. J. Pharm. Sci.* **2017,** *96*, 207-231.

35. Hofmann, A. F.; Hagey, L. R., Key Discoveries in Bile Acid Chemistry and Biology and Their Clinical Applications: History of the Last Eight Decades. *J. Lipid Res.* **2014,** *55* (8), 1553-1595.

36. Matsuoka, K.; Maeda, M.; Moroi, Y., Micelle Formation of Sodium Glyco- and Taurocholates and Sodium Glyco- and Taurodeoxycholates and Solubilization of Cholesterol into Their Micelles. *Colloids Surf. B* **2003,** *32* (2), 87-95.

37. Mazer, N. A.; Carey, M. C.; Kwasnick, R. F.; Benedek, G. B., Quasielastic Light Scattering Studies of Aqueous Biliary Lipid Systems. Size, Shape, and Thermodynamics of Bile Salt Micelles. *Biochemistry* **1979,** *18* (14), 3064-3075.

38. Ulmius, J.; Lindblom, G.; Wennerstroem, H.; Johansson, L. B. A.; Fontell, K.; Soederman, O.; Arvidson, G., Molecular Organization in the Liquid-Crystalline Phases of Lecithin-Sodium Cholate-Water Systems Studied by Nuclear Magnetic Resonance. *Biochemistry* **1982,** *21* (7), 1553-1560.

39. Nichols, J. W.; Ozarowski, J., Sizing of Lecithin-Bile Salt Mixed Micelles by Size-Exclusion High-Performance Liquid Chromatography. *Biochemistry* **1990,** *29* (19), 4600-4606.

40. Small, D. M., Size and Structure of Bile Salt Micelles. In *Molecular Association in Biological and Related Systems*, American Chemical Society: 1968; Vol. 84, pp 31-52.

41. Kawamura, H.; Murata, Y.; Yamaguchi, T.; Igimi, H.; Tanaka, M.; Sugihara, G.; Kratohvil, J. P., Spin-Label Studies of Bile Salt Micelles. *J. Phys. Chem.* **1989,** *93* (8), 3321-3326.

42. Giglio, E.; Loreti, S.; Pavel, N. V., EXAFS: A New Approach to the Structure of Micellar Aggregates. *J. Phys. Chem.* **1988,** *92* (10), 2858-2862.

43. Carey, M. C.; Small, D. M., Micelle Formation by Bile Salts: Physical-Chemical and Thermodynamic Considerations. *Arch. Intern. Med.* **1972,** *130* (4), 506-527.

44. Euston, S. R., Molecular Simulation of Biosurfactants with Relevance to Food Systems. *Curr. Opin. Colloid Interface Sci.* **2017,** *28*, 110-119.

45. Shankland, W., The Equilibrium and Structure of Lecithin-Cholate Mixed Micelles. *Chem. Phys. Lipids* **1970,** *4* (2), 109-130.

46. Small, D. M., Physicochemical Studies of Cholesterol Gallstone Formation. *Gastroenterology* **1967,** *52* (3), 607-610.

47. Hjelm, R. P.; Schteingart, C. D.; Hofmann, A. F.; Thiyagarajan, P., Structure of Conjugated Bile Salt− Fatty Acid− Monoglyceride Mixed Clloids: Studies by Small-Angle Neutron Scattering. *J. Phys. Chem. B* **2000,** *104* (2), 197-211.

48. Marrink, S. J.; Mark, A. E., Molecular Dynamics Simulations of Mixed Micelles Modeling Human Bile. *Biochemistry* **2002,** *41* (17), 5375-5382.

49. Warren, D. B.; Chalmers, D. K.; Hutchison, K.; Dang, W.; Pouton, C. W., Molecular Dynamics Simulations of Spontaneous Bile Salt Aggregation. *Colloids Surf. A* **2006,** *280* (1), 182-193.

50. Pártay, L. B.; Jedlovszky, P.; Sega, M., Molecular Aggregates in Aqueous Solutions of Bile Acid Salts. Molecular Dynamics Simulation Study. *J. Phys. Chem. B* **2007,** *111* (33), 9886-9896.

51. Pártay, L. B.; Sega, M.; Jedlovszky, P., Counterion Binding in the Aqueous Solutions of Bile Acid Salts, as Studied by Computer Simulation Methods. *Langmuir* **2008,** *24* (19), 10729-10736.

52. Turner, D. C.; Yin, F.; Kindt, J. T.; Zhang, H., Molecular Dynamics Simulations of Glycocholate−Oleic Acid Mixed Micelle Assembly. *Langmuir* **2010,** *26* (7), 4687-4692.

53. Holmboe, M.; Larsson, P.; Anwar, J.; Bergström, C. A. S., Partitioning into Colloidal Structures of Fasted State Intestinal Fluid Studied by Molecular Dynamics Simulations. *Langmuir* **2016,** *32* (48), 12732-12740.

54. Birru, W. A.; Warren, D. B.; Headey, S. J.; Benameur, H.; Porter, C. J. H.; Pouton, C. W.; Chalmers, D. K., Computational Models of the Gastrointestinal Environment. 1. The Effect of Digestion on the Phase Behavior of Intestinal Fluids. *Mol. Pharm.* **2017,** *14* (3), 566-579.

55. Suys, E. J. A.; Warren, D. B.; Porter, C. J. H.; Benameur, H.; Pouton, C. W.; Chalmers, D. K., Computational Models of the Intestinal Environment. 3. The Impact of Cholesterol Content and pH on Mixed Micelle Colloids. *Mol. Pharm.* **2017,** *14* (11), 3684-3697.

56. Verde, A. V.; Frenkel, D., Simulation Study of Micelle Formation by Bile Salts. *Soft Matter* **2010,** *6* (16), 3815-3825.

57. Nakashima, T.; Iwahashi, K.; Okazaki, S., A Molecular Dynamics Study of Sodium Chenodeoxycholate in an Aqueous Solution. *Chem. Phys. Lett.* **2006,** *420* (4), 489-492.

58. Whitcomb, D. C.; Lowe, M. E., Human Pancreatic Digestive Enzymes. *Dig. Dis. Sci.* **2007,** *52* (1), 1-17.

59. Birru, W. A.; Warren, D. B.; Ibrahim, A.; Williams, H. D.; Benameur, H.; Porter, C. J. H.; Chalmers, D. K.; Pouton, C. W., Digestion of Phospholipids after Secretion of Bile into the Duodenum Changes the Phase Behavior of Bile Components. *Mol. Pharm.* **2014,** *11* (8), 2825-2834.

60. Bennett, W. F. D.; Chen, A. W.; Donnini, S.; Groenhof, G.; Tieleman, D. P., Constant pH Simulations with the Coarse-Grained MARTINI Model — Application to Oleic Acid Aggregates. *Can. J. Chem.* **2013,** *91* (9), 839-846.

61. Morrow, B. H.; Koenig, P. H.; Shen, J. K., Atomistic Simulations of pH-Dependent Self-Assembly of Micelle and Bilayer from Fatty Acids. *J. Chem. Phys.* **2012,** *137* (19), 194902.

62. Notman, R.; Noro, M. G.; Anwar, J., Interaction of Oleic Acid with Dipalmitoylphosphatidylcholine (DPPC) Bilayers Simulated by Molecular Dynamics. *J. Phys. Chem. B* **2007,** *111* (44), 12748-12755.

63. Ngo, V. A.; Kalia, R. K.; Nakano, A.; Vashishta, P., Molecular Mechanism of Flip-Flop in Triple-Layer Oleic-Acid Membrane: Correlation between Oleic Acid and Water. *J. Phys. Chem. B* **2012,** *116* (45), 13416-13423.

64. Cerezo, J.; Zúñiga, J.; Bastida, A.; Requena, A.; Cerón-Carrasco, J. P., Atomistic Molecular Dynamics Simulations of the Interactions of Oleic and 2-Hydroxyoleic Acids with Phosphatidylcholine Bilayers. *J. Phys. Chem. B* **2011,** *115* (40), 11727-11738.

65. King, D. T.; Warren, D. B.; Pouton, C. W.; Chalmers, D. K., Using Molecular Dynamics to Study Liquid Phase Behavior: Simulations of the Ternary Sodium Laurate/Sodium Oleate/Water System. *Langmuir* **2011,** *27* (18), 11381-11393.

66. Janke, J. J.; Bennett, W. F. D.; Tieleman, D. P., Oleic Acid Phase Behavior from Molecular Dynamics Simulations. *Langmuir* **2014,** *30* (35), 10661-10667.

67. Hossain, M. S.; Berg, S.; Bergström, C. A. S.; Larsson, P., Aggregation Behavior of Medium Chain Fatty Acids Studied by Coarse-Grained Molecular Dynamics Simulation. *AAPS PharmSciTech* **2019,** *20* (2), 61.

68. Knecht, V.; Mark, A. E.; Marrink, S. J., Phase Behavior of a Phospholipid/Fatty Acid/Water Mixture Studied in Atomic Detail. *J. Am. Chem. Soc.* **2006,** *128* (6), 2030-2034.

69. Warren, D. B.; Chalmers, D. K.; Pouton, C. W., Structure and Dynamics of Glyceride Lipid Formulations, with Propylene Glycol and Water. *Mol. Pharm.* **2009,** *6* (2), 604-614.

70. Warren, D. B.; King, D.; Benameur, H.; Pouton, C. W.; Chalmers, D. K., Glyceride Lipid Formulations: Molecular Dynamics Modeling of Phase Behavior During Dispersion and Molecular Interactions Between Drugs and Excipients. *Pharm. Res.* **2013,** *30* (12), 3238-3253.

71. Birru, W. A.; Warren, D. B.; Han, S.; Benameur, H.; Porter, C. J. H.; Pouton, C. W.; Chalmers, D. K., Computational Models of the Gastrointestinal Environment. 2. Phase Behavior and Drug Solubilization Capacity of a Type I Lipid-Based Drug Formulation after Digestion. *Mol. Pharm.* **2017,** *14* (3), 580-592.

72. Kossena, G. A.; Charman, W. N.; Boyd, B. J.; Dunstan, D. E.; Porter, C. J. H., Probing Drug Solubilization Patterns in the Gastrointestinal Tract after Administration of Lipid-Based Delivery Systems: A Phase Diagram Approach. *J. Pharm. Sci.* **2004,** *93* (2), 332-348.

73. Larsson, P.; Alskär, L. C.; Bergström, C. A. S., Molecular Structuring and Phase Transition of Lipid-Based Formulations upon Water Dispersion: A Coarse-Grained Molecular Dynamics Simulation Approach. *Mol. Pharm.* **2017,** *14* (12), 4145-4153.

74. Marrink, S. J.; Risselada, H. J.; Yefimov, S.; Tieleman, D. P.; de Vries, A. H., The MARTINI Force Field: Coarse Grained Model for Biomolecular Simulations. *J. Phys. Chem. B* **2007,** *111* (27), 7812-7824.

75. Benson, S. P.; Pleiss, J., Molecular Dynamics Simulations of Self-Emulsifying Drug-Delivery Systems (SEDDS): Influence of Excipients on Droplet Nanostructure and Drug Localization. *Langmuir* **2014,** *30* (28), 8471-8480.

76. Warren, D. B.; McPhee, E.; Birru, W. A.; Benameur, H.; Chalmers, D. K.; Pouton, C. W., Location of Solvated Probe Molecules Within Nonionic Surfactant Micelles Using Molecular Dynamics. *J. Pharm. Sci.* **2019,** *108* (1), 205-213.

77. Sinko, P. J.; Singh, Y., Martin's Physical Pharmacy and Pharmaceutical Sciences: Physical Chemical and Biopharmaceutical Principles in the Pharmaceutical Sciences. Walter Kluer: 2011.

78. Moghaddasi, F.; Housaindokht, M. R.; Darroudi, M.; Bozorgmehr, M. R.; Sadeghi, A., Soybean Oil-Based Nanoemulsion Systems in Absence and Presence of Curcumin: Molecular Dynamics Simulation Approach. *J. Mol. Liq.* **2018,** *264*, 242-252.

79. Mobasheri, M.; Attar, H.; Rezayat Sorkhabadi, S. M.; Khamesipour, A.; Jaafari, M. R., Solubilization Behavior of Polyene Antibiotics in Nanomicellar System: Insights from Molecular Dynamics Simulation of the Amphotericin B and Nystatin Interactions with Polysorbate 80. *Molecules* **2015,** *21* (1), 6.

80. Suys, E. J. A.; Warren, D. B.; Pham, A. C.; Nowell, C. J.; Clulow, A. J.; Benameur, H.; Porter, C. J. H.; Pouton, C. W.; Chalmers, D. K., A Nonionic Polyethylene Oxide (PEO) Surfactant Model: Experimental and Molecular Dynamics Studies of Kolliphor EL. *J. Pharm. Sci.* **2019,** *108* (1), 193-204.

81. Kozlowska, M.; Rodziewicz, P.; Utesch, T.; Mroginski, M. A.; Kaczmarek-Kedziera, A., Solvation of Diclofenac in Water from Atomistic Molecular Dynamics Simulations – Interplay between Solute–Solute and Solute–Solvent Interactions. *Phys. Chem. Chem. Phys.* **2018,** *20* (13), 8629-8639.

82. Ghattas, M. A.; Bryce, R. A.; Al Rawashdah, S.; Atatreh, N.; Zalloum, W. A., Comparative Molecular Dynamics Simulation of Aggregating and Non-Aggregating Inhibitor Solutions: Understanding the Molecular Basis of Promiscuity. *ChemMedChem* **2018,** *13* (6), 500-506.

83. Kasimova, A. O.; Pavan, G. M.; Danani, A.; Mondon, K.; Cristiani, A.; Scapozza, L.; Gurny, R.; Möller, M., Validation of a Novel Molecular Dynamics Simulation Approach for Lipophilic Drug Incorporation into Polymer Micelles. *J. Phys. Chem. B* **2012,** *116* (14), 4338-4345.

84. Omolo, C. A.; Kalhapure, R. S.; Agrawal, N.; Rambharose, S.; Mocktar, C.; Govender, T., Formulation and Molecular Dynamics Simulations of a Fusidic Acid Nanosuspension for Simultaneously Enhancing Solubility and Antibacterial Activity. *Mol. Pharm.* **2018,** *15* (8), 3512-3526.

85. Xiang, T.-X.; Anderson, B. D., Molecular Dynamics Simulation of Amorphous Hydroxypropylmethylcellulose and Its Mixtures With Felodipine and Water. *J. Pharm. Sci.* **2017,** *106* (3), 803-816.

86. Xiang, T.-X.; Anderson, B. D., A Molecular Dynamics Simulation of Reactant Mobility in an Amorphous Formulation of a Peptide in Poly(vinylpyrrolidone). *J. Pharm. Sci.* **2004,** *93* (4), 855-876.

87. Xiang, T.-X.; Anderson, B. D., Molecular Dynamics Simulation of Amorphous Indomethacin. *Mol. Pharm.* **2012,** *10* (1), 102-114.

88. Xiang, T.-X.; Anderson, B. D., Molecular Dynamics Simulation of Amorphous Indomethacin-Poly(vinylpyrrolidone) Glasses: Solubility and Hydrogen Bonding Interactions. *J. Pharm. Sci.* **2013,** *102* (3), 876-891.

89. Xiang, T.-X.; Anderson, B. D., Distribution and Effect of Water Content on Molecular Mobility in Poly(vinylpyrrolidone) Glasses: A Molecular Dynamics Simulation. *Pharm. Res.* **2005,** *22* (8), 1205-1214.

90. Xiang, T.-X.; Anderson, B. D., Molecular Dynamics Simulation of Amorphous Hydroxypropyl-Methylcellulose Acetate Succinate (HPMCAS): Polymer Model Development, Water Distribution, and Plasticization. *Mol. Pharm.* **2014,** *11* (7), 2400-2411.

91. Xiang, T.-X.; Anderson, B. D., Effects Of Molecular Interactions On Miscibility And Mobility Of Ibuprofen In Amorphous Solid Dispersions With Various Polymers. *J. Pharm. Sci.* **2019,** *108* (1), 178-186.

92. Cascella, M.; Vanni, S., Toward Accurate Coarse-Graining Approaches for Protein and Membrane Simulations. In *Chemical Modelling* 2015; pp 1-52.

93 Tieleman, D. P.; MacCallum, J. L.; Ash, W. L.; Kandt, C.; Xu, Z.; Monticelli, L., Membrane Protein Simulations with a United-Atom Lipid and All-Atom Protein Model: Lipid–Protein Interactions, Side Chain Transfer Free Energies and Model Proteins. *J. Phys. Condens. Matter* **2006,** *18* (28), S1221-S1234.

94. Buch, I.; Harvey, M. J.; Giorgino, T.; Anderson, D. P.; De Fabritiis, G., High-Throughput All-Atom Molecular Dynamics Simulations Using Distributed Computing. *J. Chem. Inf. Model.* **2010,** *50* (3), 397-403.

95. Chandrasekhar, I.; Kastenholz, M.; Lins, R. D.; Oostenbrink, C.; Schuler, L. D.; Tieleman, D. P.; van Gunsteren, W. F., A Consistent Potential Energy Parameter Set for Lipids: Dipalmitoylphosphatidylcholine as a Benchmark of the GROMOS96 45A3 Force Field. *Eur. Biophys. J.* **2003,** *32* (1), 67-77.

96. Chandrasekhar, I.; Oostenbrink, C.; van Gunsteren, W. F., Simulating the Physiological Phase of Hydrated DPPC Bilayers: The Ester Moiety. *Soft Mater.* **2004,** *2* (1), 27-45.

97. Daura, X.; Mark, A. E.; Van Gunsteren, W. F., Parametrization of Aliphatic CHn United Atoms of GROMOS96 Force Field. *J. Comput. Chem.* **1998,** *19* (5), 535-547.

98. Hermans, J.; Berendsen, H. J. C.; Van Gunsteren, W. F.; Postma, J. P. M., A Consistent Empirical Potential for Water–Protein Interactions. *Biopolymers* **1984,** *23* (8), 1513-1518.

99. Lins, R. D.; Hünenberger, P. H., A New GROMOS Force Field for Hexopyranose-Based Carbohydrates. *J. Comput. Chem.* **2005,** *26* (13), 1400-1412.

100. Oostenbrink, C.; Villa, A.; Mark, A. E.; Van Gunsteren, W. F., A biomolecular force field based on the free enthalpy of hydration and solvation: The GROMOS Force-Field Parameter Sets 53A5 and 53A6. *J. Comput. Chem.* **2004,** *25* (13), 1656-1676.

101. Schmid, N.; Eichenberger, A. P.; Choutko, A.; Riniker, S.; Winger, M.; Mark, A. E.; van Gunsteren, W. F., Definition and Testing of the GROMOS Force-Field Versions 54A7 and 54B7. *Eur. Biophys. J.* **2011,** *40* (7), 843.

102. Schuler, L. D.; Daura, X.; van Gunsteren, W. F., An Improved GROMOS96 Force Field for Aliphatic Hydrocarbons in the Condensed Phase. *J. Comput. Chem.* **2001,** *22* (11), 1205-1218.

103. Scott, W. R. P.; Hünenberger, P. H.; Tironi, I. G.; Mark, A. E.; Billeter, S. R.; Fennen, J.; Torda, A. E.; Huber, T.; Krüger, P.; van Gunsteren, W. F., The GROMOS Biomolecular Simulation Program Package. *J. Phys. Chem. A* **1999,** *103* (19), 3596-3607.

104. Soares, T. A.; Hünenberger, P. H.; Kastenholz, M. A.; Kräutler, V.; Lenz, T.; Lins, R. D.; Oostenbrink, C.; van Gunsteren, W. F., An Improved Nucleic Acid Parameter Set for the GROMOS Force Field. *J. Comput. Chem.* **2005,** *26* (7), 725-737.

105. Fuchs, P. F. J.; Hansen, H. S.; Hünenberger, P. H.; Horta, B. A. C., A GROMOS Parameter Set for Vicinal Diether Functions: Properties of Polyethyleneoxide and Polyethyleneglycol. *J. Chem. Theory Comput.* **2012,** *8* (10), 3943-3963.

106. Horta, B. A. C.; Fuchs, P. F. J.; van Gunsteren, W. F.; Hünenberger, P. H., New Interaction Parameters for Oxygen Compounds in the GROMOS Force Field: Improved Pure-Liquid and Solvation Properties for Alcohols, Ethers, Aldehydes, Ketones, Carboxylic Acids, and Esters. *J. Chem. Theory Comput.* **2011,** *7* (4), 1016-1031.

107. Horta, B. A. C.; Merz, P. T.; Fuchs, P. F. J.; Dolenc, J.; Riniker, S.; Hünenberger, P. H., A GROMOS-Compatible Force Field for Small Organic Molecules in the Condensed Phase: The 2016H66 Parameter Set. *J. Chem. Theory Comput.* **2016,** *12* (8), 3825-3850.

108. Winger, M.; de Vries, A. H.; van Gunsteren, W. F., Force-Field Dependence of the Conformational Properties of α, ω-Dimethoxypolyethylene Glycol. *Mol. Phys.* **2009,** *107* (13), 1313-1321.

109. Kalepu, S.; Manthina, M.; Padavala, V., Oral Lipid-Based Drug Delivery Systems – An Overview. *Acta Pharm. Sin. B.* **2013,** *3* (6), 361-372.

110. Matsuura, H.; Fukuhara, K., Conformational Analysis of Poly(oxyethylene) Chain in Aqueous Solution as a Hydrophilic Moiety of Nonionic Surfactants. *J. Mol. Struct.* **1985,** *126*, 251-260.

111. Bedrov, D.; Pekny, M.; Smith, G. D., Quantum-Chemistry-Based Force Field for 1,2-Dimethoxyethane and Poly(ethylene oxide) in Aqueous Solution. *J. Phys. Chem. B* **1998,** *102* (6), 996-1001.

112. Senac, C.; Urbach, W.; Kurtisovski, E.; Hünenberger, P. H.; Horta, B. A. C.; Taulier, N.; Fuchs, P. F. J., Simulating Bilayers of Nonionic Surfactants with the GROMOS-Compatible 2016H66 Force Field. *Langmuir* **2017,** *33* (39), 10225-10238.

113. Warren, D. B.; McPhee, E.; Birru, W. A.; Benameur, H.; Chalmers, D. K.; Pouton, C. W., Improvement in the Predicted Partitioning of Alcohol and Polyethylene Oxide Groups between Water and Octanol (logP) in Molecular Dynamics Simulations. *J. Pharm. Sci.* **2019,** *108* (1), 214-222.

114. Guruge, A. G.; Warren, D. B.; Benameur, H.; Pouton, C. W.; Chalmers, D. K., Aqueous Phase Behavior of the PEO-Containing Non-Ionic Surfactant $C_{12}E_6$: A Molecular Dynamics Simulation Study. *J. Colloid Interface Sci.* **2021,** *588*, 257-268.

115. Mitchell, D. J.; Tiddy, G. J. T.; Waring, L.; Bostock, T.; McDonald, M. P., Phase Behaviour of Polyoxyethylene Surfactants with Water. Mesophase Structures and Partial Miscibility (cloud points). *J. Chem. Soc., Faraday Trans. 1* **1983,** *79* (4), 975-1000.

116. Ingólfsson, H. I.; Lopez, C. A.; Uusitalo, J. J.; de Jong, D. H.; Gopal, S. M.; Periole, X.; Marrink, S. J., The Power of Coarse Graining in Biomolecular Simulations. *Wiley Interdiscip. Rev. Comput. Mol. Sci.* **2014,** *4* (3), 225-248.

117. Takada, S., Coarse-Grained Molecular Simulations of Large Biomolecules. *Curr. Opin. Struct. Biol.* **2012,** *22* (2), 130-137.

118. El Hage, K.; Hedin, F.; Gupta, P. K.; Meuwly, M.; Karplus, M., Valid Molecular Dynamics Simulations of Human Hemoglobin Require a Surprisingly Large Box Size. *Elife* **2018**, *7*, e35560.

119. Geng, H.; Chen, F.; Ye, J.; Jiang, F., Applications of Molecular Dynamics Simulation in Structure Prediction of Peptides and Proteins. *Comput. Struct. Biotechnol. J.* **2019**, *17*, 1162-1170.

120. Okabe, T.; Kawata, M.; Okamoto, Y.; Mikami, M., Replica-Exchange Monte Carlo Method for the Isobaric–Isothermal Ensemble. *Chem. Phys. Lett.* **2001,** *335* (5), 435-439.

121. Barducci, A.; Bonomi, M.; Parrinello, M., Metadynamics. *Wiley Interdiscip. Rev. Comput. Mol. Sci.* **2011,** *1* (5), 826-843.

122. Malde, A. K.; Zuo, L.; Breeze, M.; Stroet, M.; Poger, D.; Nair, P. C.; Oostenbrink, C.; Mark, A. E., An Automated Force Field Topology Builder (ATB) and Repository: Version 1.0. *J. Chem. Theory Comput.* **2011,** *7* (12), 4026-4037.

123. Schuttelkopf, A. W.; van Aalten, D. M. F., PRODRG: A Tool for High-Throughput Crystallography of Protein-Ligand Complexes. *Acta Crystallogr. D* **2004,** *60* (8), 1355-1363.

124. Vanommeslaeghe, K.; MacKerell, A. D., Automation of the CHARMM General Force Field (CGenFF) I: Bond Perception and Atom Typing. *J. Chem. Inf. Model.* **2012,** *52* (12), 3144-3154.

125. Vanommeslaeghe, K.; Raman, E. P.; MacKerell, A. D., Automation of the CHARMM General Force Field (CGenFF) II: Assignment of Bonded Parameters and Partial Atomic Charges. *J. Chem. Inf. Model.* **2012,** *52* (12), 3155-3168.

126. Zoete, V.; Cuendet, M. A.; Grosdidier, A.; Michielin, O., SwissParam: A fast force field generation tool for small organic molecules. *J. Comput. Chem.* **2011,** *32* (11), 2359-2368.

127. Anandakrishnan, R.; Drozdetski, A.; Walker, Ross C.; Onufriev, Alexey V., Speed of Conformational Change: Comparing Explicit and Implicit Solvent Molecular Dynamics Simulations. *Biophys. J.* **2015,** *108* (5), 1153-1164.

128. Tang, X.; Huston, K. J.; Larson, R. G., Molecular Dynamics Simulations of Structure–Property Relationships of Tween 80 Surfactants in Water and at Interfaces. *J. Phys. Chem. B* **2014,** *118* (45), 12907-12918.

129. Shinoda, W.; DeVane, R.; Klein, M. L., Multi-property Fitting and Parameterization of a Coarse Grained Model for Aqueous Surfactants. *Mol. Simul.* **2007,** *33* (1-2), 27-36.

Chapter 3

Aqueous Phase Behavior of the PEO-Containing Non-Ionic Surfactant $C_{12}E_6$: A Molecular Dynamics Simulation Study

Non-ionic surfactants with polyethylene oxide (PEO) such as polysorbates (Tweens) and polyoxyl castor oils (Kolliphors) are widely used in LBFs as excipients. Thus, these surfactants play a critical role in LBFs. PEO surfactants form various colloidal systems in the aqueous environment and their phase behaviors are important for determining the fate of drug formulations in the gastrointestinal tract. Thus, to perform a better prediction, adequate modelling of the PEO surfactants through MD simulation is essential. However, the literature provides shreds of evidence that the GROMOS force field failed to model PEO molecules due to poor parameterization for oxy-functional groups and vicinal ethylene oxide groups.

At the time my PhD began, there were two force fields available in the literature: 2016H66, which was designed to model the gauche effect of PEO chains, and $53A6_{DBW,}$ which was designed to model proper interactions with water and ethylene oxide chains. However, there was no information regarding how well these two force fields model the PEO molecules in different colloidal systems. Thus, to test how efficiently two force fields, 2016H66 and $53A6_{DBW}$ model the aqueous phase behavior of PEO surfactant, we performed extensive MD simulations in micellar, hexagonal, lamellar, solid, liquid surfactants and phase-separated regions in the $C_{12}E_6$ phase diagram and we compared the simulated data with experimental measurements. The findings in this chapter facilitate us to select the most suitable force field to model PEO in our future work.

This chapter is the published article:

Guruge, A. G.; Warren, D. B.; Benameur, H.; Pouton, C. W.; Chalmers, D. K., Aqueous phase behavior of the PEO-containing non-ionic surfactant $C_{12}E_6$: A molecular dynamics simulation study. *J. Colloid Interface Sci.* **2021,** *588*, 257-268.

Journal of Colloid and Interface Science 588 (2021) 257–268

Contents lists available at ScienceDirect

Journal of Colloid and Interface Science

journal homepage: www.elsevier.com/locate/jcis

Regular Article

Aqueous phase behavior of the PEO-containing non-ionic surfactant $C_{12}E_6$: A molecular dynamics simulation study

Amali G. Guruge [a], Dallas B. Warren [b], Hassan Benameur [c], Colin W. Pouton [b], David K. Chalmers [a,*]

[a] Medicinal Chemistry Monash Institute of Pharmaceutical Sciences, Monash University, 381 Royal Parade, Parkville, Victoria 3052, Australia
[b] Drug Delivery, Disposition and Dynamics, Monash Institute of Pharmaceutical Sciences, Monash University, 381 Royal Parade, Parkville, Victoria 3052, Australia
[c] Oral Drug Delivery Innovation, Chemical Division, Lonza, Strasbourg, France

GRAPHICAL ABSTRACT

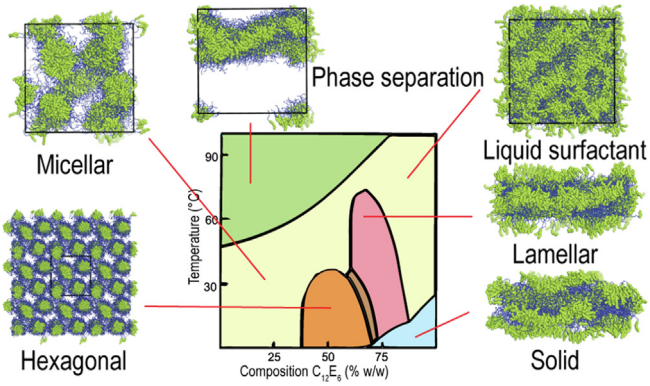

ARTICLE INFO

Article history:
Received 8 June 2020
Revised 9 December 2020
Accepted 10 December 2020
Available online 17 December 2020

Keywords:
Molecular dynamics simulation
Non-ionic surfactant
Colloids
Liquid phase behavior
Polyethylene oxide
Aqueous phase behavior

ABSTRACT

Hypothesis: Non-ionic surfactants containing polyethylene oxide (PEO) chains are widely used in drug formulations, cosmetics, paints, textiles and detergents. High quality molecular dynamics models for PEO surfactants can give us detailed, atomic-scale information about the behavior of surfactant/water mixtures.

Simulations: We used two molecular dynamics force fields (FFs), 2016H66 and $53A6_{DBW}$, to model the simple non-ionic PEO surfactant, hexaoxyethylene dodecyl ether ($C_{12}E_6$). We investigated surfactant/water mixtures that span the phase diagram of starting from randomly distributed arrangements. In some cases, we also started with prebuilt, approximate models. The simulations results were compared with the experimentally observed phase behavior.

Findings: Overall, this study shows that the spontaneous self-assembly of PEO non-ionic surfactants into different colloidal structures can be accurately modeled with MD simulations using the 2016H66 FF although transitions to well-formed hexagonal phase are slow. Of the two FFs investigated, the 2016H66 FF better reproduces the experimental phase behavior across all regions of the $C_{12}E_6$/water phase diagram.

* Corresponding author.
E-mail address: david.chalmers@monash.edu (D.K. Chalmers).

https://doi.org/10.1016/j.jcis.2020.12.032
0021-9797/

1. Introduction

Polyethylene oxide (PEO) or polyethylene glycol surfactants are the largest and most diverse group of non-ionic surfactants [1]. Due to their favorable physicochemical properties and generally low toxicity, PEO surfactants are used widely, having applications in detergents, textiles, paints, cosmetics and the pharmaceutical industry. In our research, we are interested in use of PEO surfactants as excipients in drug formulations, and particularly in lipid-based pharmaceutical formulations [2–4], where they may be used in combination with oils and cosolvents to solubilize poorly water-soluble drugs for oral delivery. To better understand the physicochemical properties of PEO surfactants and to improve these formulations, we would like to use the computational method of molecular dynamics (MD) simulation to create detailed models of drug formulations containing non-ionic surfactants and their interactions with the biological environment [5–10].

Many of the PEO surfactants used in pharmaceutical formulations, for example the polysorbates (Tween®) and polyoxyl castor oils (Kolliphor®), have complex heterogeneous compositions that can vary between batch and manufacturer [11]. This heterogeneity presents problems for molecular dynamics studies that seek to establish the relationships between the physicochemical behavior of a surfactant and its structure because the precise chemical nature of the surfactant material is unclear. In order to avoid this problem, we have chosen to study PEO alkyl ether surfactants which can be obtained as pure, well characterized materials. These surfactants consist of a linear alkyl chain and short PEO head-group and are abbreviated as C_iE_j, where *i* denotes the number of carbon atoms in the aliphatic tail of the surfactant and *j* denotes the number of ethylene oxide (EO) moieties in the head group.

Extensive analyses of C_iE_j surfactants are available in the literature. Experimental studies have measured the different properties of C_iE_j systems including the size and shape of micelles [12–17], cloud curves [18], surface and thermodynamic properties [19], dissolution rates [20] and density [21,22]. Hexaoxyethylene dodecyl ether (alternately polyoxyethylene 6 lauryl ether or $C_{12}E_6$) is a medium-sized member of the C_iE_j family and is shown in Fig. 1

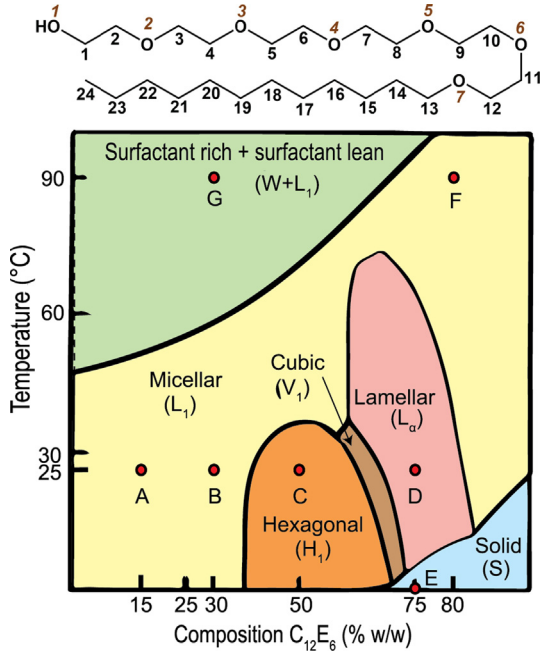

Fig. 1. Chemical structure of $C_{12}E_6$ and the phase diagram23 of the $C_{12}E_6$/water system. MD simulations were performed at points A-G.

with the atom numbering used in this paper. The experimental phase diagram for the $C_{12}E_6$/water system derived by Mitchell et al. [23] is also shown. When $C_{12}E_6$ surfactants are introduced to water in low concentrations, below the critical micelle concentration of 0.067 mM [24], the surfactant molecules remain as monomers. Further addition of the surfactant results in spontaneous aggregation into a rich variety of stable, self-assembled structures [25]. At dilute concentrations, just above the CMC, spherical micelles are present. In the mid-concentration range, hexagonal (H_1), cubic (V_1) and lamellar (L_α) regions can be seen. Increasing the temperature of a $C_{12}E_6$/water system leads to the dehydration of the PEO chains and, once the temperature passes the cloud point, the surfactant is no longer soluble and the solution becomes visually turbid. Above the cloud point, two phases are present; surfactant-rich phase and surfactant-lean phase [26]. This region is denoted as W + L_1 in the phase diagram. This system has broader colloidal regions compared to the phase diagrams of others in the C_iE_j family.

In this work, we aimed to use MD simulations to study the complex phase behavior of $C_{12}E_6$ and obtain atomic scale information regarding the formation of the different liquid phases. Such high-resolution structural information is difficult to retrieve from experimental investigations. MD simulates the natural motion of molecules in a system over a period of time [27] and accurate MD simulations require a force field (FF) that correctly models the conformational energy of the molecules present in the simulation and the interactions between molecular components. An important factor in the simulation of non-ionic surfactants is correct modelling of the conformational behavior of the PEO chains. At low temperatures, it is found that the dominant conformation around the O—C—C—O bond is gauche, which is known as the 'gauche effect' [28], while the conformation around the C—C—O—C bond favors a trans arrangement. This conformational behavior and the nature of PEO interactions with water molecules are crucial factors that influence the colloidal structure formation of non-ionic PEO surfactants.

In order to maintain consistency with our previous MD studies, we wished to use the GROMOS FF for our simulations. However, the conventional GROMOS FFs are not specifically parameterized for PEO chains, and do not correctly model the gauche effect [29]. Thus, MD simulations using standard GROMOS FFs for molecules containing PEO chains leads to relatively inaccurate computational models. In 2009, Winger et al. investigated the performance of short PEO molecules using the GROMOS FFs; 45A3, 53A6 and 53A6_OE (an extended version of 53A6) [29]. Their study identified a discrepancy between simulations and experimental data for the behavior of PEO chains when they used the 45A3 or 53A6 FFs. These issues were resolved when they used the 53A6_OE FF, which contains modified charge and van der Waals interaction parameters for ether oxygen atoms. In 2011 Horta et al. reported a GROMOS FF parameter set known as $53A6_{OXY}$ [30] for modelling of oxy-functional groups such as alcohols, ethers, aldehydes, ketones, carboxylic acids and esters. They demonstrated that optimization of atomic charges, Lennard-Jones interaction parameters and small adjustments of the covalent bonding parameters gave better agreement with experimental data for molecules with oxy-functional groups. An extension of $53A6_{OXY}$ known as $53A6_{OXY+D}$ was introduced by Fuchs et al. in 2012 [31]. This parameter set reproduced the experimental data for PEO molecules considered in the study, which is an indication of better parameterization for PEO behavior. Later, in 2016, Horta et al. introduced a GROMOS compatible parameter set known as 2016H66 for small organic molecules in the condensed phase [32]. For molecules containing oxy-functional groups or PEO chains, the 2016H66 FF uses the $53A6_{OXY}$ and $53A6_{OXY+D}$ parameters. More recently, Warren et al. introduced a FF named

53A6$_{DBW}$ for straight chain alcohols and short chain PEO molecules [33] which increases the strength of the interactions between water and ethylene oxide chains. This study found that the 53A6$_{DBW\ FF}$ better reproduces experimental octanol/water partition coefficient (logP) values than does the 53A6$_{OXY}$ FF.

A number of MD simulation studies of C_iE_j surfactants are reported in the literature. Several papers have investigated surfactant behavior at single points on the C_iE_j/water phase diagram including investigations of: the dehydration of spherical $C_{12}E_6$ micelles [34], the formation of reverse micelles of $C_{12}E_2$ [35] and $C_{12}E_4$ [36], the influence of added salt on self-assembled C_6E_6 micelles [37] the structure of the lamellar phase of $C_{12}E_2$ [38] and characterizing the effect of 1-hexanol on $C_{12}E_{10}$ micelles [39]. Recently, the 2016H66 FF was used to investigate single compositions in the lamellar regions of $C_{12}E_2$, $C_{12}E_3$, $C_{12}E_4$, $C_{12}E_5$ and $C_{14}E_4$ [40]. Some more comprehensive MD studies have investigated multiple points in the phase diagrams of C_iE_j surfactants including: phase transitions from sphere to rod in $C_{12}E_5$ [41] and $C_{12}E_6$ [42], and the lamellar phase of $C_{12}E_5$ [43]. A coarse-grained MARTINI model was used to study the self-assembly of lamellar, hexagonal and micellar phases of $C_{12}E_2$, $C_{12}E_4$ and $C_{12}E_6$ [44]. Coarse-grained models allow the simulation of longer time-scales with larger molecular systems at the expense of making substantial approximations in the nature of the intermolecular interactions, which are necessary for accurate models. In contrast, united atom models describe the intermolecular interactions with greater fidelity, although these calculations are more computationally expensive.

To date, no studies have attempted to cover the complete phase C_iE_j/water phase diagram using atomistic (united or all-atom) models. Accurate prediction of the complex molecular structures (micellar, hexagonal and lamellar phases) that form within this phase diagram would strongly indicate that the different intra- and intermolecular interactions (van der Waals, covalent, electrostatic, etc.) are correctly modelled by the force field, and would provide confidence that the force field parameters can be transferred to other nonionic PEO surfactants. In this work, we therefore aimed to model the entire phase region using MD simulations to investigate the ability of current molecular mechanics FFs to reproduce the experimentally observed phase behavior. Accordingly, we have performed multiple MD simulations of $C_{12}E_6$/water mixtures covering a wide range of different surfactant/water compositions and temperatures and correlated our simulation data with experimental observations.

2. Methods

2.1. Construction of model systems

All simulated systems contained surfactant and water molecules in a periodic cell. The initial configurations were generated as either random molecular distributions, or approximate models of lamellar or hexagonal phase. Random distributions of $C_{12}E_6$ and water molecules were built using the *random_box* script from the Silico package version 0.14 [45]. The approximate model of hexagonal phase was built in several steps: (1) Four rods of randomly distributed $C_{12}E_6$ surfactant molecules were built with a radius of 3.2 nm and placed in a hexagonal array using the *random_box* script. (2) An initial MD simulation for this system was carried out using semi-isotropic pressure coupling for 150 ns. (3) One resulting elongated rod-like micelle from this simulation was extracted, further equilibrated and used to generate a hexagonal phase containing four surfactant rods in a honeycomb packing [46]. The system was built using the scripts; *mol_rotrans* and *mol_combine* from Silico and *gmx editconf* from the GROMACS package [47,48]. The initial approximate lamellar phase model was constructed using the Silico script *bilayer_builder*. For the study of solid phase at point E (see Fig. 1) the lamellar structure resulting from simulation D^{P}_{H66} (Table 1) was used as the initial structure.

2.2. MD simulations

MD simulations were carried out on high performance computing resources provided by the Multi-modal Australian ScienceS Imaging and Visualisation Environment (MASSIVE) and the National Computational Infrastructure (NCI). All simulations were performed using GROMACS [47,48] version 2016.3 using two GROMOS compatible FFs: 2016H66 [32] and 53A6$_{DBW}$ [33]. MD simulations used the heavy hydrogen atom method, allowing an increased time step of 5 fs. In this method, the mass of hydrogen atoms is increased to 4 AMU and the additional mass of the H atom is balanced by reducing the mass of the attached heavy atom by the same amount [49]. The isothermal-isobaric ensemble (NPT) was used in all simulations. Isotropic pressure coupling was used for the systems with randomly distributed surfactants except the C_{H66}* system. Semi-isotropic coupling was used for the pre-constructed hexagonal and lamellar systems since these structures are anisotropic in nature. Temperature coupling was employed using the velocity rescale algorithm [50] with the temperature set to the appropriate point on phase diagram. A reference pressure of 1 bar and the compressibility of 4.5×10^{-5} bar^{-1} were used for the Berendsen [51] and Parrinello-Rahman [52] algorithms. Water molecules were modelled using the single point charge (SPC) model and constrained with SETTLE algorithm [53]. All other bonds were constrained by the LINCS algorithm [54]. The Verlet cut-off scheme [55] was employed for all simulations with the cut-off distance of 1.4 nm for short-range Coulombic and van der Waals interactions (non-bonded interactions). For long-range coulombic interactions, the particle-mesh Ewald (PME) technique [56] was applied with a grid spacing of 0.12 nm. The following sequential steps were followed for each modelled system.

(1) Energy minimization of 500 steps using the steepest descent method.
(2) Four short simulations were performed:
   (a) Simulation of 5000 steps using a time step of 1 fs and V-rescale temperature coupling of 0.1 ps without pressure coupling.
   (b) Simulation of 10,000 steps using a 2 fs time step and Berendsen pressure coupling with a 2 ps coupling time constant.
   (c) Simulation of 10,000 steps using a 2 fs time step and Parrinello-Rahman pressure coupling with a 2 ps coupling time constant.
   (d) Simulation of 10,000 steps of increased time step (5 fs) with a 2 ps Parrinello-Rahman pressure coupling time constant and 0.1 ps V-rescale temperature coupling time constant.
(3) The generated coordinate file was employed for the production simulation using a 5 fs time step, the Parrinello-Rahman barostat with a 2 ps pressure coupling constant and the V-rescale thermostat with a 0.1 ps coupling constant.

2.3. Simulation analysis

MD trajectories were analyzed using the GROMACS tools and PyMOL was used for visual inspection of the structures and image generation [57]. Molecular aggregation was studied using the Silico script *find_aggregate*, which assigns surfactant molecules into the same aggregate if two carbon atoms are within a cut-off distance 0.4 nm. Surfactants with no neighboring molecules within the

Table 1
Details of MD simulations performed and the structures present at the completion of the simulations.

System[a]	N_{surf}[b]	N_{water}[c]	$C_{12}E_6$[d] (% w/w)	T (°C)[e]	Approx. cell size (nm)	Pcoupl[f]	t_{sim} (ns)[g]	No. agg[h]	Average agg No[i]	Colloidal structure in	
										MD simulation	Experiment[23]
A_{H66}	676	95,871	15	25	15 × 15 × 15	I	500	3	224	Micelles	Micelles
B_{H66}	1353	78,952	30	25			350	6	224	Micelles	Micelles
C_{H66}	2255	56,394	50	25			400	1	–	Rod-like micelles	Hexagonal
D_{H66}	3382	28,197	75	25			500	1	–	Interconnected cylindrical micelles	Lamellar
F_{H66}	3608	22,557	80	90			600	1	–	Interconnected layer-like pattern	Surfactant liquid
G_{H66}	1353	78,952	30	90			200	1	–	Phase separated	Phase separated
A_{DBW}	676	95,871	15	25	15 × 15 × 15	I	300	10	66	Micelles	Micelles
B_{DBW}	1353	78,952	30	25			300	17	78	Micelles	Micelles
C_{DBW}	2255	56,394	50	25			400	11	203	Rod-like micelles	Hexagonal
D_{DBW}	3382	28,197	75	25			400	1	–	Surfactants have started to crystallize	Lamellar
F_{DBW}	3608	22,557	80	90			200	1	–	Interconnected layer-like pattern	Surfactant liquid
G_{DBW}	1353	78,952	30	90			200	1	–	Single wormy micelle	Phase separated
C^{p*}_{H66}	1340	33,511	50	25	12 × 12 × 14	S	300	4	330	Hexagonal	Hexagonal
D^{p}_{H66}	1691	14,098	75	25	18 × 18 × 5		400	1	–	Lamellar	Lamellar
E^{p}_{H66}	1691	14,098	75	0	18 × 18 × 5		400	1	–	Solid surfactant	Solid
C_{H66}*	1340	33,511	50	25	13 × 13 × 11	S	300	1	–	Rod-like micelles	Hexagonal
C^{p}_{DBW}	1340	33,511	50	25	12 × 12 × 14	S	200	4	332	Hexagonal	Hexagonal
D^{p}_{DBW}	1691	14,098	75	25	14 × 14 × 9		400	1	–	Solid (frozen $C_{12}E_6$)	Lamellar

[a] Nature of the system: A-G = point on phase diagram, H66 = 2016H66 FF, DBW = $53A6_{DBW}$ FF, * = simulations have the same composition but differ in starting structure, p = simulation commenced from pre-constructed structure.
[b] Number of $C_{12}E_6$ molecules.
[c] Number of water molecules.
[d] Weight percentage of $C_{12}E_6$.
[e] Simulation temperature.
[f] Pressure coupling: I = isotropic, S = semiisotropic.
[g] Simulation time.
[h] Number of aggregates formed in MD simulation.
[i] Average number of surfactant molecules in each aggregate.

cut-off are classified as single molecules. Radial distribution functions (RDFs), trans dihedral fractions and radii of gyration were calculated using *gmx rdf*, *gmx angle* and *gmx gyrate,* respectively. The last 10 ns of each simulation was used for these calculations. Solvent accessible surface areas (SASA) were calculated over the entire trajectory using *gmx sasa* to confirm the system had reached a stable configuration. The eccentricity of micelles was calculated [58] using the equation; $\varepsilon = 1 - I_{min}/I_{avg}$ where I_{min} is the smallest moment of inertia around the principle axes and I_{avg} is the average of the moments of inertia over the three principle axes. The *gmx gyrate* tool with the *–moi* option was used to compute this property. The potential energy of colloidal structures at point C from random and pre-built starting points was calculated using *gmx energy*. Bilayer thickness in the lamellar region was calculated using GridMAT-MD [59]. The lateral diffusion constants of $C_{12}E_6$ surfactants in the pre-constructed lamellar (point D, Fig. 1) and solid (point E, Fig. 1) structures were calculated using *gmx msd* over the last 100 ns trajectories of these simulations. The average unit cell size of the prebuilt hexagonal structures was calculated by extracting the middle coordinates of the cylinders that are in the hexagonal arrangement. To extract coordinates, 4 nm slice for xy plane from the corner of the simulation box was made using *gmx select* and *gmx editconf*. Then, xy coordinates were graphed and center coordinates in cylinders were extracted through the graph. Note that the graph was prepared enabling the periodic boundaries to illustrate the cylinders in the hexagonal arrangement.

3. Results and discussion

In this work, we wished to investigate whether MD simulations can reproduce the experimentally observed $C_{12}E_6$/water composition and temperature phase diagram. To do this, we performed a series of simulations using the two FFs, 2016H66 and $53A6_{DBW}$. We note that molecular dynamics simulations of phase behavior have a number of potential limitations which must be carefully considered when analyzing simulation results; molecular force fields are approximate, the practically achievable simulation time is short, the size of the simulation cell is small and periodic boundary conditions can introduce artifacts into the observed structure. This work aims to specifically investigate the first point but the subsequent points mean that the observed structures may not represent the true equilibrium structure. However, despite the above limitations, MD simulations can provide a deep insight into the molecular behavior of complex systems. We note that in our efforts to obtain equilibrated models in this work, we have modelled larger systems for longer simulation than have been generally reported in the literature for atomistic surfactant models.

Fig. 1 shows the simulations performed mapped on to the experimental phase diagram. Simulation parameters and the nature of the final colloidal structures formed are given in Table 1. The selected compositions cover the key phase regions: micellar (A and B), hexagonal (C), lamellar (D), solid (E), liquid surfactant (F) and a phase separated system (G). We did not attempt to model the cubic phase region of the $C_{12}E_{6/}$water phase diagram because the experimentally derived lattice parameter for the cubic colloidal structure is 11.8 nm [60], which approaches the size of our simulation cell (15 nm) and therefore the periodic boundary conditions would prevent formation of a regular, cubic structure of these dimensions.

Initially, we investigated whether the experimentally observed colloidal structures at points A, B, C, D, F and G could be achieved by self-assembly from a random distribution of surfactant molecules in water in an accessible amount of simulation time (200–600 ns). After the initial set of simulations, we found that the time

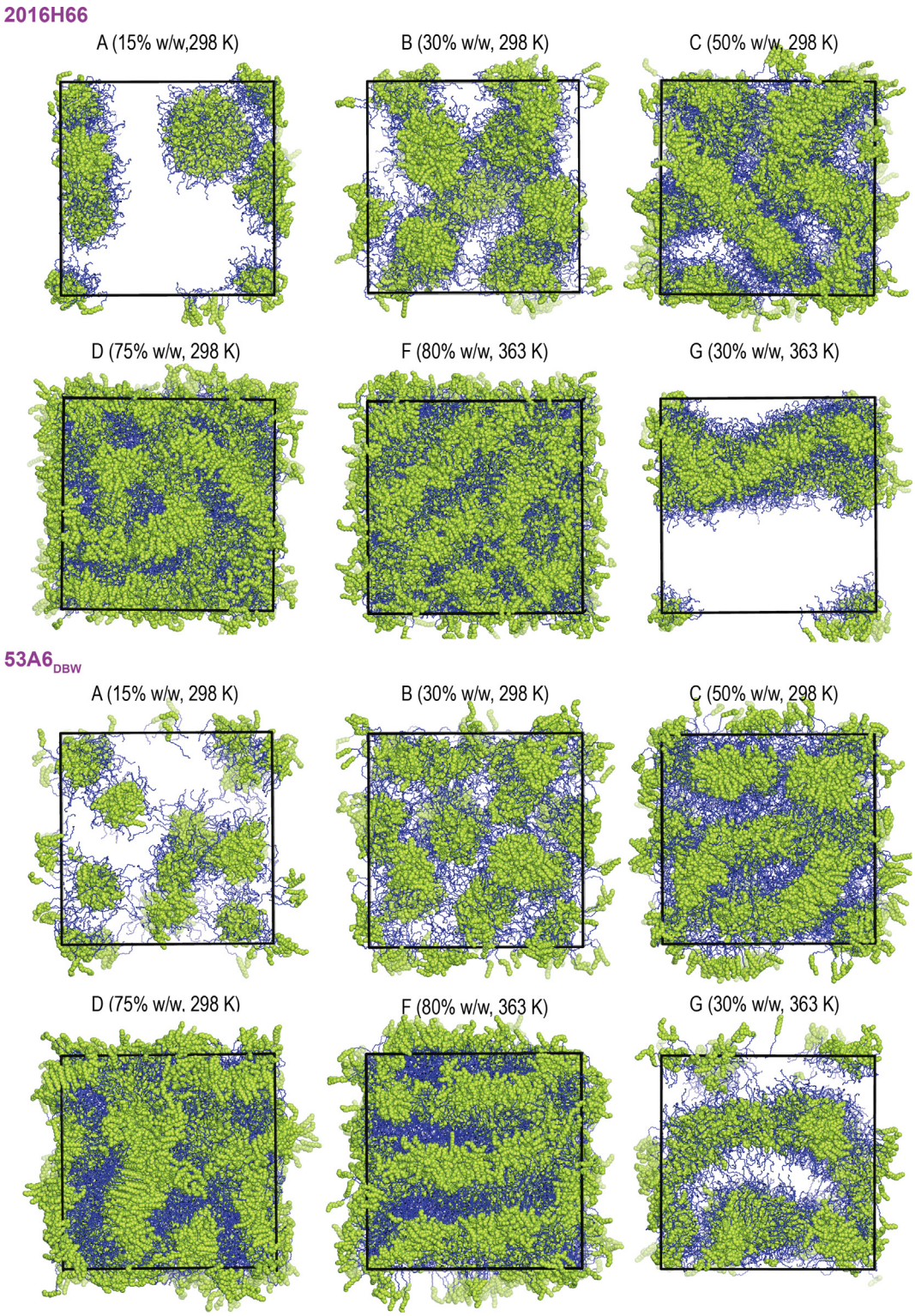

Fig. 2. Colloidal structures of $C_{12}E_6$ at points A–G (Fig. 1) formed in MD simulations using the 2016H66 and 53A6$_{DBW}$ FFs. Simulations commenced from randomly distributed surfactant and water. Surfactant coloring: tail (lime), head group (blue). $C_{12}E_6$ content and simulated temperature are shown in brackets. Box size is approximately 15 × 15 × 15 nm. Water is not shown for clarity. (For interpretation of the references to colour in this figure legend, the reader is referred to the web version of this article.)

required for the assembly of hexagonal (point C) and lamellar (point D) structures is significantly longer than these accessible simulation times, and we therefore performed additional simulations starting from pre-constructed approximate models. The final structures from MD simulations started from random distributions are shown in Fig. 2 and those from pre-built structures are in Fig. 3. Each phase region is discussed in detail below.

3.1. Micellar phase

In the micellar phase region, we performed MD simulations at points A and B using the 2016H66 and 53A6$_{DBW}$ FFs. For each simulation, the SASA was calculated to confirm the system had reached a stable configuration before doing any analysis (Supplementary Information, Fig. S1). The variation in $C_{12}E_6$ SASA in all

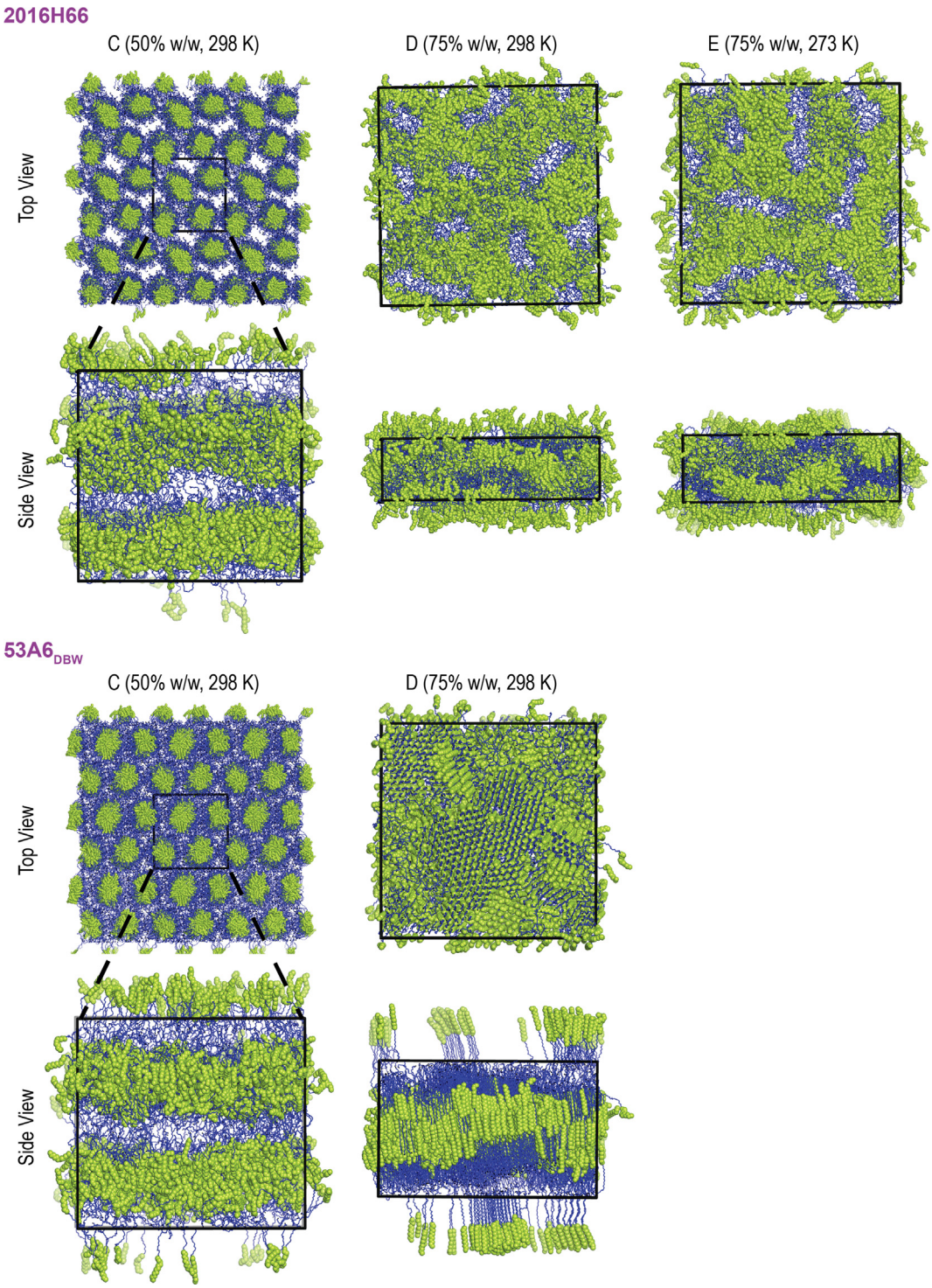

Fig. 3. Top and side views of final colloidal structures formed in MD simulations started from pre-constructed approximate structures at points C, D and E (Fig. 1) with the 2016H66 and 53A6$_{DBW}$ FFs. Surfactant coloring: tail (lime), head group (blue). $C_{12}E_6$ content and simulated temperature are shown in brackets. Box sizes: point C: 12 × 12 × 14 nm; points D and E with 2016H66 FF: 18 × 18 × 5 nm; point D with 53A6$_{DBW}$ FF: 14 × 14 × 9. Water is not shown for clarity. (For interpretation of the references to colour in this figure legend, the reader is referred to the web version of this article.)

four systems (A_{H66}, B_{H66}, A_{DBW} and B_{DBW}) was within ±2% for the last 100 ns of the simulation (see Table S1). The spontaneous evolution of the A_{H66} system over 500 ns is shown in Fig. S2 in the Supplementary Information. At the completion of the simulations, three aggregates were present in the A_{H66} system, six aggregates in the B_{H66} system, ten aggregates in the A_{DBW} system and seventeen aggregates in the B_{DBW} system (Table 1). Therefore, the 2016H66 produced larger aggregates than 53A6$_{DBW}$. Visual inspection of micelles in simulations A_{H66} and B_{H66} shows the presence of rod-like and non-spherical micelles. In contrast, simulations A_{DBW} and B_{DBW} produced only spherical micelles. This is confirmed by the ratios of the principal moments of inertia (I_1/I_2, I_1/I_3 and I_2/I_3), the eccentricity (ε) and the radii of gyration (R_g) (Table S2). All eccentricity values are close to 1 for the systems A_{DBW} and B_{DBW},

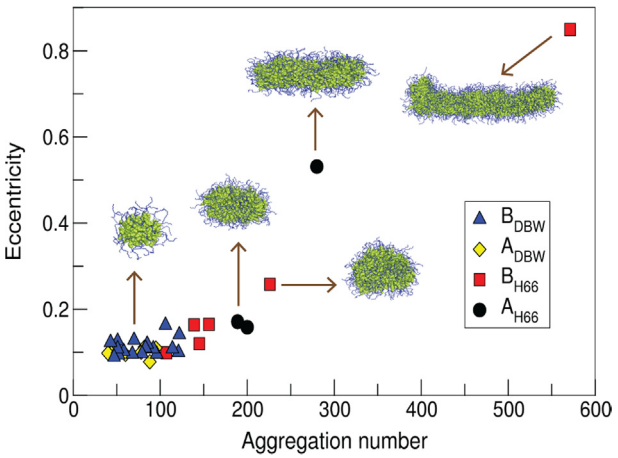

Fig. 4. Eccentricity of micelles plotted against the aggregation number for micelles taken from simulations at points A and B (Fig. 1) using the 2016H66 and 53A6$_{DBW}$ FFs. The structures of the micelles at selected points are shown. Surfactant coloring: tail (lime), head group (blue). (For interpretation of the references to colour in this figure legend, the reader is referred to the web version of this article.)

indicating that the micelles are spherical, while the eccentricity values in A_{H66} and B_{H66} systems indicates that micelles start to elongate as aggregation number increases. Fig. 4 shows how the micelle shapes vary with the aggregation number for micelles formed with the two FFs at points A and B.

To analyze the internal structural properties of the micelles formed by the two FFs, we computed the radial distribution functions (RDFs) for simulations for a selection of $C_{12}E_6$ atoms (Fig. 5). The radial distribution function, $g(r)$, describes the relative probability of finding an atom at distance r from another atom. This probability value is directly related to the free energy of interaction between the two atoms. Thus, $g(r)$ can be used to characterize the interactions between atom types in a simulation. The main atom pairs used in our analysis were selected to be: EO chain oxygen atoms (O1-O1, O4-O4 and O7-O7), EO chain and water oxygen atoms (O1-OW, O4-OW and O7-OW), and carbon atoms in the surfactant tail (C13-C13, C18-C18 and C24-C24). Fig. 5 shows that the RDFs vary with the concentration and FF. In all cases, the interactions between ether oxygens (O to O) and alkyl carbons (C to C) are stronger with the 2016H66 FF which can be seen as intense peaks in the O—O and C—C RDF graphs. In both FFs, the strongest

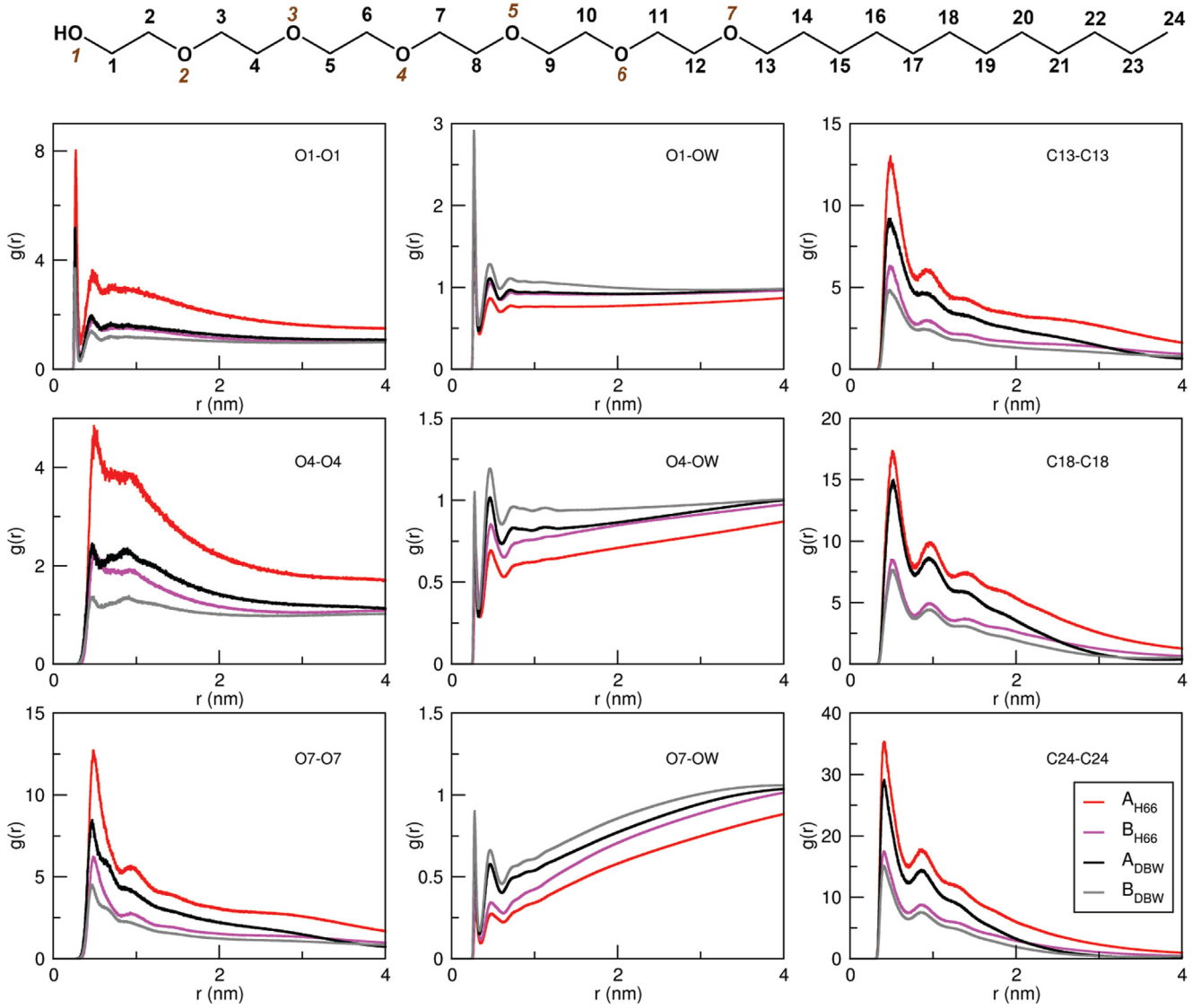

Fig. 5. Radial distribution functions for $C_{12}E_6$/water systems modelled with the 2016H66 and 53A6$_{DBW}$ FFs at points A and B (Fig. 1) in the micellar region. Red/purple: 2016H66 FF, Black/grey: 53A6$_{DBW}$. (For interpretation of the references to colour in this figure legend, the reader is referred to the web version of this article.)

O—O and C—C interactions are found at point A, which has the lowest concentration of $C_{12}E_6$. The strong peak in the O1-O1 RDF graph, around interatomic distance 0.28 nm, corresponds to the formation of a hydrogen bond between O1 hydroxyl groups, which is absent in other O—O RDFs because these are ether oxygens and cannot make hydrogen bonds to each other. On the other hand, the interactions between ether oxygens and water oxygens (O to OW) are stronger in the $53A6_{DBW}$ FF, showing that PEO chain in this FF interacts more strongly with water.

A neutron scattering study conducted by Zulauf et al. derived the aggregation number for $C_{12}E_6$ micelles at several concentrations [16]. This study found that the aggregation number lies in the range 100–200 until the $C_{12}E_6$ concentration reaches 35% w/w. Thus, the average aggregation number obtained using the 2016H66 FF (224 at both points A and B) is in good agreement this study. A coarse grain study [44] of the $C_{12}E_6$ micellar phase (20% w/w $C_{12}E_6$) found the average aggregation number to be much lower, 60 after 10 μs, the result from the current study is therefore encouraging. The size and shape of micelles in $C_{12}E_6$/water systems containing 1−10% w/w surfactant were studied by Gapiński and co-workers [13] using small angle neutron scattering, photon correlation spectroscopy and fluorescence correlation spectroscopy in the temperature range of 10–48 °C. They found that $C_{12}E_6$ forms rod-like micelles with an elliptical cross section. Consistent with this experimental observation, our MD simulations with 15% and 30% w/w $C_{12}E_6$ using 2016H66 formed rod-like micelles. In contrast, although the $53A6_{DBW}$ FF produced micelles, the aggregate number and aggregate shape deviate from experimental observations. A recent study [7] of the PEO surfactant polyethoxylated glycerol triricinoleate, a major component in Kolliphor EL®, at a concentration of 5% w/w also reported the formation of larger aggregates with the 2016H66 FF when compared to $53A6_{DBW}$.

3.2. Hexagonal phase

We tested the ability of the 2016H66 and $53A6_{DBW}$ FFs to form hexagonal phase at point C (Fig. 1). Initially, we ran MD simulations starting from random distributions of $C_{12}E_6$ in water (simulations C_{H66} and C_{DBW}). From these starting conditions, neither FF gave cylindrical micelles that were in a hexagonal lattice (Fig. 2). Both FFs did, however, produce rod-like micelles, although the micelles had no particular arrangement with respect to each other. Apart from the length of the cylindrical micelles formed, there was no significant structural difference in the structures formed by the two FFs. A previous study by Denham et al. [61] using a coarse-grained model also revealed a similar structure formation with 50–55% w/w $C_{12}E_6$ concentration, which they defined as a disordered hexagonal phase. Another MARTINI force field model showed the formation of tubular, periodic $C_{12}E_6$ micelles at 50% w/w $C_{12}E_6$ when started from random distribution when the simulation was run for more than 3 μs [44]. Recently, Grunewald et al. [62] showed the formation of tubular micelles in 50% w/w $C_{12}E_6$ using a MARTINI model in 5 out of 6 simulations and in 3 of the 6 simulations, the packing had hexagonal symmetry indicating an ideal hexagonal phase formation.

To investigate the stability of regularly packed surfactant rods, we then ran simulations using pre-built structures (simulations C^p_{H66} and C^p_{DBW}). We packed four cylindrical micelles into a single simulation cell using a hexagonal spatial arrangement and ran MD simulations. The final structures obtained with the two FFs are shown in Fig. 3. Both FFs maintained the hexagonal phase geometry during the 200 or 300 ns simulation time and did not form the wormy micelles observed in the simulations started from a random distribution.

A significant difference is evident in the behavior of the head groups of the $C_{12}E_6$ surfactants in the two studied FFs. The $53A6_{DBW}$ FF produces cylindrical micelles with head groups that are more open and solvated than 2016H66. To investigate the solvation of the PEO head groups further, we calculated RDFs for the O—O and O—OW atom pairs, which are presented in Fig. 6. As observed for the micelle simulations, the interactions between ether oxygen atoms are stronger with 2016H66, except for the interaction between O1-O1. This could be due to the structural feature we noticed with the head groups in hexagonal phase modelled with $53A6_{DBW}$ where more open (or expanded) head groups enable better hydration around the PEO chain which makes a high probability for O1-O1 interactions. In addition, the interactions between O and OW are strong in $53A6_{DBW}$, which is similar to the behavior of RDFs in the micellar region. The other interesting thing to note regarding the O-OW interactions is the high peak intensities in $53A6_{DBW}$ for the first and the second solvation shells. This clearly indicates the better solvation of PEO with $53A6_{DBW}$ due to the head group arrangement of the surfactant.

To investigate the relative stabilities of the hexagonal and disordered hexagonal phases, we ran an additional simulation ($C_{H66}{}^*$) having an identical composition to simulation C^p_{H66} but started from a random arrangement. Fig. 7(c) shows the total potential energy over the course of the 300 ns simulations. Averaged over the last half of the run, the potential energy of C^p_{H66} was lower in energy by 0.84 kJ/mol per $C_{12}E_6$ molecule, showing that the hexagonal structure is more favorable than the disordered hexagonal structure produced from an initial random arrangement (statistics are reported in Table S4). Fig. 7(d) shows that the hexagonally packed arrangement has greater exposure to solvent than disordered hexagonal.

To further establish that the pre-constructed, hexagonally packed system is an energy minimum, we took the final frame from simulation C^p_{H66} and subjected it to a 'thermal shock' by heating to 47 °C for 100 ns. The system was then returned to 25 °C for an additional 300 ns (see Table S5). On heating, the surfactant rods became thinner, more wormy and were less closely packed. On cooling, the structures returned largely to the original state although some interlinks had formed between rods (Fig. S4b). The system energy and returned to a value that was slightly greater than the original and the SASA returned to a slightly lower value (Fig. S5). These calculations confirm that the prebuilt structure is low energy.

To measure the dimensions of the hexagonal phase unit cell, we extracted coordinates of the cylinder cores through a 2D graph (Fig. 7a and b) and calculated the distances between cylinder centers. The average unit cell size (lattice parameter a) of the hexagonal phase modelled with 2016H66 FF was 6.7 ± 0.9 nm and with $53A6_{DBW}$ FF was 6.4 ± 0.4 nm. This result indicates that the cylinders are packed more closely with $53A6_{DBW}$. X-ray scattering studies performed in the hexagonal region of $C_{12}E_6$ indicates that the size of the unit cell is 5.8–6.0 nm [63,64]. Therefore, the hexagonal structure modelled with $53A6_{DBW}$, which has better solvated PEO groups, is closer to the experimental value, indicating $53A6_{DBW}$ modelled hexagonal phase more accurately. Yet, the averaged unit cell size calculated for the hexagonal structure modelled with 2016H66 FF is also in the range of experimental unit cell size of the hexagonal phase.

3.3. Lamellar phase

To investigate the lamellar phase region (point D, Fig. 1), similar to our simulations of the hexagonal phase region, we performed an initial set of simulations starting from a random distribution of surfactants and water molecules. As shown in Fig. 2, these simulations did not form lamellar phases after 400 ns. Instead, the 2016H66 FF formed disordered, interconnected cylindrical micelles. It is interesting to note that a similar colloidal structure

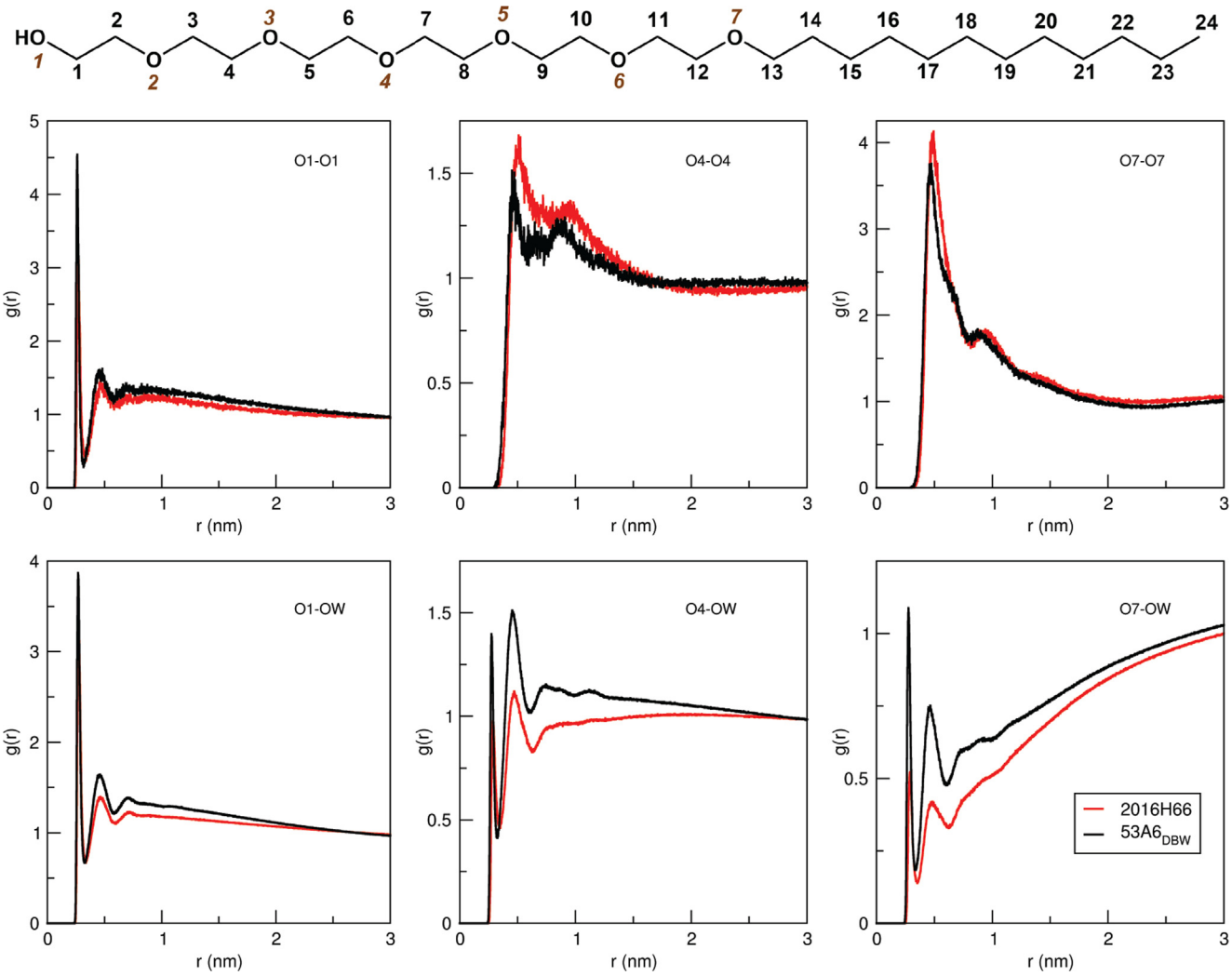

Fig. 6. Radial distribution functions for the $C_{12}E_6$/water system in the hexagonal region at point C (Fig. 1) modelled with the 2016H66 (red) and $53A6_{DBW}$ (black) FFs. (For interpretation of the references to colour in this figure legend, the reader is referred to the web version of this article.)

formation was observed in a previous coarse-grained MD study carried out at the same $C_{12}E_6$ concentration [61]. In contrast, the $53A6_{DBW}$ FF behaved very differently, producing an ordered lattice, indicating that the surfactant has started to crystallize which is in disagreement with the experimental phase diagram.

To investigate the stability of lamellar structures starting from a prebuilt structure, we constructed an approximate lamellar phase and MD simulations were carried out for 400 ns. The colloidal structures formed are shown in Fig. 3. The D_{H66} system remained as a bilayer for a 400 ns period. The D_{DBW} system solidified as we had observed previously and we therefore did not analyze this simulation any further. Visual inspection of the lamellar structure modelled with 2016H66 revealed pores and curved defects in the bilayer. The lamellar phase repeat distance/bilayer thickness, which is commonly used to characterize lamellar systems, was calculated for the pore free area of the D^p_{H66} system using GridMAT-MD, giving an average bilayer thickness of 4.80 ± 0.38 nm. We also calculated the averaged lateral diffusion constant for the D^p_{H66} system in the lamellar region which was found to be $(1.63 \pm 0.09) \times 10^{-7}$ cm^2 s^{-1}. Previous experimental studies found that the lamellar phase of the $C_{12}E_6$/water system contains highly curved defects [65,66] and pores [67], which is reproduced by 2016H66. However, the calculated bilayer thickness is overestimated by 14.3% compared to the experimental bilayer thickness reported in the literature [66,68]. These observations correlate with the previous study by Senac et al. which used 2016H66 for series of C_iE_j surfactants in the lamellar region [40]. Yethiraj et al. have investigated the diffusion of both water and surfactant in hexagonal, cubic, lamellar and micellar regions of $C_{12}E_6$ [69]. They reported the lateral diffusion coefficient for a lamellar system containing 79% w/w of $C_{12}E_6$ at 25 °C as 0.0076, which equates to a lateral diffusion constant of 1.75×10^{-7} cm^2 s^{-1} (calculated by multiplying the diffusion constant of water, 2.2995×10^{-5} cm^2 s^{-1} by 0.0076). Although we calculated the lateral diffusion constant at slightly different composition (75% w/w), it is interesting to note that the reported experimental lateral diffusion constant of $C_{12}E_6$ is close to the value we calculated from the MD simulation. Considering all these facts we discussed in this section, the bilayer modelled with 2016H66 can be considered as a plausible structural model for a real lamellar $C_{12}E_6$/water system.

3.4. Solid phase

We investigated the formation of the solid phase (point E) using 2016H66. To commence the simulations in this region, we used the colloidal structure formed in the D^p_{H66} system. Since the D^p_{DBW} crystallized, we did not run simulations with $53A6_{DBW}$ FF as this system would simply form the same crystallized structure.

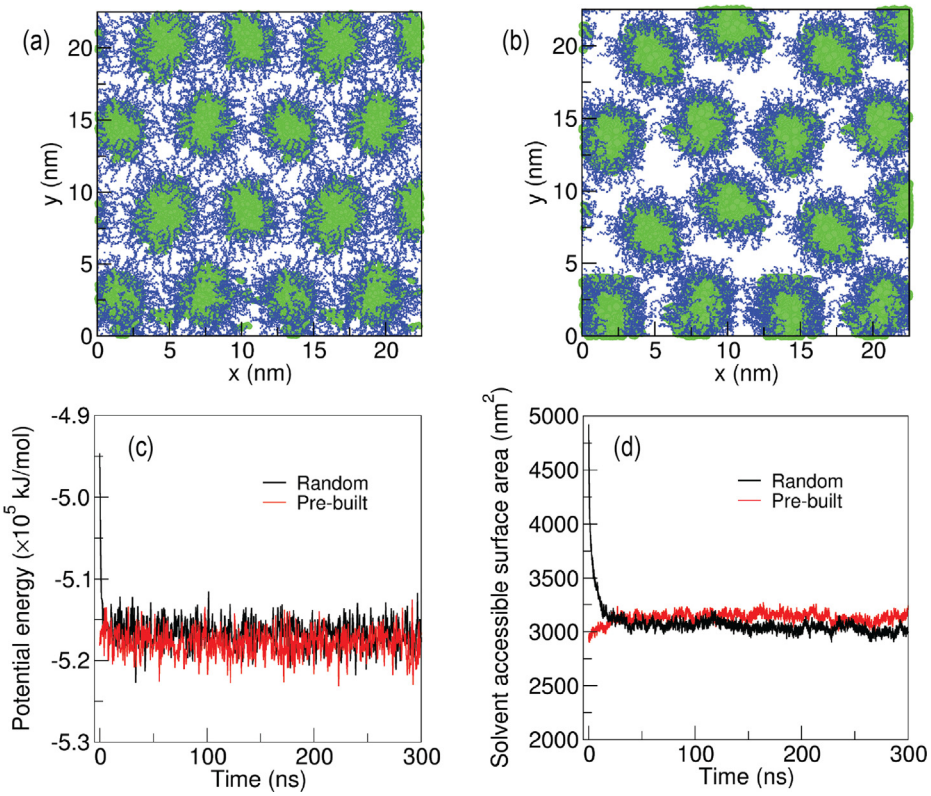

Fig. 7. Cross sections of hexagonal phase simulations that commenced from pre-built structures at point C using (a) the $53A6_{DBW}$ FF and (b) the 2016H66 FF, showing packing of the surfactant cylinders and solvation of the PEO head-groups. Coloring as in previous figures. (c) Total potential energy of simulations over time at point C started from a random distribution (simulation C_{H66}*) or from a pre-built structure (simulation C^{p}_{H66}). (d) Solvent accessible surface area of $C_{12}E_6$ in the same simulations.

The 2016H66 simulation produced a structure with highly ordered/crystalized surfactants as shown in Fig. 3, point E. To further confirm the formation of a solid, we calculated the lateral diffusion constant which was found to be $(4.2 \pm 1.8) \times 10^{-8}$ cm^2 s^{-1}, which is approximately 4 times lower than the value found in the lamellar region. This observation further confirms that $C_{12}E_6$ is in the solid phase and therefore the 2016H66 FF reproduces the experimental phase behavior in the solid surfactant region.

3.5. Liquid surfactant

To the best of our knowledge there is no experimental evidence of the exact structure formed by $C_{12}E_6$ in the liquid surfactant region. In our simulations at point F (Fig. 1), both FFs produced a structure with an interconnected layer-like pattern (Fig. 2, point F). Each layer has a lamellar-like structure with pores. It is interesting to note that coarse-grained simulations by Denham et al. [61] with 80% w/w of $C_{12}E_6$ in water produced a similar layer-like pattern, which is comparable with our result.

3.6. Phase separated (surfactant rich + surfactant lean phase)

In the phase separated region (Fig. 1, point G), simulations with both FFs produce a single aggregate in the simulation cell. The structure formed with 2016H66 is a single 'lump' while $53A6_{DBW}$ makes a worm-like micelle (Fig. 2, point G). The formation of only a single aggregate during the simulation is consistent with the formation of a phase separated system.

A number of models have been proposed to explain the cloud point phenomenon of PEO surfactants [70–72]. One model, proposed by Karlström [72] explains the cloud point behavior as being a result of conformational changes in the PEO chain. According to the model, at low temperatures, the segments of PEO chains are in a polar conformation that favors interactions with water. However, at the high temperatures, segments of PEO are in a less polar conformation that hinders interactions with water leading to the phase separation at the cloud point. Thus, we wanted to investigate the conformational changes in PEO backbone with the temperature fluctuations. For this purpose, we calculated the trans dihedral fraction (Fig. 8) for dihedral angles starting from O1—C1—C2—O2 to C12—O7—C13—C14 in the micellar and phase separated regions. Fig. 8 shows that the trans dihedral fractions of the C—C—O—C and C—O—C—C torsions are decreased in the phase separated region (at higher temperature) compared the micellar region. In contrast, the

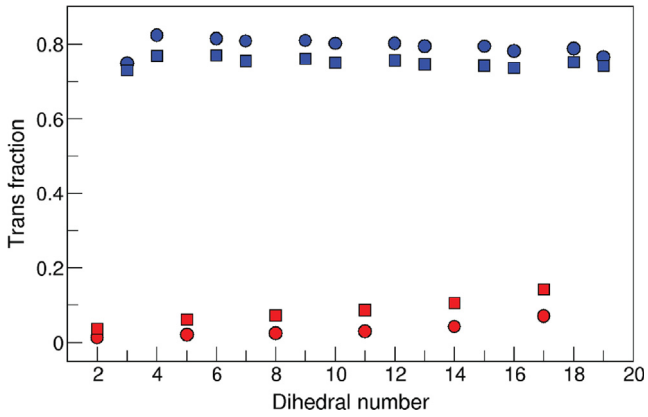

Fig. 8. Trans dihedral fraction for torsional angles calculated in micellar (point B, circles) and phase separated (point G, squares) regions using the 2016H66 FF. Coloring: O—C—C—O dihedral angle (red), C—C—O—C/C—O—C—C dihedral angle (blue) Note that the first dihedral is O1—C1—C2—O2 and the last dihedral is C12—O7—C13—C14. (For interpretation of the references to colour in this figure legend, the reader is referred to the web version of this article.)

trans dihedral fraction for the O—C—C—O torsional angle is increased (i.e. the fraction of these torsions in the gauche conformation is reduced) in the phase separated region. A Raman spectroscopy investigation [23] carried out for PEO at low temperatures also showed that the O—C—C—O torsional angle favors the gauche conformation while C—C—O—C/C—O—C—C torsional angles favor the trans conformation, but this conformational arrangement is disrupted at higher temperatures. This experimental behavior can be clearly seen in Fig. 8. Our MD simulations with the 2016H66 FF at points B and G show conformational population differences at low and high temperatures for O—C—C—O and C—C—O—C dihedrals that are consistent with the Raman study and with the model proposed by Karlström. Together, the simulations performed in the phase separated region show that 2016H66 reproduces the expected experimental phase behavior.

4. Conclusion

High-quality computational models are powerful tools to assist our understanding of surfactant phase behavior. In this work, we aimed to evaluate how well currently available FFs can model the phase behavior of PEO-containing nonionic surfactants in water and also to establish and whether conventional MD simulations, which are limited in time-scale, can form experimentally observed states within a practically accessible simulation time. Accordingly, we performed an extensive set of MD simulations covering the micelle, hexagonal, lamellar, solid, surfactant rich/surfactant lean and liquid surfactant regions of the $C_{12}E_6$/water phase diagrams using two variants of the GROMOS united atom FF: 2016H66 [32] and 53A6$_{DBW}$ [33]. This study considerably extends previous MD studies of C_iE_j/water systems, which generally investigate one, or a small number, of points on the phase diagram [34–43]. Our results show that both FFs reproduce the main features of the experimental phase behaviour [23] and can readily reproduce the primary structures of the micellar, and phase separated regions, starting from a random arrangement of surfactant molecules in water. In the hexagonal region, both FFs produce wormy micelles, a disordered hexagonal phase, but do not form clear hexagonally packed arrangements within the simulation time (400 ns). Simulations started from approximate, hexagonal rods were stable and of lower energy, suggesting that the simulations starting from a random arrangement of molecules were not able to reach the lowest energy hexagonally packed arrangement within the simulation time. Similar behavior was observed in the lamellar region where interconnected cylindrical micelles were yielded from a random distribution, but starting from the approximate model gave a porous, curved bilayer better matching the experimental lamellar phase. Overall, the 2016H66 FF reproduced the observed experimental phase behavior more accurately than the 53A6$_{DBW}$ FF. This study of the $C_{12}E_6$/water system provides confidence in using the 2016H66 FF to model other PEO-containing surfactant systems and also identifies some limitations of using MD simulations to model the more-ordered regions of the phase diagram (e.g. the hexagonal and lamellar mesophases). We expect that use of more sophisticated, enhanced-sampling approaches will be necessary to overcome the limited timescale of conventional MD simulations in these regions. We are currently applying the findings from this work to study a wider range of PEO-containing surfactants (i.e. Tween® 80 and Kolliphor® RH40) and other complex colloidal systems such as lipid-based formulations designed for loratadine/Claritin®.

CRediT authorship contribution statement

Amali G. Guruge: Investigation, Writing - original draft. **Dallas B. Warren:** Supervision, Writing - review & editing. **Hassan Benameur:** Conceptualization, Supervision. **Colin W. Pouton:** Conceptualization, Supervision, Writing - review & editing. **David K. Chalmers:** Conceptualization, Supervision, Resources, Writing - review & editing.

Declaration of Competing Interest

The authors declare that they have no known competing financial interests or personal relationships that could have appeared to influence the work reported in this paper.

Acknowledgements

This work was supported by The Multi-modal Australian ScienceS Imaging and Visualization Environment (MASSIVE) and National Computational Infrastructure (NCI). AGG gratefully acknowledges scholarship support from Oral Drug Delivery Innovation, Chemical Division, Lonza. We gratefully acknowledge provision of a GeForce GTX 1080 Ti GPU, used for MD simulations and visualization, by Nvidia Corporation.

Appendix A. Supplementary data

Figure showing the SASA of simulations at points A and B over time. Figure showing the evolution of simulation A_{H66} over time. A table showing radii of gyration data for micelles. PDB format files of the final simulation frames for each modelled system are available from Mendeley Data. DOI: 10.17632/5fbtdgyprr.1.

Supplementary data to this article can be found online at https://doi.org/10.1016/j.ultsonch.2019.104640.

References

[1] D. Bajpai, V.K. Tyagi, Nonionic surfactants: an overview, Tenside, Surfactants, Deterg. 47 (3) (2010) 190–196.
[2] C.W. Pouton, Lipid formulations for oral administration of drugs: non-emulsifying, self-emulsifying and 'self-microemulsifying' drug delivery systems, Eur. J. Pharm. Sci. 11 (2000) S93–S98.
[3] C.W. Pouton, Formulation of poorly water-soluble drugs for oral administration: physicochemical and physiological issues and the lipid formulation classification system, Eur. J. Pharm. Sci. 29 (3) (2006) 278–287.
[4] C.W. Pouton, C.J.H. Porter, Formulation of lipid-based delivery systems for oral administration: materials, methods and strategies, Adv. Drug Deliver. Rev. 60 (6) (2008) 625–637.
[5] W.A. Birru, D.B. Warren, S.J. Headey, H. Benameur, C.J.H. Porter, C.W. Pouton, D. K. Chalmers, Computational models of the gastrointestinal environment. 1. The effect of digestion on the phase behavior of intestinal fluids, Mol. Pharm. 14 (3) (2017) 566–579.
[6] W.A. Birru, D.B. Warren, S. Han, H. Benameur, C.J.H. Porter, C.W. Pouton, D.K. Chalmers, Computational models of the gastrointestinal environment. 2. Phase behavior and drug solubilization capacity of a Type I lipid-based drug formulation after digestion, Mol. Pharm. 14 (3) (2017) 580–592.
[7] E.J.A. Suys, D.B. Warren, A.C. Pham, C.J. Nowell, A.J. Clulow, H. Benameur, C.J.H. Porter, C.W. Pouton, D.K. Chalmers, A Nonionic Polyethylene Oxide (PEO) surfactant model: experimental and molecular dynamics studies of kolliphor EL, J. Pharm. Sci. 108 (1) (2019) 193–204.
[8] E.J.A. Suys, D.B. Warren, C.J.H. Porter, H. Benameur, C.W. Pouton, D.K. Chalmers, Computational models of the intestinal environment. 3. The impact of cholesterol content and pH on mixed micelle colloids, Mol. Pharm. 14 (11) (2017) 3684–3697.
[9] D.B. Warren, D.K. Chalmers, C.W. Pouton, Structure and dynamics of glyceride lipid formulations, with propylene glycol and water, Mol. Pharm. 6 (2) (2009) 604–614.
[10] D.B. Warren, D. King, H. Benameur, C.W. Pouton, D.K. Chalmers, Glyceride lipid formulations: molecular dynamics modeling of phase behavior during dispersion and molecular interactions between drugs and excipients, Pharm. Res. 30 (12) (2013) 3238–3253.
[11] Y. Wang, R. Zhang, L. Tan, H.Y. Zhang, M. Yang, Analysis of Polysorbate 80 and its related compounds by RP-HPLC with ELSD and MS detection, J. Chromatogr. Sci. 50 (7) (2012) 598–607.
[12] R.R. Balmbra, J.S. Clunie, J.M. Corkill, J.F. Goodman, Effect of temperature on the micelle size of a homogeneous non-ionic detergent, Trans. Faraday Soc. 58 (1962) 1661–1667.
[13] J. Gapiński, J. Szymański, A. Wilk, J. Kohlbrecher, A. Patkowski, R. Hołyst, Size and shape of micelles studied by means of SANS, PCS, and FCS, Langmuir 26 (12) (2010) 9304–9314.

[14] Y. Einaga, Wormlike micelles of Polyoxyethylene Alkyl ethers CiEj, Polymer J. 41 (2008) 157.
[15] S. Yoshimura, S. Shirai, Y. Einaga, Light-scattering characterization of the wormlike micelles of hexaoxyethylene Dodecyl C12E6 and hexaoxyethylene tetradecyl C14E6 ethers in dilute aqueous solution, J. Phys. Chem. B 108 (40) (2004) 15477–15487.
[16] M. Zulauf, K. Weckstrom, J.B. Hayter, V. Degiorgio, M. Corti, Neutron scattering study of micelle structure in isotropic aqueous solutions of poly(oxyethylene) amphiphiles, J. Phys. Chem. 89 (15) (1985) 3411–3417.
[17] M. Corti, V. Degiorgio, J.B. Hayter, M. Zulauf, Micelle structure in isotropic C12E8 amphiphile solutions, Chem. Phys. Lett. 109 (6) (1984) 579–583.
[18] J.P. Conroy, C. Hall, C.A. Leng, K. Rendall, G.J.T. Tiddy, J. Walsh, G. Lindblom, In Nonionic surfactant phase behavior. The effect of CH3 capping of the terminal OH. Accurate measurements of cloud curves, Darmstadt, Steinkopff, Darmstadt, 1990, pp. 253–262.
[19] M.J. Rosen, A.W. Cohen, M. Dahanayake, X.Y. Hua, Relationship of structure to properties in surfactants. 10. Surface and thermodynamic properties of 2-dodecyloxypoly(ethenoxyethanol)s, C12H25(OC2H4)xOH, in aqueous solution, J. Phys. Chem. 86 (4) (1982) 541–545.
[20] B.-H. Chen, C.A. Miller, J.M. Walsh, P.B. Warren, J.N. Ruddock, P.R. Garrett, F. Argoul, C. Leger, Dissolution rates of pure nonionic surfactants, Langmuir 16 (12) (2000) 5276–5283.
[21] H.-H. Lai, L.-J. Chen, Liquid−liquid equilibrium phase diagram and density of three water + nonionic surfactant CiEj binary systems, J. Chem. Eng. Data 44 (2) (1999) 251–253.
[22] M. Maccarini, G. Briganti, Density measurements on C12Ej nonionic micellar solutions as a function of the head group degree of polymerization (j = 5–8), J. Phys. Chem. A 104 (48) (2000) 11451–11458.
[23] D.J. Mitchell, G.J.T. Tiddy, L. Waring, T. Bostock, M.P. McDonald, Phase behaviour of polyoxyethylene surfactants with water. Mesophase structures and partial miscibility (cloud points), J. Chem. Soc., Faraday Trans. 1 79 (4) (1983) 975–1000.
[24] R.P. Frankewich, W.L. Hinze, Evaluation and optimization of the factors affecting nonionic surfactant-mediated phase separations, Anal. Chem. 66 (7) (1994) 944–954.
[25] R.I. Strey, Experimental facts: water-nonionic surfactant systems, and the effect of additives, Ber. Bunsenges. Phys. Chem. 100 (3) (1996) 182–189.
[26] K.S. Sharma, S.R. Patil, A.K. Rakshit, Study of the cloud point of C12En nonionic surfactants: effect of additives, Colloids Surf. A 219 (1) (2003) 67–74.
[27] M. Karplus, J.A. McCammon, Molecular dynamics simulations of biomolecules, Nature Struct. Biol. 9 (2002) 646.
[28] H. Matsuura, K. Fukuhara, Conformational analysis of poly(oxyethylene) chain in aqueous solution as a hydrophilic moiety of nonionic surfactants, J. Mol. Struct. 126 (1985) 251–260.
[29] M. Winger, A.H. de Vries, W.F. van Gunsteren, Force-field dependence of the conformational properties of α, ω-dimethoxypolyethylene glycol, Mol. Phys. 107 (13) (2009) 1313–1321.
[30] B.A.C. Horta, P.F.J. Fuchs, W.F. van Gunsteren, P.H. Hünenberger, New interaction parameters for oxygen compounds in the GROMOS force field: improved pure-liquid and solvation properties for alcohols, ethers, aldehydes, ketones, carboxylic acids, and esters, J. Chem. Theory Comput. 7 (4) (2011) 1016–1031.
[31] P.F.J. Fuchs, H.S. Hansen, P.H. Hünenberger, B.A.C. Horta, A GROMOS parameter set for vicinal diether functions: properties of polyethyleneoxide and polyethyleneglycol, J. Chem. Theory Comput. 8 (10) (2012) 3943–3963.
[32] B.A.C. Horta, P.T. Merz, P.F.J. Fuchs, J. Dolenc, S. Riniker, P.H. Hünenberger, A GROMOS-compatible force field for small organic molecules in the condensed phase: the 2016H66 parameter set, J. Chem. Theory Comput. 12 (8) (2016) 3825–3850.
[33] D.B. Warren, E. McPhee, W.A. Birru, H. Benameur, D.K. Chalmers, C.W. Pouton, Improvement in the predicted partitioning of alcohol and polyethylene oxide groups between water and octanol (logP) in molecular dynamics simulations, J. Pharm. Sci. 108 (1) (2019) 214–222.
[34] C.P. Fabio Sterpone, Giuseppe Brigant, Massimo Marchi, Molecular dynamics study of temperature dehydration of a $C_{12}E_6$ spherical micelle, Langmuir 20 (2004) 4311–4314.
[35] R. Allen, S. Bandyopadhyay, M.L. Klein, C12E2 reverse micelle: a molecular dynamics study, Langmuir 16 (26) (2000) 10547–10552.
[36] S. Abel, M. Waks, M. Marchi, W. Urbach, Effect of surfactant conformation on the structures of small size nonionic reverse micelles: a molecular dynamics simulation study, Langmuir 22 (22) (2006) 9112–9120.
[37] A.A. Vanin, E.N. Brodskaya, Molecular-dynamics simulation of the surface layer of a nonionic micelle, Colloid J. 79 (3) (2017) 310–316.
[38] S. Bandyopadhyay, M. Tarek, M.L. Lynch, M.L. Klein, Molecular dynamics study of the poly(oxyethylene) surfactant C12E2 and water, Langmuir 16 (3) (2000) 942–946.
[39] S. Vierros, M. Sammalkorpi, Effects of 1-hexanol on C12E10 micelles: a molecular simulations and light scattering study, Phys. Chem. Chem. Phys. 20 (9) (2018) 6287–6298.
[40] C. Senac, W. Urbach, E. Kurtisovski, P.H. Hünenberger, B.A.C. Horta, N. Taulier, P.F.J. Fuchs, Simulating bilayers of nonionic surfactants with the GROMOS-compatible 2016H66 force field, Langmuir 33 (39) (2017) 10225–10238.
[41] M. Velinova, D. Sengupta, A.V. Tadjer, S.-J. Marrink, Sphere-to-rod transitions of nonionic surfactant micelles in aqueous solution modeled by molecular dynamics simulations, Langmuir 27 (23) (2011) 14071–14077.
[42] F. Sterpone, G. Briganti, C. Pierleoni, Sphere versus cylinder: the effect of packing on the structure of nonionic C12E6 micelles, Langmuir 25 (16) (2009) 8960–8967.
[43] T.M. Ferreira, D. Topgaard, O.H.S. Ollila, Molecular conformation and bilayer pores in a nonionic surfactant lamellar phase studied with 1H–13C solid-state NMR and molecular dynamics simulations, Langmuir 30 (2) (2014) 461–469.
[44] G. Rossi, P.F.J. Fuchs, J. Barnoud, L. Monticelli, A Coarse-grained MARTINI model of polyethylene glycol and of polyoxyethylene alkyl ether surfactants, J. Phys. Chem. B 116 (49) (2012) 14353–14362.
[45] D.K. Chalmers, B.P. Roberts, Silico: A Perl Molecular Toolkit. http://silico.sourceforge.net/. http://silico.sourceforge.net.
[46] M. O'Keeffe, S. Andersson, Rod Packings, Crystal-chemistry. Acta Crystallogr. A33 (Nov) (1977) 914–923.
[47] H.J. Berendsen, D. van der Spoel, R. van Drunen, GROMACS: a message-passing parallel molecular dynamics implementation, Comput. Phys. Commun. 91 (1–3) (1995) 43–56.
[48] S. Pronk, S. Páll, R. Schulz, P. Larsson, P. Bjelkmar, R. Apostolov, M.R. Shirts, J.C. Smith, P.M. Kasson, D. Van Der Spoel, GROMACS 4.5: a high-throughput and highly parallel open source molecular simulation toolkit, Bioinformatics 29 (7) (2013) 845–854.
[49] K.A. Feenstra, B. Hess, H.J.C. Berendsen, Improving efficiency of large time-scale molecular dynamics simulations of hydrogen-rich systems, J. Comput. Chem. 20 (8) (1999) 786–798.
[50] G. Bussi, D. Donadio, M. Parrinello, Canonical sampling through velocity rescaling, J. Chem. Phys. 126 (1) (2007) 014101.
[51] H.J.C. Berendsen, J.P.M. Postma, W.F.v. Gunsteren, A. DiNola, J.R. Haak, Molecular dynamics with coupling to an external bath, J. Chem. Phys. 81 (8) (1984) 3684–3690.
[52] M. Parrinello, A. Rahman, Polymorphic transitions in single crystals: a new molecular dynamics method, J. App. Phys. 52 (12) (1981) 7182–7190.
[53] S. Miyamoto, P.A. Kollman, Settle: An analytical version of the SHAKE and RATTLE algorithm for rigid water models, J. Comput. Chem. 13 (8) (1992) 952–962.
[54] B. Hess, H. Bekker, H.J.C. Berendsen, J.G.E.M. Fraaije, LINCS: A linear constraint solver for molecular simulations, J. Comput. Chem. 18 (12) (1997) 1463–1472.
[55] L. Verlet, Computer "Experiments" on classical fluids. I. Thermodynamical properties of Lennard-Jones molecules, Phys. Rev. 159 (1) (1967) 98–103.
[56] T. Darden, D. York, L. Pedersen, Particle mesh Ewald: an N·log(N) method for Ewald sums in large systems, J. Chem. Phys. 98 (12) (1993) 10089–10092.
[57] The PyMOL Molecular Graphics System, Version 1.8 Schrödinger, LLC.
[58] M. Marchi, S. Abel, Modeling the self-aggregation of small AOT reverse micelles from first-principles, J. Phys. Chem. Lett. 6 (1) (2015) 170–174.
[59] W.J. Allen, J.A. Lemkul, D.R. Bevan, GridMAT-MD: A grid-based membrane analysis tool for use with molecular dynamics, J. Comput. Chem. 30 (12) (2009) 1952–1958.
[60] M. Clerc, A.-M. Levelut, J.-F. Sadoc, Transitions between mesophases involving cubic phases in the surfactant-water systems. Epitaxial relations and their consequences in a geometrical framework, J Phys II (Paris) 1 (10) (1991) 1263–1276.
[61] N. Denham, M.C. Holmes, A.V. Zvelindovsky, The phases in a non-ionic surfactant (C12E6)−water ternary system: a coarse-grained computer simulation, J. Phys. Chem. B 115 (6) (2011) 1385–1393.
[62] F. Grunewald, G. Rossi, A.H. de Vries, S.J. Marrink, L. Monticelli, Transferable MARTINI Model of Poly(ethylene Oxide), J. Phys. Chem. B 122 (29) (2018) 7436–7449.
[63] Y. Rancon, J. Charvolin, Epitaxial relationships during phase transformations in a lyotropic liquid crystal, J. Phys. Chem. 92 (9) (1988) 2646–2651.
[64] D. Constantin, P. Oswald, M. Impéror-Clerc, P. Davidson, P. Sotta, Connectivity of the hexagonal, cubic, and isotropic phases of the C12EO6/H2O lyotropic mixture investigated by tracer diffusion and X-ray scattering, J. Phys. Chem. B 105 (3) (2001) 668–673.
[65] M. Allain, J.-M.D. Meglio, Highly curved defects in lyotropic lamellar phases, Mol. Cryst. Liq. Cryst. 124 (1) (1985) 115–124.
[66] L. Paz, J.M. Di Meglio, M. Dvolaitzky, R. Ober, C. Taupin, Highly curved defects in lyotropic (nonionic) lamellar phases. Origin and role in hydration process, J. Phys. Chem. 88 (16) (1984) 3415–3418.
[67] D. Constantin, P. Oswald, Diffusion coefficients in a lamellar lyotropic phase: evidence for defects connecting the surfactant structure, Phys. Rev. Lett. 85 (20) (2000) 4297.
[68] J.S. Clunie, J.F. Goodman, P.C. Symons, Phase equilibria of dodecylhexaoxyethylene glycol monoether in water, Trans. Faraday Soc. 65 (1969) 287–296.
[69] A. Yethiraj, D. Capitani, N.E. Burlinson, E.E. Burnell, An NMR Study of translational diffusion and structural anisotropy in magnetically alignable nonionic surfactant mesophases, Langmuir 21 (8) (2005) 3311–3321.
[70] R. Kjellander, E. Florin, Water structure and changes in thermal stability of the system poly(ethylene oxide)–water, J. Chem. Soc. Faraday Trans. 1 77 (9) (1981) 2053–2077.
[71] R.E. Goldstein, On the theory of lower critical solution points in hydrogen-bonded mixtures, J. Chem. Phys. 80 (10) (1984) 5340–5341.
[72] G. Karlstroem, A new model for upper and lower critical solution temperatures in poly(ethylene oxide) solutions, J. Phys. Chem. 89 (23) (1985) 4962–4964.

Chapter 4

Modelling the Liquid Phase Transitions of Polyethyleneoxide Surfactant ($C_{12}E_6$)/Water Systems Using Conventional and Replica Exchange Molecular Dynamics Simulations

Polyethylene oxide (PEO) non-ionic surfactants are widely used excipient in lipid-based formulations (LBFs). Phase changes or phase transitions are observed with these non-ionic surfactant/water mixtures due to variations in temperature or compositions. Since LBFs are mixtures of lipids and surfactants, these mixtures also form different phases depending on the surfactant, oil, and water contents. We are interested in phase transitions observed with LBFs as they are in the self-gelatine capsule and then dispersed and diluted in the aqueous environment. For accurate prediction of this type of phase behavior in LBFs through molecular dynamics (MD), accurate modelling of phase transitions of PEO non-ionic surfactant/water mixtures is essential. To date, no investigation in the literature provides evidence on how effectively MD model phase transitions of PEO surfactants in water. Therefore, the work in this chapter explores how MD technique model the phase transitions of hexaoxyethylene dodecyl ether ($C_{12}E_6$)/water systems as a representative PEO surfactant.

Starting from different liquid phases of $C_{12}E_6$, we performed classical MD simulations and replica-exchange molecular dynamics simulations to study how MD reproduces the relevant phases according to the composition or temperature change. Additionally, we investigated the phases formed in the isotropic region above the hexagonal phase and isotropic region above the lamellar phase since these regions are less explored with experimental investigations.

The findings of the work in this chapter guarantee the confidence to use the 2016H66 force field in predicting the complex phase behavior of LBFs upon dispersion in the aqueous medium.

This chapter is a manuscript to be submitted for publication.

Modelling the Liquid Phase Transitions of Polyethyleneoxide Surfactant ($C_{12}E_6$)/Water Systems Using Conventional and Replica Exchange Molecular Dynamics Simulations

*Amali G. Guruge,[1] Dallas B. Warren,[2] Hassan Benameur,[3] Colin W. Pouton[2], David K. Chalmers[1]**

[1]Medicinal Chemistry and [2]Drug Delivery, Disposition and Dynamics, Monash Institute of Pharmaceutical Sciences, Monash University, 381 Royal Parade, Parkville, Victoria 3052, Australia

[3]Lonza Pharma Sciences, Strasbourg, France

Keywords

Non-ionic surfactant, poly(ethyleneoxide), colloids, phase transition, molecular dynamics simulations, replica exchange.

Abstract

Phase transitions are important in many day-to-day phenomena. Our attention has been drawn by the phase transitions that occur in pharmaceutical lipid-based drug formulations as they are dispersed in water. These phase changes can strongly influence the delivery of the drugs contained within the formulation. We are using molecular dynamics (MD) to understand the complex behavior of these drug formulations. Poly(ethyleneoxide) (PEO) surfactants are important components of many drug formulations. However, there is little information in the literature on how well MD simulations are able to simulate the phase transition processes of PEO surfactants in aqueous solution. Therefore, in this study, we investigate how effectively MD simulates phase transitions using the PEO surfactant, hexaoxyethylene dodecyl ether ($C_{12}E_6$) as a representative system. Starting from different initial $C_{12}E_6$ liquid phases, we examine how MD reproduces the relevant equilibrium colloidal structures due to changes in temperature or composition using conventional MD simulation and replica exchange MD (REMD) methods. We find that MD adequately reproduces the

phase transitions considered in the study. Also, we find that the colloidal structures are independent of the initial molecular arrangement and the final colloidal state reach is independent of the pathway. Further, the phase transition temperatures obtained from the REMD simulations agreed well with experimental phase transition temperatures. Our results also indicated that the REMD method is suitable for studying temperature phase transitions, providing significantly more thorough information compared to conventional MD simulations. Besides, we find that the colloidal structure in the isotropic region above the hexagonal phase is disordered bilayers while the colloidal structure in the isotropic region above the lamellar phase is linked porous layers.

Introduction

Mixtures of surfactants and water exhibit complex phase behavior, forming micelles, bilayers, vesicles, emulsions or other structures, depending on the precise components of the system and the degree of dilution with water. Chemical mixtures containing surfactants are important in many fields, for example, in pharmaceutical formulations where surfactants are used to solubilize poorly water-soluble drugs. In formulation development, it is well known that the presence of different colloidal phases, such as vesicles or micelles, can strongly influence the solubility of the active pharmaceutical agent included in the formulation.[1-3] Understanding of the phase behavior of pharmaceutical formulations and the transitions between phases that occur as a formulation is diluted is therefore important for developing new medicines. In drug formulation and many other areas of research, there is a need for computational predictive methods that can be used to understand the formation of different chemical phases and the transitions between these phases.

Molecular dynamics (MD) simulation is a well-established computational tool for the study of complex liquid systems[4-8] where it reveals detailed information about the molecular structure and the dynamic evolution of a given system, providing insights that cannot easily be retrieved from experimental investigations and assisting us to understand experimental observations. For good prediction of the behavior of lipid-based drug formulations in MD simulations, the formation of one colloidal structure to another due to the changes in composition or temperature is essential.

Poly(ethylene oxide) (PEO)-containing, non-ionic surfactants are important components of many industrial and consumer products. Our particular interest lies in

lipid-based drug formulations. Many of the non-ionic PEO surfactants used in drug formulations and other industrial applications are heterogeneous, complex mixtures (e.g., Tween®, Kolliphor®), which makes them difficult to model using atomistic computational methods such as molecular dynamics. In contrast, PEO alkyl ether surfactants are pure, extensively studied and well-characterized materials. This makes them useful systems to study using computational methods. PEO alkyl ether surfactants are abbreviated as C_iE_j where *i* indicates the number of carbon atoms in the hydrophobic tail and *j* specifies the number of ethylene oxide units in the hydrophilic head group. For this investigation, we selected hexaoxyethylene dodecyl ether ($C_{12}E_6$) as a representative, mid-sized surfactant from the C_iE_j family. The chemical structure and the experimental phase behavior of $C_{12}E_6$ in aqueous environment[9] are shown in Figure 1.[9]

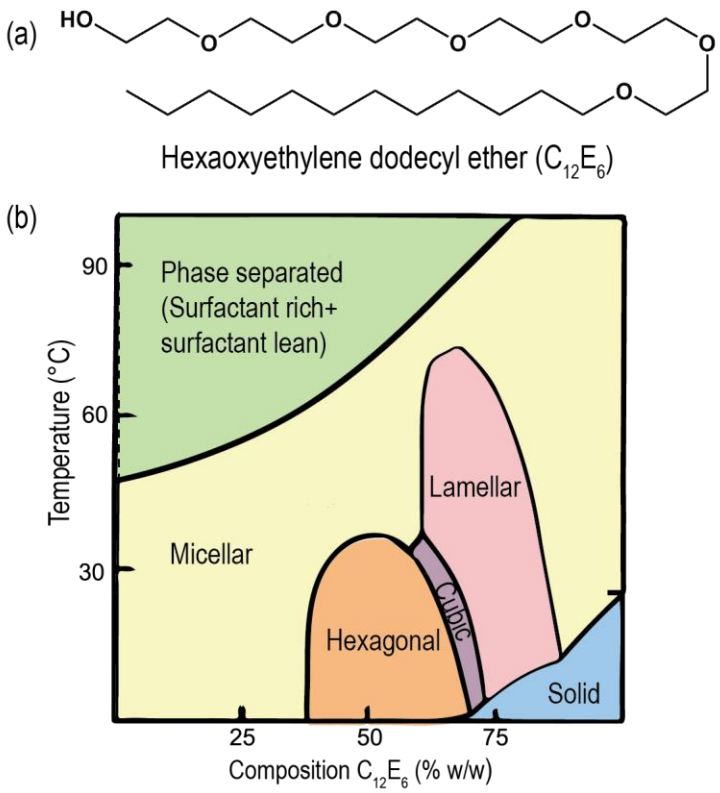

Figure 1 – (a) Chemical structure of $C_{12}E_6$. (b) Phase diagram of $C_{12}E_6$ in water.[9]

The amphiphilic nature of $C_{12}E_6$ molecules makes them self-assemble into a rich variety of stable colloidal structures. $C_{12}E_6$ in water has a critical micelle concentration (CMC) of 0.067 mM.[10] In the middle range compositions, $C_{12}E_6$ forms hexagonal and cubic phases and, at high concentrations, lamellar and solid phases. At higher temperatures, the $C_{12}E_6$/water system reaches the cloud point, forming a visually

turbid two-phase system consisting of surfactant rich and surfactant lean phases.[11] Previous experimental work on $C_{12}E_6$ has investigated the dissolution rate[12], density[13], refractive index[14], micellar structure[15-18], the effect of temperature on micelle size[19], diffusion[20-21], structural transformations of liquid crystalline phases[22], curved defects in the lamellar phase[23-24], mesomorphic phases characterization[25], orientational effects due to strong magnetic fields in hexagonal and lamellar systems containing heavy water[26], and the size, shape and polydispersity of mixed micelles composed of $C_{12}E_6$ and $C_{12}E_8$ in aqueous media[27].

Compared to the number of experimental investigations of $C_{12}E_6$, only a limited number of computational studies are available in the literature. Sterpone and co-workers investigated the hydration of spherical micelles of $C_{12}E_6$[28] in 2004 and in 2009 they investigated packing of $C_{12}E_6$ into the sphere and cylindrical micelles[7] using MD simulations. Shinoda et al. and Rossi et al. performed coarse-grained (CG) MD simulations of the self-assembly behavior of $C_{12}E_6$, considering different regions in $C_{12}E_6$/water phase diagram.[6, 29] More recently, Guruge et al. investigated the phase behavior of $C_{12}E_6$ using the 2016H66 and 53A6$_{DBW}$ force fields (FFs).[30] $C_{12}E_6$-water systems have also been studied using dissipative particle dynamics (DPD) simulations with CG models to investigate the ability of small oil molecules to control the phase structures in $C_{12}E_6$-water systems[31] and to quantitatively clarify the hydrophilic dependence of the phase structures in $C_{12}E_6$-water systems by varying the interactions between hydrophilic molecules and water molecules[32].

MD modelling of surfactant phase behavior has several limitations. The modelling results are influenced by the size of the molecular system used, the quality of the molecular model (force field) and the length of time that is simulated. A MD simulation must be large enough to not be overly influenced by the size of the simulation cell and of sufficient duration to allow the system to equilibrate to approach the experimentally observed state. Importantly, to provide a reliable model, the FF used for the simulation must accurately reproduce the conformational behavior of the surfactant and the physical interactions between PEO surfactant and with the surrounding environment.

To date, most computational studies of C_iE_j surfactants have investigated single points on surfactant phase diagrams[28, 30, 33-37] and have not attempted to study the transitions between phases, largely due to the limitations of simulation time in MD. The sphere to

rod transition of $C_{12}E_5$ has been studied by Velinova and co-workers using a CG model.[8] They investigated the self-assembly of the surfactant in the water at concentrations of $C_{12}E_5$ from 2.7 – 8.56% w/w and found that the increase of the surfactant concentration lead to a second critical micellar concentration where a transition from spherical shaped micelles to rod-like micelles occurred. Sterpone et al. investigated the same phase transition using $C_{12}E_6$ surfactant.[7] Using prebuilt spherical and cylindrical micelles, they were able to find the differences in the oil core packing, specific volume, and spatial distribution of the head groups in those two geometries. Using a prebuilt $C_{12}E_5$-water system in a lamellar arrangement, Senac et al. observed the formation of a hexagonal-like phase but they were unable to confirm whether this structure was a local or global minimum structure or whether a different structure resulted if they used a larger system for a longer simulation time.[37]

Molecular dynamics studies of phase transitions have been most extensively studied in lipid systems using CG models. In dipalmitoylphosphatidylcholine (DPPC) bilayers, transitions from the liquid to gel phase and in the reverse direction have been explored,[38] transformation of the liquid crystalline phase to the crystal phase in DPPC have also been studied.[39] Transformation of lamellar to micellar phases in dicapryloylphosphatidylcholine[40] have been modelled. Leekumjorn et al. investigated the transition of gel to liquid-crystalline states using lipid bilayers of POPC, POPE, DPPC and DPPE.[41, 42] Horta et al. also studied gel to liquid-crystal transition in monoglyceride glycerol-1-monopalmitate (GMP).[43] Their main goal was to investigate whether they could monitor the phase transition gel to liquid crystal or liquid crystal to gel on 10–100 ns time scale. They observed the gel to liquid crystal phase transition on 40 ns time scale, but the liquid crystal to gel transformation required simulation on 200 ns scale. Further, their study accurately determined phase transition temperature for the reversible phase transition from the gel to liquid crystal. Stevens investigated liquid to gel phase transition using a CG fundamental model.[44] Using another CG basic model, Hömberg and Müller studied the same phase transition of the bilayer membrane.[45] de Vries et al. studied the transformation of liquid crystalline phase to ripple phase using the lecithin lipid bilayers revealing structural information of the ripple phase.[46] We note that most of the reported phase transition investigations have used CG models.[8, 38-40, 44-45, 47] While CG models provide important and useful information about colloidal systems, in general, these models are unable to capture detail features

of colloids due to their simplified molecular representations; typically, each CG bead represents four non-hydrogen atoms. In contrast, united atom models provide more accurate molecular properties (interaction energies and geometries) and have an important role in the study of complex colloid chemistry.

The trapping of structures in local minima remains a big hurdle to modelling phase transitions. In such cases, longer simulations and enhanced sampling techniques are required to overcome energy barriers and find the global minimum. One of the standard *in silico* approaches for exploring conformational space more efficiently is temperature replica exchange molecular dynamics (REMD) simulation,[48] a combination of MD simulation and Monte Carlo algorithm. To briefly explain this method, several copies of the same system, known as replicas, are run simultaneously using MD. Each replica simulation is performed at a different temperature. A probability, given by the Metropolis criterion, is used for swapping of neighboring systems periodically based on the system potential energy. In this manner, REMD can jump over high-energy barriers by allowing systems to move to higher temperatures, exploring the conformational space more satisfactorily. An added advantage of this method is a system can be studied across a wide temperature range at the same time.[49] Also, there are many other enhanced sampling methods such as metadynamics, umbrella sampling, conformational space annealing, hyperdynamics and etc. However, these methods need predefined reaction coordinates or collective variables, and it is known that the proper predefined reaction coordinates are not easily identified for many systems.[50] Thus, we used collective variable free, REMD method for our investigation. Temperature REMD is widely used in simulations related to biological systems.[51-60] There are, however, few reported REMD studies of phase transitions of colloids conducted using atomistic models. REMD simulation of DPPC by Nagai et al. using the CG MARTINI model was used to investigate the liquid state to gel state (sol-gel) phase transition.[47, 61] They observed sol-gel phase transition around 296 K. They also observed that the lipid bilayer has two states in the gel state, a tilted gel state and an un-tilted gel state.

As described above, there have been relatively few MD studies of phase transitions in colloidal materials in general and even fewer in applied to non-ionic PEO surfactants, which are important and widely used industrial products. Further, many literature

studies have used low-resolution CG models, which are much faster, but are unable to precisely model interatomic interactions. Considering this, the first objective of our present study was to investigate whether MD simulations using a united atom force field can model the phase transitions across the whole phase diagram of the $C_{12}E_6$/water system. The second objective was to study whether REMD provides an advantage over conventional MD simulations by comparing simulations carried out with REMD method and conventional MD simulations in the study. The third objective was to explore how the starting configuration or MD simulation pathway influences the formation of relevant colloidal structures in phase transitions. Finally, we wished to gain insights into the less experimentally explored colloidal regions (i.e., isotropic regions above the hexagonal phase and lamellar phase) in $C_{12}E_6$/water phase diagram since colloidal behavior of those regions is poorly understood.

Methods

Conventional MD simulations

Starting structures for each phase transition MD simulation were frames taken from equilibrated long-timescale simulations generated in our previous investigation.[30] In some cases, the systems were modified by changing the number of molecules (i.e. water and $C_{12}E_6$). All simulations were performed using the 2016H66[62] FF with GROMACS[63-64] version 2016.3. The single point charge (SPC) model was used to model water molecules. An increased time step (5 fs) was enabled in all simulations using the heavy hydrogen atom method.[65] Hydrogen atoms were modified to have mass of 4 a.m.u. and the additional mass of the hydrogen atom was balanced by reducing the mass of the attached heavy atom. The NPT (isothermal-isobaric ensemble) was used in all simulations. The velocity rescale algorithm[66] was employed for temperature coupling and for each system the temperature was set to match with the appropriate point on the phase diagram. The pressure coupling used a reference pressure of 1 bar with the compressibility of 4.5×10^{-5} bar^{-1} for the Berendsen[67] and Parrinello-Rahman[68] algorithms. All simulations used isotropic pressure coupling, except for micellar to hexagonal phase transitions (point A to point C and point B to point C) conducted with conventional MD simulation used semi-isotropic coupling. Water bonds were constrained with SETTLE algorithm.[69] All other bonds were constrained by the LINCS algorithm.[70] For short-range non-bonded interactions

(Coulomb and van der Waals), the Verlet cut-off scheme[71] with the cut-off distance of 1.4 nm was applied. The particle-mesh Ewald (PME) technique[72] was used for long-range Coulombic interactions with a grid spacing of 0.12 nm. Before the production run, the following sequential steps were followed.

i. Energy minimization of 500 steps using the steepest descent method to remove steric clashes in atoms.

ii. Simulation of 5000 steps without pressure coupling using a time step of 1 fs and V-rescale temperature coupling of 0.1 ps.

iii. Simulation of 10,000 steps using a 2 fs time step with Berendsen pressure coupling and a 2 ps pressure coupling time constant.

iv. Simulation of 10,000 steps using 2 fs time step with Parrinello-Rahman pressure coupling and a 2 ps pressure coupling time constant.

v. Simulation of 10,000 steps of increased time step (5 fs) with a 2 ps Parrinello-Rahman pressure coupling time constant and 0.1 ps V-rescale temperature coupling time constant.

vi. The production run with 5 fs time step, 2 ps pressure coupling constant and 0.1 ps temperature coupling constant.

Replica exchange MD (REMD) simulations

In these simulations, *N* systems were simulated at *N* different temperatures. The temperature spacing was determined using the webserver (https://github.com/dspoel/remd-temperature-generator) by Patriksson and Van der Spoel,[73] which estimates temperatures required for a 0.2 probability of exchange. Before starting, each system was equilibrated at the relevant temperature for 50 ns. The interval for replica exchanges was set at 1000 steps. System information for each REMD simulation is shown in Table 2. The exact temperatures and observed exchange probabilities are given in Table S1 in the Supplementary Information (SI).

Simulation Analysis

The final simulation structures were visually examined and images generated using PyMOL.[74] The aggregate properties of colloids were analyzed using the *find_aggregate* script from the Silico package.[75] The solvent accessible surface area

(SASA) and potential energy probability distributions were calculated using *gmx sasa* and *gmx analyze* tools in GROMACS.

Results and Discussion

We modeled a series of phase transitions of the $C_{12}E_6$/water system as presented in Figure 2. Both conventional MD and REMD simulations were used to investigate how effectively these simulations could model $C_{12}E_6$ phase transitions. By performing these simulations, we also investigated whether REMD is advantageous over conventional MD for modelling phase transitions, the influence of the starting configuration and the MD simulation pathway had on the colloidal structure formation and obtained insight into the colloidal structures present in isotropic regions above the hexagonal and lamellar phases in $C_{12}E_6$/water phase diagram. The details of the systems studied are presented in Table 1 and the results of each phase transition simulation are discussed in detail below.

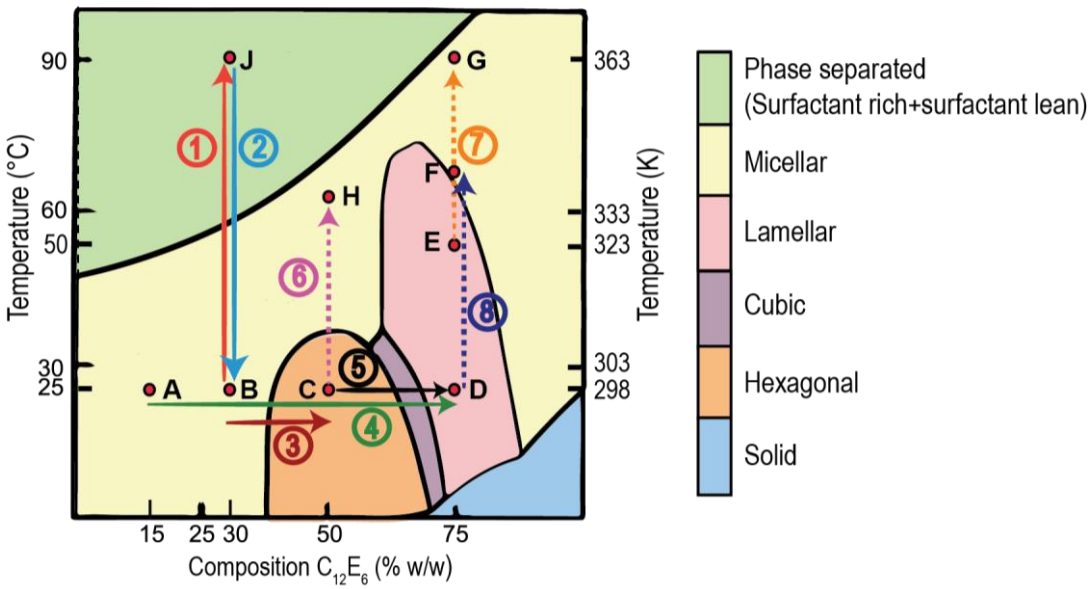

Figure 2 – Phase transitions (1 to 8) modeled in the study using molecular dynamics. Solid arrows show conventional MD simulations and dashed arrows denote the REMD method.

Table 1 – Details of phase transition MD simulations in the current study.

Sim.	Transition or point[a]	Type[b] (Num. replicas)	Transition	[$C_{12}E_6$][c] (% w/w)	Num. $C_{12}E_6$	Num. water	Temp or range (K)[d]	Approx. cell size (nm)	Pressure coupling[e]	Time[f] (ns)
R1	B	MD from random	-	30	1353	78952	298	15×15×15	I	1000
R2	J			30	1353	78952	363	15×15×15	I	500
R3	B			30	18040	1052700	298	36×36×36	I	100
1‡	B* to J	MD	Micellar to phase sep.	30	1353	78952	363	15×15×15	I	500
2‡	J* to B		Phase sep. to micellar	30	1353	78952	298	15×15×15	I	1000
3‡	B to C		Micellar to hexagonal	50	18040	451160	298	31×31×29	S	500
4‡	A‡ to D		Micellar to lamellar	75	867	7228	298	10×10×10	I	500
5‡	C to D		Hexagonal to lamellar	75	1340	11171	298	10×10×12	I	600
6‡	C to H	REMD (42)	Hexagonal to isotropic	50	1340	33511	298–334	12×12×14	I	150
7‡	E to G	REMD (32)	Lamellar to isotropic	75	1340	11171	323–364	10×10×13	I	150
8‡	D to F	REMD (34)	Lamellar[g]	75	1340	11171	298–339	10×10×13	I	300

‡Numbers are matched with the phase transitions shown in Figure 2. [a] Simulated transition or point on the phase diagram. *Unaltered final frames or ‡modified frames from a previous investigation[76] were used as starting configurations. [b] Simulation type: MD = conventional MD, REMD = replica exchange molecular dynamics. [c] Weight percentage of $C_{12}E_6$. [d] For REMD simulations, a complete list of temperatures is given in the Supplementary Information. [e] Pressure coupling method: I = isotropic, S = semi-isotropic. [f] Simulation time. [g] Note that there is no phase transition between points D and F.

Transitions across the cloud point phase boundary (B to J and J to B)

To investigate whether MD simulations effectively model transitions across the cloud point boundary, we simulated transitions between the micellar (B) and phase separated region (J) in both directions. The B to J transition (Sim **1**) was started from a system consisting of six micelles that had been equilibrated at point B; the simulation temperature was increased to 363 K and 500 ns of conventional MD simulation was carried out. The simulation in the opposite direction (Sim **2**) started with a single $C_{12}E_6$ aggregate that resulted from equilibration at point J; the temperature was set to 298 K (corresponding to point B) and conventional MD was run for 1000 ns. To evaluate whether the structure formed depended on the starting configuration or the pathway, additional simulations were performed starting from randomly distributed $C_{12}E_6$ molecules at points B and J (Sims **R1** and **R2**).

The initial and final structures of simulations **1** and **2** are shown in Figure 3. The final structures of simulation **R1** and **R2** are shown in Figure S1 in the Supplementary

Information. Sim **1** formed a lump and MD simulation at point J from random distribution also formed a similar structure. Sim **2** formed a single aggregate of all 1344 $C_{12}E_6$ surfactants creating a non-straight, branched rod-like micelle (wormy micelle). MD simulation at point B from the random distribution formed two aggregates, one is an elongated non-straight un-branched rod-like micelle (wormy micelle) with 1205 $C_{12}E_6$ surfactants while the second aggregate is a spherical micelle located close to the wormy micelle.

Figure 4 shows the convergence of the $C_{12}E_6$ SASA for simulations from phase transitions and random distributions. Above the cloud point (at point J) the SASA of the systems started from micelles (Sim **1**) and a random distribution (Sim **R2**) reach a stable value within 100 ns and maintain that value for 400 ns of simulation time (Figure 4(a)). Below the cloud point (at point B), the SASA of the systems started from a single aggregate and random distribution converge more slowly, reaching similar values after 1000 ns of simulation (Figure 4(b)).

Since we have two colloidal structures from two different pathways (i.e., from the phase transition simulation and started from random distribution) the structural properties and system energies should be the same if structure formation is independent of starting configuration or simulation pathway. Therefore, to compare energies, the averaged potential energy from the last 100 ns of each simulation was calculated. The average potential energy over the last 100 ns of the of the simulations **1** and **R2** is the same within error (Sim **1**: -2.0416 ± 0.0028 GJ/mol. Sim **R2** -2.0415 ± 0.0027 GJ/mol). The average potential energy for the colloidal structure formed in Sim **2** is -2.4088 ± 0.0023 GJ/mol and the same property for the structure formed at point B from randomly distributed molecules is -2.4099 ± 0.0023 GJ/mol. Therefore, the colloidal structure formed from randomly distributed molecules at point B is stable by ~1000 kJ/mol compared to the colloidal structure from phase transition MD simulation. Thus, the elongated non-straight un-branched rod-like micelle is more stable at point B.

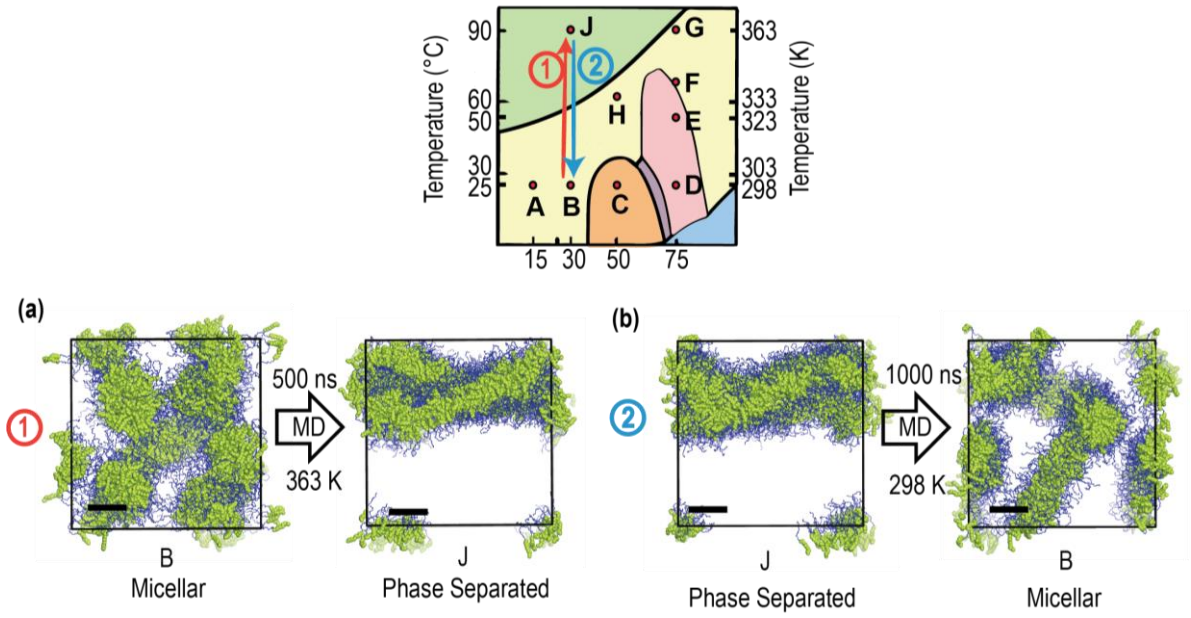

Figure 3 – Modelling of transitions across the cloud point phase boundary. (a) The transition from micellar (B) to phase separated region (J). (b) The transition from phase separated region (J) to the micellar region (B). Surfactant coloring: alkane tail (lime), PEO head group (blue). Water is not shown for clarity. The scale bar length is 3.0 nm.

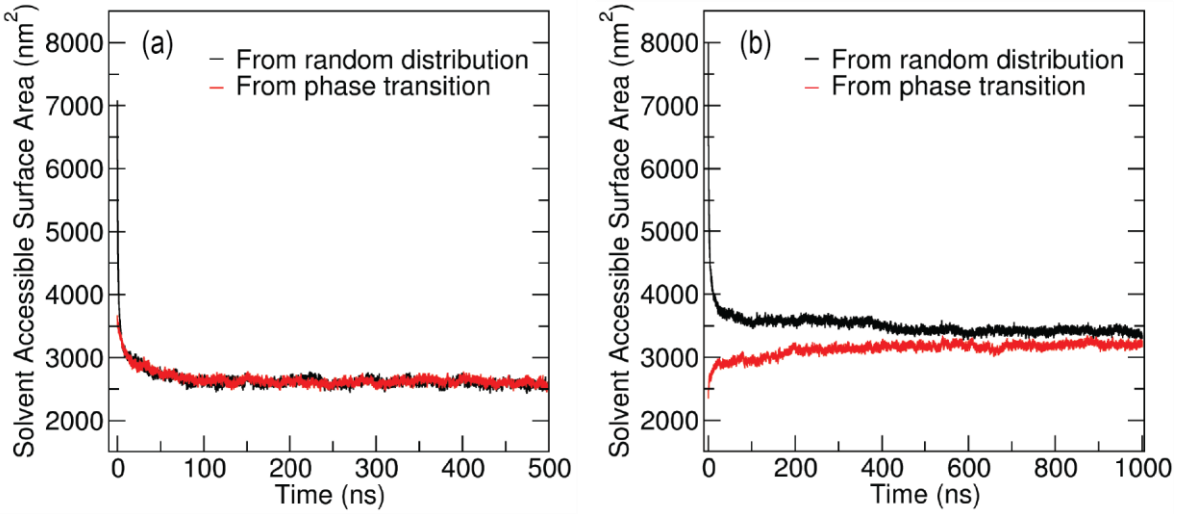

Figure 4 – Comparison of SASA in phase transition simulations with simulations started from a random distribution of surfactant molecules. (a) Simulation at point J from MD simulation from random distribution (black) and B to J phase transition MD simulation (red). (b) Simulation at point B from the random distribution (black) and J to B phase transition MD simulation (red).

Micellar to hexagonal (B to C)

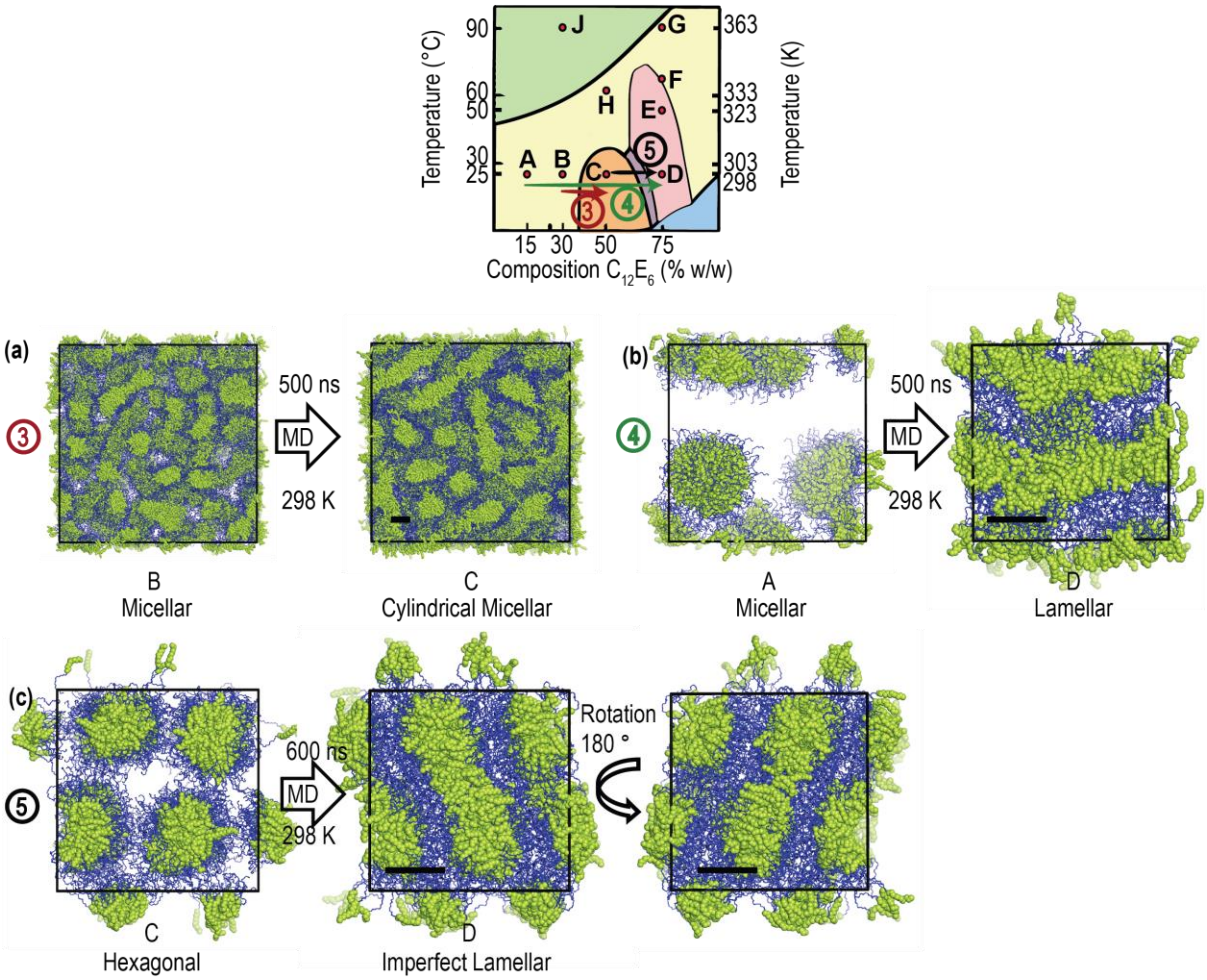

Figure 5 – Modelling of constant-temperature transitions: (a) micellar to hexagonal, (b) micellar to lamellar and (c) hexagonal to lamellar. Surfactant coloring: tail (lime), head group (blue). Water is not shown for clarity. The scale bar length is 3.0 nm and is shown only on the final frames of each phase transition. Note that the box size in simulation B to C transition is larger than the others: 31×31×29 nm.

To investigate phase transformations due to changes in $C_{12}E_6$ composition, we modeled phase transitions between the micellar and hexagonal phase regions: B to C (Sim **3**). To model the transition from B to C, we ran a MD simulation for 100 ns to get micelles at point B using ~36 nm cubic box (Sim **R3**). The simulation at point B yielded 86 aggregates (short rod-like micelles) with the average aggregation size of 208 and SASA for $C_{12}E_6$ confirmed the structure has reached a stable configuration. To model the phase transition B to C, using the micellar structure at point B, we adjusted the number of water molecules to 451,160 to resemble the water composition (50% w/w

water) at point C and the system was simulated for 500 ns at 298 K. The colloidal structure was visually inspected as shown in Figure 5(b) and SASA was calculated (see Supplementary Information, Figure S2(b)).

This simulation formed elongated cylindrical micelles which are occasionally branched. This structure is most likely trapped within a local minimum state of the conformational space, which will require a longer simulation or enhanced simulation methods to allow the system to leave the local minima. Therefore, the structure obtained is not the global minimum for this composition.

Micellar to lamellar (A to D)

The phase transition from micelles to lamellar (A to D) was modelled starting from a system of 4 micelles that had been previously equilibrated at point A, with the amount of water then reduced to match with the composition at point D. MD simulation was carried out for 500 ns (Sim **4**). The structure formed is shown in Figure 5(c). A plot of the surfactant SASA in the structure is shown in Figure S2(c) in the SI. The final equilibrated structure is a lamellar structure with pores in the layers, which is consistent with the experimental observation for the lamellar phase of $C_{12}E_6$.[77] The SASA remains constant for the last 400 ns confirming that the final system is in a stable state. It is interesting to note that, within the first 50 ns, the SASA increases significantly, indicating a drastic change in the molecular structure. The assembly of the surfactants into layers enable surfactants to interact more with water and thus the drastic increment we noticed in the SASA is due to the formation of layers from the micellar structure.

Hexagonal to lamellar (C to D)

To model the transformation between hexagonal and lamellar (C to D), we prepared a pre-built hexagonal structure resembling 75% w/w $C_{12}E_6$ in the aqueous environment and MD simulation (Sim **5**) was carried out for 600 ns with the SASA being stable (Figure S2(d) in SI) for the last 400 ns of the simulation. Inspection revealed that cylindrical micelles in the hexagonal phase are merged and formed a layer like structure from one phase of the simulation box. From the opposite phase of the simulation box (rotation by 180°), still, we observed cylindrical micellar character that

resembles the hexagonal phase (see Figure 5(d)) implying the structure is imperfect lamellar-like.

Hexagonal to isotropic phase (C to H)

The physical behavior of the isotropic phase region above the hexagonal phase of $C_{12}E_6$/water phase diagram is poorly understood. To investigate this structure, we conducted simulations from point C in the hexagonal phase region to H in the isotropic region using REMD. Starting from a prebuilt equilibrated hexagonal structure (built as described previously[76]), REMD simulation was carried for 150 ns using 42 replicas with neighbor acceptance ratio 20% (Sim **6**). To discuss the REMD simulations, we denote the simulation replicas as R_i, where i = 0 to n - 1 and n = number of system copies in the simulation. Each replica R_i is assigned a temperature, given by the temperature index T_i. For example, in this simulation, the lowest temperature index T_0 is 298 K and the highest temperature index T_{41} is 333.61 K. Figure 6(a) shows the variation of temperature indexes vs time for 4 selected replicas. The potential energy probability distributions for systems with the first 10 temperatures/replicas considering last 50 ns of the simulation time are shown in Figure 6(b) and this property calculated for all temperatures in our REMD simulation is shown in Figure S3(a) in the SI. To investigate whether the system at point H has reached a stable configuration, we calculated SASA for $C_{12}E_6$ molecules in the system with 333.61 K temperature as shown in Figure S2(b) in the SI. The colloidal structures formed at point H, near the phase boundary and point C are shown in Figure 7.

As shown in Figure 6(a), the system at 299.66 K (blue line) visited the entire temperature space. Further, it visited any given replica many times within 150 ns. This implies that replica R_0 is performing stochastic coordinate exchange with every other replica (R_2-R_{41}) during the REMD simulation. This type of behavior can be observed with many replicas in the simulation and it is a good indication that the REMD work properly[78]. Further, random walk of the replica R_0 (298 K, red line in Figure 6(a)) is restricted to the temperatures below 320.21 K (temperature index 26) and the random walk of R_{26} (320.21 K, orange line in Figure 6(a)) and R_{41} (333.61 K, green line in Figure 6(a)) is restricted to the higher (beyond the temperature index 26) temperatures. This observation implies that some replicas favor the exchange coordinates with lower temperature indexes while some replicas favor exchanges

coordinate with high temperature indexes. Also, Figure 6(b) shows that significant potential energy overlaps between adjacent pairs of temperatures and this pattern is true for all temperatures in REMD simulation (Figure S3(a) in SI). That implies exchanges between neighboring replicas in the phase transition REMD simulation are properly maintained.[79] All facts discussed so far indicate that the REMD simulation worked properly and effectively for the phase transition we considered.[48]

In this phase transition, we expect the liquid crystal (hexagonal) is deformed and transforms into an isotropic structure above the hexagonal phase region. At point H, we found two aggregates in the simulation cell, which are layers with defects (pores and curvature effect) resembling a lamellar like structure (Figure 7). We noticed a hexagonal phase arrangement in the system at 298 K, which is in a good agreement with the experimental phase diagram because point C is in the hexagonal region. The visual examination further revealed that systems at 298 K to 319.33 K possess hexagonal phase colloidal structures, though the system at 320.21 K contains a colloidal structure deviated from the hexagonal phase arrangement. This colloidal structure is no longer cylindrical micelles where two of cylindrical micelles merged and formed two aggregates with aggregation numbers 336 and 997. Further, systems beyond the temperatures 320.21 K behave similarly, forming one or two aggregates. Previously, in Figure 6(a), we noticed that the random walk of replicas R_{26} (320.21 K) and R_{41} (333.61 K) is restricted to higher temperatures and random walk of temperature R_0 (298 K) is restricted to the temperatures below 320.21 K. The reason can be clearly explained with the colloidal behavior observed in the simulation. That is, systems at 320.21 K and 333.61 K are no longer preferred to be in the hexagonal phase and thus coordinates are exchanged only with systems in higher temperatures while 298 K system is preferred to be in a hexagonal phase, thus it exchanges coordinates with systems below 320.21 K. Since we observed a structural difference at 319.33–320.21 K, the phase boundary lies between that temperature range. However, this value is approximately 10 °C away from the experimental value 309.75 K. It is important to note that force fields are not parameterized to reproduce the exact phase behavior/phase transitions of molecules and thus reproducing the phase transition within 10 °C from the experimental value is acceptable.

The experimental structure of the isotropic region above the hexagonal phase is poorly understood. However, Sallen et al. investigated pretransitional effects near hexagonal-micellar phase transition of $C_{12}E_6$/water mixture.[80] To interpret their observed experimental data, they proposed that the isotropic phase (micellar phase) is made of disordered bilayers or branched interconnected cylindrical micelles which could be broken into short segments spontaneously or it could form bridged micelles connecting close cylindrical micelles. With our simulation, we observed bridging of cylindrical micelles at 320.21 K to 331.8 K and we observed disordered bilayers at 332.71 K and 333.61 K. We did not notice fragmentation of cylindrical micelles into small segments with our REMD simulation. Thus, our simulations revealed the formation of disordered bilayers in the isotropic phase above the hexagonal region by bridging cylindrical micelles with the temperature increment. Due to the bridging of cylindrical micelles, there is no preferred orientation of molecules and that makes a decrease in the quadrupole order parameter *S* of the molecules within the cylinder, which leads to the formation of an isotropic phase at point H.

Overall, results in this section indicate that MD adequately modeled the phase transition of hexagonal to isotropic phase and we were able to determine phase transition boundary close to the experimental value. Besides, we observed structural changes when the transition occurs from hexagonal to isotropic phase. According to REMD simulation, the colloidal structure in the isotropic region above the hexagonal phase is disordered bilayers. Through REMD simulation, we can thoroughly identify structural changes due to temperature elevation, which is beneficial over conventional MD simulations.

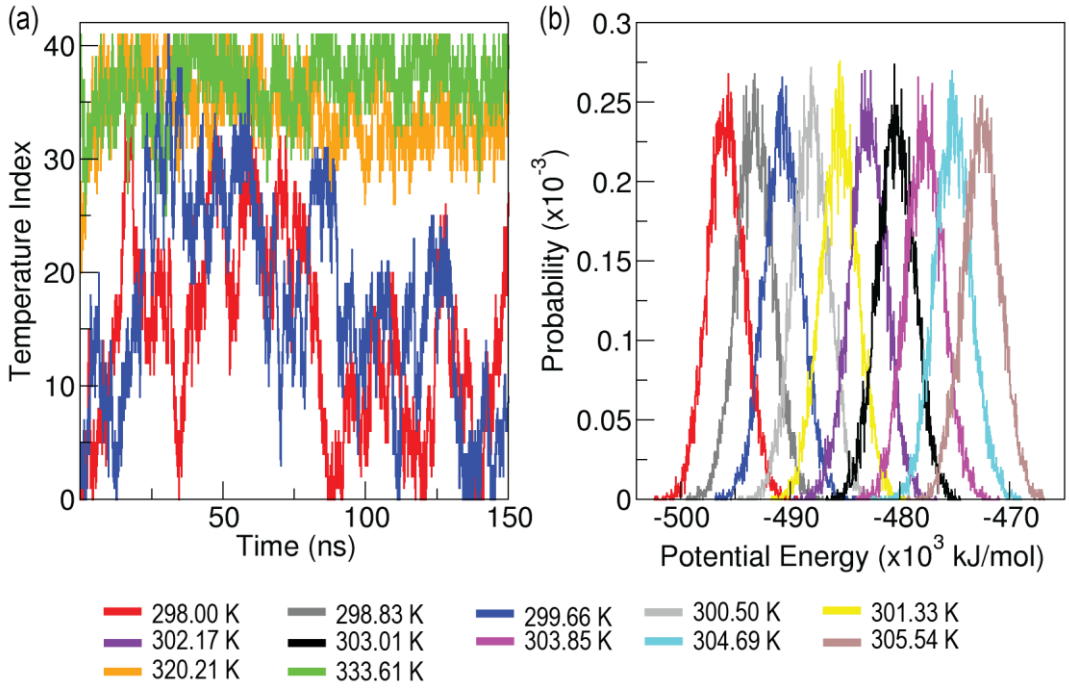

Figure 6 – (a) Random walk of replicas R_0, R_2, R_{26} and R_{41} in the temperature space. (b) The potential energy probability distribution for the first ten temperatures (298 K to 305.54 K)

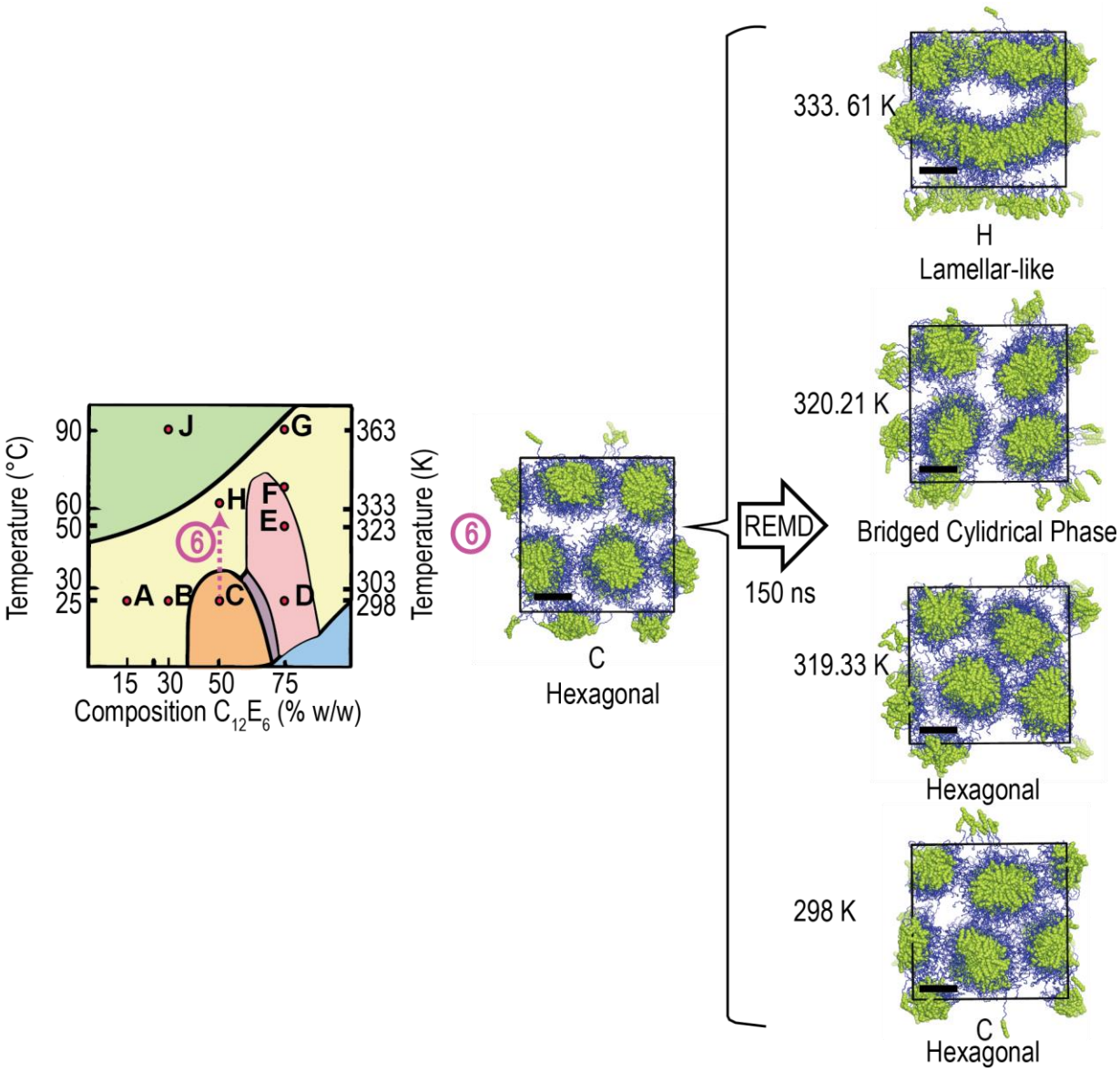

Figure 7 – REMD simulations of phase transitions from hexagonal to isotropic region. Surfactant coloring: alkane tail (lime), PEO head group (blue). Note that in the phase transition from lamellar (E) to the isotropic region (G), head groups of surfactants are not shown. Water is not shown for clarity. The scale bar length is 3.0 nm.

Lamellar to isotropic phase (E to G)

The colloidal structural behavior in the isotropic phase above the lamellar region of $C_{12}E_6$/water phase diagram is far from being understood. Thus, to determine the colloidal structure at the point G in the isotropic phase using MD and to examine how effectively MD simulates the phase transition between lamellar (point E) and isotropic phase (point G) (Figure 2), REMD simulation was conducted using 32 replicas in the temperature range 323–364.35 K.

To model this phase transition, the equilibrated initial molecular configuration was taken from the system at 323.69 K in REMD simulation carried out in the lamellar region (Sim **8** in the current study). After equilibration of replicas at relevant temperatures, the REMD simulation was conducted for 150 ns (Sim **7**). To ensure that REMD simulation is working properly, we plotted the potential energy probability distribution for the 32 replicas for the last 50 ns of simulation time (Figure S5(a) in SI) and checked the random walk of replicas within the temperature space (Figure S5(b) in SI). To check whether the system has reached a stable state at point G (363 K), SASA was calculated (Figure S5(c) in SI). We examined all final colloids formed in REMD simulation as shown in Supplementary Information, Figure S6 to study structural changes occur with the temperature elevation and to determine the phase transition boundary through the simulation. Colloids at point G and phase boundary are shown in Figure 8(b).

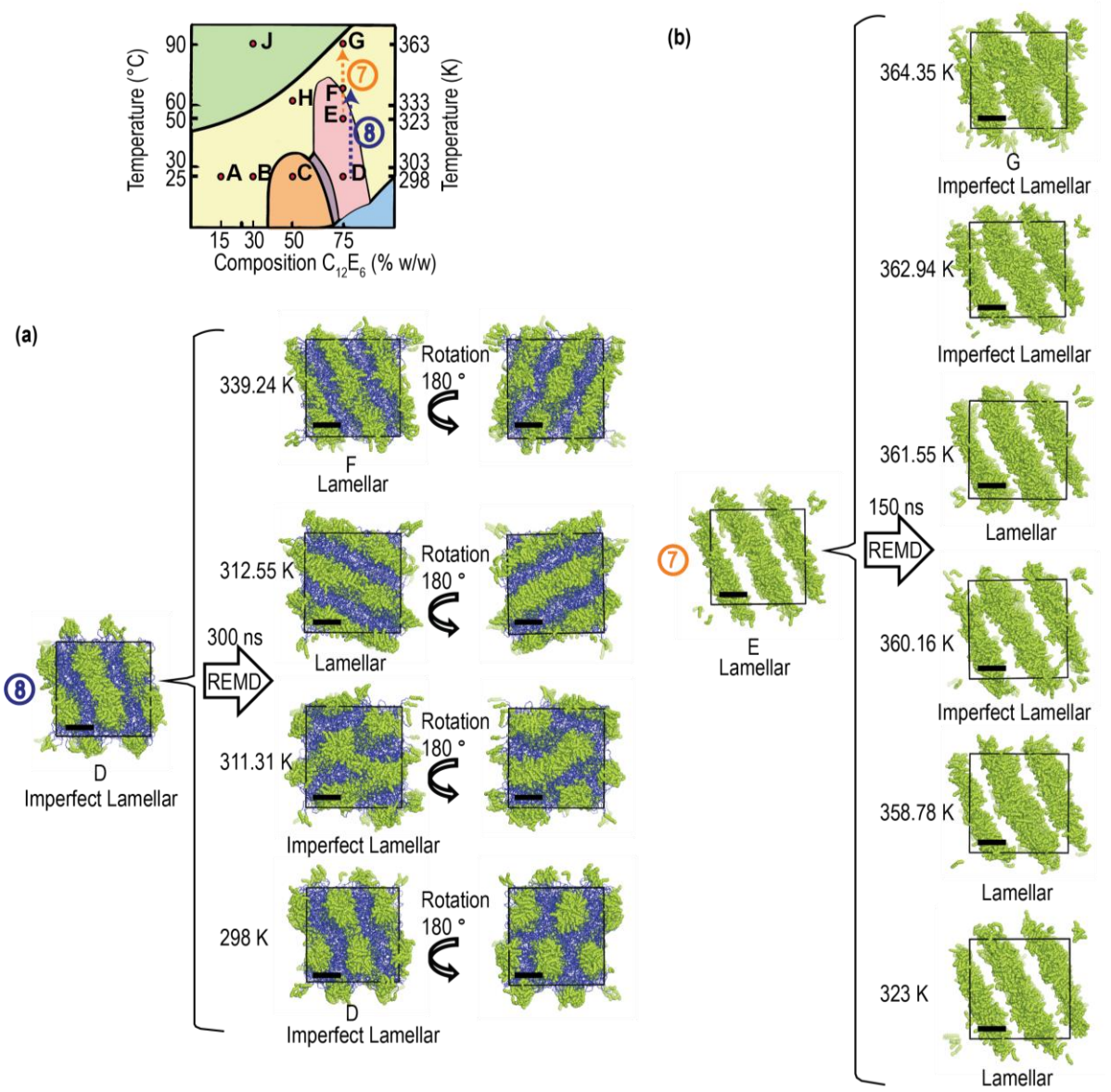

Figure 8 – (a) REMD simulations in lamellar region. (b) REMD simulations of phase transitions from lamellar to isotropic region. (Surfactant coloring: alkane tail (lime), PEO head group (blue). Water and tails of the surfactants in E to G transition are not shown for clarity. The scale bar length is 3.0 nm.

The potential energy probability distributions (Figure S5(a) in SI) in all temperatures overlap with the neighboring distribution curves, confirming that exchanges between neighboring replicas in the REMD simulation are properly maintained. Most of the random walks of replicas have visited all the temperatures, and the random walk of the first replica R_0 (323 K) is illustrated in Figure S5(b) as an example. These facts confirmed that REMD simulations worked properly and effectively. The SASA is not

changing significantly (Figure S5(c)) during the 150 ns REMD simulation time, indicating that the system has reached a stable configuration.

According to Figure 8(b) at point E, we observed the formation of porous lamellar structure, and this structure can be seen until the temperature reaches 358.78 K and at the temperature of 361.55 K. Beyond the temperature of 361.55 K and at point G, we observed a different colloidal structure compared to point E, forming interconnected or linked $C_{12}E_6$ layers with pores. The interconnection of layers in the structure occurs with two neighboring layers via a single link. Thus, there is a clear colloidal structural difference in the temperature range of 358.78–362.94 K and therefore, the phase boundary for lamellar to isotropic region lies in that temperature range. This compares favorably with the experimental phase boundary temperature of 338.25 K (calculated from the experimental phase digarm[9]).

To the best of our knowledge, there is no experimental structural information for the isotropic phase of $C_{12}E_6$ above its lamellar region. This information may not be readily accessible from experimental measurements due to the lack of long-range order and birefringence that prevent the use of experimental techniques such as X-ray diffraction and optical microscopy[81]. Yet, it is apparent from our REMD simulation that the colloidal structure in the isotropic phase above the lamellar region is layered with pores which are interconnected via single linkage. However, an experimental investigation conducted by Constantin and Oswald showed that abrupt increase in the diffusion coefficient when approaching lamellar-isotropic phase transition.[77] The study explains that is due to the defects connecting the surfactant structure. In detail, when the phase transition is approaching toward the isotropic phase, the nonpolar medium in the lamellar phase increases its connectivity, whereas the connectivity of the polar medium decreases. Thus, the defects in low temperatures are pores and defects in high temperatures are necks (Fig.1 in Reference 77). This experimental evidence matches with the two colloidal structures we observed in our REMD simulation since in perfect lamellar regions we observed pores, while at high temperatures (beyond 361.55 K), especially in the isotropic phase we observed interconnected layers through a single link, which represents the neck type defect according to the Constantin and Oswald's study. Alternatively, interconnected layers through single link type colloidal structure formation are evident at 80% w/w $C_{12}E_6$ at 363 K from our previous study conducted with the MD simulation from a random distribution.[76]

Lamellar to lamellar (D to F)

We observed the formation of an imperfect lamellar region for the phase transition from hexagonal to lamellar (point C to point D transition in Figure 2) with the conventional MD simulation in this study where it should form a lamellar structure according to the experimental phase digarm[9]. We suspected that the imperfect lamellar structure from conventional MD simulation from point C to point D phase transition is trapped in a local minimum state, which requires longer or enhanced the sampling method to get the global minimum structure at point D. Thus, to check whether we can achieve the global minimum (lamellar) at point D, we explored the conformational space in the lamellar region of $C_{12}E_6$/water phase diagram more thoroughly using an enhanced sampling method, REMD.

The final colloidal structure formed in the phase transition from hexagonal to lamellar (Sim **5** the current study) was used as the initial configuration for 34 replicas in the temperature range of 298–339.24 K. REMD simulation was carried out for 300 ns giving more simulation time (compared to the other two REMD simulations) to exchange coordinates with neighboring systems (Sim **8**). Note that point F is in the phase boundary of lamellar-isotropic phase. Thus, there is a probability that we could observe two colloidal structures with the simulation representing lamellar and isotropic phases. Similar to previous REMD simulations, we plotted the potential energy probability distribution for all temperatures considering last 50 ns of the simulation (Figure S7(a) in SI) and the random walk of replica R_3 (301.59 K) in the temperature space (Figure S7(b) in SI) to ensure that REMD worked properly. SASA was plotted for $C_{12}E_6$ using the first system in REMD simulation to identify the stability of the colloidal structure formed in the system at 298 K as shown in Figure S7(c) in SI. The visual observation of the colloidal structures at 298 K, 311.31 K, 312.55 K and at the 339.24 K is shown in Figure 8(a) while colloidal structures in all replicas are shown in Figure S8 in the SI.

Potential energy probability distributions in all temperatures are overlapped (Figure S7(a) in SI). The random walk of many replicas frequently jumps (exchange coordinates) to all temperatures in the simulation, which indicates a reasonable stochastic mixing of systems. The random walk of R_3 (301.59 K) is shown in Figure S7(b) as an example to show that R_3 (301.59 K) replica visits all temperature space.

These facts ensured that REMD simulation performed in the lamellar region worked properly and effectively. SASA (Figure S7(c)) indicates that SASA is maintained in a constant value and thus, the system is in a stable state.

With the visual examination, we noticed an imperfect lamellar structure formation at the temperature range 298–311.31 K and in these structures from the front of the simulation box, we observed layers (merged cylinders) and from the opposite side, the hexagonal character was visible. This molecular arrangement is similar to the colloid formed at point D in the phase transition from point C to point D carried out with conventional MD simulation, Sim **5**. Even though we suspected that the imperfect lamellar structure at point D is a local minimum, from the REMD method also we observed the similar colloidal structure formation at point D. We cannot be sure whether the formation of imperfect lamellar phase at 298 K (from conventional MD as well as REMD) is due to an issue with the 2016H66 force field which does not model the high concentration surfactant behavior at 298 K. On the other hand, it is possible to form imperfect lamellar structure at 298 K, but currently, we do not have any evidence to support that since this type of microstructural details are difficult to extract through experimental investigations. However, beyond 311.31 K, we detected an ideal lamellar phase with pores except for systems at temperatures 331.39 K and 336.60 K. At temperatures 331.39 K and 336.60 K, we noticed the formation of linked porous layered structure.

Conclusion

In this work, we have extensively tested how effectively MD simulates phase transitions of one of the PEO surfactant $C_{12}E_6$ in water. Phase transitions due to the temperature variations and composition changes were explored using conventional MD simulation and REMD simulations. These simulations started with one colloidal structure, translated it to a different location on the experimental phase diagram, and then determined if the expected, different equilibrium liquid phase was formed. Besides, we have also investigated whether REMD provides benefits over conventional MD simulations in phase transitions. Further, we studied how the initial configuration or MD simulation pathway influences the final colloidal structure formation. Finally, we investigated the colloidal structure formation in less

experimentally explored isotopic regions above the hexagonal and lamellar phases in $C_{12}E_6$/water phase diagram.

Our results show that all phase transitions considered successfully reproduced, except the micellar to the hexagonal phase transition. However, within that phase transition, the formation of elongated cylindrical micelles from the micellar structure was observed, the characteristic behavior of the hexagonal phase. Thus, united atom models can be used to model phase transitions of PEO surfactants effectively. REMD was also found to be a suitable method for exploring temperature phase transitions since we can explore the colloidal behavior of the surfactant in a wide temperature range by a single simulation. Alternatively, phase transition temperatures determined through REMD simulations agreed well with experimental phase transition temperatures. The only concern in this method the computational resources needed for the REMD simulation are demanding. Besides, we noticed that longer conventional MD simulations are beneficial to move the system toward global minima. In detail, we observed a change in the colloidal structures due to longer simulations even though at first sight we decided the system has reached the most stable configuration by looking at SASA calculations (i.e., phase transition of phase separation to micellar in this study). Thus, SASA needs to be used carefully for determining system stability of colloidal systems. The colloidal structure formation was found to be independent of the initial structure or pathway, only depending on the temperature and surfactant composition. Further, colloidal structures in the isotropic region above the hexagonal phase were determined as disordered bilayers while isotropic region above the lamellar phase was determined as linked porous layers.

References

1. Vithani, K.; Jannin, V.; Pouton, C. W.; Boyd, B. J., Colloidal Aspects of Dispersion and Digestion of Self-Dispersing Lipid-Based Formulations for Poorly Water-Soluble Drugs. *Adv. Drug Deliv. Rev.* **2019,** *142*, 16-34.

2. Porter, C. J. H.; Pouton, C. W.; Cuine, J. F.; Charman, W. N., Enhancing Intestinal Drug Solubilisation Using Lipid-Based Delivery Systems. *Adv. Drug Deliv. Rev.* **2008,** *60* (6), 673-691.

3. Kossena, G. A.; Boyd, B. J.; Porter, C. J. H.; Charman, W. N., Separation and Characterization of the Colloidal Phases Produced on Digestion of Common Formulation Lipids and Assessment of Their Impact on the Apparent Solubility of Selected Poorly Water-Soluble Drugs. *J. Pharm. Sci.* **2003,** *92* (3), 634-648.

4. King, D. T.; Warren, D. B.; Pouton, C. W.; Chalmers, D. K., Using Molecular Dynamics to Study Liquid Phase Behavior: Simulations of the Ternary Sodium Laurate/Sodium Oleate/Water System. *Langmuir* **2011,** *27* (18), 11381-11393.

5. Wang, Y.; Jiang, W.; Yan, T.; Voth, G. A., Understanding Ionic Liquids through Atomistic and Coarse-Grained Molecular Dynamics Simulations. *Acc. Chem. Res.* **2007,** *40* (11), 1193-1199.

6. Shinoda, W.; DeVane, R.; Klein, M. L., Coarse-Grained Molecular Modeling of Non-Ionic Surfactant Self-Assembly. *Soft Matter* **2008,** *4* (12), 2454-2462.

7. Sterpone, F.; Briganti, G.; Pierleoni, C., Sphere versus Cylinder: The Effect of Packing on the Structure of Nonionic $C_{12}E_6$ Micelles. *Langmuir* **2009,** *25* (16), 8960-8967.

8. Velinova, M.; Sengupta, D.; Tadjer, A. V.; Marrink, S.-J., Sphere-to-Rod Transitions of Nonionic Surfactant Micelles in Aqueous Solution Modeled by Molecular Dynamics Simulations. *Langmuir* **2011,** *27* (23), 14071-14077.

9. Mitchell, D. J.; Tiddy, G. J. T.; Waring, L.; Bostock, T.; McDonald, M. P., Phase Behaviour of Polyoxyethylene Surfactants with Water. Mesophase Structures and Partial Miscibility (Cloud Points). *J. Chem. Soc., Faraday Trans. 1* **1983,** *79* (4), 975-1000.

10. Frankewich, R. P.; Hinze, W. L., Evaluation and Optimization of the Factors Affecting Nonionic Surfactant-Mediated Phase Separations. *Anal. Chem.* **1994,** *66* (7), 944-954.

11. Dave, N.; Joshi, T., A Concise Review on Surfactants and Its Significance. *Int. J. Appl. Chem.* **2017,** *13* (3), 663672.

12. Chen, B.-H.; Miller, C. A.; Walsh, J. M.; Warren, P. B.; Ruddock, J. N.; Garrett, P. R.; Argoul, F.; Leger, C., Dissolution Rates of Pure Nonionic Surfactants. *Langmuir* **2000,** *16* (12), 5276-5283.

13. Maccarini, M.; Briganti, G., Density Measurements on $C_{12}E_j$ Nonionic Micellar Solutions as a Function of the Head Group Degree of Polymerization (j = 5−8). *J. Phys. Chem. A* **2000,** *104* (48), 11451-11458.

14. Chiu, Y. C.; Chen, L. J., Refractive Index of Nonionic Surfactant Solutions Containing Polyoxyethylene Mono-n-Alkylether. *Colloids Surf.* **1989,** *41*, 239-244.

15. Zulauf, M.; Weckstrom, K.; Hayter, J. B.; Degiorgio, V.; Corti, M., Neutron Scattering Study of Micelle Structure in Isotropic Aqueous Solutions of Poly(oxyethylene) Amphiphiles. *J. Phys. Chem.* **1985,** *89* (15), 3411-3417.

16. Brown, W.; Johnsen, R.; Stilbs, P.; Lindman, B., Size and Shape of Nonionic Amphiphile ($C_{12}E_6$) Micelles in Dilute Aqueous Solutions as Derived from Quasielastic and Intensity Light Scattering, Sedimentation, and Pulsed-Field-Gradient Nuclear Magnetic Resonance Self-Diffusion Data. *J. Phys. Chem.* **1983,** *87* (22), 4548-4553.

17. Gapiński, J.; Szymański, J.; Wilk, A.; Kohlbrecher, J.; Patkowski, A.; Hołyst, R., Size and Shape of Micelles Studied by Means of SANS, PCS, and FCS. *Langmuir* **2010,** *26* (12), 9304-9314.

18. Yoshimura, S.; Shirai, S.; Einaga, Y., Light-Scattering Characterization of the Wormlike Micelles of Hexaoxyethylene Dodecyl $C_{12}E_6$ and Hexaoxyethylene Tetradecyl $C_{14}E_6$ Ethers in Dilute Aqueous Solution. *J. Phys. Chem. B* **2004,** *108* (40), 15477-15487.

19. Balmbra, R. R.; Clunie, J. S.; Corkill, J. M.; Goodman, J. F., Effect of Temperature on the Micelle Size of a Homogeneous Non-Ionic Detergent. *Trans. Faraday Soc.* **1962,** *58* (0), 1661-1667.

20. Yethiraj, A.; Capitani, D.; Burlinson, N. E.; Burnell, E. E., An NMR Study of Translational Diffusion and Structural Anisotropy in Magnetically Alignable Nonionic Surfactant Mesophases. *Langmuir* **2005,** *21* (8), 3311-3321.

21. Penaloza, D. P.; Hori, K.; Shundo, A.; Tanaka, K., Spatial Heterogeneity in a lyotropic Liquid Crystal with Hexagonal Phase. *Phys. Chem. Chem. Phys.* **2012,** *14* (15), 5247-5250.

22. Rancon, Y.; Charvolin, J., Epitaxial Relationships During Phase Transformations in a Lyotropic Liquid Crystal. *J. Phys. Chem.* **1988,** *92* (9), 2646-2651.

23. Allain, M.; Meglio, J.-M. D., Highly Curved Defects in Lyotropic Lamellar Phases. *Mol. Cryst. Liq. Cryst.* **1985,** *124* (1), 115-124.

24. Paz, L.; Di Meglio, J. M.; Dvolaitzky, M.; Ober, R.; Taupin, C., Highly Curved Defects in Lyotropic (Nonionic) Lamellar Phases. Origin and role in hydration process. *J. Phys. Chem.* **1984,** *88* (16), 3415-3418.

25. Clunie, J. S.; Goodman, J. F.; Symons, P. C., Phase Equilibria of Dodecylhexaoxyethylene Glycol Monoether in Water. *Trans. Faraday Soc.* **1969,** *65* (0), 287-296.

26. Capitani, D.; Casieri, C.; Briganti, G.; La Mesa, C.; Segre, A. L., Phase Diagram of the $C_{12}E_6/D_2O$ System Revisited: Effect of Strong Magnetic Fields. *J. Phys. Chem. B* **1999,** *103* (29), 6088-6095.

27. Thomas, H. G.; Lomakin, A.; Blankschtein, D.; Benedek, G. B., Growth of Mixed Nonionic Micelles. *Langmuir* **1997,** *13* (2), 209-218.

28. Fabio Sterpone, C. P., Giuseppe Brigant, Massimo Marchi, Molecular Dynamics Study of Temperature Dehydration of a $C_{12}E_6$ Spherical Micelle. *Langmuir* **2004,** *20*, 4311-4314.

29. Rossi, G.; Fuchs, P. F. J.; Barnoud, J.; Monticelli, L., A Coarse-Grained MARTINI Model of Polyethylene Glycol and of Polyoxyethylene Alkyl Ether Surfactants. *J. Phys. Chem. B* **2012,** *116* (49), 14353-14362.

30. Guruge, A. G.; Warren, D. B.; Benameur, H.; Pouton, C. W.; Chalmers, D. K., Aqueous Phase Behavior of the PEO-Containing Non-Ionic Surfactant $C_{12}E_6$: A Molecular Dynamics Simulation Study. *J. Colloid Interface Sci.* **2021,** *588*, 257-268.

31. Denham, N.; Holmes, M. C.; Zvelindovsky, A. V., The Phases in a Non-Ionic Surfactant ($C_{12}E_6$)−Water Ternary System: A Coarse-Grained Computer Simulation. *J. Phys. Chem. B* **2011,** *115* (6), 1385-1393.

32. Nakamura, H.; Tamura, Y., Phase Diagram for Self-Assembly of Amphiphilic Molecule $C_{12}E_6$ by Dissipative Particle Dynamics Simulation. *Comput. Phys. Commun.* **2005,** *169* (1), 139-143.

33. Allen, R.; Bandyopadhyay, S.; Klein, M. L., $C_{12}E_2$ Reverse Micelle: A Molecular Dynamics Study. *Langmuir* **2000,** *16* (26), 10547-10552.

34. Abel, S.; Waks, M.; Marchi, M.; Urbach, W., Effect of Surfactant Conformation on the Structures of Small Size Nonionic Reverse Micelles: A Molecular Dynamics Simulation Study. *Langmuir* **2006,** *22* (22), 9112-9120.

35. Vanin, A. A.; Brodskaya, E. N., Molecular-Dynamics Simulation of the Surface Layer of a Nonionic Micelle. *Colloid J.* **2017,** *79* (3), 310-316.

36. Bandyopadhyay, S.; Tarek, M.; Lynch, M. L.; Klein, M. L., Molecular Dynamics Study of the Poly(oxyethylene) Surfactant $C_{12}E_2$ and Water. *Langmuir* **2000,** *16* (3), 942-946.

37. Senac, C.; Urbach, W.; Kurtisovski, E.; Hünenberger, P. H.; Horta, B. A. C.; Taulier, N.; Fuchs, P. F. J., Simulating Bilayers of Nonionic Surfactants with the GROMOS-Compatible 2016H66 Force Field. *Langmuir* **2017,** *33* (39), 10225-10238.

38. Marrink, S. J.; Risselada, J.; Mark, A. E., Simulation of Gel Phase Formation and Melting in Lipid Bilayers Using a Coarse Grained Model. *Chem. Phys. Lipids* **2005,** *135* (2), 223-244.

39. Marrink, S. J.; de Vries, A. H.; Mark, A. E., Coarse Grained Model for Semiquantitative Lipid Simulations. *J. Phys. Chem. B* **2004,** *108* (2), 750-760.

40. Marrink, S. J.; Risselada, H. J.; Yefimov, S.; Tieleman, D. P.; de Vries, A. H., The MARTINI Force Field: Coarse Grained Model for Biomolecular Simulations. *J. Phys. Chem. B* **2007,** *111* (27), 7812-7824.

41. Leekumjorn, S.; Sum, A. K., Molecular Characterization of Gel and Liquid-Crystalline Structures of Fully Hydrated POPC and POPE Bilayers. *J. Phys. Chem. B* **2007,** *111* (21), 6026-6033.

42. Leekumjorn, S.; Sum, A. K., Molecular Studies of the Gel to Liquid-Crystalline Phase Transition for Fully Hydrated DPPC and DPPE Bilayers. *Biochim. Biophys. Acta, Biomembranes* **2007,** *1768* (2), 354-365.

43. Horta, B. A. C.; de Vries, A. H.; Hünenberger, P. H., Simulating the Transition between Gel and Liquid-Crystal Phases of Lipid Bilayers: Dependence of the Transition Temperature on the Hydration Level. *J. Chem. Theory Comput.* **2010,** *6* (8), 2488-2500.

44. Stevens, M. J., Coarse-Grained Simulations of Lipid Bilayers. *J. Chem. Phys.* **2004,** *121* (23), 11942-11948.

45. Hömberg, M.; Müller, M., Main Phase Transition in Lipid Bilayers: Phase Coexistence and Line Tension in a Soft, Solvent-Free, Coarse-Grained Model. *J. Chem. Phys.* **2010,** *132* (15), 155104.

46. de Vries, A. H.; Yefimov, S.; Mark, A. E.; Marrink, S. J., Molecular Structure of the Lecithin Ripple Phase. *Proc. Natl. Acad. Sci. U.S.A.* **2005,** *102* (15), 5392-5396.

47. Nagai, T.; Ueoka, R.; Okamoto, Y., Phase Behavior of a Lipid Bilayer System Studied by a Replica-Exchange Molecular Dynamics Simulation. *J. Phys. Soc. Jpn.* **2012,** *81* (2), 024002.

48. Sugita, Y.; Okamoto, Y., Replica-Exchange Molecular Dynamics Method for Protein Folding. *Chem. Phys. Lett.* **1999,** *314* (1), 141-151.

49. Qi, R.; Wei, G.; Ma, B.; Nussinov, R., Replica Exchange Molecular Dynamics: A Practical Application Protocol with Solutions to Common Problems and a Peptide Aggregation and Self-Assembly Example. In *Peptide Self-Assembly: Methods and Protocols*, Nilsson, B. L.; Doran, T. M., Eds. Springer New York: New York, NY, 2018; pp 101-119.

50. Yang, Y. I.; Shao, Q.; Zhang, J.; Yang, L.; Gao, Y. Q., Enhanced Sampling in Molecular Dynamics. *J. Chem. Phys.* **2019**, *151* (7), 070902

51. Zhou, P.; Deng, L.; Wang, Y.; Lu, J. R.; Xu, H., Interplay between Intrinsic Conformational Propensities and Intermolecular Interactions in the Self-Assembly of

Short Surfactant-like Peptides Composed of Leucine/Isoleucine. *Langmuir* **2016,** *32* (18), 4662-4672.

52. Ngo, S. T.; Hung, H. M.; Tran, K. N.; Nguyen, M. T., Replica Exchange Molecular Dynamics Study of the Amyloid Beta (11–40) Trimer Penetrating a Membrane. *RSC Adv.* **2017,** *7* (12), 7346-7357.

53. Rhee, Y. M.; Pande, V. S., Multiplexed-Replica Exchange Molecular Dynamics Method for Protein Folding Simulation. *Biophys. J.* **2003,** *84* (2), 775-786.

54. Nishino, M.; Sugita, Y.; Yoda, T.; Okamoto, Y., Structures of a Peptide Fragment of β2-Microglobulin Studied by Replica-Exchange Molecular Dynamics Simulations – Towards the Understanding of the Mechanism of Amyloid Formation. *FEBS Lett.* **2005,** *579* (24), 5425-5429.

55. Ho, B. K.; Dill, K. A., Folding Very Short Peptides Using Molecular Dynamics. *PLoS Comput. Biol.* **2006,** *2* (4), e27.

56. Zhang, J.; Qin, M.; Wang, W., Folding Mechanism of β-Hairpins Studied by Replica Exchange Molecular Simulations. *Proteins* **2006,** *62* (3), 672-685.

57. Watts, C. R.; Gregory, A. J.; Frisbie, C. P.; Lovas, S., Structural Properties of Amyloid β(1-40) Dimer Explored by Replica Exchange Molecular Dynamics Simulations. *Proteins* **2017,** *85* (6), 1024-1045.

58. Zerze, G. H.; Uz, B.; Mittal, J., Folding Thermodynamics of β-Hairpins Studied by Replica-Exchange Molecular Dynamics Simulations. *Proteins* **2015,** *83* (7), 1307-1315.

59. Blinov, N.; Khorvash, M.; Wishart, D. S.; Cashman, N. R.; Kovalenko, A., Initial Structural Models of the Aβ42 Dimer from Replica Exchange Molecular Dynamics Simulations. *ACS Omega* **2017,** *2* (11), 7621-7636.

60. Lim, G. S.; Klähn, M., On the Stability of Proteins Solvated in Imidazolium-Based Ionic Liquids Studied with Replica Exchange Molecular Dynamics. *J. Phys. Chem. B* **2018,** *122* (39), 9274-9288.

61. Nagai, T.; Okamoto, Y., Replica-Exchange Molecular Dynamics Simulation of a Lipid Bilayer System with a Coarse-Grained Model. *Mol. Simul.* **2012,** *38* (5), 437-441.

62. Horta, B. A. C.; Merz, P. T.; Fuchs, P. F. J.; Dolenc, J.; Riniker, S.; Hünenberger, P. H., A GROMOS-Compatible Force Field for Small Organic Molecules in the Condensed Phase: The 2016H66 Parameter Set. *J. Chem. Theory Comput.* **2016,** *12* (8), 3825-3850.

63. Berendsen, H. J.; van der Spoel, D.; van Drunen, R., GROMACS: A Message-Passing Parallel Molecular Dynamics Implementation. *Comput. Phys. Commun.* **1995,** *91* (1-3), 43-56.

64. Pronk, S.; Páll, S.; Schulz, R.; Larsson, P.; Bjelkmar, P.; Apostolov, R.; Shirts, M. R.; Smith, J. C.; Kasson, P. M.; Van Der Spoel, D., GROMACS 4.5: A High-Throughput and Highly Parallel Open Source Molecular Simulation Toolkit. *Bioinformatics* **2013,** *29* (7), 845-854.

65. Feenstra, K. A.; Hess, B.; Berendsen, H. J. C., Improving Efficiency of Large Time-Scale Molecular Dynamics Simulations of Hydrogen-Rich Systems. *J. Comput. Chem.* **1999,** *20* (8), 786-798.

66. Bussi, G.; Donadio, D.; Parrinello, M., Canonical Sampling Through Velocity Rescaling. *J. Chem. Phys.* **2007,** *126* (1), 014101.

67. Berendsen, H. J. C.; Postma, J. P. M.; Gunsteren, W. F. v.; DiNola, A.; Haak, J. R., Molecular Dynamics with Coupling to an External Bath. *J. Chem. Phys.* **1984,** *81* (8), 3684-3690.

68. Parrinello, M.; Rahman, A., Polymorphic Transitions in Single Crystals: A New Molecular Dynamics Method. *J. Appl. Phys.* **1981,** *52* (12), 7182-7190.

69. Miyamoto, S.; Kollman, P. A., Settle: An Analytical Version of the SHAKE and RATTLE Algorithm for Rigid Water Models. *J. Comput. Chem.* **1992,** *13* (8), 952-962.

70. Hess, B.; Bekker, H.; Berendsen, H. J. C.; Fraaije, J. G. E. M., LINCS: A Linear Constraint Solver for Molecular Simulations. *J. Comput. Chem.* **1997,** *18* (12), 1463-1472.

71. Verlet, L., Computer "Experiments" on Classical Fluids. I. Thermodynamical Properties of Lennard-Jones Molecules. *Phys. Rev.* **1967,** *159* (1), 98-103.

72. Darden, T.; York, D.; Pedersen, L., Particle Mesh Ewald: An N·log(N) Method for Ewald Sums in Large Systems. *J. Chem. Phys.* **1993,** *98* (12), 10089-10092.

73. Patriksson, A.; van der Spoel, D., A Temperature Predictor for Parallel Tempering Simulations. *Phys. Chem. Chem. Phys.* **2008,** *10* (15), 2073-2077.

74. The PyMOL Molecular Graphics System, Version 1.8 Schrödinger, LLC.

75. Chalmers, D. K.; Roberts, B. P. Silico: A Perl Molecular Toolkit, http://silico.sourceforge.net.

76. Guruge, A. G.; Warren, D. B.; Benameur, H.; Pouton, C. W.; Chalmers, D. K., Aqueous Phase Behavior of the PEO-Containing Non-Ionic Surfactant $C_{12}E_6$: A Molecular Dynamics Simulation Study. *J. Colloid Interface Sci.* **2021,** *588*, 257-268.

77. Constantin, D.; Oswald, P., Diffusion coefficients in a lamellar lyotropic phase: Evidence for Defects Connecting the Surfactant Structure. *Phys. Rev. Lett.* **2000,** *85* (20), 4297.

78. Son, W.-J.; Jang, S.; Pak, Y.; Shin, S., Folding Simulations with Novel Conformational Search Method. *J. Chem. Phys.* **2007,** *126* (10), 104906.

79. Lee, I. H.; Kim, S. Y.; Lee, J., Transition Pathway and Its Free-Energy Profile: A Protocol for Protein Folding Simulations. *Int. J. Mol. Sci.* **2013,** *14* (8), 16058-16075.

80. Sallen, L.; Sotta, P.; Oswald, P., Pretransitional Effects Near the Hexagonal−Micellar Phase Transition of the $C_{12}EO_6/H_2O$ Lyotropic Mixture. *J. Phys. Chem. B* **1997,** *101* (25), 4875-4881.

81. Constantin, D.; Oswald, P.; Impéror-Clerc, M.; Davidson, P.; Sotta, P., Connectivity of the Hexagonal, Cubic, and Isotropic Phases of the $C_{12}EO_6/H_2O$ Lyotropic Mixture Investigated by Tracer Diffusion and X-ray Scattering. *J. Phys. Chem. B* **2001,** *105* (3), 668-673.

Chapter 5

The Colloidal Phase Behavior of Lipid-Based Formulations of Loratadine, Including Claritin®, upon Water Dispersion and Dilution: A Molecular Dynamics and Experimental Study

The previous Chapters (i.e., Chapter 3 and Chapter 4) confirmed that the 2016H66 force field is a suitable force field for modelling PEO surfactants in their wide range of colloidal behaviors. With this finding, we aimed to fill the gap in the literature by conducting MD simulations for LBFs composed of PEO surfactants to explore how MD model the phase behavior of LBFs compared to the experimental observation.

Since none of the studies in the literature used commercialised LBFs for modelling purposes, we were interested in using commercialised LBFs in our investigation. We selected two commercialised LBFs designed for 'loratadine'. One formulation is currently used by Catalent Pharma Solutions, Inc. to manufacture "Claritin® liqui-gels" and the other formulation is from another pharmaceutical company, Capsugel. To explore the influence of excipient type and content, we modified Catalent and Capsugel LBFs and made three additional LBFs for our investigation. For the comparison of MD phase behavior with experiments, we also conducted an experimental investigation that aligned with MD studies using Claritin Liqui-Gels from Bayer.

The results in this chapter provide insight into the MD ability to reproduce the experimental phase behavior of LBFs composed of PEO surfactants upon dispersion and dilution and limitations in MD on simulating such systems. Importantly, the work in this chapter fills the gap in the literature providing information on how well MD models LBFs composed of PEO surfactants.

This chapter is a manuscript to be submitted for publication.

The Colloidal Phase Behavior of Lipid-Based Formulations of Loratadine, Including Claritin®, upon Water Dispersion and Dilution: A Molecular Dynamics and Experimental Study

Amali G. Guruge[1], Dallas B. Warren[2], Hassan Benameur[3], Leigh Ford[4], Hywel D. Williams[4], Vincent Jannin[3], Colin W. Pouton[2], David K. Chalmers[1]*

[1]Medicinal Chemistry, Monash Institute of Pharmaceutical Sciences, Monash University, 381 Royal Parade, Parkville, Victoria 3052, Australia

[2]Drug Delivery, Disposition and Dynamics, Monash Institute of Pharmaceutical Sciences, Monash University, 381 Royal Parade, Parkville, Victoria 3052, Australia

[3]Lonza Pharma Sciences, Strasbourg, France

[4]Lonza Pharma Sciences, Monash Institute of Pharmaceutical Sciences, Monash University, 381 Royal Parade, Parkville, Victoria 3052, Australia

Keywords

Molecular dynamics simulations, colloids, lipid-based drug formulations, dilution, phase behavior, loratadine

Abstract

Lipid-based formulations (LBFs) combine poorly water-soluble drugs with oils, surfactants and cosolvents to deliver the drugs into the systemic circulation. However, the solubility of the drug is greatly influenced by the colloidal mixtures formed in the gastrointestinal tract after it is dispersed and makes contact with other materials present in the GI tract, such as bile. Thus, an understanding of the complex colloidal phase behavior of LBFs after oral administration is critical for designing efficient LBFs. Molecular dynamics (MD) simulation is a powerful tool for the study of these molecular systems. In this study we analysed the internal structures of five LBFs of loratadine and their phase behavior on dilution with water using 50 long time-scale MD simulations (0.4 −1.7 μs). We also conducted experimental investigations (dilution of formulations with water) including commercial Claritin® liquid softgel capsules that correlated with the MD simulations. In the process, we validate molecular models for

medium-chain triglyceride excipient (Captex® 355), medium-chain mono and diglyceride excipient (Capmul® MCM) and polyoxyl hydrogenated castor oil (Kolliphor® RH40). The simulations show that LBFs form continuous phase, water-swollen reverse micelles, bi-continuous and phase separated systems at different dilutions, which correlate with the experimental observations. We found that MD reproduces the colloidal behavior of LBFs composed of complex surfactants successfully. This implies that the models we suggest for Captex® 355, Capmul® MCM and Kolliphor® RH40 are suitable to use in future studies in LBFs. MD also shows that the polymer excipient polyvinyl pyrrolidine (Kollidon® 12PF) does not change the general phase behavior of a LBF upon dilution. However, the phase behavior of a LBF at low dilutions can change by adjusting the surfactant and oil content in the formulation (i.e., **F1** vs **F3** in the current study). MD revealed that if two formulations differ only by the water-soluble surfactant, provided the HLB (Hydrophilic Lipophilic Balance) values of the surfactants are close, then the phase behavior is similar for both formulations upon dilution. However, LBF with high HLB surfactants form small particles (i.e., water-swollen reverse micelles) upon dilution. Overall, this study provides confidence in MD simulation as a predictive tool to determine the fate of LBFs composed of medium-chain lipids, polyethylene oxide surfactants and polymers.

Introduction

Oral administration is the preferred route for the delivery of many drugs into the systemic circulation for many reasons; improved patient compliance, safety, ease of ingestion and the versatility to accommodate various types of drugs.[1] To achieve adequate absorption, the active pharmaceutical ingredient (drug) must be present in solution in the intestinal lumen. Yet, drug discovery programs often develop lipophilic compounds that are intrinsically poorly water-soluble.[2] To some extent, strategies such as lipid-based formulation (LBF) can be used to overcome the low aqueous solubility of lipophilic drugs by providing a reservoir of dissolved drug.[3-6] A major factor in the performance of LBFs is that dispersion of the formulation within the gastrointestinal (GI) tract dilutes the formulation and exposes it to bile and other materials that can modify the structure and properties of the formulation, influencing the ability of the LBF to keep the active agent in solution. Recently, molecular dynamics (MD) simulation has emerged as a powerful tool for understanding the physical behavior and

performance of drug formulations. MD is a physics-based simulation method that provides atomic-level detail about the interactions between molecules, such as drugs and the surrounding environment. MD simulations can be used to complement experimental studies and improve our understanding of these complex systems. In this work, we use MD simulations to model the behavior of lipid-based formulations (LBFs) as they are dispersed/diluted and compare the simulations to experimental observation of the diluted LBFs.

LBFs vary from simple oil blends to complex mixtures of oils, lipophilic surfactants, hydrophilic surfactants and co-solvents. As a result, a very wide range of formulations is possible.[7-8] The standard practice of assessing the performance of these drug formulations is through *in vivo* and *in vitro* studies, which are expensive and time-consuming.[9-14] With the advancement of high-performance computers, tools such as MD can provide additional insight into the performance of drug formulations on to dispersion, dilution and digestion in the GI tract with cost and time effective manner. Molecular dynamics (MD) simulations model the physical movements of atoms and molecules by solving Newtonian equations of motion numerically.[15] MD can model how the structure of a colloidal system changes with variations in composition and to other conditions such as temperature or the degree of dilution in water. Hence, by performing MD simulations of lipid-based formulations in water, we can observe details such as the types of colloidal structures formed in the formulation[16-19], the distribution of drug within the formulation[17-18, 20], the propensity for drug precipitation[18], the detailed molecular interactions within the formulation[17-18, 20] and wide range of other information. This information can give deep insight into the performance of the drug formulation. Much of the above-described information cannot be extracted using spectroscopic or diffraction techniques, which indicates the great potential of MD in drug formulation field.

Applications of MD to formulation design have been reviewed by Boyd et al. and by Hasmukh et al. in 2019.[21-22] Although the technique shows great promise, the application of MD simulation to the study of LBFs is still quite limited. Few studies in the literature investigate the behavior of LBFs upon dispersion, dilution or in the presence of bile components[16-19], and published studies are restricted to simple formulations; oily blends that do not contain surfactants such as the Kolliphors® or Polysorbates that are widely used in LBFs. One study reports simulations of self-

emulsifying drug delivery systems containing poly(ethylene glycol).[20] There is a gap in the literature regarding surfactant-containing LBFs. To extend our understanding of how MD simulation can be applied to the study of more complex LBFs, we set out to investigate a collection of formulations based on commercialized or developed LBFs containing loratadine, including the leading product, Claritin®.

Loratadine (Figure 1) is an antihistamine used to treat the symptoms of allergic reactions. It is a poorly water-soluble drug that belongs to Class II with reference to the Biopharmaceutics Classification System (BCS).[23] Loratadine is a second-generation antihistamine that does not cause sedation or other central nervous system effects.[24] The usual adult oral dose for allergic rhinitis and chronic urticaria is 10 mg once a day[25], delivered using one of a range of dosage forms such as syrups, tablets or capsules. Loratadine is a widely studied drug in the literature, but it is rarely modelled using MD.[26-27] An experimental and computational study by Zhang et al. investigated the effects of hydroxylpropylmethyl cellulose acetate succinate and poly(vinylpyrrolidone-co-vinyl-acetate) polymers on supersaturation state of loratadine solid dispersions.[26] Another study combined density functional theory (DFT) and MD to investigate reactive properties of loratadine.[27]

In this study, our attention was drawn by the formulation invented by Okutan and co-workers[28] (patent number US20120301544A1), which overlaps with excipients in the marketed “Claritin® liqui-gels” (Figure S1 in SI). The excipient content of this formulation (denoted **F1**) is shown in Table 1. To compare the performance of LBF **F1**, an additional formulation designed by us, for delivery in a soft gelatin capsule is also investigated in the current study (formulation, **F5**). We investigated three additional modified LBFs that were designed to identify changes in the phase behavior due to variation in surfactant and polymer excipients.

There is little information in the literature regarding how well MD models the phase behavior of complex LBFs that contain nonionic surfactants based on polyoxyethylene chains. Additionally, there have been no MD studies of marketed LBFs. The aims of the current investigation are three-fold. First, we wished to investigate the performance of MD models of marketed LBFs designed for loratadine. Second, we aimed to validate computational models for the surfactant, polyoxyl hydrogenated castor oil (Kolliphor® RH40) and the oily excipients, medium-chain triglyceride (Captex® 355) and medium-

chain mono and diglyceride (Capmul® MCM). To our knowledge, this is the first study that models these three excipients with MD. Thirdly, we wished to investigate how phase behavior of these formulations varies with the excipient and composition. To achieve this, we modified the compositions of formulations **F1** and **F5**, creating formulations **F2**, **F3,** and **F4**. For each formulation (**F1**-**F5**), we model the dilution of the formulation in water considering dry formulation, to mimic the LBF in the soft gelatin capsule, and diluted formulation, to mimic the LBF after oral administration. Finally, we compare the MD studies with experimental observations of diluted loratadine formulations.

Materials and Methods

Materials

Claritin® liqui-gel capsules were purchased from CVS pharmacy (US, Figure S1 in the Supplementary Information). Polysorbate 80, Capmul® MCM and Kolliphor® RH40 were obtained from Sigma-Aldrich (US), ABITEC Corporation (Janesville, US) and BASF (Germany), respectively. Loratadine was obtained from Merck (Castle Hill, Australia). Water was obtained from a Milli-Q water purification system (Millipore, Bedford, MA).

Experimental Methods

Formulation F1. Diluted formulations were made by placing suitable weight amounts taken from Claritin® liqui-gels (Figure S1 (a)) with water into glass sample vials which were mixed to make 10-90% w/w of Claritin® aqueous solutions. Samples were vortex-mixed, stored at 37 °C and equilibrated for at least 24 hours before use. Samples were mixed thoroughly before visual inspection.

Formulation F3. Appropriate amounts of Claritin® liqui-gels were taken and Polysorbate 80 was added to make the total Polysorbate 80 weight percentage 30%. This prepared **F3** formulation was vortexed and kept at the room temperature. Appropriate weight amounts from that prepared **F3** formulation and water were put into glass sample vials and mixed to make 10-90% w/w of **F3** aqueous solutions. Samples were vortexed, stored at 37 °C and equilibrated for at least 24 hours prior to use. Samples were mixed thoroughly before the visual inspection.

Formulation F4. Following the excipient ratios listed in Table 1(**F4**), the appropriate amount of loratadine, Capmul® MCM and Polysorbate 80 were vortexed in glass sample vials and kept at room temperature. From this prepared **F4** formulation, suitable amounts were taken and mixed with water to prepare 10-90% w/w of **F4** aqueous solutions. Samples were vortexed, stored at 37 °C and equilibrated for at least 24 hours before use. Samples were mixed thoroughly before the visual inspection.

Formulation F5. As for formulation **F4** but Polysorbate 80 was replaced with Kolliphor® RH40.

MD Simulation

Modelling excipients in drug formulations

Captex® 355 is a mixture of medium chain triglycerides which was modelled as a combination of 55% w/w tricaprylin and 45% w/w tricaprin. Capmul® MCM is a product of medium chain mono- and diglycerides that contains monocaprylin, monocaprin, dicaprylin and dicaprin. It was modelled as a mixture of 85% w/w caprylic glyceride and 15% w/w capric glyceride. Both excipients were modelled following the composition described in brochures from ABITEC Corporation[29-30] and in the literature.[31] The monoglyceride to diglyceride ratio in Capmul® MCM was modelled as 60:40% w/w. Polysorbate 80 is a complex mixture and the precise chemical nature of this surfactant material can vary from manufacturing batch to batch.[32] However, it was modelled as a pure compound using a simplified topology (Figure 1, $w = x = y = z = 5$). Kolliphor® RH40 is also a heterogeneous mixture, lacking a single well-defined chemical structure. We used a single molecular representation for this excipient (Figure 1, l, $n = 13$ and $m = 14$). Kollidon® 12PF is a polymer that has a molecular weight of 2000–3000 g/mol[33] (Figure 1). We modelled this excipient as a 25-monomer unit with alternating S and R configuration at the chiral centers (marked with * in Figure 1). The structures of molecules used in modelling the excipients in formulations **F1** to **F5** are shown in Figure 1.

Topologies

The caprylic and capric mono, di- and triglycerides in Captex® 355 and Capmul® MCM topologies were parameterized with the 2016H66 force field. Polysorbate 80 was

modelled using the topology generated by Tang et al. using the 2016H66 force field.[34] The loratadine and Kollidon® 12PF, topologies were taken from Automated Topology Builder (ATB).[35] The Kolliphor® RH40 topology was adapted from the Kolliphor® EL topology using 2016H66 FF developed in a previous study.[36]

Construction of systems

All formulations systems were constructed with total formulation content varying from 10% w/w to 100% w/w followed by addition of water to composition to 100%. Depending on the formulation (i.e., **F1** to **F5**), the model systems contained some number of capric and caprylic mono, di and triglycerides, Polysorbate 80, Kollidon® 12PF, loratadine, Kolliphor® RH40 and water. At the beginning of the MD simulation all molecules were randomly distributed in the simulation cell.

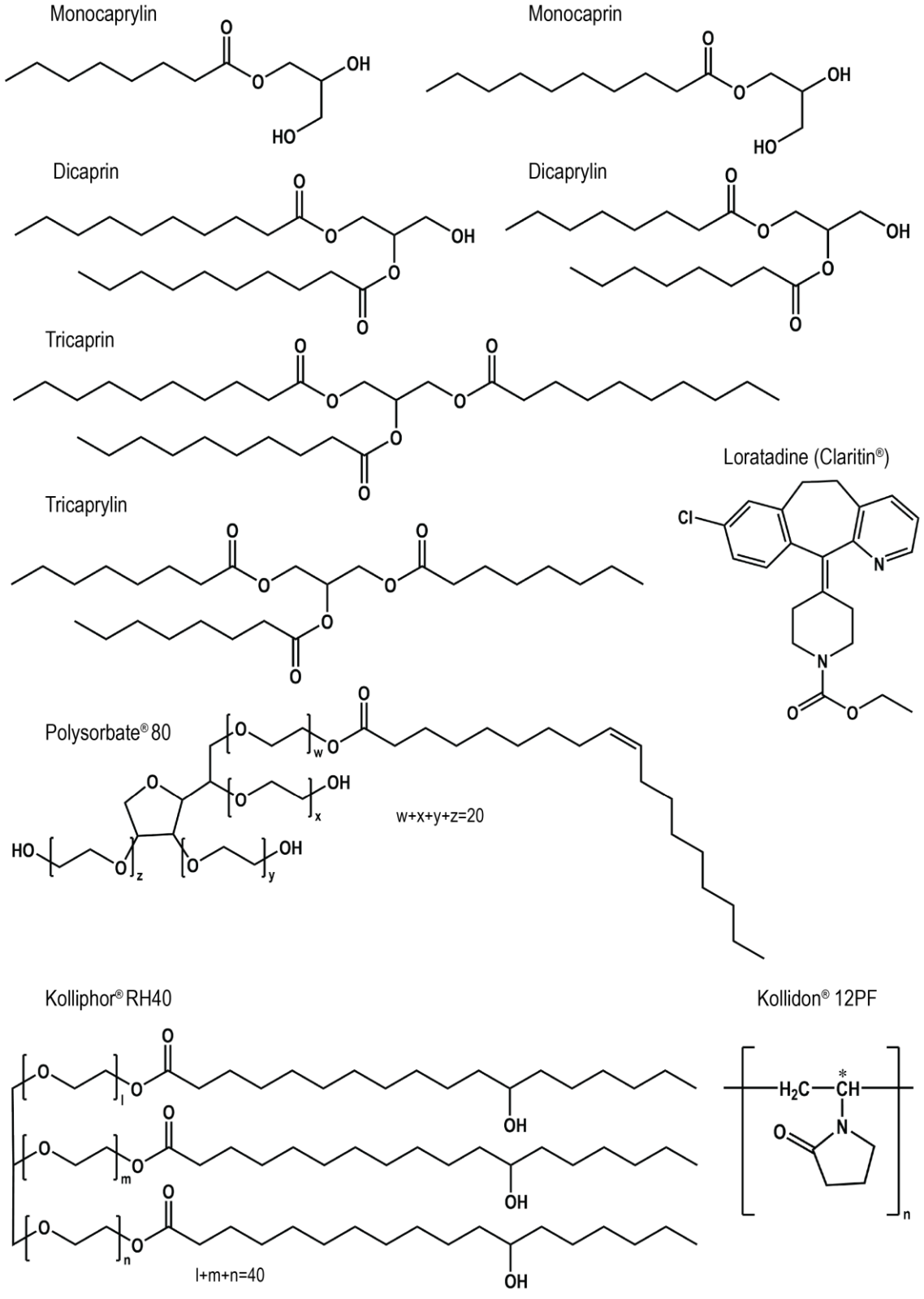

Figure 1 – Chemical structures of glycerides (in Captex® 355 and Capmul® MCM) and other excipients in formulations **F1** to **F5**. For Polysorbate 80 and Kolliphor® RH 40, the nominal chemical structures are shown.

MD Simulations

MD simulations were performed using the 2016H66[37] FF with GROMACS[38-39] version 2018.8. In all simulations, an increased time step (5 fs) was enabled using the heavy H atom (4 amu) method.[40] The isothermal-isobaric ensemble (NPT) was used in all simulations. The velocity rescale algorithm[41] was employed for the temperature coupling and all systems were simulated at 310 K. A reference pressure of 1 bar and compressibility of 4.5×10^{-5} bar^{-1} were used for pressure coupling with the Berendsen[42] and Parrinello-Rahman[43] algorithms. Isotropic pressure coupling was employed in all simulations. Water was modelled using the single point charge (SPC) model constrained with SETTLE algorithm.[44] All other bonds were constrained by the LINCS algorithm.[45] For short-range non-bonded interactions (Coulomb and van der Waals), the Verlet cut-off scheme[46] with the cut-off distance of 1.4 nm was applied. For long-range Coulombic interactions, the particle-mesh Ewald (PME) technique[47] with a grid spacing of 0.12 nm was applied. The following steps were followed before the production run.

i. Energy minimization of 500 steps using the steepest descent method to remove steric clashes.

ii. Simulation of 5000 steps using a time step of 1 fs and V-rescale temperature coupling with 0.1 ps time constant without pressure coupling.

iii. Simulation of 10,000 steps using a 2 fs time step with the Berendsen pressure coupling and a 2 ps pressure coupling time constant.

iv. Simulation of 10,000 steps using 2 fs time step with Parrinello-Rahman pressure coupling with 2 ps pressure coupling time constant.

v. Simulation of 10,000 steps of increased time step (5 fs) with Parrinello-Rahman pressure coupling time constant and 0.1 ps v-rescale temperature coupling time constant.

The production run was carried out with 5 fs time step, 2 ps pressure coupling constant and 0.1 ps temperature coupling constant.

Simulation Analysis

The final frames in MD simulations were visually examined using VMD[48] and images for this publication were generated using the same graphics package. MD trajectories were analyzed with the GROMACS tools. The aggregate properties of colloidal structures were analyzed using the *find aggregate* script from the Silico package.[49] Solvent accessible surface area (SASA), diffusion of water and radius of gyration were calculated using *gmx sasa*, *gmx msd* and *gmx gyrate* tools in GROMACS. For the calculation of moment of inertia, *gmx gyrate* tool with *moi* option was used. Calculations of moments of inertia, radius of gyration and SASA per molecule used the last 10 ns of the simulation, extracting data at 50 ps time intervals.

Results

Molecular dynamics simulations

In this study, we performed molecular dynamics simulations of five LBFs (formulations **F1** to **F5**). Details of each formulation are given in Table 1. For each formulation, we modelled the effects of dilution by varying the water content from 0-90% w/w. Note that 0% w/w added water systems in formulations **F1** to **F3** contain a trace amount of water due to the presence of 1.44 - 2.0% w/w water in the neat formulation (Table 2). A total of fifty MD simulations were performed. Each simulation began using a random arrangement of formulation components. Details of system compositions, simulation time and the final structures obtained at the end of each simulation are presented in Table 3.

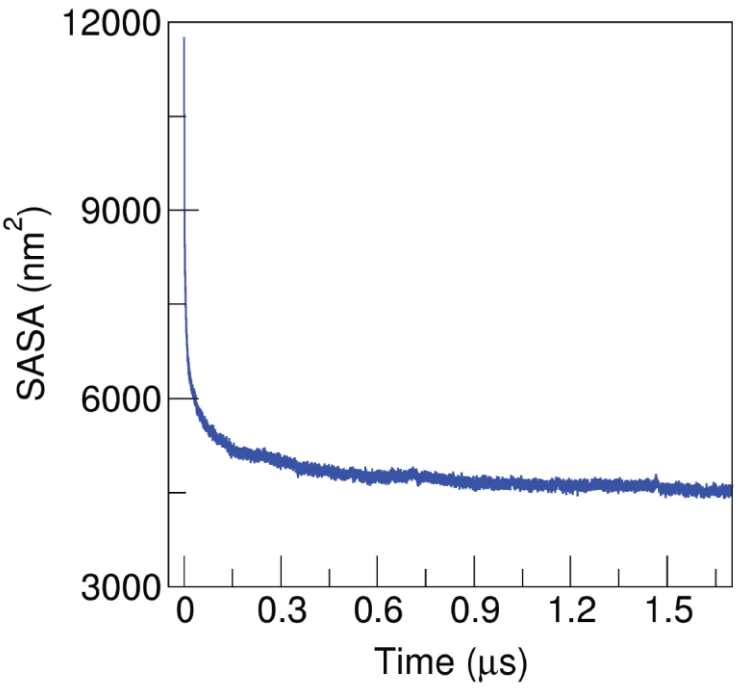

Figure 2 – Solvent accessible surface area (SASA) of non-water components over time for formulation **F2** diluted with 20% w/w water (Simulation number 14).

To make a reliable prediction of the final phases formed in dilutions of formulations, it is important that the MD simulations have reached an equilibrated state. Our previous study showed that SASA can be used as an indicator in MD to determine the stability of colloidal structure formation.[50] Therefore, to find whether systems have reached stable equilibrium, the total SASA of non-water components were calculated for all systems (shown in Figures S2 to S6 in the Supplementary Information). The change in SASA over time for the simulation of formulation **F2** diluted with 20% w/w water is shown in Figure 2 as an example. Figure 2 indicates that SASA remains constant for a long time (more than 1 µs), which confirms that there is no major change in the colloidal structure and system has reached a stable configuration. Similar behavior was observed for all simulated systems. It is also clear from the SASA calculations that, when a system forms a continuous phase (excipients distributed throughout the simulation cell) or bi-continuous phase (oil and water channels interspersed in the system), it stabilizes very quickly (in less than 50 ns). However, when a system forms water aggregates that are dispersed in an oil environment; the system equilibrates slowly and for such systems, we extended the simulations to more than 0.4 µs. We also observed that in systems with very high-water content (e.g., 90% w/w) the SASA

can reduce in steps, due to combining of individual aggregates over time and SASA remains constant once all aggregates have assembled into a single cluster.

Table 4 – Source and compositions of the formulations considered in this study.

Formulation	**F1**	**F2**	**F3**	**F4**	**F5**
Source	Okutan et al.[28]‡	**F1** without Kollidon® 12PF	**F1** with increased Polysorbate 80	**F5** with Polysorbate 80	Capsugel
Excipients	**Content (% w/w)**				
Loratadine	6.30	6.70	4.55	6.30	6.30
Medium-chain triglyceride (Captex® 355)	41.20	43.90	29.73	-	-
Medium-chain mono and diglyceride (Capmul® MCM)	41.20	43.90	29.73	70.30	70.30
Polysorbate 80	3.10	3.30	30.00	23.40	-
Polyoxyl hydrogenated castor oil (Kolliphor® RH40)	-	-	-	-	23.40
Polyvinyl pyrrolidine (Kollidon® 12PF)	6.30	0.00	4.55	-	-
Water	2.00	2.10	1.44	-	-

‡ Marketed “Claritin® liqui-gels”

Table 5 – Composition, MD simulation details and outcomes of simulations performed for formulations **F1** to **F5**.

Formulation	Simulation number	Formulation (% w/w)	Loratadine	Polysorbate® 80	Kolliphor® RH40	Kollidon® 12PF	Water	TGL		DGL		MGL		Approx. cell size (nm)	Simulation time (ns)	Final structure
								C8	C10	C8	C10	C8	C10			
F1	1	100	793	114	0	109	5347	2319	1610	1959	297	4637	725	20×20×20	400	C
	2	90	713	103	0	98	31547	2087	1449	1763	268	4174	653	20×20×20	1000	WSRM
	3	80	634	91	0	87	57749	1856	1288	1567	238	3710	580	20×20×20	1000	WSRM
	4	70	555	80	0	76	83949	1623	1127	1371	208	3246	507	20×20×20	1000	WSRM/PS*
	5	60	476	68	0	65	110150	1392	966	1175	178	2782	435	20×20×20	400	PS
	6	50	396	57	0	54	136351	1160	805	979	149	2319	363	20×20×20	400	PS
	7	40	317	46	0	43	162551	928	644	783	119	1855	290	20×20×20	400	PS
	8	30	238	34	0	32	188752	696	483	588	89	1391	217	20×20×20	400	PS
	9	20	159	23	0	22	214952	464	322	392	59	927	145	20×20×20	400	PS
	10	10	79	11	0	11	241153	232	161	196	30	464	72	20×20×20	400	PS
	11	10	325	47	0	45	987763	950	659	802	122	1899	297	32×32×32	450	PS
F2	12	100	843	121	0	0	5614	2471	1715	2087	317	4941	773	20×20×20	400	C
	13	90	759	109	0	0	31788	2224	1544	1879	285	4447	695	20×20×20	1500	WSRM
	14	80	674	97	0	0	57963	1977	1372	1670	253	3953	618	20×20×20	1700	WSRM
	15	70	590	85	0	0	84136	1730	1201	1461	222	3459	541	20×20×20	800	WSRM/PS*
	16	60	506	73	0	0	110311	1483	1029	1252	190	2965	464	20×20×20	400	PS
	17	50	422	61	0	0	136484	1236	856	1044	158	2471	386	20×20×20	400	PS
	18	30	253	36	0	0	188832	741	514	626	95	1482	232	20×20×20	400	PS
	19	10	84	12	0	0	241179	247	171	209	32	494	77	20×20×20	400	PS
F3	20	100	573	1104	0	79	3850	1674	1162	1414	215	3346	523	20×20×20	400	C
	21	90	515	993	0	71	30200	1506	1045	1272	193	3012	471	20×20×20	400	BC
	22	80	458	883	0	63	56551	1339	929	1131	172	2677	419	20×20×20	400	BC
	23	70	401	773	0	55	82901	1172	813	990	150	2342	366	20×20×20	600	PS
	24	60	344	662	0	47	109252	1004	697	848	129	2008	314	20×20×20	400	PS
	25	50	286	552	0	39	135602	837	581	707	107	1673	262	20×20×20	400	PS
	26	40	229	441	0	32	161952	669	465	565	86	1339	209	20×20×20	400	PS
	27	30	172	331	0	24	188303	502	348	424	64	1004	157	20×20×20	400	PS
	28	20	115	221	0	16	214653	335	232	283	43	669	105	20×20×20	400	PS
	29	10	57	110	0	8	241003	167	116	141	21	335	52	20×20×20	400	PS
	30	10	235	452	0	32	987150	686	476	579	88	1371	214	32×32×32	400	PS

TGL – triglyceride, DGL – diglyceride, MGL – monoglyceride, C8 – caprylic glyceride, C10 – capric glyceride. C – continuous, BC – bi-continuous, PS – phase separated, WSRM – water-swollen reverse micelles. *Classification of system not definitive because the colloidal structure spans half of the simulation cell size.

Table 6 (continued) – Composition, MD simulation details and outcomes of simulations performed for formulations F1 to F5.

Formulation	Simulation number	Formulation (% w/w)	Loratadine	Polysorbate® 80	Kolliphor® RH40	Kollidon® 12PF	Water	TGL		DGL		MGL		Approx. cell size (nm)	Simulation time (ns)	Final structure
								C8	C10	C8	C10	C8	C10			
F4	31	100	793	861	0	0	0	0	0	3343	507	7913	1237	20×20×20	400	C
	32	90	713	775	0	0	26735	0	0	3008	457	7122	1114	20×20×20	400	BC
	33	80	634	689	0	0	53471	0	0	2674	406	6330	990	20×20×20	1500	WSRM
	34	70	555	603	0	0	80206	0	0	2340	355	5539	866	20×20×20	800	WSRM
	35	60	476	516	0	0	106942	0	0	2006	304	4748	742	20×20×20	800	PS
	36	50	396	430	0	0	133677	0	0	1671	254	3956	619	20×20×20	800	PS
	37	40	317	344	0	0	160412	0	0	1337	203	3165	495	20×20×20	600	PS
	38	30	238	258	0	0	187148	0	0	1003	152	2374	371	20×20×20	400	PS
	39	20	159	172	0	0	213883	0	0	669	101	1583	247	20×20×20	400	PS
	40	10	79	86	0	0	240618	0	0	334	51	791	124	20×20×20	400	PS
F5	41	100	793	0	417	0	0	0	0	3343	507	7913	1237	20×20×20	400	C
	42	90	713	0	376	0	26735	0	0	3008	457	7122	1114	20×20×20	400	BC
	43	80	634	0	334	0	53471	0	0	2674	406	6330	990	20×20×20	1000	WSRM
	44	70	555	0	292	0	80206	0	0	2340	355	5539	866	20×20×20	800	WSRM
	45	60	476	0	250	0	106942	0	0	2006	304	4748	742	20×20×20	800	WSRM/PS*
	46	50	396	0	209	0	133677	0	0	1671	254	3956	619	20×20×20	800	PS
	47	40	317	0	167	0	160412	0	0	1337	203	3165	495	20×20×20	600	PS
	48	30	238	0	125	0	187148	0	0	1003	152	2374	371	20×20×20	600	PS
	49	20	159	0	83	0	213883	0	0	669	101	1583	247	20×20×20	400	PS
	50	10	79	0	42	0	240618	0	0	334	51	791	124	20×20×20	400	PS

TGL – triglyceride, DGL – diglyceride, MGL – monoglyceride, C8 – caprylic glyceride, C10 – capric glyceride. C – continuous, BC – bi-continuous, PS – phase separated, WSRM – water-swollen reverse micelles. *Classification of system not definitive because the colloidal structure spans half of the simulation cell size.

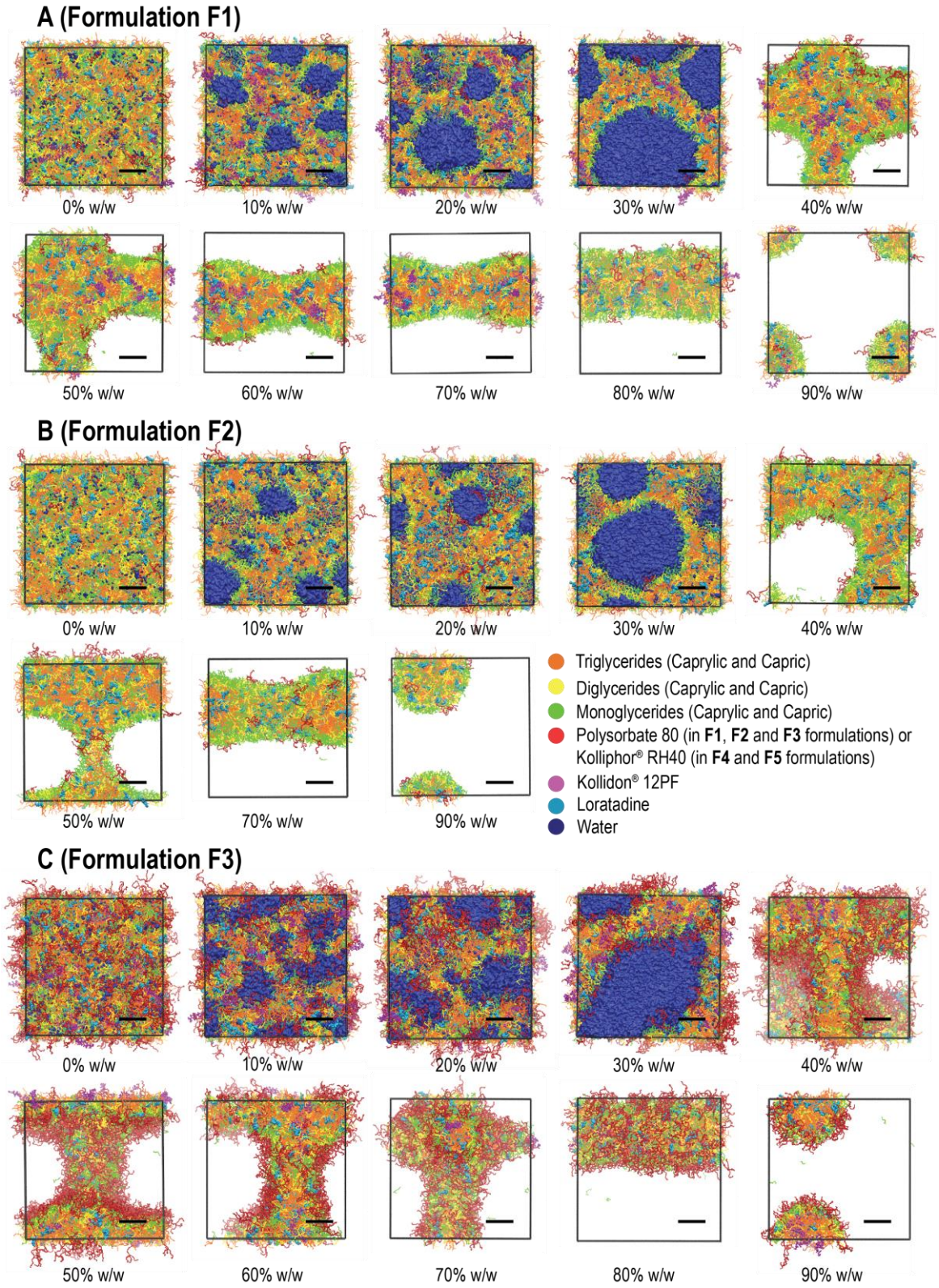

Figure 3 – Final molecular structures formed in MD simulations of formulations **F1**-**F3** (A-C) as they are diluted in water. The percentage below each image indicates the water content included in the system. Water is not shown for simulations with > 30% water content. The scale bar length is 4.0 nm.

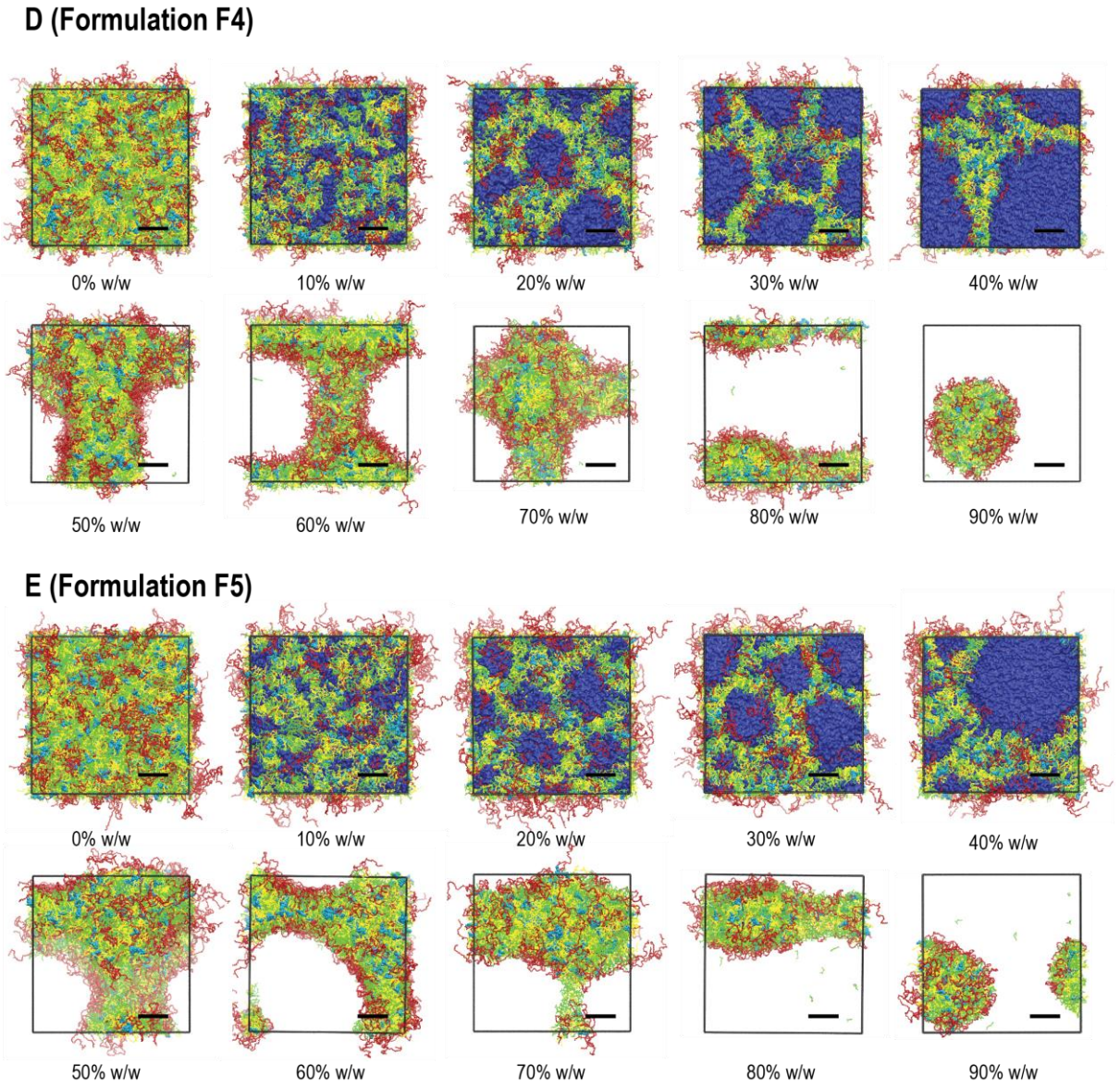

Figure 3 (continued) – Final molecular structures formed in formulations **F4** and **F5** (D, E).

During the simulations, all model systems, started from random arrangements, self-assembled into the various colloidal structures shown in Figure 3. These final frames were classified as follows. Structures with a homogeneous distribution of molecules within the simulation cell were classified as “continuous phase”. Systems with water aggregates that were dispersed in the oil environment were classified as “water-swollen reverse micelles”. The formation of a large single aggregate (cluster) in the simulation cell was classified as “phase separated”. When water and oil channels are interspersed and separated from the oil medium by surfactant monolayer, the structure was classified as “bi-continuous phase”. The thickness of the water channels can vary between thin or swollen as shown in Figure 4. Note that the formation of a single oily cluster in MD indicates the formation of massive

particles (the structure spans the simulation box). Thus, the relevant structure formation in such systems is restricted by the simulation cell size and the periodic boundary condition.

Formulation **F1** corresponds to the commercial loratadine product. Final structures from MD simulations of this formulation neat and diluted with water are shown in Figure 3A. Neat formulation **F1**, which contains a trace amount of water, formed a continuous phase without any significant structuring. Addition of water between 10 and 30% w/w led to the formation of discrete water globules that are dispersed in the oil continuous phase (the oil content varies from ~84% to ~63% w/w), indicating that the structures formed are water-swollen reverse micelles. The water pools are almost spherical, and swell with the addition of water. One of the reverse micelles in 30% w/w water is extremely large and expands half of the box size, which implies that the simulation cell is too small to form a larger molecular structure that is most likely in a phase-separated state. In water-swollen reverse micellar structures, the MGLs, DGLs and surfactants are arranged at the oil-water interface, TGLs are located in the hydrophobic region of the structure. Once 40%w/w water is reached, phase separation occurs which is indicated by the formation of a single aggregate and a single large water pool. Phase separation is also observed for systems with 50 to 90% w/w water and particularly the system with 90% w/w water formed an almost spherical aggregate ($I_3>I_2>I_1$ and $I_1/I_2 \approx I_2/I_3 \approx 1$, see Table S1 for data), which contains 1245 molecules (aggregation number). The radius of gyration (R_g) for this aggregate is 4.54±0.01 nm. To establish that this system is in phase-separated state and not in an oil droplet dispersed in the aqueous phase (e.g., oil-in-water microemulsion), we performed an additional simulation using a larger simulation cell (32 × 32 × 32 nm). The final frame of this simulation is shown in Figure S7(a) in the SI. The SASA for non-water components and Figure S7(b) shows that the system is still moving toward the most energy minimum state that is combining two current aggregates into a single beyond 450 ns. Thus, we can confirm that the system is in a phase-separated state rather than a simple oil droplet dispersed in water.

To investigate the influence of the polymer excipient polyvinyl pyrrolidine (Kollidon® 12PF) we modelled formulation **F2,** which contains the same excipients as **F1** except that the polymer excipient was removed. In simulations of this formulation (Figure 3B), we observed similar continuous phase, water-swollen reverse micellar and phase-separated structures seen for formulation **F1**. Differences to formulation **F1** were observed in the size of water pools in the reverse micelles. These are discussed in the next section.

Even though formulation **F1** is classified as Type III,[8] its surfactant content is relatively low. To investigate effect of increasing the surfactant content, we modelled formulation **F3**, which contains a much higher Polysorbate 80 content (30% w/w). The neat formulation gave a continuous phase (Figure 3C). At 10-20% w/w water, formulation **F3** formed a bi-continuous phase where the water channels widened with the addition of water. With 30% w/w added water, the formulation formed phase separated state and remained in the same state through to 90% w/w water. The 90% w/w water system formed a single spherical aggregate (See Table S1 for sphericity data and R_g). Further, studying this system with a larger simulation cell showed that the formation of a single aggregate is the most favorable state (Figure S8 in SI).

To investigate the influence of surfactant type in the phase behavior of LBFs, we modified formulation **F5** by replacing the surfactant polyoxyl hydrogenated castor oil with Polysorbate 80 to derived formulation **F4**. This formulation does not contain the excipient medium-chain triglyceride or the polymer excipient polyvinyl pyrrolidine as found in formulations **F1** - **F3**. In the absence of water, this formulation formed a continuous phase (Figure 3D). Addition of 10% w/w to the formulation led to the formation of thin water channel network. The water channels were closely associated with surfactant molecules, indicating the system forms a bi-continuous phase. Further addition of water (20-30% w/w) to **F4** produced reverse micelles and the size of these structures increased with the addition of water. From 40% w/w to 90% w/w water, the systems formed phase-separated states.

Formulation **F5** models an alternative loratadine formulation. The surfactant in this formulation is the polyethoxylated fatty acid derivative Kolliphor® RH40/polyoxyl hydrogenated castor oil. This formulation forms a continuous phase at 0% w/w water, a bi-continuous phase at 10% w/w water and water-swollen reverse micellar phases at 20-30% w/w water (Figure 3E). At 40% w/w water, this formulation formed water-swollen reverse micelles. Two of these structures are extremely large and expand half of the simulation box. This indicates that this structure could be in phase-separated state and not in water-swollen reverse micellar. From 50-90% w/w water, the systems formed phase-separated states.

Water distribution within formulations

Changes in the phase markedly affect the water structure within the system. Figure 4 illustrates the diverse arrangements of water molecules found within different phases produced by the simulations. The figure shows 4 nm sections from the *xy*, *yz* and *xz* planes. The white space in between water and cell border (black) is filled with other excipients in the

system that are not shown. The images give an idea of how water distributes throughout the system, its interactions with the surrounding formulation and the likely effects on water diffusion. For example, water molecules in the interior of the water pools in Figure 4(b) only make contact with other water molecules and do not interact with other (more viscous) excipients in the systems and thus they can move fast. However, water molecules on the surface of the pools interact strongly with surrounding molecules which hinders their diffusion. This effect results in their being fast and slow components of water diffusion in the -reverse-micellar state.

All formulations formed water-swollen reverse micelles at lower dilutions except for formulation **F3** which instead produced more extended channels. To investigate how excipient content and type influences reverse micelle formation, we measured the sizes of the water pools in the reverse micellar structures formed in each simulation. The average and largest aggregation numbers were calculated for water pools with more than 1000 water molecules (Figure 5). Table S2 in the Supplementary Information shows the total number of water pools with > 1000 water molecules in each diluted system. Note that the size of these water pools is affected by the simulation cell size and simulation time. The size of the simulation cell and the periodic boundary conditions used could introduce artifacts that affect the formation of these water pools and longer simulations potentially could result in formation of larger water pools.

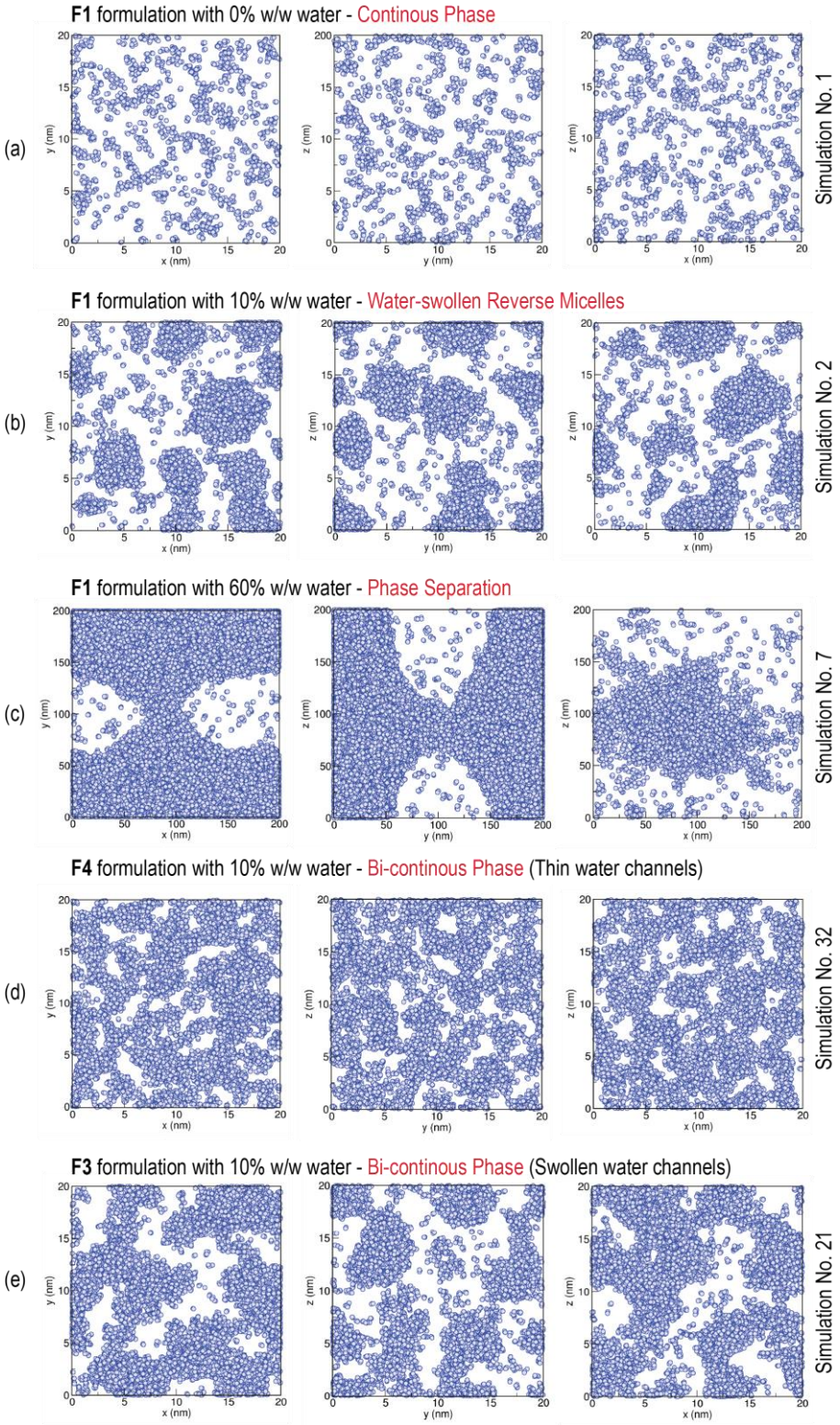

Figure 4 – Arrangement of water in MD simulations of different phase regions of diluted loratadine formulations. (a) Continuous phase. (b) Water-swollen reverse micelles. (c) Phase separated state. (d) Bi-continuous phase with thin water channels. (e) Bi-continuous phase with swollen water channels.

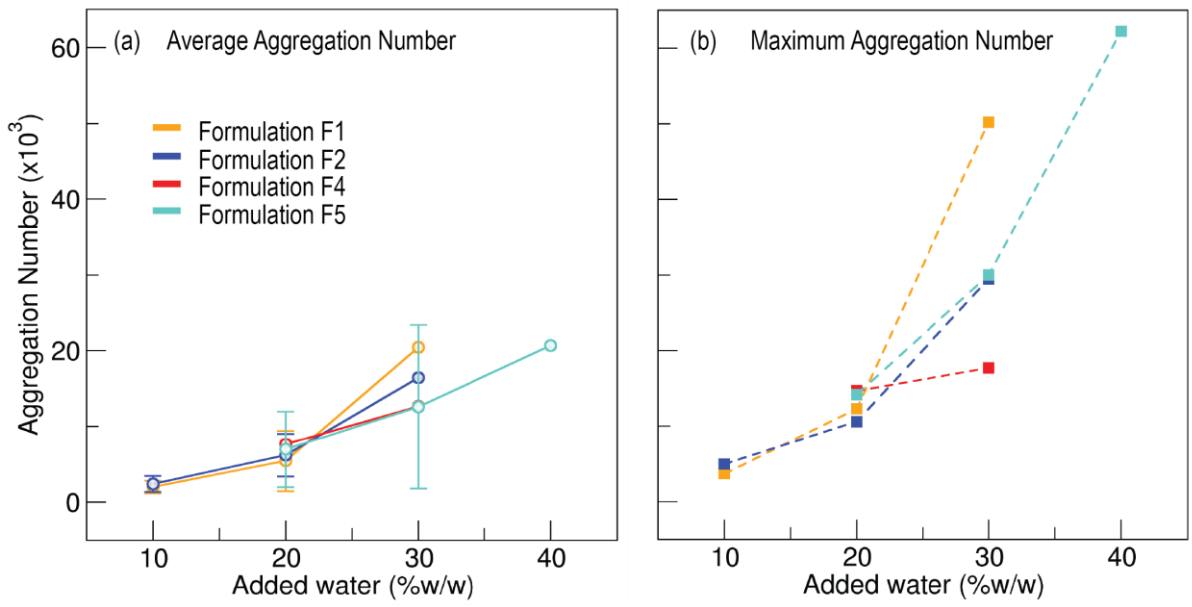

Figure 5 – Aggregation numbers for water pools formed in water-swollen reverse micellar systems. (a) Average sizes. (b) Maximum sizes. Error bars represent RMSD.

Figure 5 shows the average and maximum numbers of water molecules in each water pool as a function of water content (values are not shown when the pools become very large). In all cases, the addition of water increases the size of water pools. It is notable that similar formulation types show similar relationships between pool size and water content. Particularly, water pool size in formulations **F1** and **F2** is the same at 10% and 20% w/w water. Similar behavior is observed with formulations **F4**, **F5** at 20% and 30% w/w water. The low RMSD values for formulations **F1**, **F2** formulations at 10-20% w/w water and formulations **F4**, **F5** at 20% w/w water suggest that the reverse micelle water pools are monodisperse in these ranges. Figure 4(b) indicates that the maximum aggregation numbers for water pools formed in formulations **F1**, **F2** and **F5** at 30-40% w/w water is extremely large and structures suggesting that these formulations are phase separated above 30% w/w water.

Diffusion of Water

Changes in the molecular structure of a system strongly affect molecular mobility. Figure 6 shows the fast and slow components self-diffusion constant of water for each of the studied systems. The fast diffusion component can be attributed to water in the interior of the water pools whereas slow diffusion is due to water bound to polar groups in glycerides and surfactants.

Figure 6(a) shows that for formulations **F1** and **F2** (which behave similarly) the fast diffusion increases as the systems change from continuous phase to the water-swollen reverse micellar phase. Also, within the water-swollen reverse micellar phase region, fast diffusion increases with the addition of water. However, at 40% w/w water, fast diffusion drops as the phase structure is transformed from the reverse micelles to phase separated. Beyond this point, diffusion again increases with the addition of water and reaches a maximum value corresponding to the self-diffusion of bulk water.

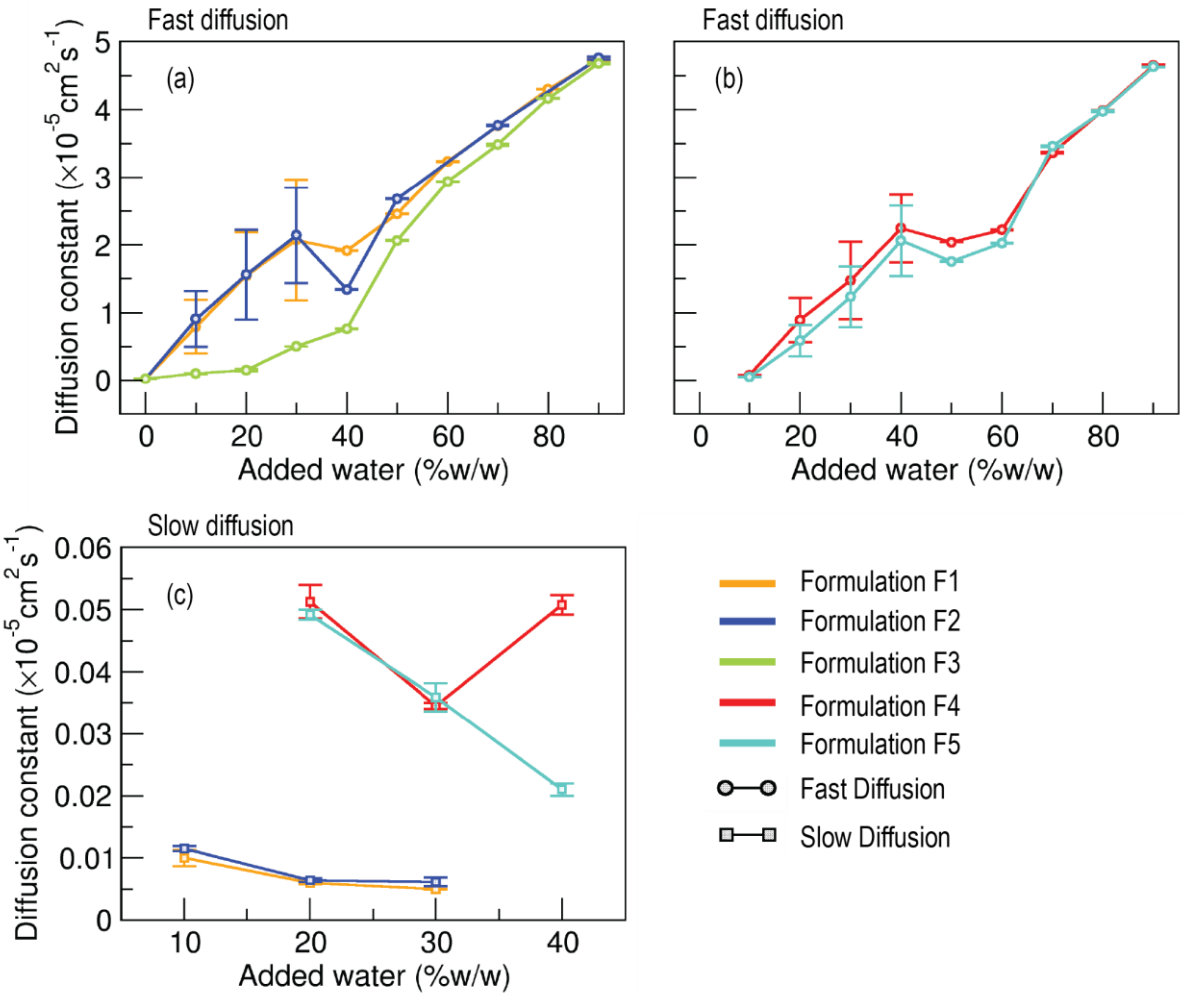

Figure 6 – Self-diffusion constants of water in formulations **F1** to **F5** from MD simulation. (a) Fast diffusion of water in formulation **F1** and variants **F2** and **F3**. (b) Fast diffusion of water in **F4** and its variant **F5**. (c) Slow diffusion of water in formulations **F1**, **F2**, **F4**, and **F5**. Error bars show RMSD.

Formulation **F3**, the fast diffusion of water is lower in the range 20-80% w/w water and behaves differently (i.e., the shape of the graph differs) from the previous cases. However, fast diffusion increases with the addition of water and reached the highest value at 90% w/w

water showing diffusion of bulk water. There is no dropdown of fast diffusion when formulation transforms from bi-continuous to phase separated states. This observation suggests that diffusion of water is fast in the single water pool in the phase separation compared to water in channels.

Formulations **F4** and **F5** have similar fast diffusion profiles, although the values for formulation **F4** formulation are slightly higher in the range 20-60% w/w water. A reduction in the diffusion rate is observed at 50% w/w water as the formulations change from reverse micellar to phase separated.

The slow diffusion constants behave similarly in related formulations (i.e., **F1**, **F2**, and **F4**, **F5**). However, at 40% w/w water systems **F4** and **F5** behave differently where **F4** formulation has a higher value. This is due to the cluster formed in phase separation (**F4** at 40% w/w water) restricts having interactions of water with other excipients compared to the formulation in water-swollen reverse micelles (**F5** at 40% w/w water). Thus, fewer interactions for water in **F4** formulation enabled fast diffusion at 40% w/w water.

Interaction of Excipients with Water

To investigate the interactions between components of the formulation with water, we calculated SASA per molecule of each individual molecular species. Figure 7 shows the changes in exposure as each formulation is diluted. It is apparent that that SASA per molecule in DGLs (C8 and C10), MGLs (C8 and C10), loratadine and Polysorbate 80 is high in formulations **F1** and **F2** (>10% w/w water) compared to the other three formulations. Further, the SASA per molecule in MGLs and DGLs, behave similarly within formulations **F1** and **F2** and formulations **F4** and **F5**. Even though **F3** is a variant of **F1** formulation, the SASA in DGLs and MGLs in **F3** formulation behaves similar to **F4**, **F5** formulations. A sudden drop in the values for DGLs and MGLs components in **F1**, **F2** formulations is observed at 40% w/w water due to the change of molecular arrangement from reverse micellar to phase separated, but it is increased again after that point. SASA per TGLs (both C8 and C10) in **F1**, **F2** and **F3** behave similarly with no significant change with the addition of water or formulation type.

Loratadine SASA per molecule behaves similarly in **F1**, **F2** and **F3**, **F4**, **F5** formulations. Also, SASA per Polysorbate 80 behaves the same way in **F1**, **F2** and **F3**, **F4** formulations. Furthermore, SASA per polyvinyl pyrrolidine behaves similarly in **F1** and **F3** formulations.

SASA per polyoxyl hydrogenated castor oil is less exposed to water when it is in bi-continuous phase, but when this surfactant is in bulky water it is more exposed to water.

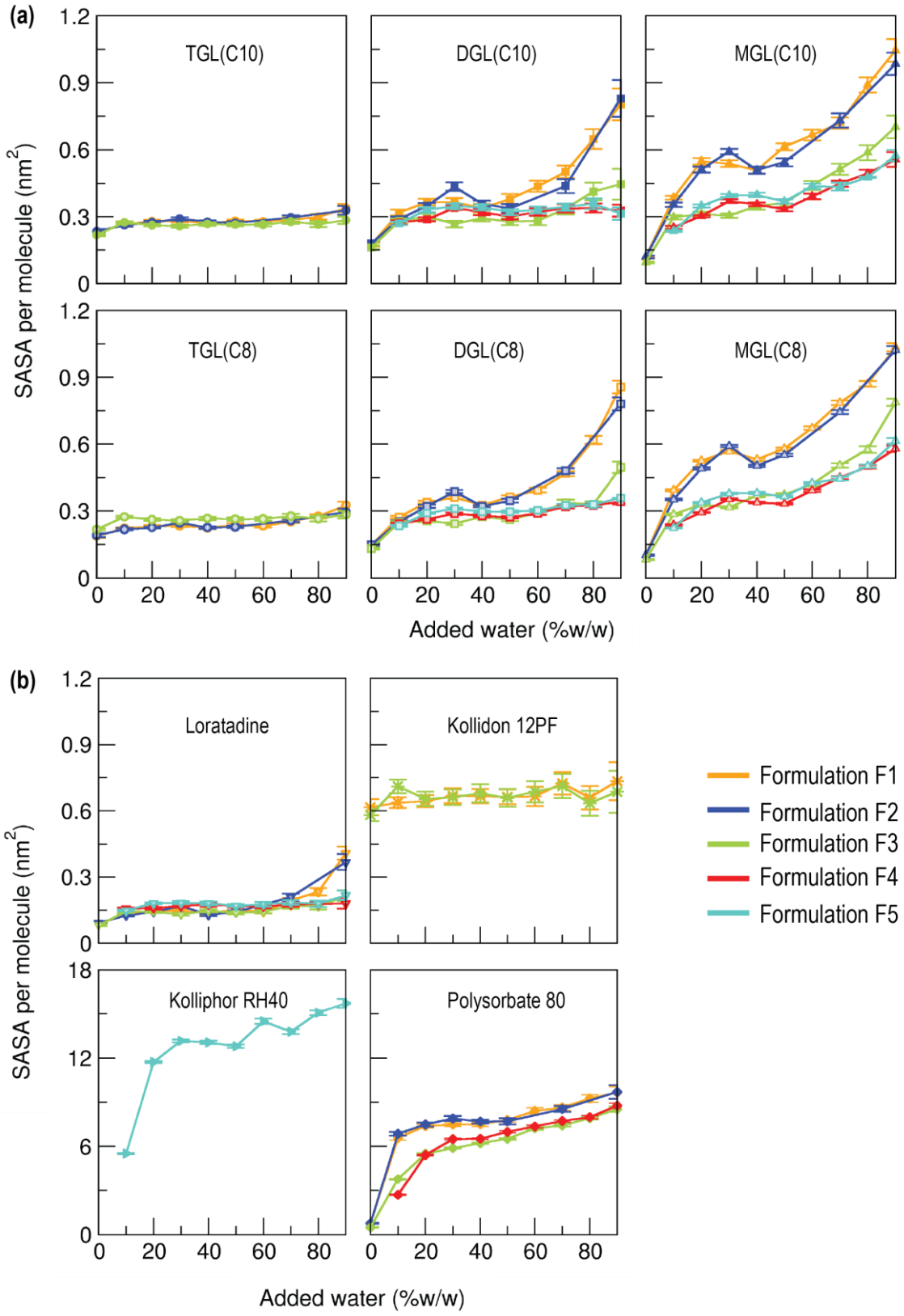

Figure 7 – SASA per molecule for each excipient component in diluted LBFs as a function of water content. Error bars show RMSD.

Aggregation of Loratadine

Since loratadine is a poorly water-soluble drug, to gain insight into the possibility of drug precipitation on dilution, we calculated the aggregation behavior of loratadine in each simulation. Detailed aggregation properties are shown in Table S2 of the SI. As an example, Figure 8(a) shows the average and maximum aggregation numbers in formulation **F3** as a function of water content. In this example, the average aggregation number varies from 2 to 3 and the average cluster size does not change significantly as the formulation as diluted. Figure 8(b) shows the loratadine aggregates within the colloidal structure formed in 90% w/w water simulation of formulation **F3**. The low aggregation numbers and lack of variation as the formulation is diluted suggest that formulation **F3** will effectively maintain loratadine in solution as it is dispersed within the GI tract. Similar behavior was observed for all other formulations (see Table S2 in SI).

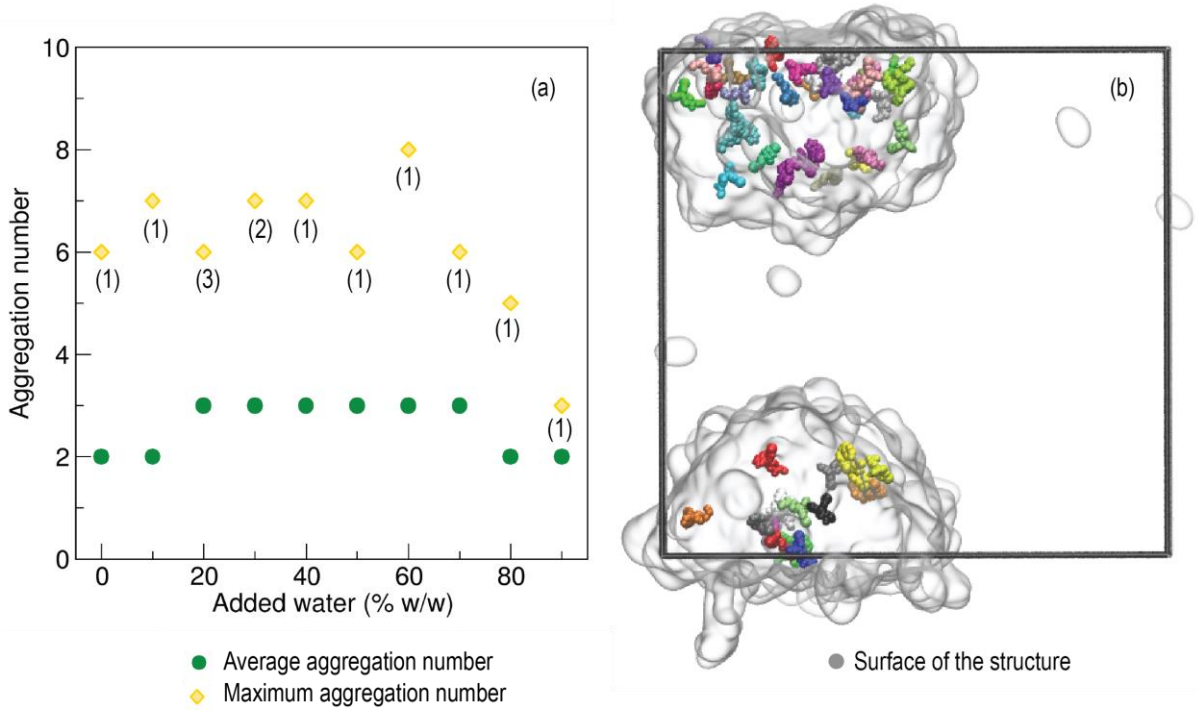

Figure 8 – (a) Average and maximum loratadine aggregation numbers in formulation **F3** as it is diluted with water. The number shows in brackets indicates the number of aggregates present of the maximum size. (b) Loratadine aggregates formed in **F3** diluted with 90% w/w water. Colors indicate different loratadine aggregates within the structure.

Experimental Phase Behavior of Diluted Formulations.

To compare the MD simulations with experimental data, we performed experimental studies that parallel the simulations. Formulations **F1**, **F3**, **F4**, and **F5** were diluted with water 10-90% w/w and the resulting solutions are shown in Figure 9.

We observed clear solutions at 10-20% w/w water in **F1** and **F3** formulations and milky solutions in the rest of the dilutions in two formulations. Both formulations **F4** and **F5** behaved differently compared to **F1** and **F3**. In particular, **F4** and **F5** formulations with 10% w/w water dilutions appeared as clear solutions, 20-30% w/w water dilutions formed translucent solutions and 40-90% w/w water dilutions yielded milky solutions.

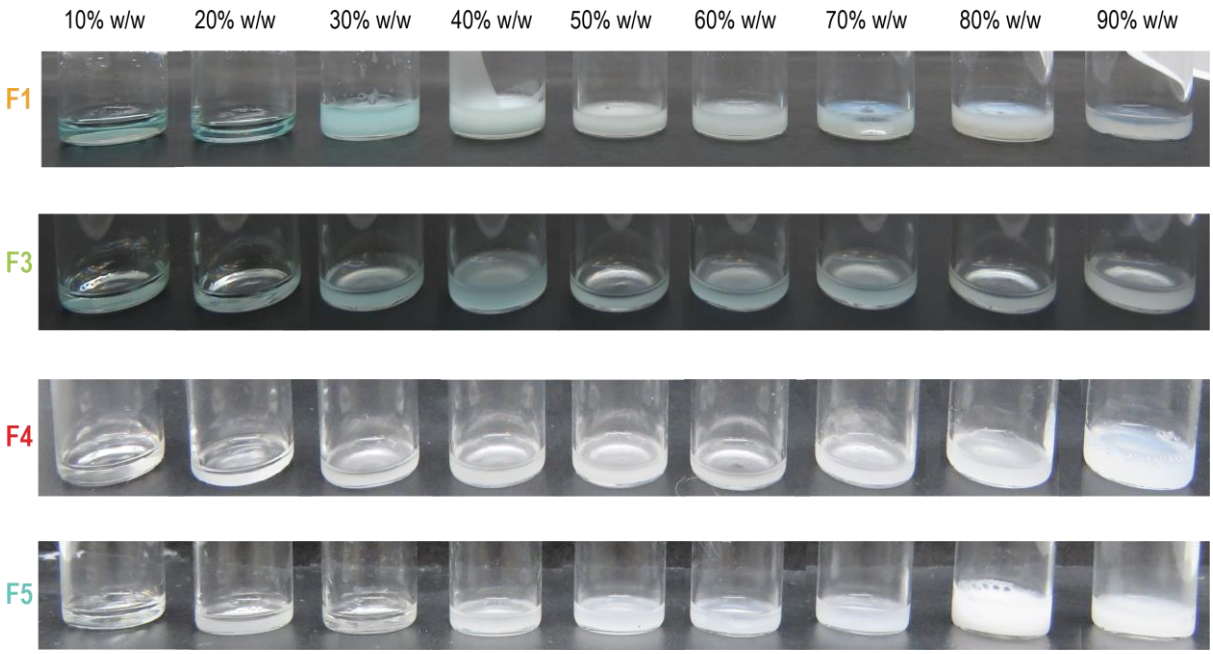

Figure 9 – Experimental phase behavior of formulations **F1**, **F3**, **F4** and **F5**. Since the liquid in the capsules is blue, a slight blue color is present in diluted formulations **F1** and **F3**.

Discussion

We are interested in the use of MD simulations to understand the performance of LBFs. Here, we have evaluated two loratadine formulations; the first is the commercial formulation from Okutan and co-workers[28] (**F1**) and the second is a formulation designed by us. (**F5)**. The differences between these two formulations are: i) **F1** includes triglycerides, but **F5** is free from triglycerides, ii) **F1** contains the polymer excipient polyvinyl pyrrolidine (Kollidon® 12PF) and iii) **F1** contains the surfactant Polysorbate 80 and **F5** contains polyoxyl hydrogenated castor oil (Kolliphor® RH40). We were also interested in studying the contributions made by specific excipients, so we altered formulations **F1** and **F5** to create

three modified examples. In formulation **F2**, we studied the effect of removing the polymer, polyvinyl pyrrolidine from **F1**. In formulation **F3**, we increased the total Polysorbate 80 content to 30% w/w, since formulation **F1** has a low surfactant content (3.1% w/w) compared to the more standard amounts used in Type III formulations in the lipid formulation classification system[8]. In the third case (**F4**), we replaced polyoxyl hydrogenated castor oil with Polysorbate 80. In each case, the effect of diluting the formulation in water was modelled by running simulations with added water content ranging from 0-90%.

Phase Behavior of Formulations (MD vs Experimental)

A wide range of colloidal structures can be formed by oil-surfactant-water-mixtures. Since their characteristics are important for the comparison of our computational and experimental data some of the structures are described here. An emulsion is a mixture of two immiscible liquids where the droplet form of one liquid is firmly dispersed in the other due to slow coalescence or a barrier to coalescence.[51] Water in oil (W/O) emulsions disperse water-swollen micelles covered with surfactants in an oil-rich phase while oil-in-water (O/W) emulsions disperse oil droplets in a continuous water phase.[52] The droplet size in O/W or W/O systems can vary from nanometer to micron scale.[53] W/O or O/W nanoemulsions and microemulsions can appear as clear or translucent solutions[54-55] while emulsions generally have a milky white appearance.[56] Bi-continuous microemulsions are single-phase, thermodynamically stable, clear solutions[55] formed by mixing almost equal amounts of oil and water with a large amount of surfactant (such as 50% weight) to produce continuous water and oil channels.[57]

In our simulations of diluted formulations, we observed progressive changes in phase with increasing water content (Figure 3). The neat formulations form a continuous phase. Addition of water progressively produces, swollen reverse micelles, bi-continuous phases and, finally, two-phase systems with separated oil and water compounds. Self-assembled MD structures similar to those observed the current study in continuous phase,[16] water-swollen reverse micellar,[16-17, 57] bi-continuous phase[57] and phase separated state[16-19, 58-59] have been previously reported in a variety of colloidal systems. Additionally, some of the observed changes microstructures have also previously seen in MD simulations, such as the increase in reverse micellar size[16-17] and the swelling behavior of water channels.[57] Finally, we note that the oily structures observed in phase separated states (i.e., a cluster or reverse micellar structure that spans half of the simulation box size) do not directly represent

the equilibrium structure of the system due to the fact that the final particle size is more massive than the simulation cell. This issue has been discussed in the literature.[16-19, 58-59]

Experimentally we observed clear solutions at low water content, followed by translucent, then milky solutions at higher water content (Figure 9). Comparison of the MD structures with experiment shows that reverse micellar structures with lower water aggregation number (5,500 – 12,500 molecules) correspond to clear experimental solutions; larger, water-swollen reverse micellar structures (water aggregation number 5,500 – 12,500) are matched by translucent solutions; bi-continuous phases are matched with clear solutions and phase separated states; and finally, cases where the formulation makes a cluster or separate aggregate that extends to the half of the simulation box (water aggregation number **>**12,500) are matched with milky solutions. Thus, the structural features in MD can be related to the experimental observations. Further, both MD and experiments indicate that reverse micellar systems (e.g., formulation **F1** with 10-20% w/w water and formulations **F4** and **F5** with 20-30% w/w water) could be either nano- or microemulsions. The size of the oily particles in the emulsion is not able to be determined from the simulation, because they are larger than the size of the simulation cell.

Each of the formulations diluted in the current study varies in oil, water, and surfactant concentration even though surfactant to oil ratio is the same for a particular formulation studied. The literature provides information that changes in water/oil proportion or both determine the emulsion type in the system.[60] That is the reason for the formation of different emulsion types such as water swollen reverse micelles, bicontinuous and phase separation (emulsion) with LBFs (i.e., **F1** to **F5**) upon dilution. Furthermore, surfactant type and concentration also play an important role in emulsification.[61] The simulations formulations of F**4** and F**5**, which differ only in the water-soluble surfactant, have similar phase behavior upon dilution as demonstrated by the similar colloidal structures formed on dilution (Figures 3D and E) and the similar profiles for the fast component of the water diffusion. Because the two formulations are composed with same proportions of oil, surfactant and water contents, the explored systems (Table 6, simulation 31 to 50) are the same in two formulations. Thus, the phase behavior is the same in two LBFs upon dilution. However, the surfactants polysorbate 80 and polyoxyl hydrogenated castor oil have similar HLB[62] values (e.g., 14-16[63] for and 15 respectively). Some differences are apparent in the simulations of 20% dilution where the formulation containing polyoxyl hydrogenated castor oil (**F4**), which has

better self-emulsifying properties, forms smaller water-swollen reverse micelles, which is in agreement with previous studies.[64-66]

MD simulations also provide the opportunity to study the effect of different components on formulation behavior. Here we investigated the effect of polyvinyl pyrrolidine polymer on phase behavior. The simulations of **F2**, which lacks the polymer, are very similar to the **F1** simulations in structure (Figures 3A and B) and in diffusion behavior (Figure 7), showing that this excipient does not greatly affect the phase behavior of a formulation. This component is likely included in the formulation to enhance the uniform dispersibility/solubility and compatibility of the capsule fill.[28, 67]

Interaction of Excipients with Water

MD provides insight into how the individual excipients interact with water in different phases. From this study, we can make several observations. 1) The oily TGLs are buried inside the lipid structures and do not change their interactions with water significantly due to changes in formulation type or the degree of dilution. 2) In formulations with the same general phase behavior (i.e., **F1** and **F2** are similar and **F4** and **F5** are similar), excipients interact similarly with water upon dilution. 3) Higher concentrations of Polysorbate 80 in the formulation limit interactions of MGLs, DGLs and surfactant itself with water due to the steric hindrance caused by branched and large surfactant nature of Polysorbate 80. Finally, 4) the polymer excipient, polyvinyl pyrrolidine does not change its interactions with water on the addition of water or the formation of different colloidal structure. In general, the simulations show that the interaction of excipients with water is closely linked to the phase structures formed.

Aggregation Behavior of Loratadine

The aggregation behavior of loratadine in the MD simulations provides insight into the propensity of loratadine to precipitate upon dispersion. This property is significant in formulation design since precipitation reduces the bioavailability of the drug.[4, 68] In all dilutions, the drug was mainly located in the lipidic region with minimum contact of water, consistent with its low solubility in water. We did not see aggregation of loratadine in any of the five formulations, which suggests that all of these lipid formulations are able to keep the drug solubilized within the system.

Conclusion

MD simulations provide additional insight into the complex phase behavior of LBFs upon dispersion and dilution. In this study, we have explored how well MD simulates the phase behavior of PEO mixed LBFs upon dispersion and dilution compared with experimental observation. Accordingly, we performed long (0.4–1.7 μs) 50 MD simulations for commercialized and modified LBFs considering 0-90% w/w dilution with water and carried out an experimental investigation, which aligns with MD. This study provides further confidence to use MD in modelling and extracting atomic details in designing efficient drug formulations since none of the earlier studies explored LBFs with PEO surfactants and commercialized LBFs.[16-20] Our results show that under different compositions and excipients, MD self-assembled randomly distributed molecular species into continuous phase, water-swollen reverse micelles, bi-continuous and phase separation. These structures well explain the experimental behavior indicating MD reproduce the experimental phase behavior. Thus, computational models we suggest for Captex® 355, Capmul® MCM, and Kolliphor® RH40 excipients are suitable for future studies. MD revealed that the effect of Kollidon® 12PF on phase behavior is minimum. MD also show that the phase behavior of a formulation at low dilutions can change by surfactant content and oil content in the formulation (**F1** vs **F3** in the study). Further, MD reveal that when formulation contains water soluble surfactant with closer HLB values, phase behavior does not change on surfactant type. However, the surfactant with high HLB tends to form smaller particles (i.e., water-swollen reverse micelles). Additionally, MD provide qualitative information such as the behavior of SASA of molecular species, swelling behavior reverse micelles and channels in bi-continuous phases, self-diffusion of water, drug location within the colloid and propensity of drug precipitation in different environments, which hard to extract through experimental methods but greatly helps us to understand the complex phase behavior of LBFs upon dilution.

Furthermore, potential experimental approaches can be used further to compare and test the validity of MD observations in the current study. The SEM/TEM images or diffraction or light scattering techniques can be used for particle sizing in formulation systems. However, there are some limitations associated with these techniques such as low water content systems cannot adequately be sized by either electron microscopy or diffraction or light scattering techniques. Because low water content systems are viscous mixtures that are largely water-in-oil until a point at approximately 50% water when a phase inversion occurs.

At this stage, the particle size of a dispersed formulation depends on the extent to which the formulation has been homogenised. Also, to validate the diffusion behavior of water obtained in MD, Pulsed Field Gradient Spin-Echo NMR technique[69] can be used. Even though we performed a limited number of experiments in the study to compare MD results, we believe the work in this paper confirms that MD can be used as a prediction tool to investigate the fate of LBFs after release from the soft-gelatine capsule in the GI tract. This will considerably help to accelerate the process of designing efficient LBFs for poorly water-soluble drugs.

References

1. Sastry, S. V.; Nyshadham, J. R.; Fix, J. A., Recent Technological Advances in Oral Drug Delivery–A Review. *Pharmaceut. Sci. Tech. Today* **2000,** *3* (4), 138-145.

2. Lipinski, C. A., Drug-Like Properties and the Causes of Poor Solubility and Poor Permeability. *J. Pharmacol. Toxicol. Methods* **2000,** *44* (1), 235-249.

3. Kuentz, M., Lipid-Based Formulations for Oral Delivery of Lipophilic Drugs. *Drug Discov. Today Technol.* **2012,** *9* (2), e97-e104.

4. Feeney, O. M.; Crum, M. F.; McEvoy, C. L.; Trevaskis, N. L.; Williams, H. D.; Pouton, C. W.; Charman, W. N.; Bergström, C. A. S.; Porter, C. J. H., 50 Years of Oral Lipid-Based Formulations: Provenance, Progress and Future Perspectives. *Adv. Drug Deliv. Rev.* **2016,** *101*, 167-194.

5. Porter, C. J. H.; Trevaskis, N. L.; Charman, W. N., Lipids and Lipid-Based Formulations: Optimizing the Oral Delivery of Lipophilic Drugs. *Nat. Rev. Drug Discov.* **2007,** *6* (3), 231-248.

6. Mu, H.; Holm, R.; Müllertz, A., Lipid-Based Formulations for Oral Administration of Poorly Water-Soluble Drugs. *Int. J. Pharm.* **2013,** *453* (1), 215-224.

7. Pouton, C. W., Lipid Formulations for Oral Administration of Drugs: Non-Emulsifying, Self-Emulsifying and Self-Microemulsifying Drug Delivery Systems. *Eur. J. Pharm. Sci.* **2000,** *11*, S93-S98.

8. Pouton, C. W., Formulation of Poorly Water-Soluble Drugs for Oral Administration: Physicochemical and Physiological Issues and the Lipid Formulation Classification System. *Eur. J. Pharm. Sci.* **2006,** *29* (3), 278-287.

9. Williams, H. D.; Sassene, P.; Kleberg, K.; Bakala-N'Goma, J.-C.; Calderone, M.; Jannin, V.; Igonin, A.; Partheil, A.; Marchaud, D.; Jule, E., Toward the Establishment of Standardized In Vitro Tests for Lipid-Based Formulations, Part 1: Method Parameterization and Comparison of In Vitro Digestion Profiles Across a Range of Representative Formulations. *J. Pharm. Sci.* **2012,** *101* (9), 3360-3380.

10. Williams, H. D.; Anby, M. U.; Sassene, P.; Kleberg, K.; Bakala-N'Goma, J. C.; Calderone, M.; Jannin, V.; Igonin, A.; Partheil, A.; Marchaud, D.; Jule, E.; Vertommen, J.; Maio, M.; Blundell, R.; Benameur, H.; Carrière, F.; Müllertz, A.; Pouton, C. W.; Porter, C. J., Toward the Establishment of Standardized In Vitro Tests for Lipid-Based Formulations. 2. The Effect of Bile Salt Concentration and Drug Loading on the Performance of Type I, II, IIIA, IIIB, and IV Formulations During In Vitro Digestion. *Mol. Pharm.* **2012,** *9* (11), 3286-300.

11. Williams, H. D.; Sassene, P.; Kleberg, K.; Calderone, M.; Igonin, A.; Jule, E.; Vertommen, J.; Blundell, R.; Benameur, H.; Müllertz, A.; Pouton, C. W.; Porter, C. J. H.; on behalf of the, L. C., Toward the Establishment of Standardized In Vitro Tests for Lipid-Based Formulations, Part 3: Understanding Supersaturation Versus Precipitation Potential During

the In Vitro Digestion of Type I, II, IIIA, IIIB and IV Lipid-Based Formulations. *Pharm. Res.* **2013,** *30* (12), 3059-3076.

12. Williams, H. D.; Sassene, P.; Kleberg, K.; Calderone, M.; Igonin, A.; Jule, E.; Vertommen, J.; Blundell, R.; Benameur, H.; Müllertz, A.; Porter, C. J. H.; Pouton, C. W., Toward the Establishment of Standardized In Vitro Tests for Lipid-Based Formulations, Part 4: Proposing a New Lipid Formulation Performance Classification System. *J. Pharm. Sci.* **2014,** *103* (8), 2441-2455.

13. Porter, C. J. H.; Kaukonen, A. M.; Taillardat-Bertschinger, A.; Boyd, B. J.; O'Connor, J. M.; Edwards, G. A.; Charman, W. N., Use of In Vitro Lipid Digestion Data to Explain the In Vivo Performance of Triglyceride-Based Oral Lipid Formulations of Poorly Water-Soluble Drugs: Studies with Halofantrine. *J. Pharm. Sci.* **2004,** *93* (5), 1110-1121.

14. Kollipara, S.; Gandhi, R. K., Pharmacokinetic Aspects and In Vitro-In Vivo Correlation Potential for Lipid-Based Formulations. *Acta Pharm. Sin. B.* **2014,** *4* (5), 333-49.

15. Andersen, H. C., Molecular Dynamics Simulations at Constant Pressure and/or Temperature. *J. Chem. Phys.* **1980,** *72* (4), 2384-2393.

16. Warren, D. B.; Chalmers, D. K.; Pouton, C. W., Structure and Dynamics of Glyceride Lipid Formulations, with Propylene Glycol and Water. *Mol. Pharm.* **2009,** *6* (2), 604-614.

17. Warren, D. B.; King, D.; Benameur, H.; Pouton, C. W.; Chalmers, D. K., Glyceride Lipid Formulations: Molecular Dynamics Modeling of Phase Behavior During Dispersion and Molecular Interactions Between Drugs and Excipients. *Pharm. Res.* **2013,** *30* (12), 3238-3253.

18. Birru, W. A.; Warren, D. B.; Han, S.; Benameur, H.; Porter, C. J. H.; Pouton, C. W.; Chalmers, D. K., Computational Models of the Gastrointestinal Environment. 2. Phase Behavior and Drug Solubilization Capacity of a Type I Lipid-Based Drug Formulation after Digestion. *Mol. Pharm.* **2017,** *14* (3), 580-592.

19. Larsson, P.; Alskär, L. C.; Bergström, C. A. S., Molecular Structuring and Phase Transition of Lipid-Based Formulations upon Water Dispersion: A Coarse-Grained Molecular Dynamics Simulation Approach. *Mol. Pharm.* **2017,** *14* (12), 4145-4153.

20. Benson, S. P.; Pleiss, J., Molecular Dynamics Simulations of Self-Emulsifying Drug-Delivery Systems (SEDDS): Influence of Excipients on Droplet Nanostructure and Drug Localization. *Langmuir* **2014,** *30* (28), 8471-80.

21. Boyd, B. J.; Bergström, C. A. S.; Vinarov, Z.; Kuentz, M.; Brouwers, J.; Augustijns, P.; Brandl, M.; Bernkop-Schnürch, A.; Shrestha, N.; Préat, V.; Müllertz, A.; Bauer-Brandl, A.; Jannin, V., Successful Oral Delivery of Poorly Water-Soluble Drugs Both Depends on the Intraluminal Behavior of Drugs and of Appropriate Advanced Drug Delivery Systems. *Eur. J. Pharm. Sci.* **2019,** *137*, 104967.

22. Mehta, C. H.; Narayan, R.; Nayak, U. Y., Computational Modeling for Formulation Design. *Drug Discov. Today* **2019,** *24* (3), 781-788.

23. Savla, R.; Browne, J.; Plassat, V.; Wasan, K. M.; Wasan, E. K., Review and Analysis of FDA Approved Drugs Using Lipid-Based Formulations. *Drug Dev. Ind. Pharm.* **2017,** *43* (11), 1743-1758.

24. Kay, G. G.; Harris, A. G., Loratadine: A Non-Sedating Antihistamine. Review of Its Effects on Cognition, Psychomotor Performance, Mood and Sedation. *Clin. Exp. Allergy* **1999,** *29* (S3), 147-150.

25. Clissold, S. P.; Sorkin, E. M.; Goa, K. L., Loratadine. *Drugs* **1989,** *37* (1), 42-57.

26. Zhang, S.; Sun, M.; Zhao, Y.; Song, X.; He, Z.; Wang, J.; Sun, J., Molecular Mechanism of Polymer-Assisting Supersaturation of Poorly Water-Soluble Loratadine Based on Experimental Observations and Molecular Dynamic Simulations. *Drug Deliv. Transl. Res.* **2017,** *7* (5), 738-749.

27. Armaković, S.; Armaković, S. J.; Abramović, B. F., Theoretical Investigation of Loratadine Reactivity in Order to Understand Its Degradation Properties: DFT and MD Study. *J. Mol. Model.* **2016,** *22* (10), 240.

28. Okutan, B.; Draper, P.; Draper, J., Pharmaceutical Formulations of Loratadine for Encapsulation and Combinations Thereof. Google Patents: 2012.

29. Captex®. https://www.abiteccorp.com/media/2794/abitec-abitec-literature-captex-brochure.pdf (Accessed January 04, 2021).

30. Capmul®. https://www.abiteccorp.com/media/2795/abitec-abitec-literature-capmul-brochure.pdf (Accessed January 04, 2021).

31. Prajapati, H. N.; Dalrymple, D. M.; Serajuddin, A. T. M., A Comparative Evaluation of Mono-, Di- and Triglyceride of Medium Chain Fatty Acids by Lipid/Surfactant/Water Phase Diagram, Solubility Determination and Dispersion Testing for Application in Pharmaceutical Dosage Form Development. *Pharm. Res.* **2012,** *29* (1), 285-305.

32. Zhang, R.; Wang, Y.; Tan, L.; Zhang, H. Y.; Yang, M., Analysis of Polysorbate 80 and Its Related Compounds by RP-HPLC with ELSD and MS Detection. *J. Chromatogr. Sci.* **2012,** *50* (7), 598-607.

33. Bühler, V., Soluble Polyvinylpyrrolidone (povidone). In *Polyvinylpyrrolidone Excipients for Pharmaceuticals: Povidone, Crospovidone and Copovidone* 2005; pp 5-124.

34. Tang, X.; Huston, K. J.; Larson, R. G., Molecular Dynamics Simulations of Structure–Property Relationships of Tween 80 Surfactants in Water and at Interfaces. *J. Phys. Chem. B* **2014,** *118* (45), 12907-12918.

35. Malde, A. K.; Zuo, L.; Breeze, M.; Stroet, M.; Poger, D.; Nair, P. C.; Oostenbrink, C.; Mark, A. E., An Automated Force Field Topology Builder (ATB) and Repository: Version 1.0. *J. Chem. Theory Comput.* **2011,** *7* (12), 4026-4037.

36. Suys, E. J. A.; Warren, D. B.; Pham, A. C.; Nowell, C. J.; Clulow, A. J.; Benameur, H.; Porter, C. J. H.; Pouton, C. W.; Chalmers, D. K., A Nonionic Polyethylene Oxide (PEO)

Surfactant Model: Experimental and Molecular Dynamics Studies of Kolliphor EL. *J. Pharm. Sci.* **2019,** *108* (1), 193-204.

37. Horta, B. A. C.; Merz, P. T.; Fuchs, P. F. J.; Dolenc, J.; Riniker, S.; Hünenberger, P. H., A GROMOS-Compatible Force Field for Small Organic Molecules in the Condensed Phase: The 2016H66 Parameter Set. *J. Chem. Theory Comput.* **2016,** *12* (8), 3825-3850.

38. Berendsen, H. J.; van der Spoel, D.; van Drunen, R., GROMACS: A Message-Passing Parallel Molecular Dynamics Implementation. *Comput. Phys. Commun.* **1995,** *91* (1-3), 43-56.

39. Pronk, S.; Páll, S.; Schulz, R.; Larsson, P.; Bjelkmar, P.; Apostolov, R.; Shirts, M. R.; Smith, J. C.; Kasson, P. M.; Van Der Spoel, D., GROMACS 4.5: A High-Throughput and Highly Parallel Open Source Molecular Simulation Toolkit. *Bioinformatics* **2013,** *29* (7), 845-854.

40. Feenstra, K. A.; Hess, B.; Berendsen, H. J. C., Improving Efficiency of Large Time-Scale Molecular Dynamics Simulations of Hydrogen-Rich Systems. *J. Comput. Chem.* **1999,** *20* (8), 786-798.

41. Bussi, G.; Donadio, D.; Parrinello, M., Canonical Sampling Through Velocity Rescaling. *J. Chem. Phys.* **2007,** *126* (1), 014101.

42. Berendsen, H. J. C.; Postma, J. P. M.; Gunsteren, W. F. v.; DiNola, A.; Haak, J. R., Molecular Dynamics with Coupling to an External Bath. *J. Chem. Phys.* **1984,** *81* (8), 3684-3690.

43. Parrinello, M.; Rahman, A., Polymorphic Transitions in Single Crystals: A New Molecular Dynamics Method. *J. Appl. Phys.* **1981,** *52* (12), 7182-7190.

44. Miyamoto, S.; Kollman, P. A., Settle: An Analytical Version of the SHAKE and RATTLE Algorithm for Rigid Water Models. *J. Comput. Chem.* **1992,** *13* (8), 952-962.

45. Hess, B.; Bekker, H.; Berendsen, H. J. C.; Fraaije, J. G. E. M., LINCS: A Linear Constraint Solver for Molecular Simulations. *J. Comput. Chem.* **1997,** *18* (12), 1463-1472.

46. Verlet, L., Computer "Experiments" on Classical Fluids. I. Thermodynamical Properties of Lennard-Jones Molecules. *Phys. Rev.* **1967,** *159* (1), 98-103.

47. Darden, T.; York, D.; Pedersen, L., Particle Mesh Ewald: An N·log(N) Method for Ewald Sums in Large Systems. *J. Chem. Phys.* **1993,** *98* (12), 10089-10092.

48. Humphrey, W.; Dalke, A.; Schulten, K., VMD: Visual Molecular Dynamics. *J. Mol. Graph.* **1996,** *14* (1), 33-38.

49. Chalmers, D. K.; Roberts, B. P. Silico: A Perl Molecular Toolkit http://silico.sourceforge.net.

50. Guruge, A. G.; Warren, D. B.; Benameur, H.; Pouton, C. W.; Chalmers, D. K., Aqueous Phase Behavior of the PEO-Containing Non-Ionic Surfactant $C_{12}E_6$: A Molecular Dynamics Simulation Study. *J. Colloid Interface Sci.* **2021,** *588*, 257-268.

51. Kilpatrick, P. K., Water-in-Crude Oil Emulsion Stabilization: Review and Unanswered Questions. *Energy Fuels* **2012,** *26* (7), 4017-4026.

52. Tadros, T. F., Emulsion Formation, Stability, and Rheology. In *Emulsion Formation and Stability* 2013; pp 1-75.

53. Goodarzi, F.; Zendehboudi, S., A Comprehensive Review on Emulsions and Emulsion Stability in Chemical and Energy Industries. *Can. J. Chem. Eng.* **2019,** *97* (1), 281-309.

54. Solans, C.; Izquierdo, P.; Nolla, J.; Azemar, N.; Garcia-Celma, M. J., Nano-Emulsions. *Curr. Opin. Colloid Interface Sci.* **2005,** *10* (3), 102-110.

55. Ita, K., Chapter 6 - Microemulsions. In *Transdermal Drug Delivery*, Ita, K., Ed. Academic Press: 2020; pp 97-122.

56. Benito, J. M.; Cambiella, A.; Lobo, A.; Gutiérrez, G.; Coca, J.; Pazos, C., Formulation, Characterization and Treatment of Metalworking Oil-in-Water Emulsions. *Clean Technol. Environ. Policy* **2010,** *12* (1), 31-41.

57. Negro, E.; Latsuzbaia, R.; de Vries, A. H.; Koper, G. J. M., Experimental and Molecular Dynamics Characterization of Dense Microemulsion Systems: Morphology, Conductivity and SAXS. *Soft Matter* **2014,** *10* (43), 8685-8697.

58. Suys, E. J. A.; Warren, D. B.; Porter, C. J. H.; Benameur, H.; Pouton, C. W.; Chalmers, D. K., Computational Models of the Intestinal Environment. 3. The Impact of Cholesterol Content and pH on Mixed Micelle Colloids. *Mol. Pharm.* **2017,** *14* (11), 3684-3697.

59. Birru, W. A.; Warren, D. B.; Headey, S. J.; Benameur, H.; Porter, C. J. H.; Pouton, C. W.; Chalmers, D. K., Computational Models of the Gastrointestinal Environment. 1. The Effect of Digestion on the Phase Behavior of Intestinal Fluids. *Mol. Pharm.* **2017,** *14* (3), 566-579.

60. Salager, J.-L.; Márquez, L.; Peña, A. A.; Rondón, M.; Silva, F.; Tyrode, E., Current Phenomenological Know-How and Modeling of Emulsion Inversion. *Ind. Eng. Chem. Res.* **2000**, *39* (8), 2665-2676.

61. Adeyeye, C. M.; Price, J. C., Effect of Non-Ionic Surfactant Concentration and Type on the Formation and Stability of W/O/W Multiple Emulsions: Microscopic and Conductometric Evaluations. *Drug Dev. Ind. Pharm.* **1991**, *17* (5), 725-736.

62. Hydrophilic–Lipophilic Balance (HLB): Classical Indexation and Novel Indexation of Surfactant. In *Encyclopedia of Biocolloid and Biointerface Science 2V Set*, 2016; pp 570-574.

63. Reintjes, T., Solubility Enhancement with BASF Pharma Polymers: Solubilizer Compendium. *BASF: Ludwigshafen, Germany* **2011**.

64. Niamprem, P.; Rujivipat, S.; Tiyaboonchai, W., Development and Characterization of Lutein-Loaded SNEDDS for Enhanced Absorption in Caco-2 cells. *Pharm. Dev. Technol.* **2014**, *19* (6), 735-742.

65. Khan, A. W.; Kotta, S.; Ansari, S. H.; Sharma, R. K.; Ali, J., Self-Nanoemulsifying Drug Delivery System (SNEDDS) of the Poorly Water-Soluble Grapefruit Flavonoid Naringenin: Design, Characterization, In Vitro and In Vivo Evaluation. *Drug Deliv.* **2015**, *22* (4), 552-561.

66. Chatterjee, B.; Hamed Almurisi, S.; Ahmed Mahdi Dukhan, A.; Mandal, U. K.; Sengupta, P., Controversies with Self-Emulsifying Drug Delivery System from Pharmacokinetic Point of View. *Drug Deliv.* **2016**, *23* (9), 3639-3652.

67. Yudina, D. V.; Blynskaja, E. V.; Alekseev, K. V.; Marakhova, A. I., Polymers for the Enhancement of Solubility of Pharmaceutical Substances in Solid Drug Formulations. *Russ. Chem. Bull.* **2018**, *67* (5), 787-791.

68. Khan, J.; Rades, T.; Boyd, B., The Precipitation Behavior of Poorly Water-Soluble Drugs with an Emphasis on the Digestion of Lipid Based Formulations. *Pharm. Res.* **2016**, *33* (3), 548-562.

69. Naoui, W., Bolzinger, M.A., Fenet, B., Pelletier, J., Valour, J.P., Kalfat, R., Chevalier, Y., Microemulsion Microstructure Influences the Skin Delivery of an Hydrophilic Drug. *Pharm. Res.* **2011**, *28* (7), 1683-1695.

Chapter 6

Phase Behavior of Phospholipid/Bile Salt/Water Mixtures with a Coarse-Grained MD Approach

The presence of bile in the GI tract, which includes phospholipids, bile salts and cholesterol also self-assembled into a series of colloidal structures such as micelles, mixed micelles, unilamellar and multilamellar vesicles that increase the solubilization of the drug in a formulation.[1] Therefore, bile components play a significant role in the fate of drug/drug formulations.[2-3] Thus, a clear picture of the fate of LBFs can be obtained from introducing bile components to the MD simulation of LBFs. Unfortunately, vesicle-like structures that are prone to form in the presence of bile are not possible to model with united atom models due to their larger structural nature. Thus, as a solution, we used coarse-grained (CG) molecular dynamics (MD) simulations for our investigation of modelling the phase behavior of bile components in water mixtures.

At the time this work began, there were no systematic CG MD investigations on the phase behavior of phospholipid/bile salt/water mixtures. Thus, we undertook a preliminary investigation using the MARTINI CG models to test whether this method could reproduce the experimental phase behavior. Our ultimate goal is to introduce bile components to the LBFs to obtain the fate of LBFs after oral administration. We aim to further extend this study to make this chapter publishable.

6.1 Introduction

6.1.1 Gastro-Intestinal (GI) Tract Lumen and Drug Absorption

The GI tract is a complex environment. The digestion of triglycerides/diglycerides from the formulation and solubilisation of the drug in the small intestine is a complicated process that is described in Porter and co-workers a review article.[1] In detail, once a drug formulation is orally administered, it contacts with bile, digestive enzymes, foods, and digested foods and is exposed to a dynamically pH changing environment. Subsequently, LBFs from an orally administrated drug are dispersed in the stomach and gastric lipase starts to digest triglycerides into diglycerides and free fatty acids. Amphiphilic products from the initial digestion then facilitate emulsification of the drug formulation. On entering into the small intestine, pancreatic lipase, and co-lipase complete the breakdown of the remaining triglycerides into diglycerides, monoglycerides and free fatty acids. The secretion of bile from the gall bladder into the small intestine further facilitates the self-assembly of these components into micelles, mixed micelles and vesicles that significantly enhances the solubility of poorly water-soluble drugs incorporated in the LBF. This highlights the importance of bile components in drug absorption.

Bile is a heterogeneous mixture composed mainly of bile salts, phospholipids and cholesterol.[4] Detailed information regarding these components is given in Chapter 2. Due to the significant contribution of bile components in drug absorption, the colloidal behavior of bile salts, phospholipids and cholesterol in different systems has been investigated in the literature.[5-9] Of the different experimental investigations, our attention was drawn by a study conducted by Birru et al.[5] who investigated the phase behavior of phospholipid, 1-palmitoyl-2-oleoyl-sn-glycerol-3-phosphocholine (POPC), glycochenodeoxycholate (GDX) and digested products of POPC and found a clear difference in the phase behavior between undigested and digested phospholipids in the transition of phases from micelles to vesicles. They also developed a ternary phase diagram for POPC/GDX/water mixtures. Later, this phase diagram was further extended for the high concentration of POPC by Birru and co-workers[10] in 2017 assuming that the position of the phase boundary does not change with the increased lipid concentration (i.e., the boundary at lower concentration was extrapolated), which we used for the work in this chapter.

6.1.2 MD Studies with Bile Components

The MD approach has been widely used to study bile components. Previous studies have investigated bile salt aggregation or its phase behavior[10-15], mixed micelle formation[13, 16], the impact of cholesterol on the colloidal behavior of bile[17], molecular interactions of colloids present in fasted state intestinal fluid[18] and counterion binding in bile salt micelles[19] using all-atom, united-atom or coarse-grained models. There are also numerous investigations on digested products of bile, especially of fatty acids, which investigate their role in membranes/bilayers under various conditions using all-atom[20-21], united-atom[22] and CG models[23-24]. Additionally, the phase behavior of fatty acids in different environments and under different conditions have also been investigated with a united-atom[25-26] model and a CG model[27-28]. These studies are discussed in detail in Chapter 2.

However, there were no systematic MD investigations in the literature that explore how effectively MD coarse-grained models reproduce the phase behavior of phospholipid/bile salt/water mixtures. Thus, we aimed to investigate whether MARTINI coarse-grained models could reproduce the experimental phase behavior of POPC/glycochenodeoxycholate/water mixtures in the micellar and vesicular regions of experimentally derived POPC/glycodeoxycholic acid sodium salt/water ternary phase diagram.

6.1.3 The MARTINI Force Field

The 'MARTINI' force field was introduced in 2003 by Marrink and Mark where they studied the spontaneous aggregation of phospholipid, dipalmitoylphosphatidylcholine (DPPC) into unilamellar vesicles.[29] In this force field, molecules are simplified by a grouping of several atoms into a virtual bead. Through this simple molecular representation, Marrink's research group mainly aimed to provide a simple model for MD simulations that can be easy to use, computationally fast and applicable to a large range of biomolecular systems.[30] After introducing this force field, several extensions of these force fields have been released to improve the MARTINI force field for different systems.[30-34] Thus, this force field has been used to explore more complex systems such as self-assembly of vesicles, vesicle fusion, the formation of gel and liquid order phases and phase transitions.[29, 31, 35-40]

The MARTINI force field is based on four-to-one mapping where on average four heavy atoms with their associated hydrogens are represented by a single interaction centre known as a bead.[41] To be consistent with four-to-one mapping criteria, for modelling water, four water molecules are mapped to a CG water bead. However, this mapping pattern is not

used with ions and small ring-like fragments. For example, Na^+ ion is represented by a single CG bead and benzene like molecules are mapped with high resolutions, such as two non-hydrogen atoms to one CG bead. Based on the chemical nature of the structure, CG beads are assigned a type as polar (P), non-polar (N), apolar (C) or charged (Q). Within these four types, subtypes are assigned again either by a letter, implying their hydrogen-bonding capabilities or by a number implying the degree of polarity. In detail, assigning a subtype with letters, 'd' denotes donor, 'a' denotes acceptor, 'da' denotes both donor and acceptor and 'o' denotes none. When assigning subtype with the degree of polarity, 1 to 5 numbers are used where number 1 used to imply low polarity and number 5 used to imply high polarity.

Bonded interactions are described with energy functions commonly used in classical force fields such as harmonic bond/angle and dihedral potentials. Non-bonded interactions are described by a Lennard-Jones potential and Coulombic energy function. In general, MARTINI simulations are stable with timesteps of up to 40 fs or 20 fs in molecules with rings or proteins.[41] Currently, a list of MARTINI CG models for different molecules such as lipids, sterols, peptides, sugars, proteins, polymers can be found on the official MARTINI website. All CG molecules employed in this work are from that MARTINI website, http://cgmartini.nl/.

6.2 Methods

6.2.1 Construction of Systems

MD simulations were performed at Australia's specialised high-performance computing facility for imaging and visualisation, The Multi-modal Australian ScienceS Imaging and Visualisation Environment (MASSIVE). All systems were prepared by placing POPC, bile salt and water in a random orientation using *random_box* script from Silico[42] package in the approximate box size of 50×50×50 nm except for one simulation (simulation at point B* in Table 1). The number of molecules to be placed in the box was calculated from the weights of POPC, bile salt and water. When the system contained bile salt, Na^+ ions were added to the system according to the number of bile salts in the system. This step was conducted to neutralize the total charge in systems with bile salts. The following procedure was followed for MD simulations on constructed systems.

6.2.2 Topologies

POPC, cholic acid sodium salt (CHOX) and water modelled parameters from MARTINI force filed in http://cgmartini.nl/ website.

6.2.3 MD Simulations

All simulations were performed using GROMACS version 2018.4 with a time step of 25 fs. The isothermal-isobaric ensemble (NPT ensemble) was used in all simulations. Temperature coupling was used with the velocity rescale algorithm with a temperature coupling time constant of 1 ps. The reference temperature was set to 310 K. The reference pressure, 1 bar and compressibility of 3×10^{-4} bar^{-1} were used for the Parrinello-Rahman[43] algorithms. MARTINI water beads (one bead representing four water molecules) and Na^{+} ions were modelled using the parameters in the default itp files from http://cgmartini.nl/ website. All other bonds were constrained by the LINCS algorithm.[44] A Verlet cut-off scheme[45] was employed for all simulations with the cut-off distance of 1.1 nm for short-range Coulombic and van der Waals interactions (non-bonded interactions). For long-range Coulombic interactions, the reaction-field was applied. Before the production run, all systems were subjected to energy minimization of 1000 steps with a time step of 40 fs using the steepest descent method.

MD trajectories were analysed using GROMACS tools while resulting colloidal structures were visually inspected using PyMOL.[46] The self-assembled structures were studied using *find_aggregate* script in the Silico package[42]. This script assigns molecules into the same aggregate if two carbon atoms are within a cut-off distance. To use this script with CG models, we used a cut-off distance of 0.8 nm. The solvent accessible surface area (SASA) was calculated using *gmx_sasa* to confirm that the system has reached a stable configuration.

6.3 Results

In this work, we wished to investigate whether MD simulations using the MARTINI CG model could successfully reproduce the experimentally observed aqueous phase behavior of phospholipid and bile salt mixtures. For this purpose, we performed MD simulations for POPC/CHOX/water mixtures that align with A to E points as shown in Figure 1 in micellar and vesicle regions of an experimentally derived ternary phase diagram.[5, 10]

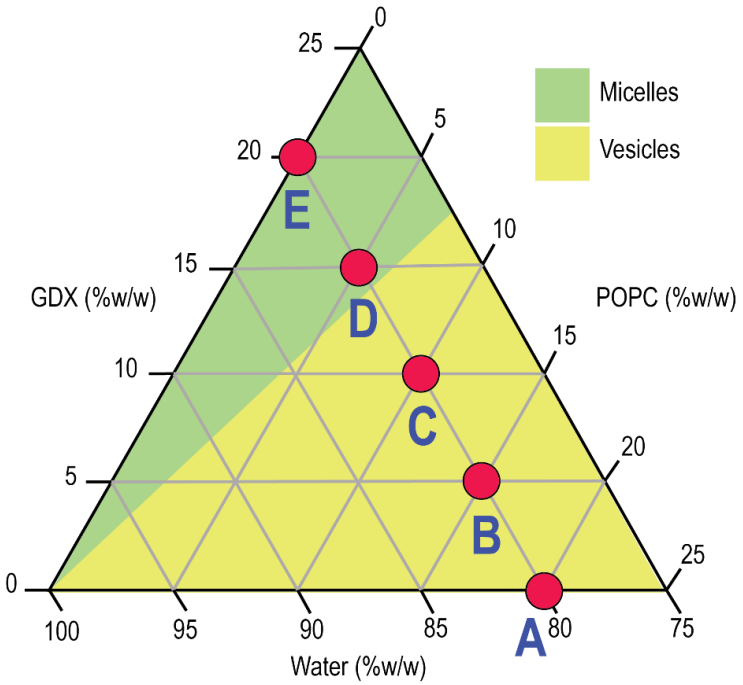

Figure 1 – Ternary phase diagram for POPC/GDX/water mixtures at 310 K.[5, 10] Points selected for MD simulations in the current study are shown in A to E. *Adapted with permission from Birru, W. A.; Warren, D. B.; Headey, S. J.; Benameur, H.; Porter, C. J. H.; Pouton, C. W.; Chalmers, D. K., Computational Models of the Gastrointestinal Environment. 1. The Effect of Digestion on the Phase Behavior of Intestinal Fluids. Mol. Pharm.* ***2017,*** *14 (3), 566-579. Copyright (2017) American Chemical Society.*

Even though this ternary phase diagram was derived using glycodeoxycholic acid sodium salt, the unavailability of MARTINI parameters for glycodeoxycholic acid sodium salt molecule led us to use cholic acid sodium salt (3*a*-7*a*-12*a*-trihydroxy-5*b*-cholanic acid sodium salt) instead of glycodeoxycholic acid sodium salt. The chemical structures of POPC, glycodeoxycholic acid sodium salt and cholic acid sodium salt are shown in Figure 2. All simulations were started from random orientation and details of system composition, simulation time, final structures obtained in these systems are presented in Table 1.

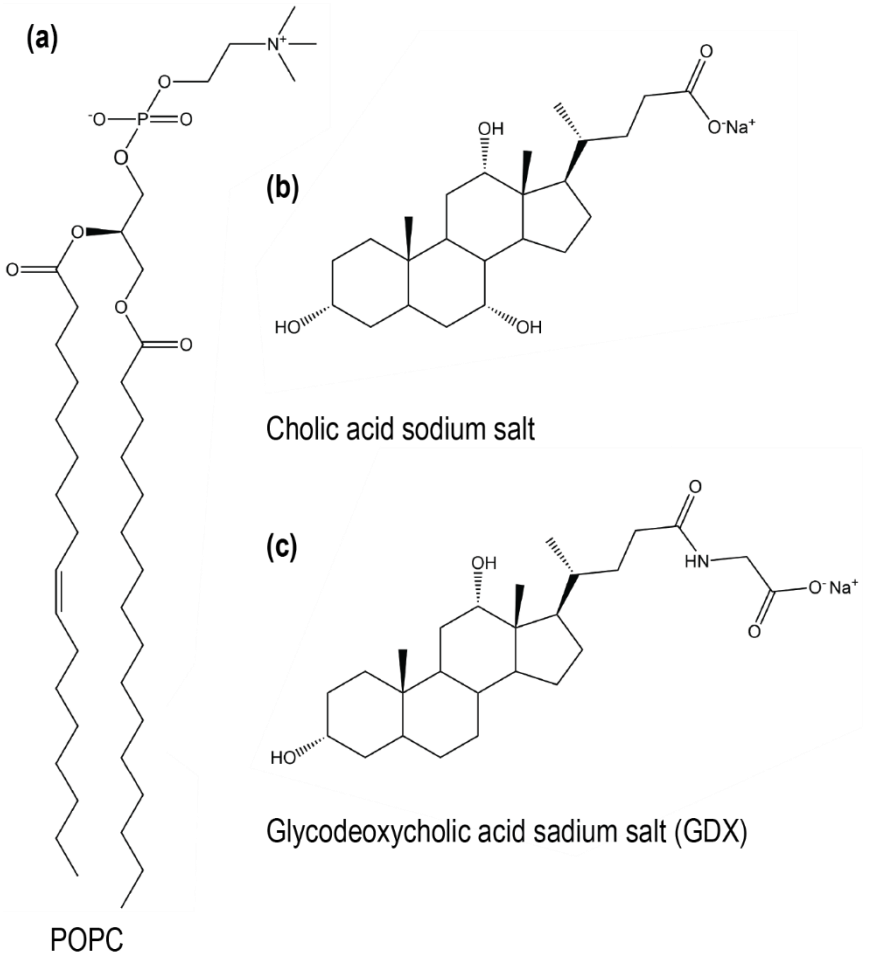

Figure 2 – Chemical structures of (a) POPC, (b) cholic acid sodium salt and (c) glycodeoxycholic acid sodium salt.

To determine the final structures at points A to E, system equilibration is essential. Our previous work showed that solvent accessible surface area (SASA) can be used as an indicator to identify the system stability of a colloidal system.[47] Thus, in this work, we calculated the SASA for POPC, except for the system at point E to determine the system stability (Figure 3). For the system at point E, we calculated SASA for bile salt since that system does not contain POPC. A constant value of SASA for a significant time indicates that a particular system has reached a stable state. Figure 3 suggests that the systems have reached stable configurations except at point E, which is still stabilizing toward a minimum structure. Yet, at point E, the fluctuation of SASA values with respect to the simulation time is small and that indicates the molecular arrangement is not going to change drastically.

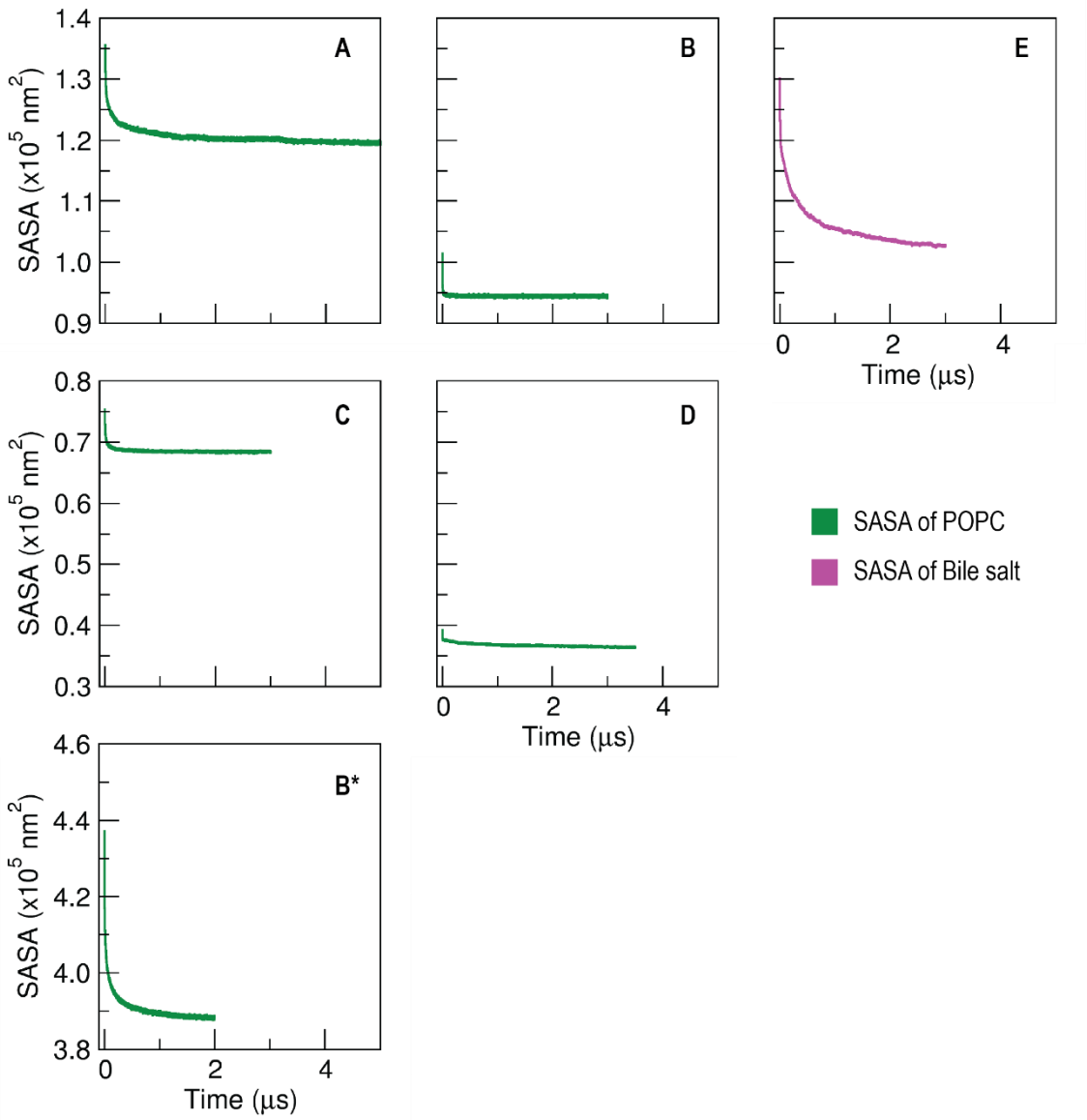

Figure 3 – SASA calculated for POPC or bile salt in simulated systems at point A to E

Table 1 – Composition, MD simulation details and outcomes of simulations performed for points A to E

point on the phase diagram	POPC		bile salt		water		163pprox. . cell size (nm)	tim e (μs)	colloidal structure in	
	N_{POPC}	% w/w	N_{bile_salt}	% w/w	N_{water}	% w/w			MD	exp.[10]
A	19807	20	0	0	835481	80	50×50×50	5	vesicles	vesicles
B	14855	15	8741	5	835481	80	50×50×50	3	bilayer‡	vesicles
B*	60847	15	35803	5	3422129	80	80×80×80	2	bicelles	vesicles
C	9904	10	174–82	10	835481	80	50×50×50	3	micelles	vesicles
D	4952	5	26223	15	835481	80	50×50×50	3.5	micelles	micelles
E	0	0	34964	20	835481	80	50×50×50	3	micelles	micelles

N_{POPC} – number of POPC molecules, N_{bile_salt} – number of bile salt molecules, N_{water} – number of water molecules, % w/w – weight percentage of POPC or bile salt or water, exp. – experimental, ‡Structure spans the simulation box size, *Simulation of point B with larger box size

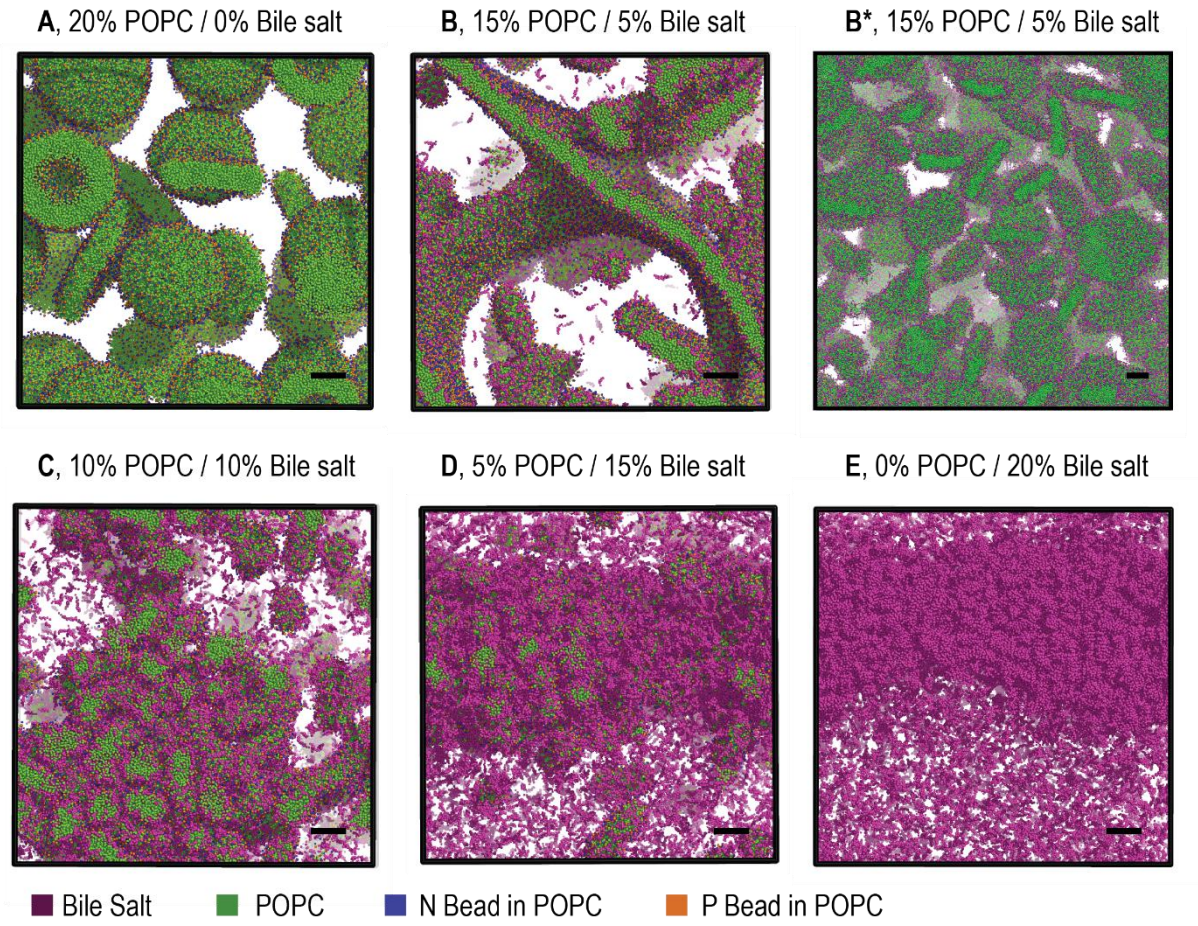

Figure 4 – Final structures formed in MD simulations performed at points A to E in the experimental phase diagram. % Indicates weight percentages of the POPC and bile salt in each system. The scale bar length is 5.0 nm.

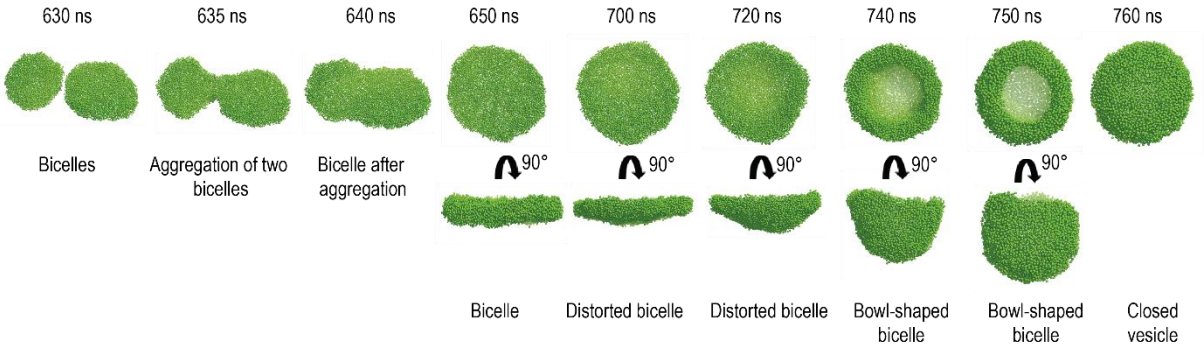

Figure 5 – Formation of vesicular structure with the progression of time

All simulations started from random distributions self-assembled into different structures as shown in Figure 4. At point A, the system formed monodisperse vesicles (average aggregation number was 1157±192) and the arrangement of POPC into a vesicular structure was a dynamic process. The formation of one vesicle in the system at point A over time is shown in Figure 5.

We observed that small bicelles (an aggregate that has a flat bilayer-like and curved micelle-like arrangement) that were close to each other merged to form a single large bicelle structure (630 – 650 ns in Figure 5). After the formation of the larger bicelle, it started to distort (700 −720 ns in Figure 5) and changed its shape to a bowl-shaped bicelle (740 −750 ns). This bowl-shaped bicelle further curled up and formed a closed unilamellar vesicle at 760 ns. The diameter measured from the centre of the vesicle to the outer surface of the vesicle is ~13.7 – 14 nm. Also, the analysis of vesicles revealed that the average aggregation number was 1157±192. The maximum and minimum aggregation number for vesicles in the system were 3507 and 924, respectively. With vesicle structures, we also noticed that the system contains bicelles as well. The aggregation number in bicelle structures varies from 866 – 214.

On introduction of bile salt, CHOX to the POPC/water mixture at point A, the system formed a different structure. This structure is a large bilayer that spans the simulation cell. The simulation cell was therefore not large enough for the formation of the relevant colloidal structure at point B. Thus, we conducted an additional simulation (B* simulation in Table 1) using an ~80 nm cubic box. Interestingly, the simulation with a larger simulation cell yielded bicelles. In this system, almost all bile salts in the system are positioned on the surface of bicelle structures and a very small number of bile salts were free to move in water. The aggregation number varied in a wide range, 64 – 1643, with an average of 503.

Further addition of bile salt to the system yielded micelles at point C. The micellar aggregation number varied over a wide range (23-685) with an average of 168 molecules. With the increment of the aggregation number, the micellar shape changed from spherical to worm-like. A small number of bile salt molecules were on the surface of micelles and most of the bile salts were free to move or interact with water.

Point D is on the phase boundary of the vesicle to micelle transition. At this point, the system remained in the micellar phase. The maximum micellar aggregation number was 186 molecules. Similar to the previous system, the micellar shape changed from spherical to wormy-like. The system at point E does not contain POPC. Consistent with the experiment observation at point E, MD simulation formed micelles at that point.

6.4 Discussion

We aimed to introduce bile salts and phospholipids to LBFs and perform MD simulations to investigate the fate of LFs more precisely. As the initial step, we investigated how well the

CG MARTINI model reproduces the aqueous phase behavior of phospholipid/bile salt mixtures. For this purpose, we performed MD simulations in vesicular and micellar regions of experimentally derived POPC/GDX/water ternary phase diagram.

The formation of vesicles at point A is matched experimental observation since point A is in the vesicular region of the experimentally derived phase diagram. Furthermore, the process of vesicle formation through a bicelle revealed that small bicelles merge to obtain an appropriate number of POPC molecules to form a vesicle. One could argue that the phase at point A is not in pure vesicular nature due to the presence of both vesicles and bicelles. However, a longer simulation could change the existence of bicelles and vesicles and reach a phase with only vesicles. The small RMSD value in the average aggregation number at point A confirms that vesicles are monodispersed. The simple molecular model in the CG force field led to the formation of vesicles within ~150 ns simulation time, which cannot be observed within this time scale using all-atom or united-atom models. Interestingly, a previous study using a DPPC (dipalmitoylphosphatidylcholine) and DPPE (dipalmitoylphosphatidylethanolamine) mixture formed a vesicle at 340 K using MARTINI CG models through bicelle formation, similar to the POPC vesicle formation we observed in the system at point A.[48] Even though POPC and DPPC differ slightly in chain length and the degree of saturation, the POPC vehicle diameter measured from the simulation is closer to the minimal size of DPPC unilamellar vesicles (about 20 nm) reported in the literature.[49]

According to the experimental observation, point B is in the vesicular region. However, the initial simulation at point B formed a bilayer that spanned the box, which disappeared with the use of a larger simulation cell. This confirms that artifacts could be introduced due to the size of the simulation box and the periodic boundary conditions that hinder the relevant structure formation. This issue has frequently been reported for colloidal systems using other force fields (i.e., all-atom and united atom).[10, 17, 50-53] The simulation at point B shows that this problem can occur even with CG force fields, where system space is not enough for the relevant structure formation. It is promising that the simulation of a larger box yielded bicelles that could form vesicles upon extension of the simulation following the dynamic behavior we noticed in vesicle formation at point A. Also, we observed that the system at point A formed many vesicular structures within the first 1 μs. However, the presence of POPC with bile salt (simulation at point B) slow-down the process of vesicle formation compared to the system with POPC alone. Furthermore, the bicelle aggregation number is still small compared to

the bicelle aggregation number at point A, which suggests the bicelles at point B are still growing.

According to the experimental phase diagram, point C is in the vesicular region. However, the simulation at point C formed micelles instead of vesicles. This could be due to the different bile salts used here (i.e., glycodeoxycholic acid sodium salt vs cholic acid sodium salt). In detail, glycodeoxycholic acid sodium salt is a bile salt with two OH groups while cholic acid sodium salt is a bile salt with three OH groups. Thus, cholic acid sodium salt is more hydrophilic and better solvated. Therefore, the system with cholic acid sodium salt could more readily form micelles at point C rather than vesicles. At point D, the system remained in the micellar phase. Since point D is experimentally in the micellar region this MD observation is matched with the experimental observation. Interestingly, when POPC and bile salt formed micelles (e.g., points C and D), the shape of the micelle changed from spherical to wormy-like with the increment of aggregation number. To the best of our knowledge, there is no information in the literature regarding the shape of micelles formed when higher bile salt concentrations (15% w/w to 20% w/w) are mixed with POPC (5%-10% w/w). However, a theoretical model developed in the literature by Kozlov and co-workers suggests that mixed micelles formed from phospholipids and bile salts tend to form cylindrical micelles[54], which agrees with the current study. Additionally, a previous experimental investigation also observed the formation of cylindrical micelles at the transition from vesicle to micelles in the cholate-phosphatidylcholine system.[55]

The micellar phase formed in the simulation at point E matches the experimental observation. However, the system at point E could not be analysed with the *find_aggregate* script since the MARTINI CHOX model lacks C beads, which must use with the script.

6.5 Conclusion

In this work, we were interested in introducing phospholipids and bile salts to LBFs to investigate the fate of LBFs more precisely after oral administration. Therefore, we investigated how well the MARTINI CG model reproduces the experimental behavior of POPC/CHOX/water mixtures. We performed MD simulations for different points in micellar and vesicular regions of experimentally derived POPC/GDX/water phase diagram.[5, 10] However, due to the unavailability of CG parameters for GDX on the MARTINI official website, we used cholic acid sodium salt (CHOX) instead, GDX. Our results show that CG MARTINI model MD simulations self-assembled randomly distributed POPC/CHOX/water

molecules into vesicles or micelles depending on the POPC and bile salt composition. Further, the structures reproduced through MD match well with the experimental observation except for a single point (i.e., point C), which could be due to the use of two different bile salts in MD and experiments (cholic acid sodium salt vs glycodeoxycholic acid sodium salt). It is promising that the vesicle formation is observed through a bicelle structure that curls up and formed a closed vesicle, which is in agreement with a previous study in the literature for DPPC and DPPE mixture.[48] Also, the micellar shape we observed with POPC/CHOX/water systems is matched with the micellar shape stated in the literature for phospholipids/bile salt/water mixtures.[54-55] Since none of the studies in the literature systematically investigate the phase behavior of phospholipids, bile salt and water mixtures, the findings in this study provide information covering the unexplored area in the literature. We believe this work provides the confidence to use MARTINI POPC and bile salt models in LBFs to investigate the fate of formulations more precisely after oral administration.

6.6 References

1. Porter, C. J. H.; Trevaskis, N. L.; Charman, W. N., Lipids and Lipid-Based Formulations: Optimizing the Oral Delivery of Lipophilic Drugs. *Nat. Rev. Drug Discov.* **2007,** *6* (3), 231-248.

2. Holm, R.; Müllertz, A.; Mu, H., Bile Salts and Their Importance for Drug Absorption. *Int. J. Pharm.* **2013,** *453* (1), 44-55.

3. Pouton, C. W.; Porter, C. J. H., Formulation of Lipid-Based Delivery Systems for Oral Administration: Materials, Methods and Strategies. *Adv. Drug Deliv. Rev.* **2008,** *60* (6), 625-637.

4. O'Connor, C. J.; Wallace, R. G., Physico-Chemical Behavior of Bile Salts. *Adv. Colloid Interface Sci.* **1985,** *22* (1), 1-111.

5. Birru, W. A.; Warren, D. B.; Ibrahim, A.; Williams, H. D.; Benameur, H.; Porter, C. J. H.; Chalmers, D. K.; Pouton, C. W., Digestion of Phospholipids after Secretion of Bile into the Duodenum Changes the Phase Behavior of Bile Components. *Mol. Pharm.* **2014,** *11* (8), 2825-2834.

6. Yeap, Y. Y.; Trevaskis, N. L.; Porter, C. J. H., Lipid Absorption Triggers Drug Supersaturation at the Intestinal Unstirred Water Layer and Promotes Drug Absorption from Mixed Micelles. *Pharm. Res.* **2013,** *30* (12), 3045-3058.

7. Yeap, Y. Y.; Trevaskis, N. L.; Quach, T.; Tso, P.; Charman, W. N.; Porter, C. J., Intestinal Bile Secretion Promotes Drug Absorption from Lipid Colloidal Phases via Induction of Supersaturation. *Mol. Pharm.* **2013,** *10* (5), 1874-1889.

8. Small, D.; Bourges, M.; Dervichian, D., The Biophysics of Lipidic Associations: I. The Ternary Systems Lecithin-Bile Salt-Water. *Biochim. Biophys. Acta, Lipids Lipid Metab.* **1966,** *125* (3), 563-580.

9. Hernell, O.; Staggers, J. E.; Carey, M. C., Physical-Chemical Behavior of Dietary and Biliary Lipids During Intestinal Digestion and Absorption. 2. Phase Analysis and Aggregation States of Luminal Lipids During Duodenal Fat Digestion in Healthy Adult Human Beings. *Biochemistry* **1990,** *29* (8), 2041-2056.

10. Birru, W. A.; Warren, D. B.; Headey, S. J.; Benameur, H.; Porter, C. J. H.; Pouton, C. W.; Chalmers, D. K., Computational Models of the Gastrointestinal Environment. 1. The Effect of Digestion on the Phase Behavior of Intestinal Fluids. *Mol. Pharm.* **2017,** *14* (3), 566-579.

11. Warren, D. B.; Chalmers, D. K.; Hutchison, K.; Dang, W.; Pouton, C. W., Molecular Dynamics Simulations of Spontaneous Bile Salt Aggregation. *Colloids Surf. A* **2006,** *280* (1), 182-193.

12. Pártay, L. B.; Jedlovszky, P.; Sega, M., Molecular Aggregates in Aqueous Solutions of Bile Acid Salts. Molecular Dynamics Simulation Study. *J. Phys. Chem. B* **2007,** *111* (33), 9886-9896.

13. Turner, D. C.; Yin, F.; Kindt, J. T.; Zhang, H., Molecular Dynamics Simulations of Glycocholate−Oleic Acid Mixed Micelle Assembly. *Langmuir* **2010,** *26* (7), 4687-4692.

14. Nakashima, T.; Iwahashi, K.; Okazaki, S., A Molecular Dynamics Study of Sodium Chenodeoxycholate in an Aqueous Solution. *Chem. Phys. Lett.* **2006,** *420* (4), 489-492.

15. Verde, A. V.; Frenkel, D., Simulation Study of Micelle Formation by Bile Salts. *Soft Matter* **2010,** *6* (16), 3815-3825.

16. Marrink, S. J.; Mark, A. E., Molecular Dynamics Simulations of Mixed Micelles Modeling Human Bile. *Biochemistry* **2002,** *41* (17), 5375-5382.

17. Suys, E. J. A.; Warren, D. B.; Porter, C. J. H.; Benameur, H.; Pouton, C. W.; Chalmers, D. K., Computational Models of the Intestinal Environment. 3. The Impact of Cholesterol Content and pH on Mixed Micelle Colloids. *Mol. Pharm.* **2017,** *14* (11), 3684-3697.

18. Holmboe, M.; Larsson, P.; Anwar, J.; Bergström, C. A. S., Partitioning into Colloidal Structures of Fasted State Intestinal Fluid Studied by Molecular Dynamics Simulations. *Langmuir* **2016,** *32* (48), 12732-12740.

19. Pártay, L. B.; Sega, M.; Jedlovszky, P., Counterion Binding in the Aqueous Solutions of Bile Acid Salts, as Studied by Computer Simulation Methods. *Langmuir* **2008,** *24* (19), 10729-10736.

20. Morrow, B. H.; Koenig, P. H.; Shen, J. K., Atomistic Simulations of pH-Dependent Self-Assembly of Micelle and Bilayer from Fatty Acids. *J. Chem. Phys.* **2012,** *137* (19), 194902.

21. Ngo, V. A.; Kalia, R. K.; Nakano, A.; Vashishta, P., Molecular Mechanism of Flip-Flop in Triple-Layer Oleic-Acid Membrane: Correlation between Oleic Acid and Water. *J. Phys. Chem. B* **2012,** *116* (45), 13416-13423.

22. Cerezo, J.; Zúñiga, J.; Bastida, A.; Requena, A.; Cerón-Carrasco, J. P., Atomistic Molecular Dynamics Simulations of the Interactions of Oleic and 2-Hydroxyoleic Acids with Phosphatidylcholine Bilayers. *J. Phys. Chem. B* **2011,** *115* (40), 11727-11738.

23. Bennett, W. F. D.; Chen, A. W.; Donnini, S.; Groenhof, G.; Tieleman, D. P., Constant pH Simulations with the Coarse-Grained MARTINI Model — Application to Oleic Acid Aggregates. *Can. J. Chem.* **2013,** *91* (9), 839-846.

24. Notman, R.; Noro, M. G.; Anwar, J., Interaction of Oleic Acid with Dipalmitoylphosphatidylcholine (DPPC) Bilayers Simulated by Molecular Dynamics. *J. Phys. Chem. B* **2007,** *111* (44), 12748-12755.

25. King, D. T.; Warren, D. B.; Pouton, C. W.; Chalmers, D. K., Using Molecular Dynamics to Study Liquid Phase Behavior: Simulations of the Ternary Sodium Laurate/Sodium Oleate/Water System. *Langmuir* **2011,** *27* (18), 11381-11393.

26. Knecht, V.; Mark, A. E.; Marrink, S.-J., Phase Behavior of a Phospholipid/Fatty Acid/Water Mixture Studied in Atomic Detail. *J. Am. Chem. Soc.* **2006,** *128* (6), 2030-2034.

27. Janke, J. J.; Bennett, W. F. D.; Tieleman, D. P., Oleic Acid Phase Behavior from Molecular Dynamics Simulations. *Langmuir* **2014,** *30* (35), 10661-10667.

28. Hossain, M. S.; Berg, S.; Bergström, C. A. S.; Larsson, P., Aggregation Behavior of Medium Chain Fatty Acids Studied by Coarse-Grained Molecular Dynamics Simulation. *AAPS PharmSciTech* **2019,** *20* (2), 61.

29. Marrink, S. J.; Mark, A. E., Molecular Dynamics Simulation of the Formation, Structure, and Dynamics of Small Phospholipid Vesicles. *J. Am. Chem. Soc.* **2003,** *125* (49), 15233-15242.

30. Monticelli, L.; Kandasamy, S. K.; Periole, X.; Larson, R. G.; Tieleman, D. P.; Marrink, S.-J., The MARTINI Coarse-Grained Force Field: Extension to Proteins. *J. Chem. Theory Comput.* **2008,** *4* (5), 819-834.

31. Marrink, S. J.; Risselada, H. J.; Yefimov, S.; Tieleman, D. P.; de Vries, A. H., The MARTINI Force Field: Coarse Grained Model for Biomolecular Simulations. *J. Phys. Chem. B* **2007,** *111* (27), 7812-7824.

32. Lopez, C. A., Martini Force Field: Extension To Carbohydrates. *Biophys. J.* **2009,** *96* (3), 405a.

33. Rossi, G.; Monticelli, L.; Puisto, S. R.; Vattulainen, I.; Ala-Nissila, T., Coarse-Graining Polymers with the MARTINI Force-Field: Polystyrene as a Benchmark Case. *Soft Matter* **2011,** *7* (2), 698-708.

34. Shivgan, A. T.; Marzinek, J. K.; Huber, R. G.; Krah, A.; Henchman, R. H.; Matsudaira, P.; Verma, C. S.; Bond, P. J., Extending the Martini Coarse-Grained Forcefield to N-Glycans. *J. Chem. Inf. Model.* **2020**, *60* (8), 3864-3883.

35. Marrink, S. J.; Mark, A. E., The Mechanism of Vesicle Fusion as Revealed by Molecular Dynamics Simulations. *J. Am. Chem. Soc.* **2003,** *125* (37), 11144-11145.

36. Marrink, S. J.; de Vries, A. H.; Mark, A. E., Coarse Grained Model for Semiquantitative Lipid Simulations. *J. Phys. Chem. B* **2004,** *108* (2), 750-760.

37. Marrink, S. J.; Risselada, J.; Mark, A. E., Simulation of Gel Phase Formation and Melting in Lipid Bilayers Using a Coarse Grained Model. *Chem. Phys. Lipids* **2005,** *135* (2), 223-44.

38. Risselada, H. J.; Marrink, S. J., The Molecular Face of Lipid Rafts in Model Membranes. *Proc. Natl. Acad. Sci. U. S. A.* 2**008,** *105* (45), 17367-17372.

39. Nagai, T.; Ueoka, R.; Okamoto, Y., Phase Behavior of a Lipid Bilayer System Studied by a Replica-Exchange Molecular Dynamics Simulation. *J. Phys. Soc. Jpn.* **2012,** *81* (2), 024002.

40. Nagai, T.; Okamoto, Y., Replica-Exchange Molecular Dynamics Simulation of a Lipid Bilayer System with a Coarse-Grained Model. *Mol. Simul.* **2012,** *38* (5), 437-441.

41. Marrink, S. J.; Tieleman, D. P., Perspective on the Martini Model. *Chem. Soc. Rev.* **2013,** *42* (16), 6801-6822.

42. Chalmers, D. K.; Roberts, B. P. Silico: A Perl Molecular Toolkit. http://silico.sourceforge.net.

43. Parrinello, M.; Rahman, A., Polymorphic Transitions in Single Crystals: A New Molecular Dynamics Method. *J. Appl. Phys.* **1981,** *52* (12), 7182-7190.

44. Hess, B.; Bekker, H.; Berendsen, H. J. C.; Fraaije, J. G. E. M., LINCS: A Linear Constraint Solver for Molecular Simulations. *J. Comput. Chem.* **1997,** *18* (12), 1463-1472.

45. Verlet, L., Computer "Experiments" on Classical Fluids. I. Thermodynamical Properties of Lennard-Jones Molecules. *Phys. Rev.* **1967,** *159* (1), 98-103.

46. The PyMOL Molecular Graphics System, Version 1.8 Schrödinger, LLC.

47. Guruge, A. G.; Warren, D. B.; Benameur, H.; Pouton, C. W.; Chalmers, D. K., Aqueous Phase Behavior of the PEO-Containing Non-Ionic Surfactant $C_{12}E_6$: A Molecular Dynamics Simulation Atudy. *J. Colloid Interface Sci.* **2021,** *588*, 257-268.

48. Chng, C.-P., Effect of Simulation Temperature on Phospholipid Bilayer–Vesicle Transition Studied by Coarse-Grained Molecular Dynamics Simulations. *Soft Matter* **2013,** *9* (30), 7294-7301.

49. Cornell, B. A.; Fletcher, G. C.; Middlehurst, J.; Separovic, F., The Lower Limit to the Size of Small Sonicated Phospholipid Vesicles. *Biochim. Biophys. Acta, Biomembranes* **1982,** *690* (1), 15-19.

50. Larsson, P.; Alskär, L. C.; Bergström, C. A. S., Molecular Structuring and Phase Transition of Lipid-Based Formulations upon Water Dispersion: A Coarse-Grained Molecular Dynamics Simulation Approach. *Mol Pharm* **2017,** *14* (12), 4145-4153.

51. Birru, W. A.; Warren, D. B.; Han, S.; Benameur, H.; Porter, C. J. H.; Pouton, C. W.; Chalmers, D. K., Computational Models of the Gastrointestinal Environment. 2. Phase Behavior and Drug Solubilization Capacity of a Type I Lipid-Based Drug Formulation after Digestion. *Mol. Pharm.* **2017,** *14* (3), 580-592.

52. Warren, D. B.; Chalmers, D. K.; Pouton, C. W., Structure and Dynamics of Glyceride Lipid Formulations, with Propylene Glycol and Water. *Mol. Pharm.* **2009,** *6* (2), 604-614.

53. Warren, D. B.; King, D.; Benameur, H.; Pouton, C. W.; Chalmers, D. K., Glyceride Lipid Formulations: Molecular Dynamics Modeling of Phase Behavior During Dispersion and Molecular Interactions Between Drugs and Excipients. *Pharm. Res.* **2013,** *30* (12), 3238-3253.

54. Kozlov, M. M.; Lichtenberg, D.; Andelman, D., Shape of Phospholipid/Surfactant Mixed Micelles: Cylinders or Disks? Theoretical Analysis. *J. Phys. Chem. B* **1997,** *101* (33), 6600-6606.

55. Walter, A.; Vinson, P. K.; Kaplun, A.; Talmon, Y., Intermediate Structures in the Cholate-Phosphatidylcholine Vesicle-Micelle Transition. *Biophys. J.* **1991,** *60* (6), 1315-1325.

Conclusion

The phase behavior and the nature of the colloids formed within a drug formulation after oral administration determines how effectively the formulated drug is dissolved in the gastrointestinal (GI) lumen. However, the complex and dynamic environment in the GI tract hinders studies of lipid-based formulations (LBFs) after the formulation is released from the soft-gelatine capsule. With the advancement of high-performance computers, molecular dynamics (MD) has emerged as a powerful tool that provides atomic information about such complex systems. Information from MD greatly helps us understand the experimental observations. Thus, our aim was to explore how well the MD technique models the phase behavior of LBFs in the GI tract. If MD can model the phase behavior successfully in a range of physiological conditions, the atomic information from the simulations is useful to design and develop efficient LBFs for poorly water soluble drugs. To that end, we systematically conducted several investigations, as described below.

In Chapter 3, we observed that the conventional GROMOS force field failed to reproduce the experimental phase behavior of polyethylene oxide (PEO) molecules. Therefore, we modelled the aqueous phase behavior of $C_{12}E_6$ surfactant in different regions of the phase diagram using two recently released force fields, 2016H66 and $53A6_{DBW}$. The findings of this study give us confidence to select the 2016H66 force field over the $53A6_{DBW}$ force field, since the 2016H66 force field better reproduced the experimental colloidal behavior of $C_{12}E_6$ in many regions of the $C_{12}E_6$/water phase diagram. Furthermore, we also found that the 2016H66 force field has some limitations, since it does not model mesophases accurately (i.e., $C_{12}E_6$ hexagonal phase is more precisely modelled with $53A6_{DBW}$).

Extending the above work, we modelled phase transitions of $C_{12}E_6$ using conventional MD and replica-exchange molecular dynamics (REMD) to test how effectively MD could model phase transitions. Through this investigation, we found that MD with the 2016H66 force field successfully modelled the phase transitions and phase boundaries (since phase transition temperatures were reproduced through REMD). Further, we found that the colloidal structure formation is independent of the MD simulation pathway. Furthermore, we determined that the colloidal structure in the isotropic region above the hexagonal phase as disordered bilayers while the isotropic region above the lamellar phase forms linked porous

layers. Importantly, the studies in Chapter 3 and Chapter 4 together provide confidence to use MD and united atom force field, 2016H66 to model complex PEO surfactants and complex phase behaviors.

In Chapter 5, we investigated the phase behavior of commercialized LBFs for loratadine. To date, this is the first study that systemically investigates LBFs containing PEO non-ionic surfactants since previously, the unavailability of proper force field parameters to model PEO molecules hindered simulating such LBFs. Furthermore, this study was the first investigation to explore a commercialized LBF through the MD technique. This study found that the experimental phase behavior of the LBFs was reproduced successfully with MD. Through this investigation, we developed computational models for excipients Capmul® MCM, Captex® 355 and Kolliphor® RH40 which can be used with future studies in LBFs. Also, we revealed how general phase behavior is affected by changes in excipient type and content. Additionally, MD disclosed microstructural details of colloidal structure formation, which cannot extract through experimental investigations (such as: the drug location within colloids and solvent accessible surface area changes in excipients with the phase structures and degree of the dilution). All this atomic information reveals the factors that affect the changes in phase behavior or microstructural features of the colloids. Therefore, when we design a formulation for a poorly water soluble drug, we can adjust the concentration and nature of the excipients used, to obtain phases that enhance the solubility of the drug upon dispersion and avoid using excipients and compositions that promote drug precipitation.

In the last chapter, we studied how well the MARTINI force field models the phase behavior of phospholipids/bile salt/water mixtures. The study showed that MARTINI coarse-grained models for POPC/cholic acid sodium salt/water mixtures reproduced the experimental phase behavior in micellar and vesicular regions. MD data further revealed that POPC self-assembled into vesicles through bicelle structures. However, MD also revealed that introduce of bile salt, cholic acid sodium salt slows down the self-assembling of vesicles compared to a system with POPC and water.

Since the MARTINI coarse-grained model successfully reproduced the phase behavior of phospholipid/bile salt/water mixtures, future studies can be focused on introducing the bile components to the LBFs. By introducing bile salts and phospholipid species in simulations, we could observe the fate of LBFs after oral administration more precisely in cost effective manner. The atomic information through simulations will greatly help understand more

complex structure formations (i.e., mixed micelles and vesicles) or phase behavior of LBFs. Ultimately, information through MD will assist in designing better LBFs for poorly water-soluble drugs.

APPENDICES

APPENDIX 1

Supporting information for the journal article in Chapter 3

Aqueous Phase Behavior of the PEO-Containing Non-Ionic Surfactant $C_{12}E_6$: A Molecular Dynamics Simulation Study

Amali G. Guruge, Dallas B. Warren, Hassan Benameur, Colin W. Pouton, David K. Chalmers

Additional simulations to test the stability of the hexagonal phase

Methods

We performed two additional MD simulations (Sim1 and Sim2) to test whether the pre-built hexagonal structure we model at point C has reached the proper thermodynamic equilibrium. For Sim1 (Table S5), we increased the temperature of the hexagonal arrangement to 320 K (47 °C) and MD simulation was carried out for 100 ns. Using the final frame of Sim1, the second simulation was done at 298 K (25 °C) for 300 ns. All these simulations used the 2016H66 force field.

Results

We conducted two additional simulations (see Table S3) where we 'thermally shocked' the $C_{H66}{}^{p}$ hexagonal system by heating to 47 °C and running the simulation for 300 ns (Sim 1), followed by cooling the system again to 25 °C and running for another 300 ns (Sim 2). On heating, the surfactant rods became thinner, more wormy and were less closely packed (Figure S4a). On cooling, the structures returned largely to the original state although some interlinks remained between rods (Figure S4b). The potential energy of the new system remained higher than the starting arrangement (Figure S5a). The average potential energy calculated over the last 150 ns at point C started from the pre-built structure (-517910±1688.32 kJ/mol) (simulation $C_{H66}{}^{P}$) and Sim2 (-517509±1692.2 kJ/mol) indicates that the hexagonal arrangement is stabilized by 401 kJ/mol. This shows the that interlinked system is higher in energy than the original and that therefore the original prebuilt arrangement is the more stable arrangement. The SASA for Sim2 and point C simulations starting from the random arrangement and pre-constructed hexagonal phase is shown in Figure S5b. Over the course of Sim2 the surfactant SASA moves towards the value

measured for simulation C_{H66}^{p}, also showing that the pre-built geometry is the more stable arrangement.

Figures

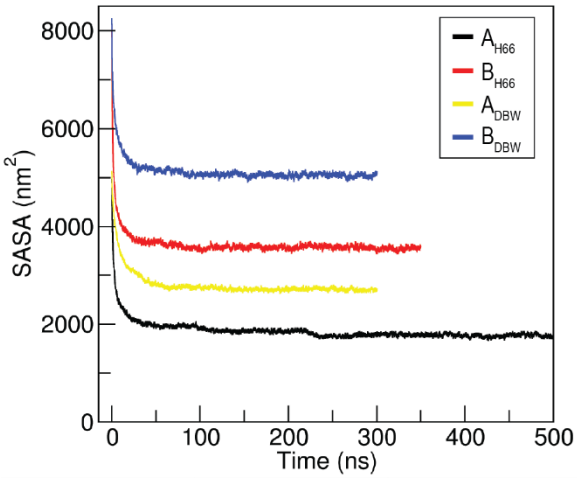

Figure S1 – Solvent accessible surface area (SASA) of $C_{12}E_6$ micelles formed at points A and B with the 2016H66 and 53A6$_{DBW}$ FFs

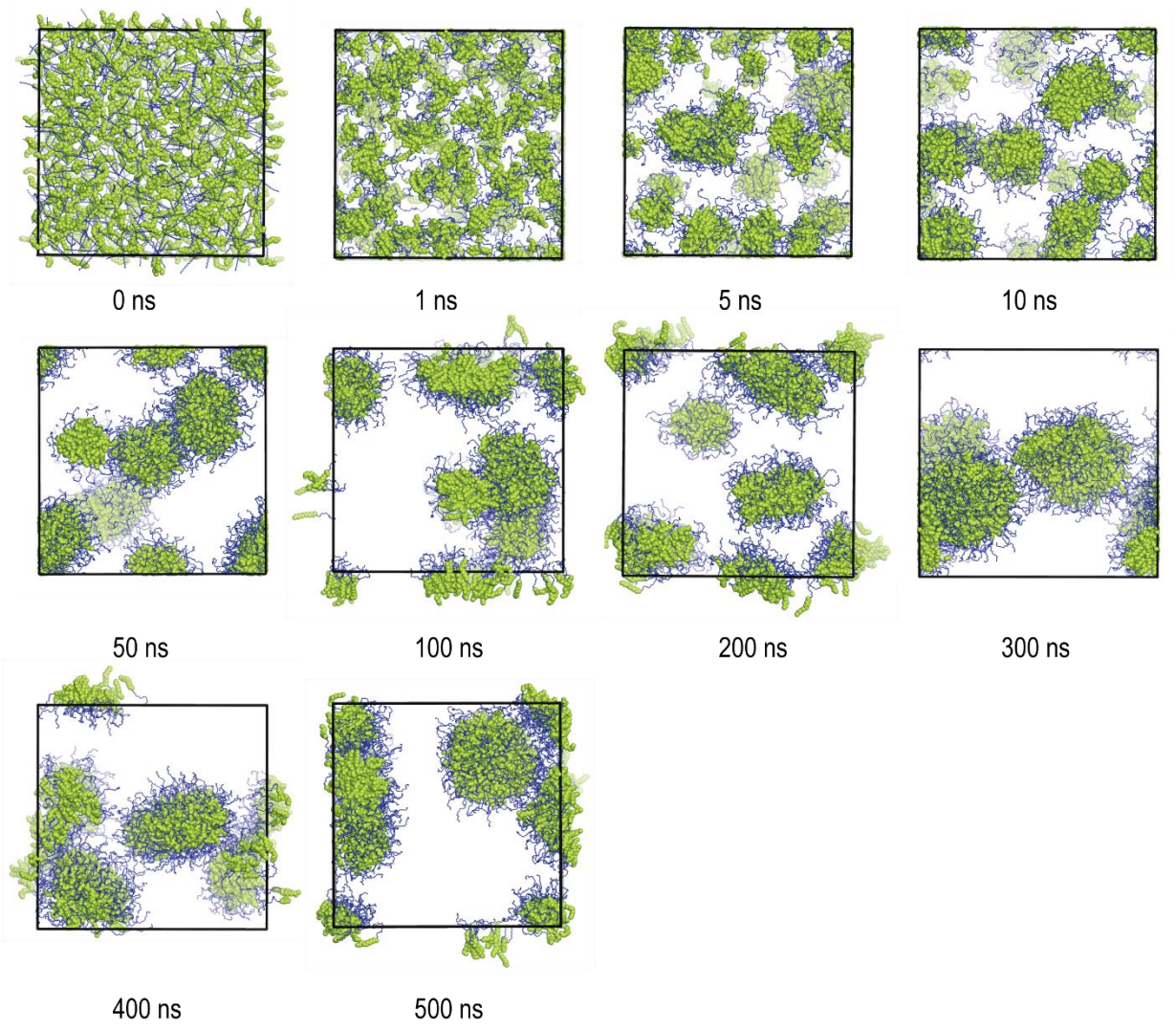

Figure S2 – Formation of micelles in the system A_{H66} over a 500 ns simulation

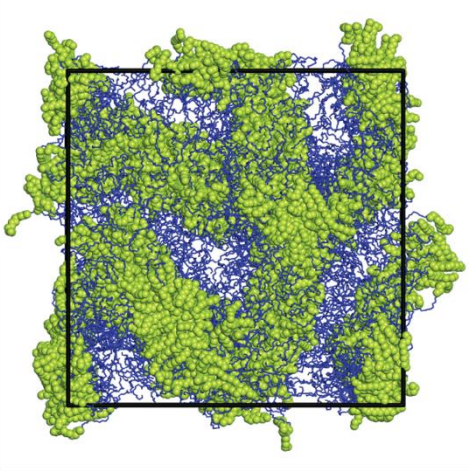

Figure S3 – Colloidal structure at point C from the random distribution with 13×13×11 nm box. We have another simulation at point C starting with random distribution with simulation box size 15×15×15 nm. This structure contains rod-like micelles and consistent with the simulation at point C with a 15×15×15 nm box.

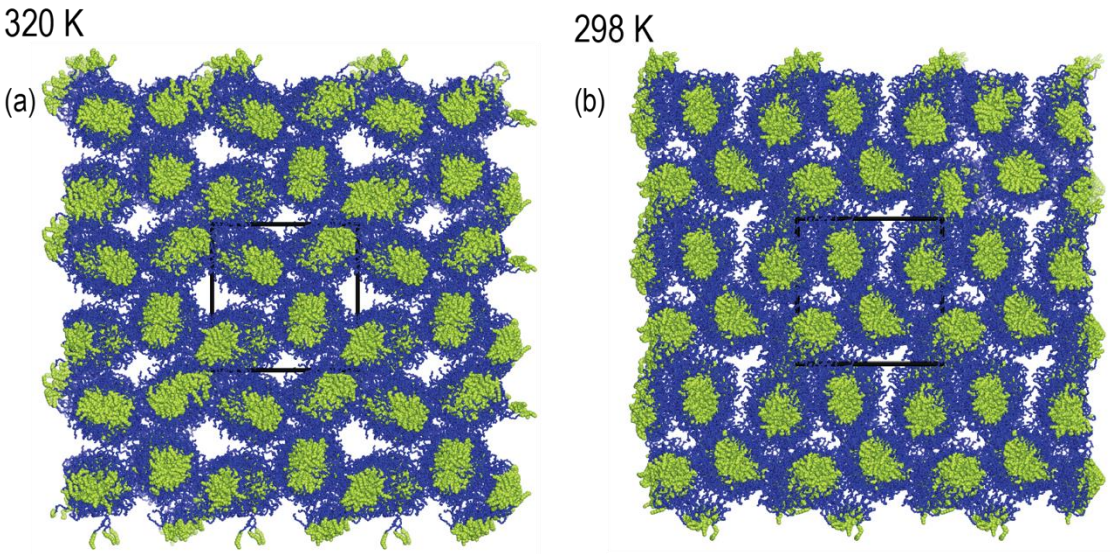

Figure S4 – Colloidal structure at point C from the final obtained from successive 300 ns simulations at 320K (Sim1, left) and 298K (Sim2, right). Simulations used the 2016H66 force field. Sim1 commenced from the final frame of simulation $C_{H66}{}^{p}$. These simulations show that the pre-built hexagonal phase is a stable, low energy structure.

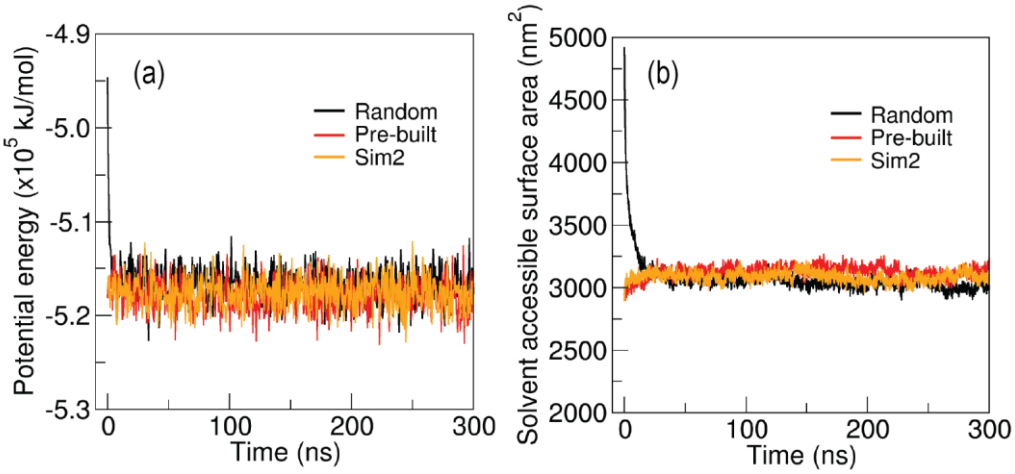

Figure S5 – Plots showing (a) the energy and (b) the SASA of Sim2 compared to systems with the same molecular compositions started from pre-built (simulation C_{H66}^{p}) and random (simulation C_{H66}) arrangements of surfactants.

Tables

Table S1– Coefficient of variation of the solvent accessible surface area (SASA) for the last 100 ns of equilibrated micelle systems

System	SASA coefficient of variation
A_{H66}	1.79
B_{H66}	1.07
A_{DBW}	0.97
B_{DBW}	0.76

Table S2– Radius of gyration (R_g), moments of inertia along principal axes (I_1/I_2, I_1/I_3 and I_2/I_3) and eccentricity (ε) calculated for micelles formed with the 2016H66 and 53A6$_{DBW}$ force fields.

System	Agg. no.	R_g (nm)	I_1/I_3	I_1/I_2	I_2/I_3	ε
A_{H66}	280	3.66±0.09	0.36±0.03	0.38±0.03	0.94±0.09	0.53±0.07
	200	2.93±0.02	0.70±0.03	0.88±0.04	0.80±0.04	0.16±0.01
	189	2.87±0.01	0.69±0.03	0.86±0.05	0.80±0.04	0.17±0.01
B_{H66}	571	6.93±0.10	0.10±0.00	0.11±0.00	0.98±0.04	0.85±0.06
	226	3.08±0.02	0.61±0.02	0.72±0.03	0.85±0.04	0.26±0.02
	156	2.68±0.02	0.71±0.03	0.84±0.03	0.84±0.03	0.17±0.01
	145	2.59±0.01	0.77±0.03	0.90±0.04	0.86±0.04	0.12±0.01
	139	2.58±0.02	0.73±0.04	0.82±0.04	0.90±0.05	0.16±0.01
	107	2.35±0.01	0.82±0.03	0.90±0.03	0.91±0.04	0.10±0.01
A_{DBW}	95	2.38±0.02	0.81±0.04	0.88±0.04	0.92±0.04	0.11±0.01
	88	2.33±0.02	0.85±0.03	0.93±0.03	0.92±0.04	0.08±0.00
	82	2.28±0.02	0.81±0.03	0.88±0.04	0.92±0.04	0.11±0.01
	78	2.27±0.02	0.82±0.05	0.89±0.05	0.92±0.06	0.10±0.01
	60	2.15±0.02	0.83±0.04	0.90±0.05	0.92±0.05	0.10±0.01
	55	2.07±0.03	0.82±0.05	0.89±0.05	0.92±0.06	0.10±0.01
	50	2.02±0.03	0.81±0.06	0.87±0.06	0.93±0.06	0.12±0.01
	48	1.97±0.02	0.83±0.05	0.90±0.05	0.92±0.05	0.10±0.01
	44	1.93±0.03	0.83±0.05	0.90±0.05	0.92±0.05	0.10±0.01
	40	1.89±0.03	0.83±0.05	0.90±0.06	0.92±0.06	0.10±0.01
B_{DBW}	122	2.55±0.02	0.76±0.05	0.84±0.06	0.91±0.06	0.14±0.01
	121	2.53±0.02	0.81±0.03	0.91±0.03	0.90±0.03	0.10±0.01
	114	2.51±0.01	0.80±0.03	0.90±0.03	0.89±0.03	0.11±0.01
	106	2.46±0.03	0.74±0.05	0.81±0.05	0.91±0.06	0.16±0.02
	96	2.37±0.01	0.82±0.04	0.90±0.04	0.91±0.04	0.10±0.01
	92	2.34±0.02	0.81±0.04	0.89±0.03	0.91±0.04	0.11±0.01
	85	2.31±0.02	0.80±0.04	0.87±0.04	0.92±0.05	0.12±0.01
	83	2.29±0.02	0.81±0.03	0.88±0.04	0.92±0.04	0.11±0.01
	79	2.26±0.02	0.82±0.04	0.90±0.05	0.91±0.04	0.10±0.01
	70	2.21±0.02	0.80±0.04	0.85±0.04	0.94±0.04	0.13±0.01
	68	2.16±0.03	0.84±0.05	0.89±0.06	0.95±0.06	0.10±0.01
	58	2.08±0.02	0.82±0.04	0.89±0.04	0.92±0.04	0.10±0.01
	52	1.98±0.02	0.83±0.05	0.90±0.05	0.93±0.05	0.09±0.01
	51	1.98±0.02	0.79±0.05	0.86±0.05	0.92±0.05	0.13±0.01
	51	1.97±0.02	0.81±0.05	0.89±0.05	0.90±0.05	0.11±0.01
	47	1.93±0.02	0.84±0.05	0.91±0.05	0.92±0.05	0.09±0.01
	43	1.90±0.02	0.78±0.05	0.88±0.05	0.88±0.06	0.12±0.01

Table S4 – Difference in the potential energy of simulations over time at point C started from a random distribution (simulation C_{H66}^{*}) or from a pre-built structure (simulation C_{H66}^{P}). Ensemble average is calculated over the last half of the 300 ns simulations. The standard deviation is calculated using block averages (10 x 150 ns blocks).

	Difference in total energy (kJ/mol)	**Energy difference per $C_{12}E_6$ molecule (kJ/mol)**
< PE(sim C_{H66}^{P}) - PE(sim C_{H66}^{*}) >	-1122	-0.84
Block av. standard deviation	199	0.15

Table S5 – Investigation of the stability of the pre-built hexagonal phase using the 2016H66 force field. Sim1 (300 ns) started from the final frame of C_{H66}^{P}. Sim2 was returned to the lower temperature and was also run for 300 ns.

System	**N_{surf}**	**N_{water}**	**w/w % $C_{12}E_6$**	**T (°C)**	**Approx cell size (nm)**	**Pcoupl**	**t_{sim} (ns)**	**Colloidal structure in**	
								MD simulation	**Experiment**
Sim1	1340	33511	50	47	12×12×14	SI	100	less-ordered cylindrical micelles with some interconnections	disordered bilayers or branched interconnected cylindrical micelles[1]
Sim2	1340	33511	50	25			300	cylindrical micelles with some interconnections	hexagonally packed cylindrical micelles[2]

References

1. Sallen, L.; Sotta, P.; Oswald, P., Pretransitional Effects Near the Hexagonal−Micellar Phase Transition of the $C_{12}EO_6/H_2O$ Lyotropic Mixture. *J. Phys. Chem. B* **1997,** *101* (25), 4875-4881.

2. Mitchell, D. J.; Tiddy, G. J. T.; Waring, L.; Bostock, T.; McDonald, M. P., Phase Behavior of Polyoxyethylene Surfactants with Water. Mesophase Structures and Partial Miscibility (Cloud Points). J. Chem. Soc., Faraday Trans. 1 **1983**, 79 (4), 975-1000.

APPENDIX 2

Supporting information for the manuscript in Chapter 4

Modelling the Liquid Phase Transitions of Polyethyleneoxide Surfactant ($C_{12}E_6$)/Water Systems Using Conventional and Replica Exchange Molecular Dynamics Simulations

Amali G. Guruge, Dallas B. Warren, Leigh Ford, Hywel D. Williams, Vincent Janin, Hassan Benameur, Colin W. Pouton, David K. Chalmers

Tables

Table S1 – Temperatures and exchange probabilities in three REMD simulations

Phase transition	**Temperatures (K) in REMD**	**Exchange probabilities**
Hexagonal to isotropic phase (C to H)	298.00, 298.83, 299.66, 300.50, 301.33, 302.17, 303.01, 303.85, 304.69, 305.54, 306.39, 307.24, 308.09, 308.94, 309.80, 310.65, 311.51, 312.37, 313.23, 314.10, 314.96, 315.83, 316.70, 317.58, 318.45, 319.33, 320.21, 321.09, 321.97, 322.85, 323.74, 324.63, 325.52, 326.41, 327.30, 328.20, 329.09, 329.99, 330.90, 331.80, 332.71, 333.61.	0.19, 0.18, 0.19, 0.21, 0.21, 0.19, 0.16, 0.12, 0.19, 0.19, 0.17, 0.23, 0.28, 0.15, 0.19, 0.20, 0.23, 0.21, 0.17, 0.22, 0.22, 0.18, 0.14, 0.15, 0.22, 0.20, 0.21, 0.21, 0.19, 0.17, 0.17, 0.17, 0.22, 0.23, 0.16, 0.19, 0.26, 0.16, 0.17, 0.21, 0.18
Lamellar to isotropic phase (E to G)	323.00, 324.27, 325.55, 326.83, 328.11, 329.40, 330.69, 331.98, 333.28, 334.59, 335.90, 337.21, 338.52, 339.84, 341.17, 342.50, 343.83, 345.17, 346.51, 347.85, 349.21, 350.56, 351.92, 353.28, 354.65, 356.02, 357.40, 358.78, 360.16, 361.55, 362.94 and 364.35.	0.16, 0.16, 0.18, 0.17, 0.17, 0.18, 0.17, 0.18, 0.17, 0.18, 0.18, 0.18, 0.18, 0.18, 0.17, 0.18, 0.18, 0.18, 0.18, 0.17, 0.17, 0.18, 0.18, 0.18, 0.17, 0.17, 0.18, 0.18, 0.18, 0.18, 0.18, 0.18
Lamellar to lamellar boundary (D to F)	298.00, 299.19, 300.39, 301.59, 302.80, 304.01, 305.22, 306.43, 307.64, 308.86, 310.08, 311.31, 312.55, 313.78, 315.02, 316.27, 317.39, 318.64, 319.90, 321.16, 322.42, 323.69, 324.96, 326.24, 327.52, 328.80, 330.09, 331.39, 332.69, 333.99, 335.29, 336.60, 337.92, 339.24	0.16, 0.18, 0.16, 0.17, 0.15, 0.13, 0.15, 0.18, 0.17, 0.16, 0.16, 0.16, 0.18, 0.18, 0.16, 0.23, 0.16, 0.19, 0.15, 0.18, 0.15, 0.19, 0.20, 0.17, 0.19, 0.15, 0.16, 0.18, 0.16, 0.16, 0.17, 0.19, 0.18

Figures

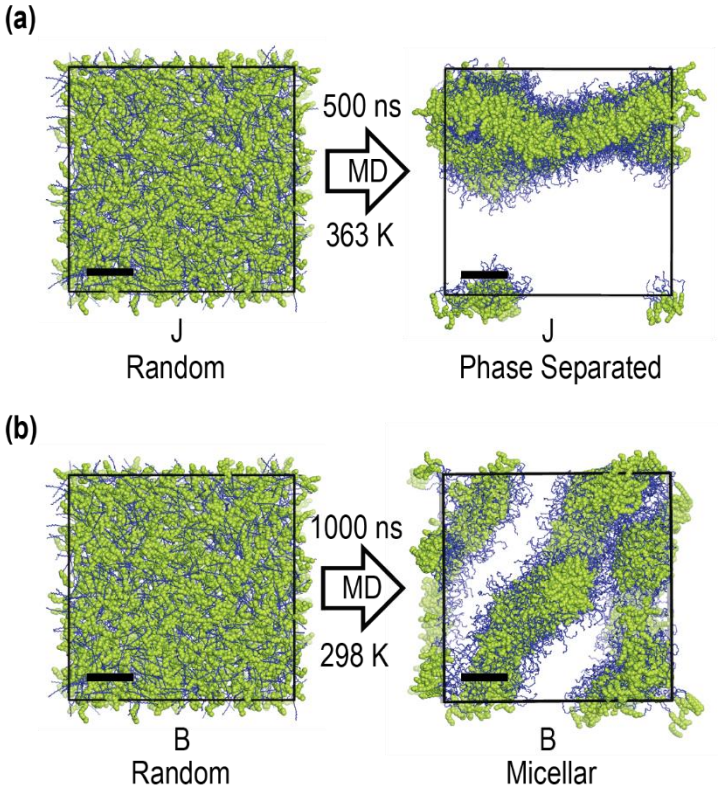

Figure S1 – Final frames of the point J and B. (a) Simulation at point J starting from the random distribution. (b) Simulation at point B starting from the random distribution.

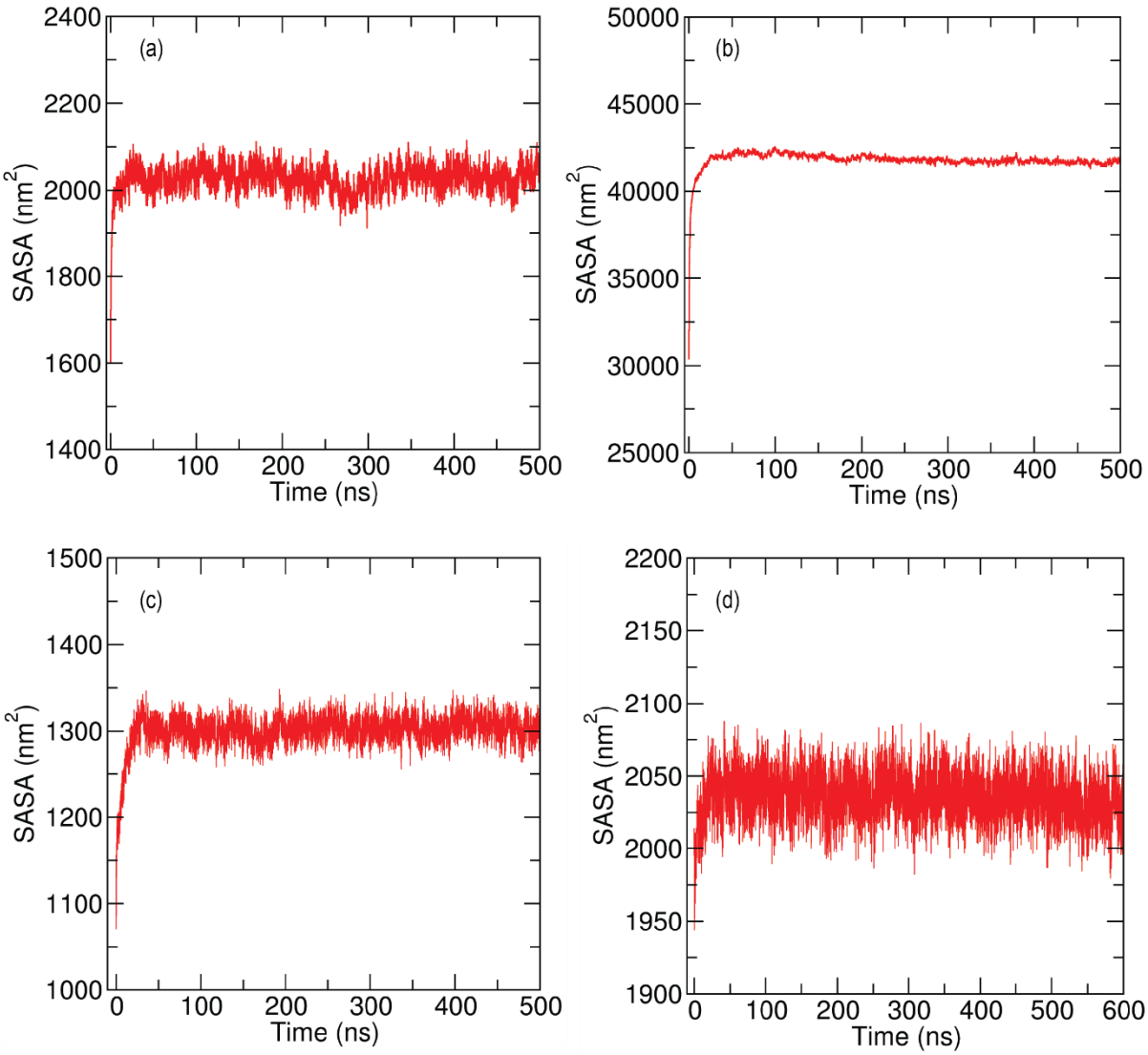

Figure S2 – (a) - SASA calculated for $C_{12}E_6$ molecules in the phase transition MD simulation carried out from micellar to hexagonal (point A to point C), (b) – SASA calculated for $C_{12}E_6$ molecules in the phase transition MD simulation carried out from micellar to hexagonal (point B to point C), (c) - SASA calculated for $C_{12}E_6$ molecules in the phase transition MD simulation carried out from micellar to lamellar (point A to point D), (d) - SASA calculated for $C_{12}E_6$ molecules in the phase transition MD simulation from hexagonal to lamellar (point C to point D)

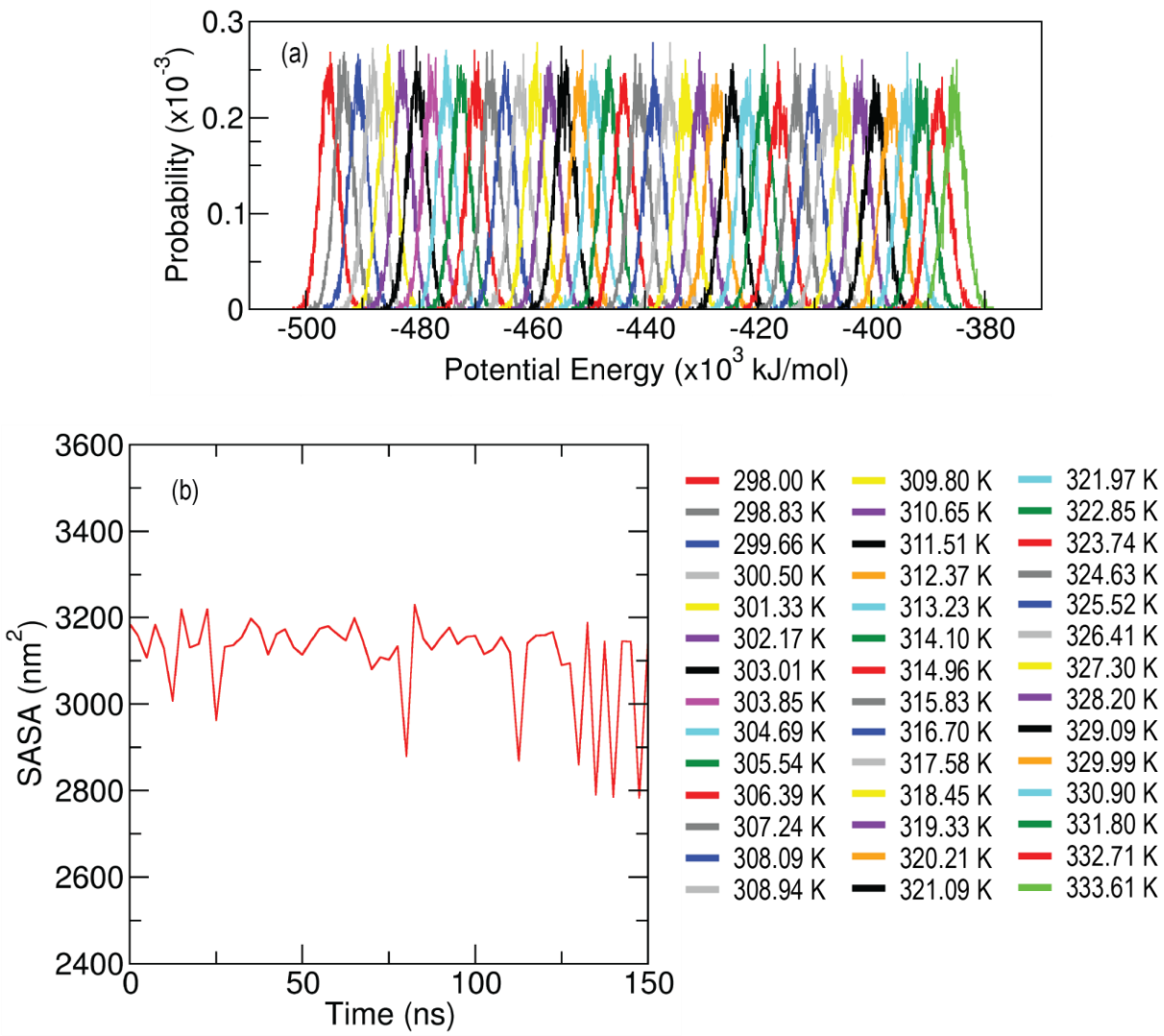

Figure S3 – (a) - Potential energy probability distributions for 42 temperatures in the phase transition from hexagonal to isotropic phase (point C to point H) carried out with REMD, (b) - Solvent accessible surface area (SASA) calculated for $C_{12}E_6$ molecules in the colloidal system formed at point H (333.61 K)

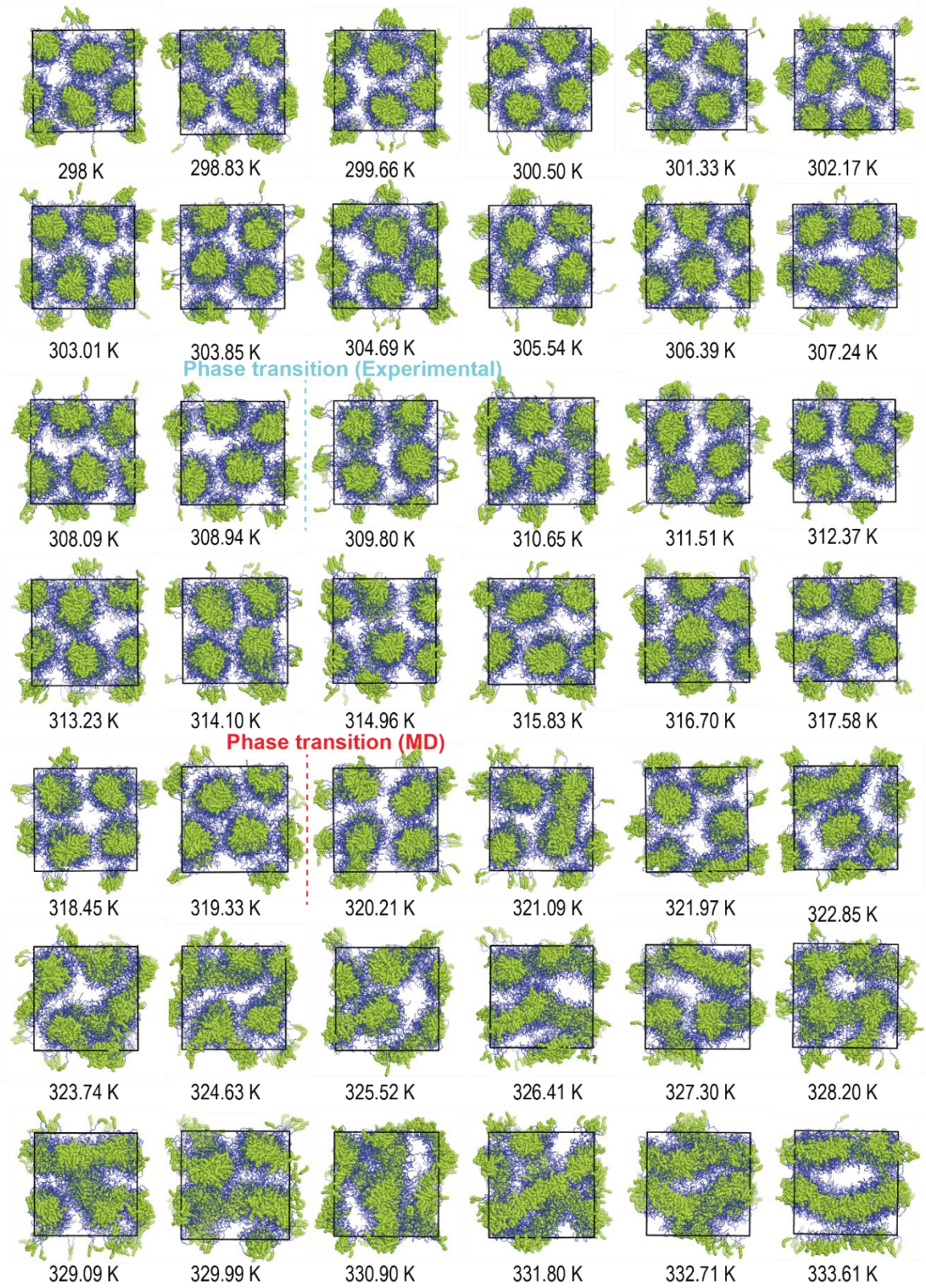

Figure S4 – Colloidal structures formed in REMD simulation of the phase transition from hexagonal to the isotropic region (point C to point H), Red colour dash line represents the phase transition boundary with respect to the colloidal structure formed in the REMD simulation, Blue colour dash line represents the experimental phase transition boundary, Surfactant coloring: alkane tail (lime), PEO head group (blue). Water is not shown for clarity.

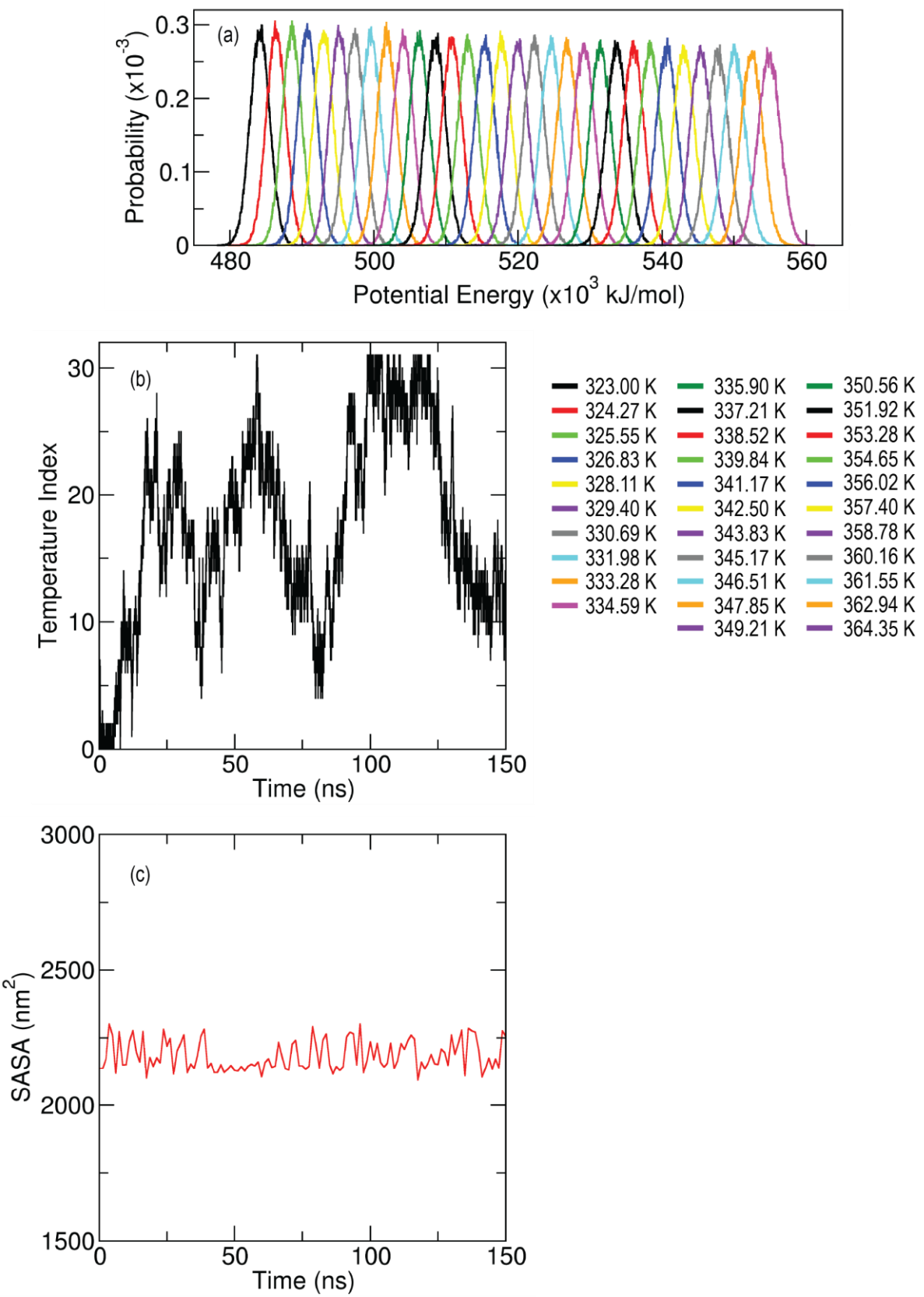

Figure S5 – (a) – Potential energy probability distributions for 32 temperatures in the phase transition from lamellar to isotropic phase (point E to point G), (b) – Random walk of the replica R_0 (323 K) in the temperature space, (c) – Solvent accessible surface area (SASA) for $C_{12}E_6$ surfactants in the colloidal structure at point G.

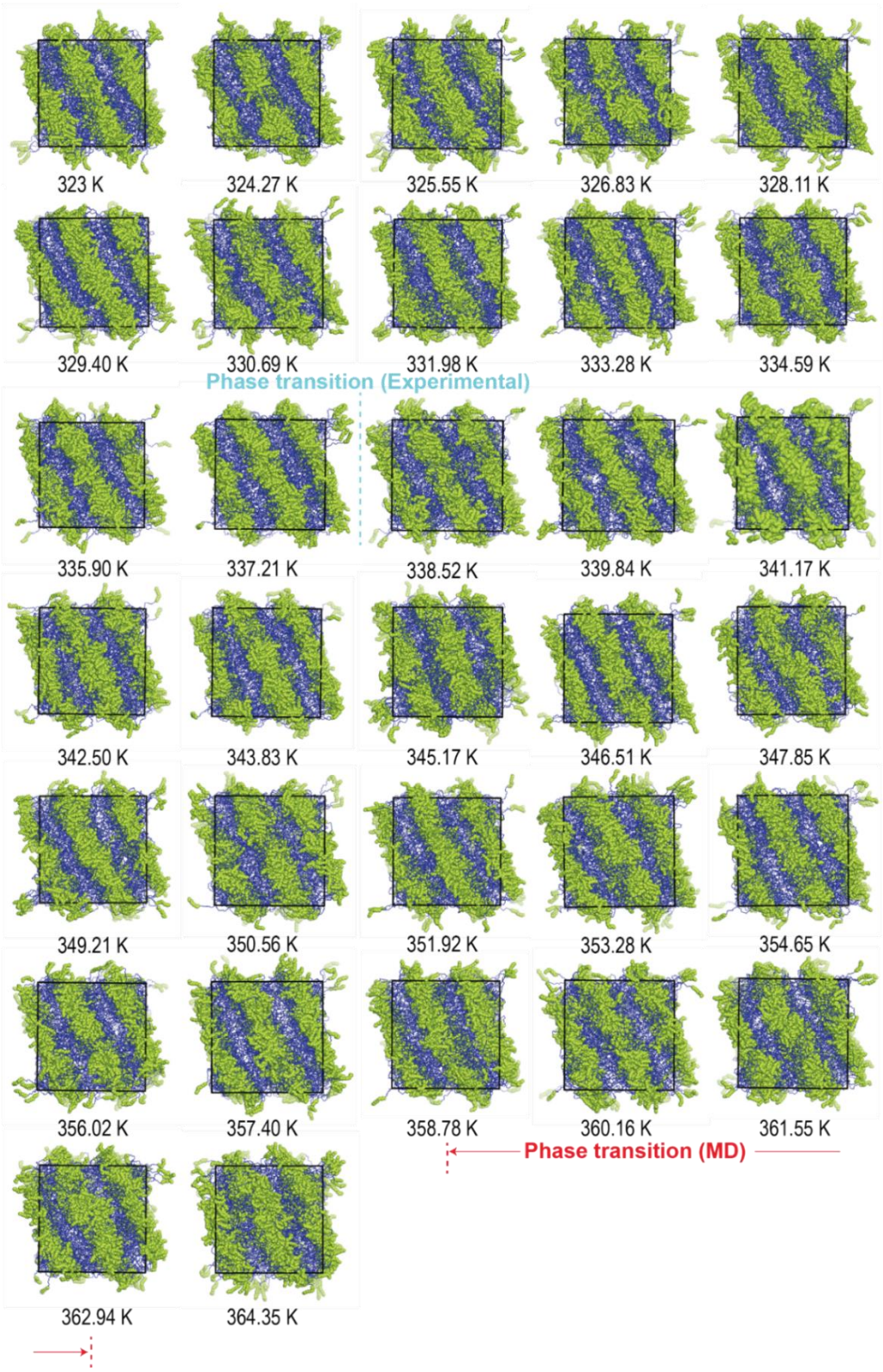

Figure S6 – Colloidal structures formed in the phase transition from lamellar to isotropic phase (point E to point G), Red colour dash line represents the phase transition boundary with respect to the colloidal structure formed in the REMD simulation, Blue colour dash line represents the experimental phase transition boundary, Surfactant coloring: alkane tail (lime), PEO head group (blue). Water is not shown for clarity.

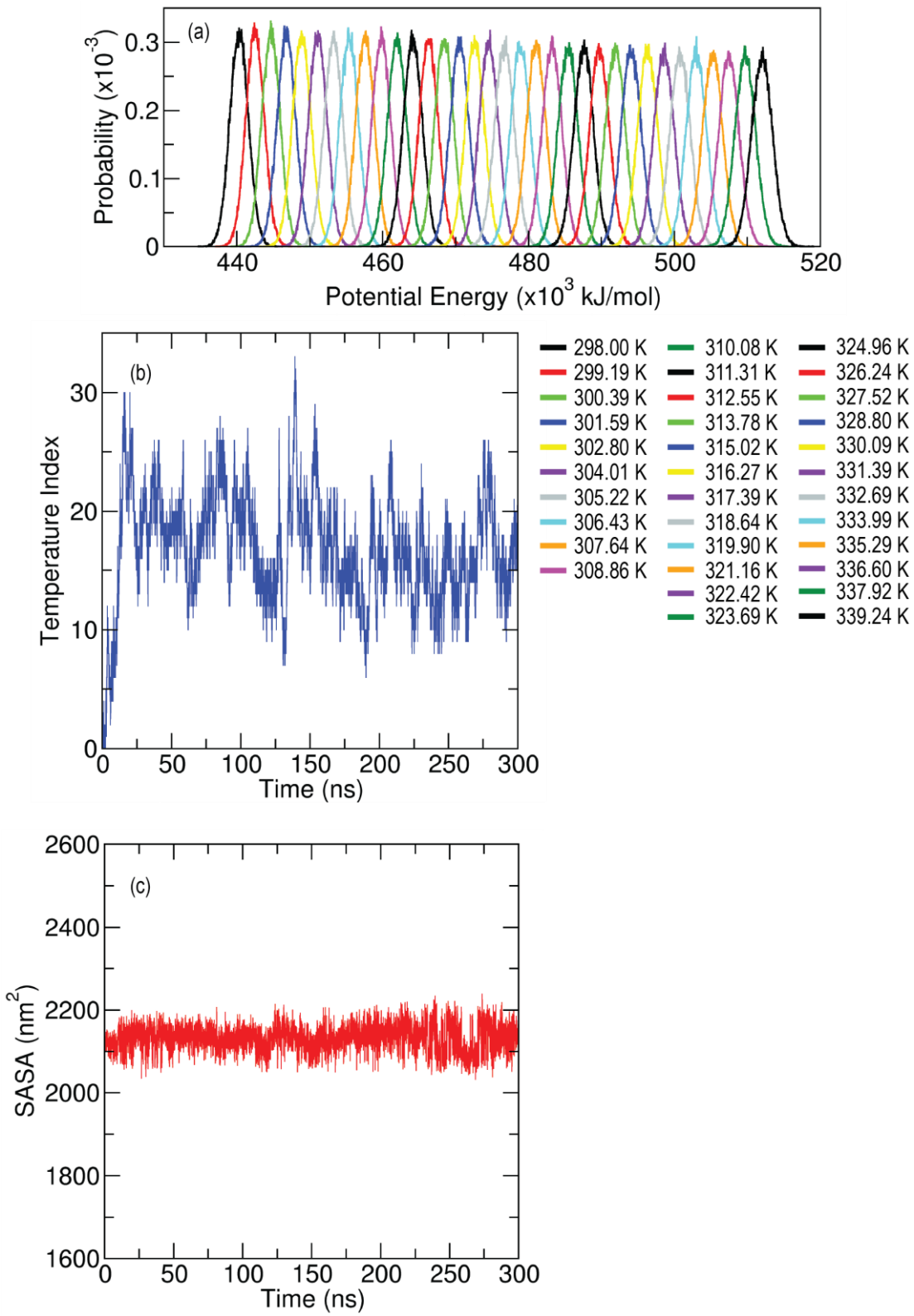

Figure S7 – (a) – Potential energy probability distributions for 34 temperatures in the lamellar region (D to F) REMD simulation, (b) – Random walk of the temperature of replica R_3 (301.59 K) in the temperature space, (c) - SASA for $C_{12}E_6$ molecules in the 298 K system in the REMD simulation.

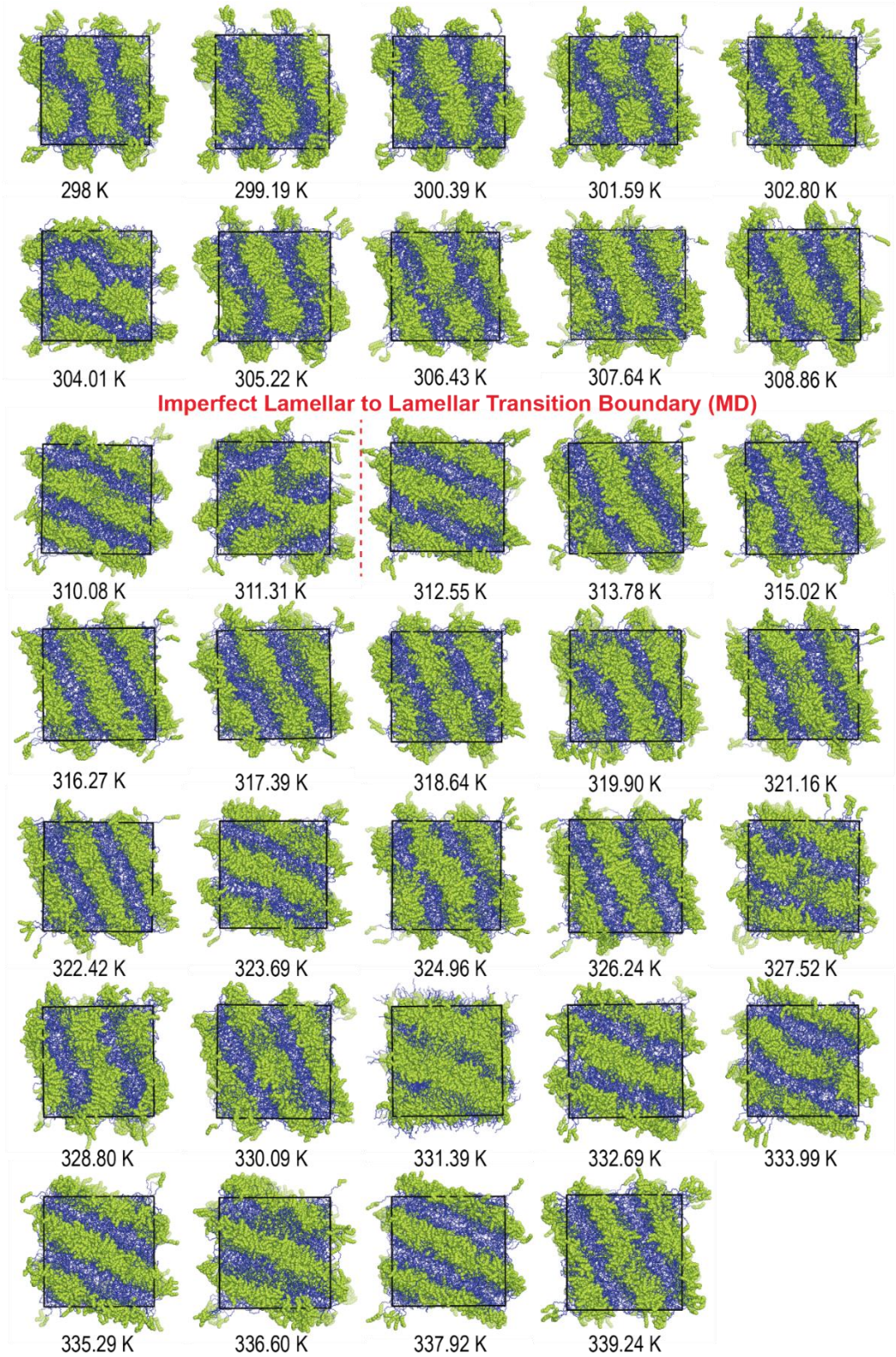

Figure S8 – Colloidal structures formed in replica exchange molecular dynamics (REMD) simulation in the lamellar region (D to F), Red colour dash line represents the imperfect lamellar to the lamellar boundary with respect to the colloidal structure formed in the REMD simulation, Surfactant coloring: alkane tail (lime), PEO head group (blue). Water is not shown for clarity.

APPENDIX 3

Supporting information for the manuscript in Chapter 5

The Colloidal Phase Behavior of Lipid-Based Formulations of Loratadine, Including Claritin®, upon Water Dispersion and Dilution: A Molecular Dynamics and Experimental Study

Amali G. Guruge, Dallas B. Warren, Hassan Benameur, Leigh Ford, Hywel D. Williams, *Vincent Jannin*, *Colin W. Pouton, David K. Chalmers*

Figures

Figure S1 – (a), (b) Liqui-gel capsules purchased from the market, (c) Inactive ingredients mentioned in the purchased Claritin® liqui gels.

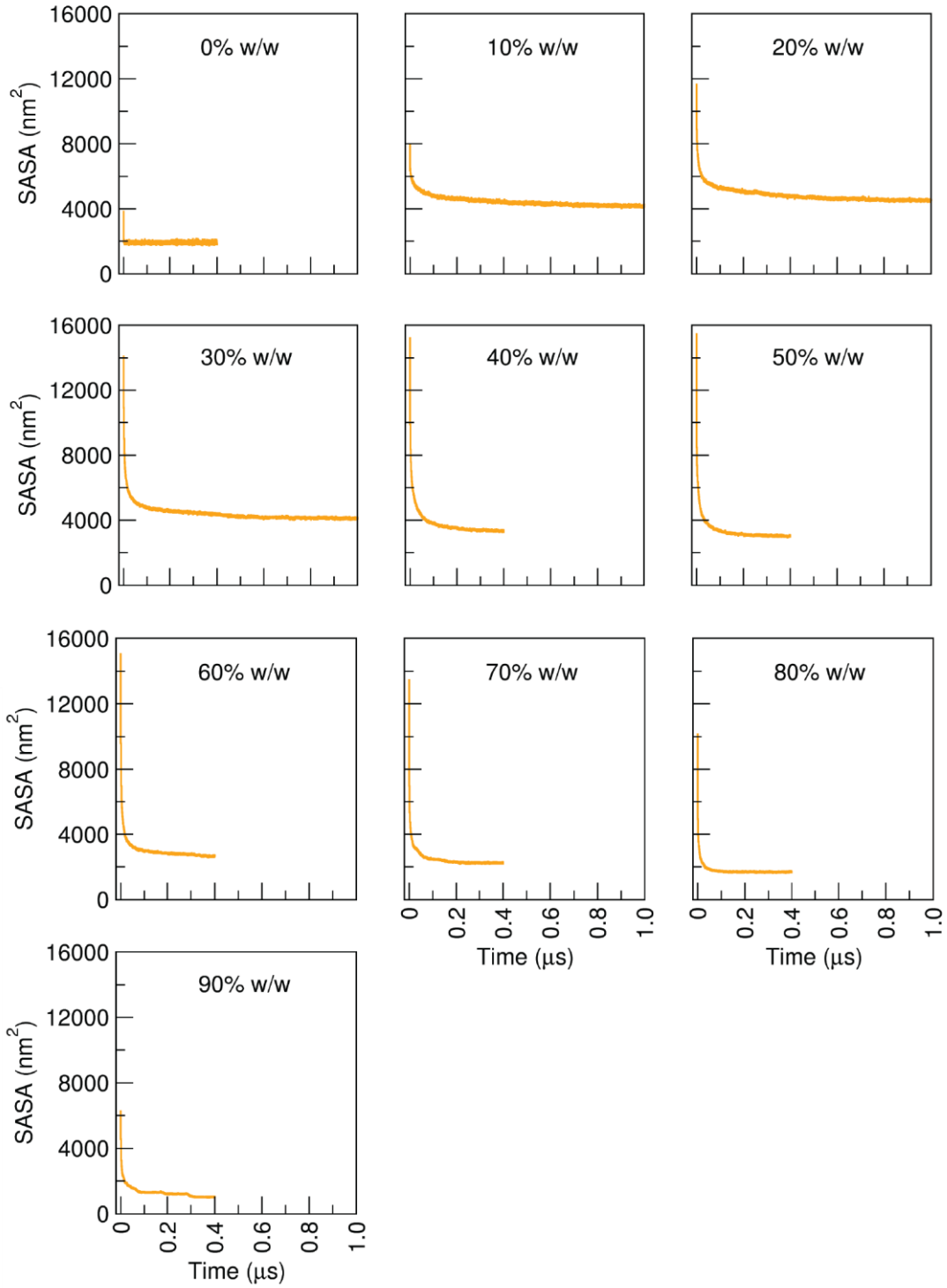

Figure S2 – Solvent accessible surface area (SASA) for non-water components in 0% w/w to 90% w/w added water systems in **F1** formulation.

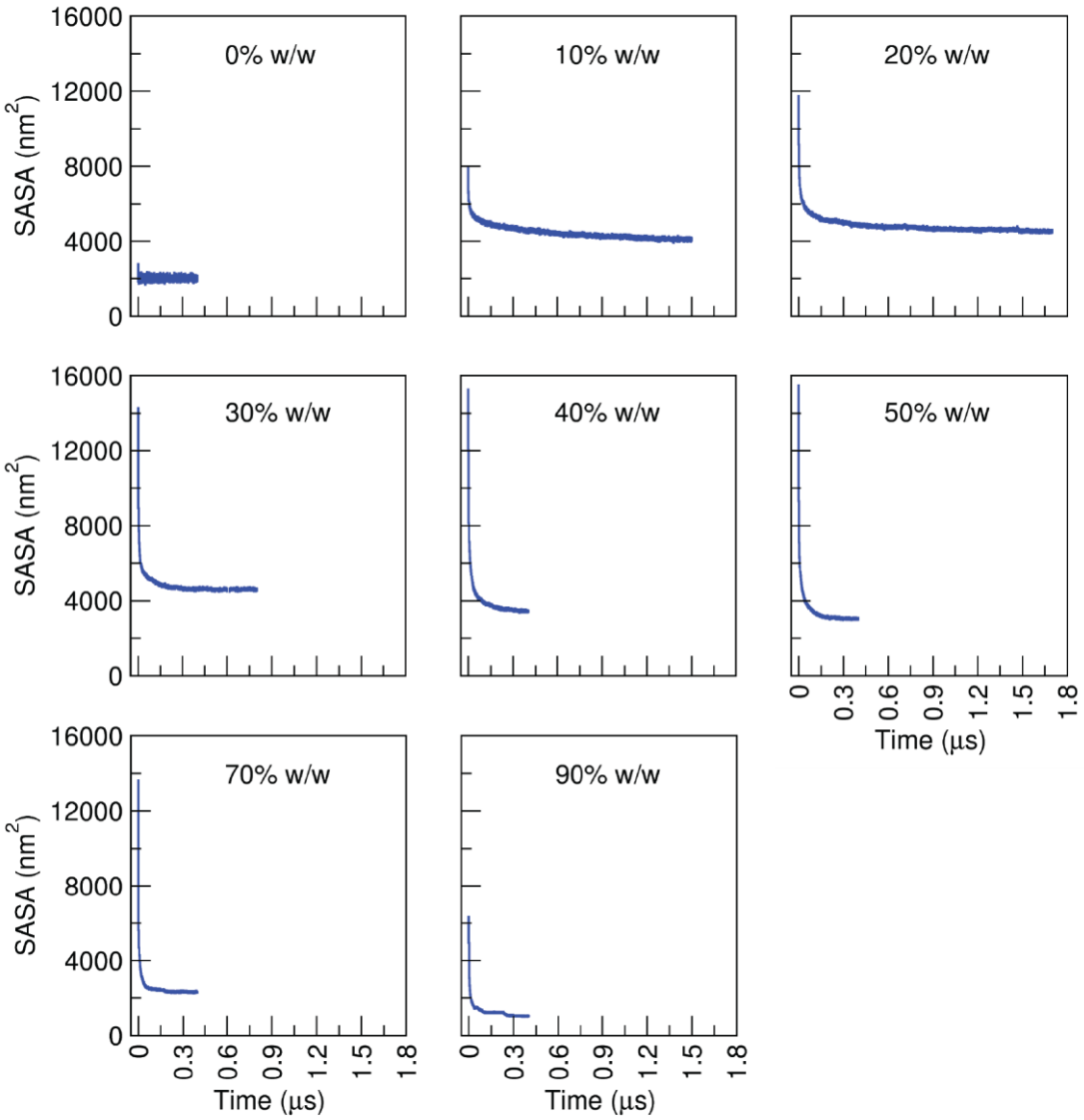

Figure S3 – Solvent accessible surface area (SASA) for non-water components in 0% w/w to 90% w/w added water systems in **F2** formulation.

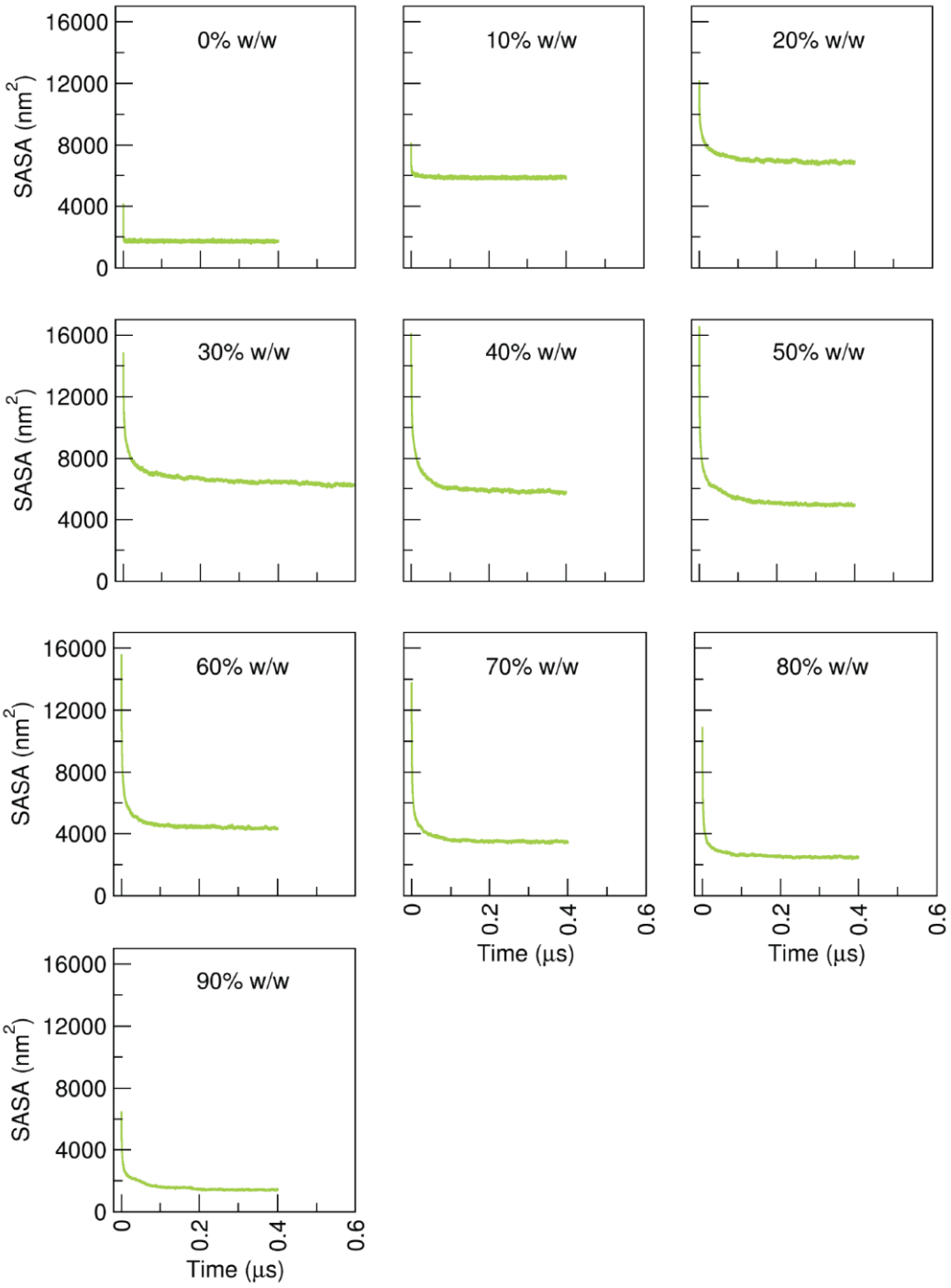

Figure S4 – Solvent accessible surface area (SASA) for non-water components in 0% w/w to 90% w/w added water systems in **F3** formulation.

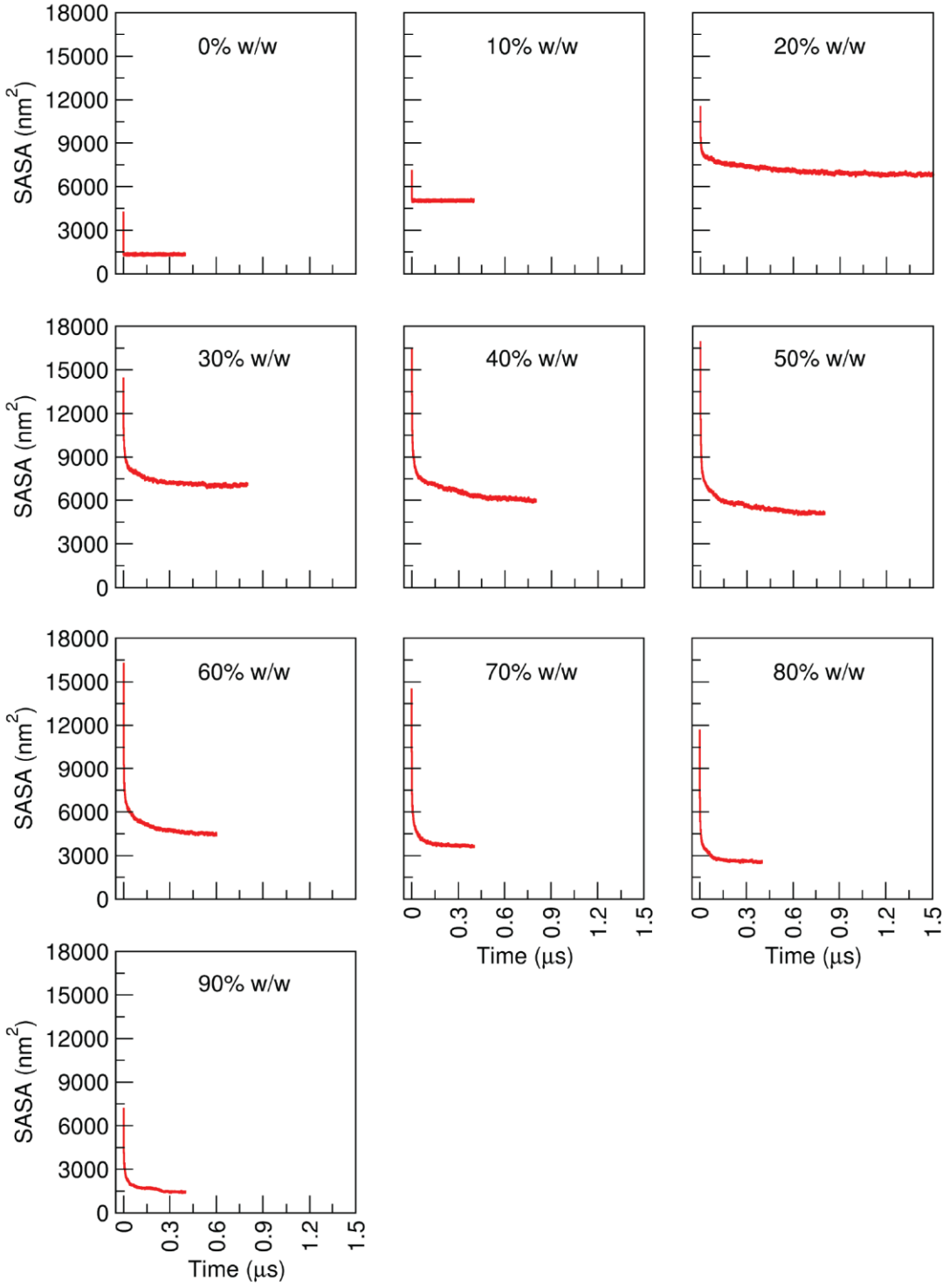

Figure S5 – Solvent accessible surface area (SASA) for non-water components in 0% w/w to 90% w/w added water systems in **F4** formulation.

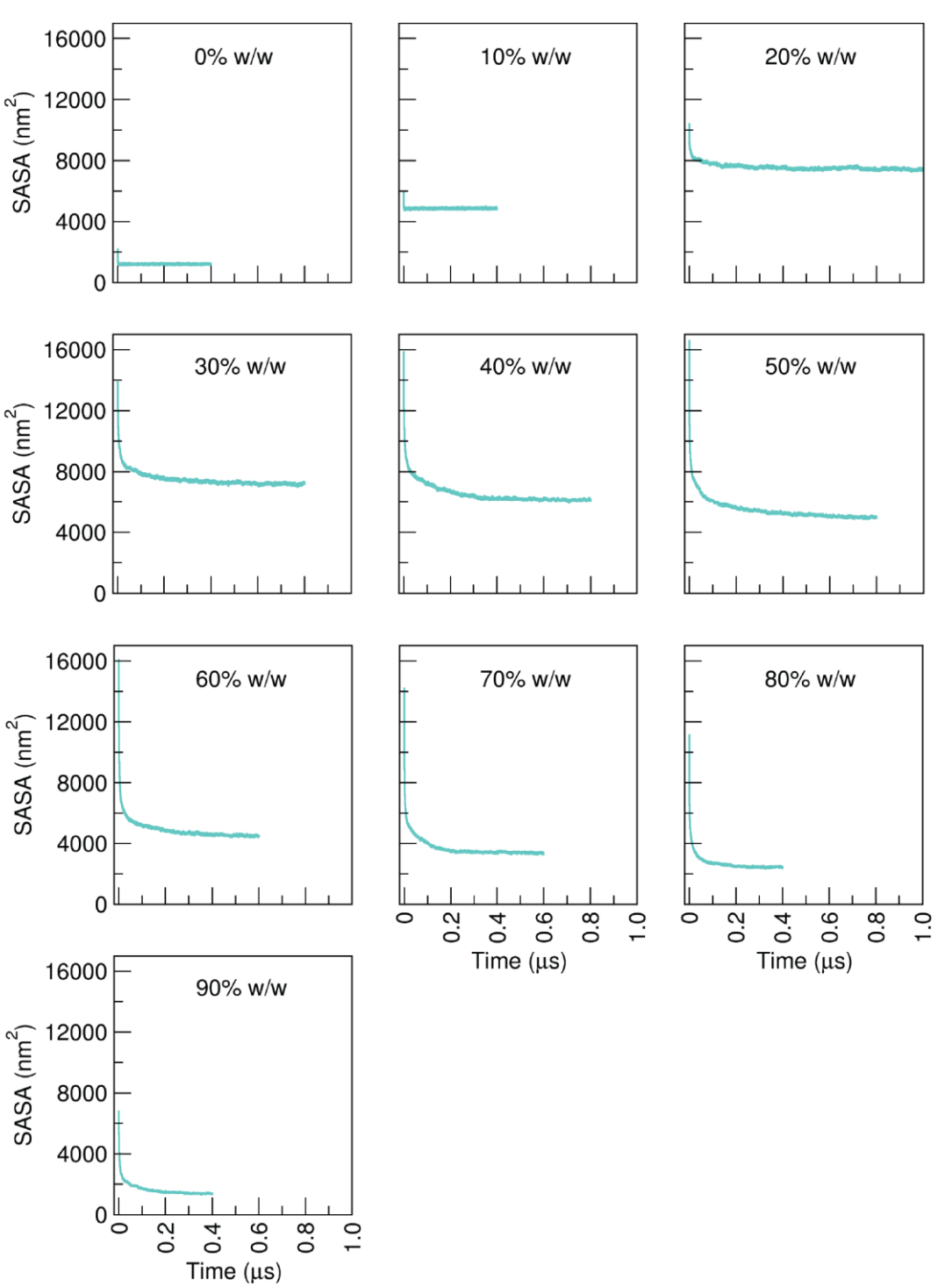

Figure S6 – Solvent accessible surface area (SASA) for non-water components in 0% w/w to 90% w/w added water systems in **F5** formulation.

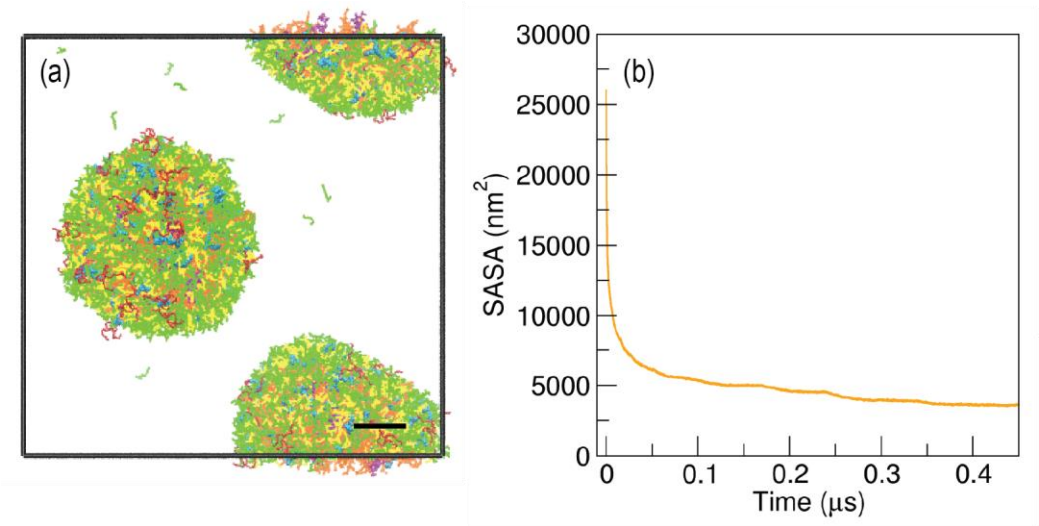

Figure S7 – (a) Colloidal structure formed in 90% w/w water with **F1**. (b) SASA for non-water component in the same system. The scale bar length is 4.0 nm.

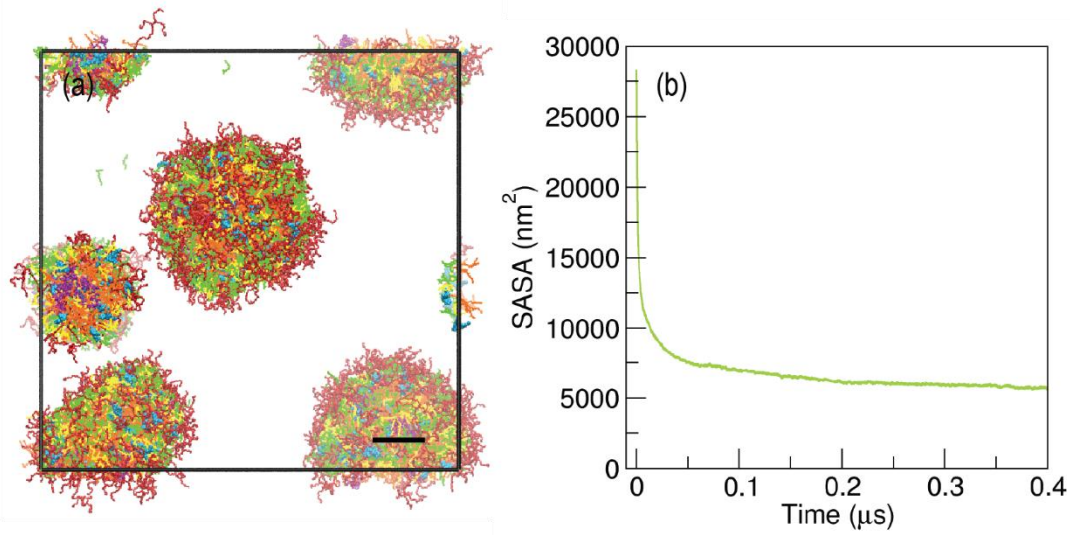

Figure S8 – (a) Colloidal structure formed in 90% w/w water with **F3**. (b) SASA for non-water component in the same system. The scale bar length is 4.0 nm.

Tables

Table S1 – Ratios of moments of inertia along principal axes and averaged radius of gyration for **F1**, **F2**, **F3**, **F4** and **F5** formulations at 90% w/w systems.

Formulation	Simulation number	No. of aggregates	Aggregation no.	I_1/I_2	I_2/I_3	I_1/I_3	Rg (nm)
F1	10	1	1245	0.940±0.019	0.950±0.020	0.892±0.013	4.535±0.006
F2	19	1	1322	0.923±0.013	0.973±0.015	0.898±0.018	4.638±0.007
F3	29	1	984	0.956±0.019	0.931±0.018	0.889±0.014	4.597±0.007
F4	40	1	1461	0.939±0.013	0.955±0.014	0.897±0.010	4.709±0.009
F5	50	1	1416	0.701±0.011	0.904±0.011	0.634±0.010	4.964±0.014

Table S2 – Total number of aggregates (more than 1000 water molecules) formed in water-swollen reverse micellar systems in **F1**, **F2**, **F4** and **F5** formulations.

Water (%w/w)	Number of Aggregates			
	F1	**F2**	**F4**	**F5**
10	12	10	-	-
20	10	9	6	7
30	4	5	6	6
40	-	-	-	5

Table S3 – Aggregation properties of loratadine in all systems

formulation	system	water (%w/w)	no. of agg.[a]	max. agg.no[b]	average agg. no.[c]	mode agg.no.[d]
1	1	0	131	9 (1)	3	2 (84)
	2	10	117	9 (1)	3	2 (84)
	3	20	118	6 (2)	3	2 (77)
	4	30	102	7 (4)	3	2 (66)
	5	40	80	8 (2)	3	2 (51)
	6	50	71	9 (1)	3	2 (44)
	7	60	50	11 (1)	3	2 (31)
	8	70	39	12 (1)	3	2 (25)
	9	80	26	6 (1)	3	2 (20)
	10	90	14	5 (1)	3	2 (8)
2	12	0	147	9 (1)	3	2 (98)
	13	10	138	9 (1)	3	2 (84)
	14	20	119	8 (1)	3	2 (75)
	15	30	93	7 (1)	3	2 (56)
	16	40	96	7 (3)	3	2 (60)
	17	50	72	16 (1)	3	2 (43)
	18	70	41	8 (1)	3	2 (28)
	19	90	14	5 (1)	2	2 (12)
3	20	0	90	6 (1)	2	2 (66)
	21	10	82	7 (1)	2	2 (63)
	22	20	66	6 (3)	3	2 (46)
	23	30	63	7 (2)	3	2 (41)
	24	40	55	7 (1)	3	2 (37)
	25	50	46	6 (1)	3	2 (31)
	26	60	40	8 (1)	3	2 (24)
	27	70	23	6 (1)	3	2 (15)
	28	80	20	5 (1)	2	2 (16)
	29	90	10	3 (2)	2	2 (8)
4	31	0	131	8 (1)	3	2 (87)
	32	10	124	11 (1)	3	2 (79)
	33	20	110	11 (1)	3	2 (61)
	34	30	97	8 (1)	3	2 (58)
	35	40	82	13 (1)	3	2 (35)
	36	50	80	8 (2)	3	2 (46)
	37	60	60	13 (1)	3	2 (41)
	38	70	47	8 (1)	3	2 (27)
	39	80	28	14 (1)	3	2 (17)
	40	90	15	4 (1)	2	2 (11)
5	41	0	134	6 (1)	3	2 (84)
	42	10	132	9 (1)	3	2 (84)
	43	20	128	10 (1)	3	2 (78)
	44	30	99	9 (1)	3	2 (57)
	45	40	78	8 (2)	3	2 (48)
	46	50	71	11 (1)	3	2 (37)
	47	60	58	7(1)	3	2 (31)
	48	70	52	6 (1)	3	2 (30)
	49	80	33	7(1)	3	2 (16)
	50	90	13	8(1)	3	2 (5)

[a]Number of aggregates in a system, [b]Maximum aggregation number in a system and the values in the brackets indicates the number of aggregates in that aggregate number, [c]Average aggregation number, [d]Mode aggregation number and the values in brackets indicate number of aggregates in that aggregation number.